Title

Accounting for Vs Spatial Variability and Modeling Errors in 1D Site Response Analyses

Author

Pretell Ductram, Anthony Renmin

Publication Date

2022

Peer reviewed|Thesis/dissertation

Accounting for V_S Spatial Variability and Modeling Errors in 1D Site Response Analyses

By

ANTHONY RENMIN PRETELL DUCTRAM

DISSERTATION

Submitted in partial satisfaction of the requirements for the degree of

DOCTOR OF PHILOSOPHY

in

Civil and Environmental Engineering

in the

OFFICE OF GRADUATE STUDIES

of the

UNIVERSITY OF CALIFORNIA

DAVIS

Approved:

Katerina Ziotopoulou, Chair

Norman A. Abrahamson

Ellen M. Rathje

Committee in Charge

2022

To my parents, Jenny and Justo,

to my brother, Rutsy,

and to my wife, Fiorella,

for their unconditional love and support

ACKNOWLEDGMENTS

I am incredibly grateful to my advisors Prof. Katerina Ziotopoulou and Prof. Norman Abrahamson. I will always be thankful to Katerina for taking me as a student, trusting my judgment, and providing freedom to my research curiosity. I appreciate Katerina's contributions to my growth as a well-rounded professional and her guidance through the different academic avenues I took and challenges I faced. I am deeply thankful to Norm, who has always been willing to share his time and knowledge, despite his many duties. Norm's devotion to teaching and selfless mentorship is admirable. I was extremely fortunate to take his class during my first year and to interact and work with him ever since.

I am sincerely grateful to Prof. Ellen Rathje for kindly accepting to serve as a member of my dissertation committee and for sharing her valuable time and knowledge.

During my graduate school journey, I have been fortunate to work with and interact with many exceptional professionals. I have significantly benefited from discussions with Dr. Albert R. Kottke, Prof. Jack Montgomery, and Dr. Jennie Watson-Lamprey. I am thankful for all the excellent professors I have learned from at UC Davis, especially Prof. Ross Boulanger, Prof. Jason DeJong, and Prof. Alejandro Martinez. I enjoyed learning from Ross during lectures and meetings we had while pursuing my master's degree. His passion and enthusiasm are contagious and inspiring. Jason always had his office door open to answer my questions on laboratory and field testing, or any other subject. My interactions with Ross and Jason greatly contributed to the formation of a solid and diverse technical foundation. It was always fun to have Spanglish conversations with Alejandro.

I am immensely thankful for the friends I made at UC Davis, Francisco Humire, Patrick Bassal, and Sumeet Sinha. Their friendship made my graduate school years an enjoyable journey; countless discussions on where pisco really is from, soccer days, dinner with our spouses, and so much more. These are memories that I will always cherish. Through my time at Davis, I have also been fortunate to meet a diverse group of amazing people, whose friendship I value. I would like to acknowledge Dr. Barry Zheng, Laura Hernández-Bassal, Miki Doan, Prof. Anubhab Gupta, Mandeep Basson, Hussain Alshawaf, Lin Huang, Matt Burrall, and Maya El Kortbawi.

My early interest in pursuing graduate school was strengthened by multiple interactions with friends, colleagues, and mentors during my years as a practicing engineer with Golder Associates. In particular, I would like to acknowledge Terry Eldridge, Dr. Manuel Monroy, Dr. Gordan Gjerapic, and Daniel Torres.

Lastly, I would like to thank my family. Agradezco a mi familia, a mi abuela Leonor, a mis padres Jenny y Justo, a mi hermano Rutsy, a mis tíos Víctor y Martín, y a mis primos Sashenka y Pavel, por ser el motor de mi motivación y siempre confiar en mis decisiones, aunque no comprendan bien de qué se trata. Above all, I thank my wife, Fiorella, whose sacrifice and patience made all this possible, and who supported me along the way since the beginning of this adventure far away from home.

Financial support for the work presented in this dissertation was provided by the Department of Civil and Environmental Engineering at UC Davis, Pacific Gas and Electric Company, and the California Strong Motion Instrumentation Program. The support of these organizations is appreciated.

ABSTRACT

One-dimensional site response analysis (1D SRA) remains the world state of practice for assessing site-specific site response in engineering projects. The 1D SRA numerical approach condenses the complexities of the 3D wave propagation phenomena into a simple horizontally polarized wave vertically traveling through a soil column, thus leading to errors in site response predictions. This dissertation proposes two approaches: (1) an approach to capture the effect of shear-wave velocity (V_S) spatial variability on site response using 1D SRAs, and (2) an approach for conducting 1D SRAs to account for the effect of unmodeled features affecting site response (e.g., inclined waves) and the potential for higher site amplifications. These approaches and the findings learned during their development are herein presented to provide practical recommendations expected to improve site response predictions using 1D SRAs.

A numerical investigation using 2D and 1D SRAs is conducted to develop an approach for capturing 2D V_S spatial variability effects on site response using 1D SRAs with randomized V_S profiles. The limitations of 1D SRAs with V_S randomization are mainly due to (1) the excessive randomization and the assumption that the resulting mean site response is representative, and (2) the intrinsic inability of 1D SRAs to capture wave propagation effects (e.g., constructive interference). Results from this investigation indicate that the 84th seismic response estimated from 1D SRAs conducted with fifty randomized V_S profiles generated using the Toro model (1995) with V_S standard deviation, $\sigma_{\ln V_S} = 0.25$ approximates well the median 2D site response at the site's fundamental frequency, regardless of what the site-specific $\sigma_{\ln V_S}$ is. Comparisons with data from four borehole sites classified as Group A (Tao and Rathje, 2020) support this observation.

An approach for conducting 1D SRAs is developed based on comparisons between 1D SRA predictions and borehole ground-motion data, with two objectives: (1) to improve site response predictions, and (2) to account for the 1D-SRA bias and the potential for underpredicting the estimated seismic response. The first objective is achieved by using randomized V_S profiles with $\sigma_{\ln V_S}$ and damping multipliers (D_{mul}) that reduce intrinsic errors carried in 1D SRAs, such as the overpredictions at the site's resonant frequency. Results from this work indicate that the $\sigma_{\ln V_S}$-D_{mul} pair leading to the lowest root mean square error between the observed and 1D SRA-based transfer functions and amplification factors is $\sigma_{\ln V_S} = 0.25$ and $D_{mul} = 3$. The second objective is achieved by acknowledging the 1D-SRA bias $\left(c_{3D}^{SRA}\right)$ and the potential for under- and overpredictions due to modeling errors carried by 1D SRAs, quantified as the standard deviation of the site-specific bias-corrected mean residuals $\left(\phi_{S2S}^{SRA}\right)$. The c_{3D}^{SRA} is used to bias-correct results from 1D SRAs with V_S randomization, thus obtaining the best estimate site response. The potential for higher site amplifications is subsequently accounted for by computing the 95th site response percentile using ϕ_{S2S}^{SRA}.

TABLE OF CONTENTS

LIST OF FIGURES

uncorrected FAS and uncorrected PSA response spectra (median of all input motions) at surface; (g) and (h): best estimate, and 5^{th} and 95^{th} percentiles of bias-corrected FAS and PSA response spectrum at surface (median of all input motions).

LIST OF TABLES

CHAPTER 1

INTRODUCTION

BACKGROUND

One-dimensional site response analyses (1D SRAs) remain the world state of practice for estimating site-specific site response, despite the ample evidence of discrepancies between ground-motion data and site response predictions. These analyses condense the three-dimensional nature of wave propagation to horizontally polarized vertically propagating shear (SH) waves traveling upward through a soil column, which implies a soil deposit of horizontal layers that extend infinitely in the lateral directions. Such simplifications challenge the 1D SRA's ability to capture the effect of non-1D features affecting site response, such as a dipping bedrock or the incidence of inclined waves, and their influence on site response leads to errors in site response predictions, in this dissertation referred to as modeling errors.

The shear-wave velocity (V_S) spatial variability is a critical site-specific feature affecting site response given its ubiquitous nature in the field, and it is perhaps the only one intended to be addressed in practice. For instance, it is common in the design of nuclear facilities (1) to conduct 1D SRAs using three base-case V_S profiles to account for the epistemic uncertainty, and (2) to randomize each one of these base-case V_S profiles to account for aleatory variability using the model proposed by Toro (1995). This approach, however, has been found to underestimate site response predictions due to the excessive amount of V_S randomization recommended by Toro (e.g., Teague and Cox, 2016) or the lack of lateral correlation between the randomized V_S profiles

(Pehlivan, 2013). Nevertheless, 1D SRAs conducted using randomized V_S profiles reduce the overprediction at the resonant frequencies (Tao and Rathje, 2019) and the peak-to-trough ratio in transfer functions (De la Torre et al., 2021), which thus make V_S randomization a potential tool for improving site response predictions.

Improving site response predictions in engineering practice is a difficult task. The simple parameterization and broad implementation of 1D SRAs in engineering practice limit the alternatives for improving site response predictions to: (1) altering the site response input parameters (e.g., V_S and damping), (2) post-processing 1D SRA estimates such that a more accurate site response is obtained (e.g., using scaling factors), and (3) a combination of (1) and (2). Previous studies explored the effect of calibrating damping to capture wave scattering effects and thus improve linear elastic SRAs. For instance, Tao and Rathje (2019), based on observations from four borehole array sites, found that increasing the minimum damping estimated based on Darendeli (2001) by factors ranging from 1.5 to 5 can improve the prediction of different ground motion intensity measures or metrics of interest (e.g., peak ground velocity, transfer functions). The calibration of damping or other alternative approaches (e.g., randomizing V_S profiles) can lead to improved 1D SRA-based predictions. Since such predictions are never flawless; thus, the reduced amount of modeling errors should be quantified and considered.

The site response modeling errors are neglected in current practice, and the accuracy of site response predictions is assumed to depend on the quality of input parameters alone, which is an unrealistic assumption (e.g., Stewart and Afshari, 2020). Site response modeling errors can be quantified as the difference between ground-motion data from borehole sites and site response predictions, and separated into a global method bias, and aleatory components. Once quantified, the method bias can be accounted for by adding it to the predicted site response, and the potential

for higher site amplifications can be considered by estimating site response percentiles higher than the median.

DISSERTATION SCOPE

This dissertation is a collection of manuscripts published or to be submitted for review and future publication. This dissertation provides the following main contributions: (1) an approach for capturing 2D V_S variability effects on site response using 1D SRAs conducted with V_S randomization, and (2) an approach for conducting 1D SRAs to account for modeling errors that uses (a) calibrated amounts of damping and V_S randomization that improve site response predictions, and (b) models for the bias and variability in the site terms (i.e., bias corrected site-specific mean residual) associated with 1D SRAs conducted with the calibrated damping and V_S randomization. A brief description of the subsequent chapters and the authorship roles are described in the following sections.

CHAPTER 2

The second chapter compares results from 2D SRAs on random fields and 1D SRAs on randomized V_S profiles to evaluate the ability of the latter to capture 2D V_S spatial variability effects. The amount of V_S randomization required along with the V_S model by Toro (1995) is calibrated, and its sensitivity to various 2D V_S variability features (e.g., degree of V_S variability, horizontal and vertical correlation lengths) is evaluated. The consistency of findings from this numerical study is evaluated against ground-motion data from borehole array sites.

The contents of this chapter were originally published as a journal paper in Earthquake Spectra titled “Conducting 1D site response analyses to capture 2D V_S spatial variability effects,” by R. Pretell, K. Ziotopoulou, and N.A. Abrahamson. Pretell was the lead researcher, responsible

for the methods, analyses, and writing of the manuscript, and Ziotopoulou and Abrahamson were the faculty advisors and reviewed the manuscript. The contents of Appendix A (referred in this chapter) were originally published as a conference paper titled "Numerical investigation of V_S spatial variability effects on the seismic response estimated using 2D and 1D site response analyses," by R. Pretell, K. Ziotopoulou and N.A. Abrahamson, presented during GeoCongress 2022 in Charlotte, North Carolina (March 2022). Pretell was the lead researcher, responsible for the methods, analyses, and writing of the paper, Ziotopoulou and Abrahamson were the faculty advisors and reviewed the paper.

CHAPTER 3

The third chapter presents an approach for conducting 1D SRAs with two objectives (1) to improve site response predictions, and (2) to account for the bias in 1D SRAs and the potential for under- and overpredictions carried by site response estimates. This chapter uses ground-motion data from borehole sites to calibrate damping and V_S randomization.

The contents of this chapter will be submitted for journal publication with title "A borehole data-based approach for conducting 1D site response analyses I: damping and V_S randomization," by R. Pretell, N.A. Abrahamson, and K. Ziotopoulou. Pretell was the lead researcher, responsible for the methods, analyses, and writing of the manuscript, and Abrahamson and Ziotopoulou were the faculty advisors and reviewed the manuscript.

CHAPTER 4

The fourth chapter builds on the third chapter to quantify the site response residuals associated with 1D SRAs conducted with the calibrated amount of damping and V_S randomization. The site response residuals are partitioned into their different components, mainly the global site response

bias $\left(c_{3D}^{SRA}\right)$ and the site-specific mean bias-corrected residuals ($\delta S2S_S^{SRA}$) with standard deviation ϕ_{S2S}^{SRA}, and their sensitivity due to site type (1D- or 3D-like), region, and the presence of pseudo-resonances are discussed. Models for c_{3D}^{SRA} and ϕ_{S2S}^{SRA} are proposed, and guidelines are provided for conducting 1D SRAs using the calibrated damping, V_S randomization, and considering c_{3D}^{SRA} and ϕ_{S2S}^{SRA} to account for modeling errors.

The contents of this chapter will be submitted for journal publication with title "A borehole data-based approach for conducting 1D site response analyses II: accounting for modeling errors," by R. Pretell, N.A. Abrahamson, and K. Ziotopoulou. Pretell was the lead researcher, responsible for the methods, analyses, and writing of the manuscript, and Abrahamson and Ziotopoulou were the faculty advisors and reviewed the manuscript.

CHAPTER 5

The fifth chapter of this dissertation summarizes the main findings of the previous three chapters and presents future research directions.

CHAPTER 2

CONDUCTING 1D SITE RESPONSE ANALYSES TO CAPTURE 2D V_S SPATIAL VARIABILITY EFFECTS

AUTHOR'S NOTE

The contents of this chapter were originally published in Earthquake Spectra, by Pretell R, Ziotopoulou K and Abrahamson NA. Minor formatting changes were made to the original publication. Authorship roles are provided in Chapter 1.

PUBLICATION

Pretell R, Ziotopoulou K and Abrahamson NA (2022) Conducting 1D site response analyses to capture 2D V_S spatial variability effects. *Earthquake Spectra* 00(0): 1–25. 10.1177/87552930211069400

2.1. ABSTRACT

One-dimensional site response analyses (1D SRAs) with shear-wave velocity (V_S) randomization are commonly performed to estimate median site-specific amplification factors (AFs) under the implicit assumption that this approach yields a realistic response. In this work, an investigation is conducted to determine the appropriate amount of V_S randomization $(\sigma_{\ln V_S})$ needed to capture a median response that accounts for 2D V_S spatial variability effects. Results from 2D SRAs and 1D SRAs with V_S randomization show that the median 2D seismic responses are generally higher than 1D responses at the site's fundamental frequency, and that higher V_S variability has a mild impact

on the median 2D seismic response amplitude at the fundamental frequency, whereas it significantly reduces the median 1D response. Findings indicate that the 84th percentile AFs based on 1D SRAs conducted with V_S randomization using $\sigma_{\ln V_S} = 0.25$, approximate well with the more realistic median 2D SRA-based AFs around the fundamental frequency, while the 70^{th} to 60^{th} percentiles might be more appropriate at higher frequencies. The benefit of using percentiles of the 1D SRA-based AFs higher than the median is shown for different site conditions and supported by comparisons against empirical data from four downhole sites.

2.2. INTRODUCTION

The estimation of the seismic response at the ground surface is a key component in the seismic design of structures. One-dimensional site response analyses (1D SRAs) are commonly used to assess the amplification or deamplification of seismic waves as they travel from a source at depth, through soil deposits, and reach the ground surface. This simplified analysis is widely used in engineering practice given that it requires a relatively simple site characterization, and it is computationally inexpensive. However, 1D SRAs condense the 3D nature of wave propagation to horizontally polarized vertically propagating shear (SH) waves traveling upward through a 1D soil column, which is representative of a soil deposit of horizontal layers that extend infinitely in the lateral directions. Given this simplification, observed discrepancies between empirical data and 1D SRA-based estimations are unsurprising (e.g., Afshari and Stewart, 2019; Baise et al., 2011; Kaklamanos et al., 2011, 2013; Kottke, 2010; Regnier, 2013; Regnier et al., 2018; Stewart et al., 2008; Tao and Rathje, 2019; Thompson et al., 2012; Zalachoris and Rathje, 2015). These discrepancies are generally attributed to (1) uncertainties associated with shear-wave velocity (V_S) and (2) conflicts between field reality and the 1D SRAs' underlying assumptions, such as laterally homogeneous V_S structure. In this work, 2D V_S spatial variability effects on the median seismic

response are studied, and an approach for capturing these effects using 1D SRAs is investigated. In reality, there are no 2D sites, but rather 3D sites that unavoidably encompass a wide range of site conditions (e.g., variable V_S, inclined bedrock, inclined wave propagation) affecting the seismic response. However, herein, the expression "2D V_S spatial variability" is used to be explicit about the assumptions of this study, and the range of applicability of the conclusions drawn.

The effect of V_S spatial variability on the seismic response has been studied by regulators and researchers. For nuclear facilities, it is common to follow the guidelines by the Electric Power Research Institute (EPRI, 2013) to conduct 1D SRAs. These guidelines recommend using three base-case V_S profiles to account for the epistemic uncertainty on the V_S profile and to randomize each one of these base-case V_S profiles to account for aleatory variability. This approach, however, has been found to underestimate site response predictions (Teague and Cox, 2016). Previous research efforts have also studied spatial variability and other non-1D effects. Pehlivan (2013) performed 2D equivalent-linear SRAs on V_S random fields and 1D equivalent-linear SRAs on randomized V_S profiles and found that mean spectral accelerations from 2D SRAs are higher by 15% – 40%. De Martin et al. (2013) performed 3D, 2D, and 1D SRAs using the spectral-element method and concluded that small deviations from 1D wave propagation theory strongly affect the period and amplitude of the system's resonant modes. Bielak et al. (1999) compared the estimations from 2D and 1D SRAs against observations from the 1988 Armenia Earthquake and concluded that results from 2D SRAs provide a better agreement.

In this article, 2D and 1D linear elastic SRAs are conducted to investigate a methodology for capturing 2D V_S spatial variability effects on the seismic response using 1D SRAs with V_S randomization. SRAs performed on 2D V_S correlated random fields and on 1D randomized V_S profiles are generated using the Toro model (1995). Various site conditions are considered to

generate the 2D random fields, whereas the standard deviation of V_S $(\sigma_{\ln V_S})$ for 1D randomization is calculated from the 2D models and generic values are also used. Differences between the median 2D SRA- and 1D SRA-based seismic responses are discussed, and residuals are estimated. Two criteria for estimating a more realistic 2D seismic response using 1D SRAs are evaluated, and findings are contrasted against empirical data. Results from this study provide insights into the biases carried when estimating the seismic response using 1D SRAs with V_S randomization, and practical guidance is provided to conduct these analyses such that a more realistic seismic response that accounts for 2D V_S spatial variability effects is captured.

2.3. RATIONALE FOR V_S RANDOMIZATION

One-dimensional SRAs are commonly conducted using randomized V_S profiles with two objectives: (1) to account for the spatial variability of natural soil deposits (e.g., Griffiths et al., 2016a; Kaklamanos et al., 2020; Tao and Rathje, 2019; Toro, 1995) and (2) to correct for overpredictions of the site amplification observed at the site's fundamental frequency when using 1D SRAs (e.g., Rodriguez-Marek et al., 2020; Zalachoris and Rathje, 2015). While these two aspects justify the use of randomized V_S profiles, there is limited guidance on how to conduct V_S randomization, and whether it yields a more realistic seismic response is unclear. Commonly, the amount of V_S randomization, that is, the deviation from the baseline or "seed" V_S profile, is controlled by $\sigma_{\ln V_S}$ and determined from V_{S30}-based site classes (e.g., EPRI, 2013). However, V_{S30} is an index that cannot capture site-specific features affecting seismic amplification and thus V_S randomization based on V_{S30} does not necessarily lead to a more realistic response.

A number of site-specific features and wave propagation mechanisms play a role in the site amplification (or deamplification), such as changes in soil's impedance, V_S spatial variability,

constructive interference, wave reflections and focusing effects, surface waves, and so on (Figure 2.1). Out of all these, 1D SRAs that are most commonly used in practice can only explicitly model the changes in impedance and resonance effects. We hypothesize that each unmodeled site-specific feature can be uncoupled and implicitly captured in 1D SRAs using a selected amount of $\sigma_{\ln V_S}$. For instance, the seismic response for a site with spatially variable V_S and a dipping bedrock can be estimated from 1D SRAs with randomized V_S profiles generated using $\sigma_{\ln V_S} = \sigma_{\ln V_{S,1}} + \sigma_{\ln V_{S,2}}$, where $\sigma_{\ln V_{S,1}}$ is used to capture the V_S spatial variability effects on the seismic response, and $\sigma_{\ln V_{S,2}}$ is used to capture the dipping bedrock effects.

In this work, an approach for using V_S randomization and estimating an appropriate seismic response is investigated. The proposed approach for conducting 1D SRAs with V_S randomization has two parts: (1) using contributions to $\sigma_{\ln V_S}$ from each unmodeled site-specific feature and (2) estimating a realistic seismic response based on a calibrated or selected criterion (e.g., a percentile higher than the median or a scaled response). In this article, attention is placed on the amount of V_S randomization for capturing the V_S spatial variability effects on the median seismic response at ground surface, that is, $\sigma_{\ln V_S}$. V_S randomization is conducted using the model for V_S proposed by Toro (1995).

2.3.1. V_S RANDOMIZATION MODEL BY TORO

Toro (1995) proposed a V_S randomization model for the probabilistic characterization of V_S in SRAs with several sets of parameters for different V_{S30}-based site classes (Boore et al., 1994; Toro, 1995). The model's main parameters are $\sigma_{\ln V_S}$ and an auto-regressive functional form that determines the interlayer correlation. This model relies on the observation that V_S approximately varies with a log-normal distribution (e.g., Li and Assimaki, 2010), and it assumes a constant $\sigma_{\ln V_S}$

with depth. Toro also proposed models for randomizing layer thicknesses, and depth to bedrock, which are commonly used along with the model for randomizing V_S. In this work, only V_S is randomized.

2.4. NUMERICAL INVESTIGATION

2.4.1. EVALUATION APPROACH

Three sets of SRAs are conducted (Figure 2.2): (1) 2D SRAs on random fields constructed for several target $\sigma_{\ln V_S}$, (2) 1D SRAs with V_S randomization using several specified values of $\sigma_{\ln V_S}$, and (3) 1D SRAs on sampled V_S profiles extracted from the 2D random field models. The 2D ground-motion response is recorded at equally spaced locations along the ground surface. These results, which are herein assumed to represent a more realistic seismic response, are compared against 1D SRA-based estimates. The sampled V_S profiles consist of profiles numerically sampled from the 2D models at the recording locations (Figure 2.2). Results from this set of 1D SRAs provide insight into the ability of 1D SRAs to estimate an accurate seismic response when multiple flawlessly measured V_S profiles are available. Results from the three sets are compared in terms of transfer functions (TFs) for Fourier amplitudes and amplification factors (AFs) for response spectral values. All SRAs are linear elastic.

2.4.2. NUMERICAL MODEL

The 2D and 1D models consist of 1 m × 1 m square elements with different V_S values, which allow for an appropriate propagation of waves with frequencies lower than about 12.5 Hz (Kuhlemeyer and Lysmer, 1973). The 2D model's width is selected such that a seismic response along the middle zone, that is "recording zone," is unaffected by wave reflections from the edges of the model. Various model widths (or width-to-height W:H ratios) were tested for a 1D-type

model (Figure 2.3a) until the estimated seismic response is comparable to the one obtained using 1D SRAs. A model width of 600 m (i.e., W:H = 20) is used to allow for a 100-m wide recording zone which results in errors in the TFs of less than 5% (Figure 2.3b and 2.3c). Each model has 21 recording locations equally spaced every 5 m along the surface. Preliminary analyses not presented herein for brevity indicated that shorter recording spacings do not provide additional benefit in the accuracy of the estimated seismic response.

A damping ratio of 10% is used for all soils in the numerical sections of this article. Note that damping is not used as a means to account for unmodeled natural phenomena such as wave scattering, instead, V_S randomization is used for that. The selection of a 10% damping ratio was led by a balance between the number of recorded responses along the model's surface, model size, and computational demand. Had a more realistic (lower) damping ratio been used, then a significantly larger 2D numerical model or more 2D models would have been required to obtain the same number of ground motion responses along the surface. Using this value of damping ratio does not affect the observed trends and conclusions drawn in this study, as indicated in a later section. The bedrock was modeled as a rigid base to isolate the effects of the soil–bedrock impedance ratio. The finite element software QUAD4MU (Hudson et al., 1994, 2003) is used to conduct 2D and 1D SRAs.

2.4.3. BASELINE 2D RANDOM FIELD MODELS

The 2D sites consist of 30-m-deep correlated V_S random fields over a horizontally oriented bedrock. The random fields are developed using the covariance matrix approach (Vanmarcke, 1983), based on a 1D seed V_S profile and a correlation function ρ. The seed V_S profile is developed

using the relations proposed by Kamai et al. (2016) for sites in California with a V_{S30} = 200 m/s, and ρ is an exponential model with no nugget, given by:

$$\rho = \exp\left(-2\frac{\Delta_{hor}}{\theta_{hor}}\right)\exp\left(-2\frac{\Delta_{ver}}{\theta_{ver}}\right) \quad (2.1)$$

in which Δ_{hor} and Δ_{ver} are the lag distances along the horizontal and vertical directions, respectively, and θ_{hor} and θ_{ver} are the horizontal and vertical V_S correlation lengths, selected as 50 and 5 m, respectively. The selected correlation lengths yield a correlation anisotropy of 10, common in soil properties and geological environments (DeGroot, 1996; Phoon and Kulhawy, 1996, 1999). The 2D random field models are generated for target $\sigma_{\ln V_S}$ = 0.2, 0.3, 0.4, and 0.5, commonly observed in nature (e.g., Holzer et al., 2005; Wills and Clahan, 2006). Figure 2.2 shows a sample 2D random field model for a target $\sigma_{\ln V_S}$= 0.2, and Figure 2.4 shows the correlation functions for $\ln(V_S)$ in the horizontal direction. The correlation values are presented in $\tanh^{-1}$ scale to produce an approximately normal distribution (Abrahamson et al., 1991) and are estimated for a maximum lag distance of half the model width to prevent biases induced by the number of available data pairs. The agreement between the theoretical and the mean simulated correlation functions confirms that the target correlation model is well captured by the generated profiles.

2.4.4. 1D SRAs WITH V_S RANDOMIZATION

The seismic response is assessed through 1D SRAs on a suite of 50 randomized V_S profiles (Toro, 1995). The seed profile used for V_S randomization is calculated as the geometric mean of multiple profiles sampled from the recording zone, considered as the only portion of the 2D models affecting the seismic response, whereas $\sigma_{\ln V_S}$ is the standard deviation of the same profiles, used for V_S randomization. Hereafter, this standard deviation is referred to as "model-specific $\sigma_{\ln V_S}$." This approach is similar to practical applications where multiple V_S profiles are measured in the

field and then used to estimate a representative V_S profile and $\sigma_{\ln V_S}$ (e.g., Griffiths et al., 2016b; Teague and Cox, 2016). Evaluations not included herein indicate that the ultimate seismic response is not sensitive to the location, or the number of the selected V_S profiles sampled within the zone of influence when more than 10 V_S profiles are used. In total, 50 V_S profile realizations are generated as it leads to stable results, with standard errors for the mean AF lower than 5% for most cases and lower than 8% for models with highly variable V_S. Using more realizations does not impact the results. Each set of results presented in this article are based on a different set of 50 V_S randomized profiles, such that conclusions are not based on a single one. The V_S randomization model was used with the interlayer correlation parameters recommended for sites with V_{S30} ranging from 180 to 360 m/s. These correlation parameters and those recommended for sites with V_{S30} ranging from 360 to 760 m/s are similar and using either set of parameters for a given seed V_S profile leads to practically the same seismic response.

2.4.5. INPUT GROUND MOTION

The ground motion from the M7.6 Chi-Chi earthquake (1999) recorded at the TCU075 station (Figure 2.5) was downloaded from the Pacific Earthquake Engineering Research Center (PEER) Database (Ancheta et al., 2013) and is applied uniformly as vertically incident SH waves along the model base as acceleration. For linear elastic SRAs, a single input ground motion is sufficient for estimating the response in terms of TFs. In the case of AFs, we assume that any additional contribution to the variability that comes from multiple input ground motions is minimal compared to the variability already included using 2D V_S random fields and randomized 1D V_S profiles. This assumption is supported by additional analyses with different ground motions, not presented herein and a previous study by Bazzurro and Cornell (2004).

2.5. BASELINE RESULTS

Results indicate discrepancies between 2D and 1D SRAs in terms of TFs and AFs. Figures 2.6 and 2.7 present TFs and AFs for four representative 2D models, each with different model-specific $\sigma_{\ln V_S}$, and the associated sampled and randomized 1D models. The discrepancies are consistently observed for different $\sigma_{\ln V_S}$and are due to (1) amplification effects captured by 2D SRAs but missed by 1D SRAs, such as wave scattering and constructive interference, and (2) a stronger shifting of the 1D fundamental frequencies due to V_S randomization, which leads to the cancelation of peaks and troughs and thus lower median TFs and AFs, and overall highly variable responses across frequencies compared to the 2D results. This effect has also been pointed out by other researchers (e.g., Tao and Rathje, 2019; Teague and Cox, 2016). In all cases, the median 2D SRA-based TF is higher than the median 1D SRA-based TF from sampled V_S profiles around the fundamental frequency, and the latter is higher than the 1D SRA-based TF from randomized V_S profiles.

The cancelation of peaks and troughs is less significant in the case of 1D SRAs on sampled profiles given the stronger correlation of the 1D columns compared to the randomized V_S profiles. These results also suggest that highly variable sites present a weaker second mode TF when estimated based on 2D SRAs, which is due to wave scattering caused by soil heterogeneities (De la Torre et al., 2019). Similar trends are observed in the median 2D SRA- and 1D SRA-based AFs (Figure 2.7), although with milder differences given that AFs have contributions from a range of Fourier spectrum frequencies at a single oscillator frequency (Bora et al., 2016). These observations are consistent with previous similar studies (e.g., Bielak et al., 1999; Nour et al., 2003; Pehlivan, 2013).

Importantly, this numerical evaluation indicates that the site's V_S variability, captured through $\sigma_{\ln V_S}$, has a different impact on the 2D and 1D seismic responses. In other words, using model-specific $\sigma_{\ln V_S}$ values for 1D SRAs with V_S randomization does not necessarily lead to a more realistic seismic response. It is worth noting that 2D SRA-based TFs generally show higher amplitudes than 1D SRA-based TFs. Various researchers have observed that 1D SRAs overpredict the responses at the site's fundamental frequency (e.g., Rodriguez-Marek et al., 2020; Zalachoris and Rathje, 2015). It is therefore likely that 2D SRAs suffer from a similar issue. Assuming that the degree of overprediction is similar in 2D as in 1D SRAs, results from this work are not affected, as the relative differences between 2D and 1D SRAs are studied rather than absolute amplitudes. An immediate approach to test the validity of conclusions drawn from this numerical evaluation can rely on empirical data, as presented in a later section.

2.5.1. V_S RANDOMIZATION TO ACCOUNT FOR 2D V_S SPATIAL VARIABILITY

The previous section shows that randomizing V_S with model-specific $\sigma_{\ln V_S}$ values does not necessarily lead to an appropriate median seismic response. Here, an evaluation of the ability of V_S randomization with a generic $\sigma_{\ln V_S}$ = 0.25 to capture 2D V_S spatial variability effects is conducted, and the performance of a generic $\sigma_{\ln V_S}$ is compared against model-specific $\sigma_{\ln V_S}$ values.

The results in terms of TFs and AFs are, respectively, presented in Figures 2.8 and 2.9 for the same representative sites selected for Figures 2.6 and 2.7. In all cases investigated, that is, $\sigma_{\ln V_S}$ = 0.16 to 0.48, the 84th percentile TFs and AFs at the fundamental frequency estimated using a generic $\sigma_{\ln V_S}$ = 0.25 are similar to those estimated using model-specific $\sigma_{\ln V_S}$ values. Using $\sigma_{\ln V_S}$ = 0.25 leads to TFs slightly broader compared to the ones from model-specific $\sigma_{\ln V_S}$ for sites

with low V_S variability, and narrower TFs in the case of highly variable sites. These results suggest that $\sigma_{\ln V_S} = 0.25$ could be used to capture 2D V_S spatial variability effects on the seismic response.

2.6. CRITERIA FOR ESTIMATING A REPRESENTATIVE SEISMIC RESPONSE

Results indicate that median 1D SRA-based TFs and AFs (with or without V_S randomization) are lower than the median 2D SRA-based TFs and AFs, around the fundamental frequency. This suggests that the median 2D response cannot be captured by the median 1D response. As such, two criteria to approximate the median 2D response using 1D SRAs with V_S randomization are investigated: (1) 1D seismic response percentiles higher than the median, and (2) scaling factors to adjust the median 1D seismic response. Results in this section are presented in terms of AFs only, but similar trends are observed for TFs.

2.6.1. POTENTIAL CRITERION I: PERCENTILES HIGHER THAN THE MEDIAN 1D SRA-BASED SEISMIC RESPONSE

This approach aims at capturing a median response that accounts for 2D V_S spatial variability effects using a percentile higher than the median 1D SRA-based response. To evaluate the benefit from this approach, residuals are estimated for the nth percentile of the 1D SRA-based AFs as:

$$Residual = \ln\left(AF_{2D,\, median}\right) - \ln\left(AF_{1D,\, n^{th}\, percentile}\right) \qquad (2.2)$$

where n^{th} can be the median, 60^{th}, 70^{th}, 84^{th}, or the 90^{th} percentile. Positive and negative residuals indicate underprediction and overprediction, respectively. Figures 2.10 and 2.11 present residuals for AFs estimated using 10 2D random fields, and the corresponding randomized 1D V_S profiles generated using model-specific $\sigma_{\ln V_S}$, indicated in the top left corners, and a generic $\sigma_{\ln V_S} = 0.25$. In both figures, solid lines represent the median residuals estimated from all the 10 2D random

fields, each one with a different model-specific $\sigma_{\ln V_S}$ affecting the seismic response, hence the range of $\sigma_{\ln V_S}$ values. In Figure 2.10 (model-specific $\sigma_{\ln V_S}$), residuals for median 1D SRA-based AFs (95% CI) vary from 20.5 to 0.75, with scatter increasing with $\sigma_{\ln V_S}$. Logically, these residuals decrease, that is, they transition from underprediction to overprediction, as higher percentiles of the 1D SRA-based AFs are considered. The 84th – 90th percentile AFs have residuals near zero at the fundamental frequency (i.e., around 1.8 Hz), whereas the 60th – 70th percentile AFs reach near-zero residuals at higher frequencies. In Figure 2.11 (generic $\sigma_{\ln V_S}$ = 0.25), the differences between 2D and 1D SRA-based AFs at the fundamental frequency are similar to those obtained when using model-specific $\sigma_{\ln V_S}$ values. However, at higher frequencies, the overprediction is slightly higher for sites with low V_S variability ($\sigma_{\ln V_S}$ from 0.16 to 0.19), and lower for sites with high V_S variability ($\sigma_{\ln V_S}$ from 0.3 to 0.48). For highly variable sites, the 60th percentile AF appears to be high enough to capture the median 2D SRA-based response at frequencies other than the fundamental.

2.6.2. POTENTIAL CRITERION II: SCALING FACTORS TO ADJUST THE MEDIAN 1D SRA-BASED SEISMIC RESPONSE

This approach aims at capturing a median response that accounts for 2D V_S spatial variability effects by scaling the median 1D SRA-based response. This approach is similar to using correction factors to account for 2D or 3D effects (e.g., Chavez-Garcia and Faccioli, 2000). The scaling factors are estimated as:

$$Scaling\ Factor = \frac{AF_{2D,\,median}}{AF_{1D,\,median}} \qquad (2.3)$$

in which AF_{2D}, median is the median 2D SRA-based AF estimated for a site, and AF_{1D}, median is the median 1D SRA-based AF for a set of 50 randomized V_S profiles used to assess the seismic response of the same site. Generally, scaling factors vary from 0.5 to 2.3 (Figure 2.12). Higher factors are estimated for more variable sites. For instance, a median factor of 1.5 could be applied to a 1D SRA-based AF to estimate the median 2D AF at the fundamental frequency for sites with $\sigma_{\ln V_S}$ from 0.4 to 0.48.

Using scaling factors presents two limitations: (1) they depend on the site's frequency modes, the site's $\sigma_{\ln V_S}$, and vary across frequencies, which makes them challenging to know and calibrate for a wide range of site conditions, and (2) they are highly variable even at a single frequency, often with factors lower and higher than 1 and a median near 1 that do not properly correct neither overprediction nor underprediction. This approach might be appropriate for site-specific projects, where a few 2D SRAs can be conducted to calibrate scaling factors (e.g., Anderson et al., 2018), but appears unsuitable for a generalized recommendation.

2.7. PARAMETRIC EVALUATION

A parametric evaluation is conducted to study the consistency of the observed trends of the residuals in AFs for different site conditions. This evaluation is conducted for 2D random fields developed for a target $\sigma_{\ln V_S}$ = 0.2 and varying other baseline conditions one at the time. These conditions are the underlying bedrock, the V_S heterogeneity (correlation model, $\sigma_{\ln V_S}$, and correlation lengths), the site's stiffness and fundamental frequency (V_{S30} and depth), and the soils' damping ratio. All the investigated parameters and values are listed in Table 2.1. TFs and AFs are estimated with model-specific $\sigma_{\ln V_S}$, and the residuals for the median and 84th percentile AFs are calculated and compared against results for the baseline case. In this case, residuals are shown

against the normalized frequency, f/f_0, where f_0 is the site's fundamental frequency, to remove the effect of differences in f_0 of different sites. Herein, attention is placed on the consistency of the improved performance of the 84th percentile over the median 1D SRA-based AFs, at the fundamental frequency (f/f_0 = 1). A study of the effects of the site conditions on the 2D SRA-based TFs and AFs and the sampled 1D SRA-based TFs and AFs is presented in Appendix A (Pretell et al., 2022).

2.7.1. EFFECT OF UNDERLYING BEDROCK CONDITIONS

The baseline site was modeled using a rigid base to isolate the influence of the soil–bedrock impedance ratio. A rigid base does not allow for the dissipation of energy when seismic waves bounce back down to the model base. Here, the effect of this assumption is studied. An elastic base allows for some energy dissipation, which is a more common field condition. The elastic base is modeled for three $V_{S,\,bedrock}$ = 500, 760, and 1500 m/s. The results indicate that the presence of an elastic base leads to a mild reduction of residuals, with lower V_S values leading to lower residuals (Figure 2.13a). At the fundamental frequency, the 1D SRA-based median AF underpredicts the response, while 84th percentile AFs are relatively stable and lead to near zero residuals. At higher frequencies, the median and 84th percentile 1D SRA-based AFs generally overpredict the response. The relative difference between the residuals corresponding to a rigid and an elastic base is minor and follows the same trends as observed for the baseline site. Thus, a rigid base is used for further parametric analyses.

2.7.2. EFFECT OF CORRELATION MODEL

The correlation model controls how fast the V_S correlation decays with distance. The baseline site was developed using V_S random fields that follow an exponential correlation model. The effect of

the selected correlation is evaluated using the spherical, the polynomial decaying, and the squared exponential correlation models (e.g., Lloret-Cabot et al., 2014). The results do not show a significant variation of the residuals for different correlation models compared to the baseline site (Figure 2.13b). Overall, all residuals for the median and 84th percentile AFs cluster closely and vary within a narrow range of 0.1 ln units.

2.7.3. EFFECT OF HORIZONTAL CORRELATION LENGTH

The horizontal correlation length, θ_{hor} determines the span within which V_S is highly correlated in the horizontal direction. Sites with longer θ_{hor} have a more similar V_S in the lateral direction and thus are more compliant to the 1D SRA assumption of lateral continuity. Another interpretation for longer θ_{hor} is for sites with low V_S variability relative to the size of the structure of interest. The baseline site's θ_{hor} of 50 m is decreased and increased (θ_{hor} = 5, 25, and 500 m) to evaluate the effect of shorter and longer horizontal correlation lengths. The results indicate that sites with longer θ_{hor} lead to smaller residuals, that is, the 2D and 1D seismic responses are more similar (Figure 2.13c), whereas sites with shorter θ_{hor}, that is, more variable in the lateral direction, lead to further underpredictions of the 2D SRA-based median AFs at the fundamental frequencies.

2.7.4. EFFECT OF VERTICAL CORRELATION LENGTH

The vertical correlation length, θ_{ver}, determines the span within which V_S is correlated in the vertical direction. Sites with longer θ_{ver} are representative of soil deposits with thicker layers of approximately uniform V_S. The baseline site's θ_{ver} of 5 m is increased (θ_{ver} = 10, 25, 50 m) to evaluate the effect of longer vertical correlation lengths. The results indicate that longer θ_{ver} values lead to higher overpredictions of the seismic response at the fundamental frequency (Figure 2.13d).

The residuals for the 1D SRA-based median and 84th percentile AFs are not significantly affected by θ_{ver} and vary within 0.2 ln units across frequencies.

2.7.5. EFFECT OF SITE'S DEPTH

The baseline site had a depth of 30 m and a θ_{ver} of 5 m. The effect of the site depth on the estimated residuals is evaluated for the depths of 50, 100, and 200 m through two scenarios: (1) deeper sites with constant θ_{ver} and (2) deeper sites with constant θ_{ver}/depth. When necessary, the 2D baseline model geometry and element dimensions are changed to accommodate the larger (deeper and wider) models while balancing the number of recordings and the computational demand. The results indicate that the AFs for deeper sites with θ_{ver} = 5 m are generally underpredicted by the median 1D SRA-based AFs at the fundamental and some high-frequency modes, and that 1D SRA-based 84th percentile AFs are more representative of median 2D SRA-based AFs at f/f_0 (Figure 2.13e). Similar trends are observed in the case of deeper sites with constant θ_{ver}/depth (Figure 2.13f).

2.7.6. EFFECT OF SITE'S V_{S30}

The baseline site was generated to have an overall V_{S30} of 200 m/s following the relations by Kamai et al. (2016). The effect of V_{S30} is evaluated for the values of 300, 400, and 500 m/s. In all cases, the parameters used to generate 1D V_S profiles are the same and correspond to sites with V_{S30} from 180 to 360 m/s (Toro, 1995). The results indicate that median 1D SRA-based AFs underpredict the median 2D SRA-based AFs at the site's fundamental frequency and they might under- or overpredict AFs at higher frequencies (Figure 2.13g). The 84th percentile 1D SRA-based AFs lead to near zero residuals at the fundamental frequency and higher overprediction at higher frequencies.

2.7.7. EFFECT OF SOIL DAMPING

The dissipation of energy during wave propagation is controlled by the damping ratio. The baseline site's materials are modeled with a damping ratio of 10%. The effect of using different critical damping ratios is evaluated for damping ratio values of 2%, 5%, and 15%. The results indicate a significant impact of damping on the residuals, with lower damping leading to higher and a more erratic variability of residuals (Figure 2.13h). The effect of damping on the absolute seismic responses is important. However, the effect of damping on the relative difference between the seismic responses estimated using 2D and 1D SRAs is relatively minor. Given a selected damping ratio, the difference between the residuals corresponding to the 1D SRA-based median and 84th percentile 1D SRA-based AFs is similar to the previous scenarios in variability across frequencies and magnitude.

2.7.8. CONCLUSION FROM PARAMETRIC EVALUATION

The parametric evaluation indicates some variability in the magnitude of residuals for different site conditions but consistent trends in the differences between the residuals from the median and 84th percentile 1D SRA-based AFs. Therefore, it is concluded that the applicability of the potential criteria for estimating a more realistic median seismic response is not limited to the baseline case.

2.8. EMPIRICAL CONSISTENCY

The ability of 1D SRAs with V_S randomization using $\sigma_{\ln V_S} = 0.25$ combined with the selection of a percentile higher than the median seismic response to be approximate a more realistic response that captures V_S spatial variability effects is evaluated against ground-motion data. Toward this end, data from four downhole sites are used: (1) Delaney Park (Alaska), (2) Garner Valley (California), (3) HYGH10 (Japan), and (4) IBRH13 (Japan). These stations are selected as they

are identified as sites unlikely to be exposed to non-1D effects and their seismic response to be dominated by true resonances (Tao and Rathje, 2020). Nevertheless, 1D SRAs might still lead to underestimation of the median empirical TF amplitudes, except at the fundamental frequency where overprediction is well known to occur. We argue that while these sites do not present complex geological structures, observed discrepancies between theoretical and empirical responses are mainly due to the V_S spatial variability inherent to natural deposits. Therefore, these sites offer an opportunity to examine the trends and findings obtained from the numerical work discussed earlier. Key features of the downhole sites, including the taxonomy by Tao and Rathje (2020) and Thompson et al. (2012), are presented in Table 2.2. A description of the sites' geology is presented by Combellick (1999) for Delaney Park, Bonilla et al. (2002) for Garner Valley, and borehole logs for HYGH10 and IBRH13 are available on the Kiban Kyoshin Network (KiK-net) website (National Research Institute for Earth Science and Disaster Resilience (NIED), 2019).

2.8.1. GROUND-MOTION RECORDINGS

Ground-motion recordings are collected from the Network for Earthquake Engineering Simulations (NEES) database for Delaney Park and Garner Valley and from the KiK-net database for the HYGH10 and IBRH13 sites. In the case of Delaney Park and Garner Valley, which have sensors at multiple depths, ground-motion recordings from the deepest sensor are used to work with the widest possible ground-motion frequency band. The ground motions are used as recorded, without any rotation. The recordings are processed, baseline corrected, and filtered with a Butterworth band-pass filter (0.5 – 25 Hz) using the software PRISM (Jones et al., 2017). The recordings are then selected for the site response evaluation based on the following two criteria: (1) an average signal-to-noise ratio (SNR) higher than 5 within the frequency range of interest (Ktenidou et al., 2011) and (2) peak accelerations lower than 0.01 g in the sensor at depth such

that SRAs remain within the linear elastic range (e.g., Kaklamanos et al., 2013). A summary of the number of records that meet these criteria is presented in Table 2.2.

2.8.2. EVALUATION AND RESULTS

The baseline V_S profiles for each site, reported by Tao (2018), are randomized using the model proposed by Toro (1995) to generate 50 V_S profiles. For these sites, the previously investigated generic $\sigma_{\ln V_S} = 0.25$ is used alongside with correlation parameters for sites with V_{S30} from 180 to 360 m/s. Previous studies have suggested that $\sigma_{\ln V_S}$ for V_S randomization should decrease with depth and its selection should be guided by geological information (Tao and Rathje, 2019). However, given that enough data are not commonly available, a constant value of $\sigma_{\ln V_S}$ is used in this study. The evaluation does not account for epistemic uncertainty on the baseline V_S profile. Theoretical TFs are computed using the code NRATTLE, written by C. Mueller, modified by R. Herrmann, and included in the strong-motion programs by Boore (2005). NRATTLE uses the Thomson–Haskell solution to compute the 1D SH-wave TF (Haskell, 1953; Thomson, 1950) based on a V_S profile, density, and the inverse of the quality factors (Q_S^{-1}). Values for Q_S are estimated as one-tenth of V_S (Olsen et al., 2003), and damping as half the inverse of the Qs (Joyner and Boore, 1988). For this, the baseline V_S profiles are considered, regardless of V_S randomization, which leads to damping values ranging from 0.5% to 3.2% (Delaney Park), 0.15% to 2.6% (Garner Valley), 0.35% to 3.7% (HYGH10), and 0.15% to 3% (IBRH13). Alternative relations for quality factors as a function of damping have been proposed for California (Campbell, 2009) and KiK-net sites (Cabas et al., 2017). These relations generally lead to higher damping values and thus ultimate lower theoretical TFs and AFs are also possible. Vertical incident waves are assumed in all cases.

Theoretical and empirical TFs and AFs are compared in Figures 2.14 and 2.15, and residuals for AFs presented in Figure 2.16. For each site, 50 theoretical TFs are calculated along with 50 theoretical AFs per ground-motion recording. Unsurprisingly, given the sites' classification as A (Tao and Rathje, 2020), the fundamental frequency mode is well captured by the theoretical TFs, except at HYGH10 where some discrepancy is observed. This discrepancy is attributed to errors in the baseline V_S profile and can be addressed in practice using multiple baseline profiles (e.g., EPRI, 2013).

Results in terms of TFs show that amplitudes of the first mode empirical median TFs are better approximated by the 84th percentile than by the median theoretical TFs. At higher frequencies, the median to the 84th percentile theoretical TFs fluctuate from overprediction to underprediction at different frequency ranges. Basically, the higher modes are smoothed out by V_S randomization as previously pointed out by Tao and Rathje (2019). Results in terms of AFs, generally used in engineering design, present three different behaviors: (1) at Delaney Park and Garner Valley, the median theoretical AF is near or higher than the empirical median AF, and thus higher percentiles overpredict the AF consistently across frequencies; (2) at IBRH13, the median and 70th percentile theoretical AFs are generally lower than the empirical median AF, and the 84th percentile captures well the empirical median AF across frequencies; and (3) at HYGH10, results fluctuate between ranges of under- and overprediction for the median and higher percentile AFs. The overprediction of the seismic response at Delaney Park might be due to the high V_S variability inferred from geological conditions at this site (Tao and Rathje, 2019). It is therefore always recommended to estimate site-specific $\sigma_{\ln V_S}$ based on measured V_S profiles to guide the selection of a more appropriate percentile (60th or 70th AFs) at frequencies other than the fundamental.

The seismic response estimated using empirical data from downhole vertical arrays shows consistency with results and trends obtained from the numerical investigation. To evaluate the overall benefit of using a higher percentile, mean residuals for the median, the 70th, and the 84th percentile 1D AFs are estimated for the numerical investigation considering all the baseline sites for a generic $\sigma_{\ln V_S}$ = 0.25 (Figure 2.11) and for the empirical data (Figure 2.15). This preliminary statistical evaluation indicates consistency between the numerical and empirical trends (Figure 2.17). Using percentiles higher than the median seismic response reduces the underpredictions to residuals near zero at the fundamental frequency observed for HYGH10 and IBRH13 in Figure 2.16, although with site-specific differences as observed in Figures 2.14 and 2.15.

2.9. CONCLUSIONS

One-dimensional site response analyses (1D SRAs) with shear-wave velocity (V_S) randomization are commonly conducted to estimate the median site-specific seismic amplification (or deamplification) under the implicit assumption that this approach leads to a realistic response. The results from the numerical evaluation using 2D SRAs and 1D SRAs with V_S randomization indicate that the latter leads to TFs lower by 30 – 50% and AFs lower by 10 – 40%, around the sites' fundamental frequency. Meanwhile, the observed underpredictions are either lower or overpredictions at higher frequencies. The inability of 1D SRAs with V_S randomization to capture a more realistic 2D response is mainly due to the combined effects of (1) the shifting of the individual 1D responses' fundamental modes that lead to the coincidence of peaks and troughs at common frequencies that cancel each other out when the median seismic response is estimated, and (2) the intrinsic limitations of 1D SRAs to capture the amplification effects other than those caused by impedance changes and resonance (e.g., constructive interference). Results from this

numerical evaluation do not support the use of median AFs from 1D SRAs with V_S randomization for the design of structures.

AFs estimated using 1D SRAs with V_S randomization ($\sigma_{\ln V_S} = 0.25$) and percentiles higher than the median capture well the median 2D AFs that account for the effect of V_S spatial variability, at the fundamental frequency. Results from the numerical evaluation suggest that in most cases, $\sigma_{\ln V_S} = 0.25$ for V_S randomization has a similar or superior performance in preventing underpredictions using model-specific $\sigma_{\ln V_S}$ computed from the 2D random fields for capturing 2D V_S spatial variability effects. The percentile 84th AF is an appropriate estimate at the fundamental frequency, the 70th percentile AF is a better alternative at higher frequencies for sites with slightly to moderately variable V_S ($\sigma_{\ln V_S}$ lower than 0.3), and the 60th percentile AF for highly variable sites ($\sigma_{\ln V_S}$ higher than 0.3). These findings are supported by a numerical evaluation using linear elastic 2D and 1D SRAs on sites with spatially variable V_S across multiple site conditions, and an initial analysis using empirical data from four downhole vertical arrays. The trends are consistent in numerical results across different site conditions, but three behaviors are observed for the performance of higher percentiles from 1D SRAs in the empirical evaluation, ranging from consistent overprediction of AFs to consistent underprediction, or a mixture of both. It is expected that avoiding overpredictions from the 84th percentile AFs would require conducting 2D or 3D SRAs with appropriate V_S models.

Results from this study also show that $\sigma_{\ln V_S}$, used for V_S randomization, has a different impact on 2D and 1D SRAs. In 2D SRAs, a higher $\sigma_{\ln V_S}$ leads to mild variations of the median seismic response (TFs and AFs) amplitudes and a moderate increase in the response variability. In 1D SRAs with V_S randomization, a higher $\sigma_{\ln V_S}$ leads to a significant decrease in the median

seismic response amplitudes and a significant increase in the response variability across frequencies. At the same time, $\sigma_{\ln V_S}$ has a strong impact on TFs than it has on AFs. Due to these effects, conducting V_S randomization with site-specific $\sigma_{\ln V_S}$ does not necessarily lead to a more appropriate median seismic response, particularly for sites with highly variable V_S ($\sigma_{\ln V_S}$ higher than 0.3). Nevertheless, using measured V_S profiles in site-specific SRAs is critical, and knowing the site-specific $\sigma_{\ln V_S}$ can guide the selection of a representative seismic response percentile at frequencies other than the fundamental. The measurement of site-specific V_S profiles is encouraged.

This study focused on the estimation of a median seismic response that captures 2D V_S spatial variability effects. Linear elastic 2D SRAs were conducted on correlated V_S random fields with $\sigma_{\ln V_S}$ values from 0.16 to 0.48, and 1D SRAs on randomized V_S profiles developed using the model proposed by Toro (1995) for V_S randomization only. Empirical data from sites classified as A using the taxonomy proposed by Tao and Rathje (2020) were compared against the results from SRAs conducted using damping ratios estimated based on quality factors and V_S values (Joyner and Boore, 1988; Olsen et al., 2003). Findings from this work are subject to the above considerations and have not been tested against other conditions, such as sites inferred to be exposed to non-1D effects and complex geology. Further investigations are deemed necessary to investigate the effects of additional 2D features affecting the seismic response, the soil's nonlinearity, among others. Similarly, a comprehensive statistical evaluation of the residuals associated with the seismic response estimated as a percentile higher than the median from 1D SRAs with V_S randomization should be conducted.

2.10. ACKNOWLEDGMENTS

The authors thank Prof. Ellen M. Rathje, Prof. Adrian Rodriguez-Marek, Dr. Albert R. Kottke, and Dr. Jennie A. Watson-Lamprey for the valuable discussions and feedback. They also thank Prof. Brady R. Cox and the two anonymous reviewers for their comments and suggestions that greatly improved this article. Any opinions or conclusions expressed herein are those of the authors and do not necessarily reflect the views of any of the above people or the represented organizations.

2.11. REFERENCES

Abrahamson NA, Schneider JF and Stepp JC (1991) Spatial coherency of shear waves from the Lotung, Taiwan large-scale seismic test. *Structural Safety* 10: 145–162.

Afshari K and Stewart JP (2019) Insights from California vertical arrays on the effectiveness of ground response analysis with alternative damping models. *Bulletin of the Seismological Society of America* 109: 1250–1264.

Ancheta TD, Darragh RB, Stewart JP, Seyhan E, Silva WJ, Chiou BSJ, Wooddell KE, Graves RW, Kottke AR, Boore DM, Kishida T and Donahue JL (2013) *PEER NGA-West2 database.* Report PEER 2013/03, May. Berkeley, CA: Pacific Earthquake Engineering Research Center (PEER), University of California, Berkeley.

Anderson LM, Kottke AR and McHood M (2018) Using 2D analyses to augment probabilistic 1D site response analysis. In: *Proceedings of the 5th decennial GEESD conference (geotechnical special publication)*, Austin, TX, 10–13 June, Vol. 291, pp. 210–216. Reston, VA: American Society of Civil Engineers (ASCE).

Baise LG, Thompson EM, Kaklamanos J and Dorfmann L (2011) Complex site response: Does one-dimensional site response work. In: *Proceedings of the 4th international association of seismology and physics of the earth's interior/international Association of earthquake engineering international symposium on the effects of surface geology on seismic motion (ESG4)*, Santa Barbara, CA, 23–26 August.

Bazzurro P and Cornell CA (2004) Ground-motion amplification in nonlinear soil sites with uncertain properties. *Bulletin of the Seismological Society of America* 94(6): 2090–2109.

Bielak J, Xu J and Ghattas O (1999) On earthquake ground motion and structural response in alluvial valleys. *Journal of Geotechnical and Geoenvironmental Engineering* 125: 413–423.

Bonilla LF, Steidl JH, Gariel JC and Archuleta RJ (2002) Borehole response studies at the Garner Valley Downhole Array, Southern California. *Bulletin of the Seismological Society of America* 92(8): 3165–3179.

Boore DM (2005) *SMSIM–Fortran programs for simulating ground motions from earthquakes: Version 2.3–A revision of OFR 96–80-A.* United States Geological Survey (USGS) Open File Report 2000–509 revised.

Boore DM, Joyner WB and Fumal TE (1994) *Estimation of response spectra and peak accelerations from western North American earthquakes; An interim report, Part 2.* United States Geological Survey (USGS) Open File Report 94-127.

Bora SS, Scherbaum F, Kuehn N and Stafford P (2016) On the relationship between Fourier and response spectra: Implications for the adjustment of empirical ground-motion prediction equations (GMPEs). *Bulletin of the Seismological Society of America* 106(3): 1235–1253.

Cabas A, Rodriguez-Marek A and Bonilla LF (2017) Estimation of site-specific Kappa (κ_0)-consistent damping values at KiK-net sites to assess the discrepancy between laboratory-based damping models and observed attenuation (of seismic waves) in the field. *Bulletin of the Seismological Society of America* 107(5): 2258–2271.

Campbell KW (2009) Estimates of shear-wave Q and κ_0 for unconsolidated and semiconsolidated sediments in Eastern North America. *Bulletin of the Seismological Society of America* 99(4): 2365–2392.

Chavez-Garcia FJ and Faccioli E (2000) Complex site effects and building codes: Making the leap. *Journal of Seismology* 4: 23–40.

Combellick RA (1999) *Simplified geologic map and cross sections of Central and East Anchorage, Alaska.* Preliminary interpretive report no. 1999-1, August. Fairbanks, AK: Alaska Division of Geological & Geophysical Surveys.

De la Torre C, McGann C, Bradley B and Pletzer A (2019) 3D seismic site response with soil heterogeneity and wave scattering in OpenSees. In: *Proceedings of the 1st Eurasian conference on OpenSees: OpenSees Days Eurasia*, Hong Kong, China, 20–21 June, pp. 255–262. Hong Kong, China: Department of Building Services Engineering, Faculty of Construction and the Environment, The Hong Kong Polytechnic University.

De Martin F, Matsushima S and Kawase H (2013) Impact of geometric effects on near-surface Green's functions. *Bulletin of the Seismological Society of America* 103(6): 3289–3304.

DeGroot DJ (1996) Analyzing spatial variability of in situ soil properties. In: *Proceedings of the uncertainty in the geologic environment: From theory to practice (Uncertainty'96)*, Madison, WI, 31 July–3 August, vol. 1, pp. 210–238. New York: ASCE.

Electric Power Research Institute (EPRI) (2013) *Seismic evaluation guidance: Screening, prioritization and implementation details (SPID) for the resolution of Fukushima near-term task force recommendation 2.1: Seismic*. Report no. 1025287, 28 February. Palo Alto, CA: EPRI.

Griffiths SC, Cox BR, Rathje EM and Teague DP (2016a) Mapping dispersion misfit and uncertainty in V_S profiles to variability in site response estimates. *Journal of Geotechnical and Geoenvironmental Engineering* 142(11): 04016062.

Griffiths SC, Cox BR, Rathje EM and Teague DP (2016b) Surface-wave dispersion approach for evaluating statistical models that account for shear-wave velocity uncertainty. *Journal of Geotechnical and Geoenvironmental Engineering* 142(11): 04016061.

Haskell NA (1953) The dispersion of surface waves on multilayered media. *Bulletin of the Seismological Society of America* 43: 17–34.

Holzer TL, Bennett MJ, Noce TE and Tinsley JC (2005) Shear-wave velocity of surficial geologic sediments in Northern California: Statistical distributions and depth dependence. *Earthquake Spectra* 21(1): 161–177.

Hudson MB, Idriss IM and Beikae M (1994) QUAD4M: User's manual for a computer program to evaluate the seismic response of soil structures using finite-element procedures and incorporating a compliant base. Report, Center for Geotechnical Modeling, University of California, Davis, Davis, CA, May.

Hudson MB, Idriss IM and Beikae M (2003) QUAD4MU: Addendum to user's manual for QUAD4M for updates to the QUAD4MU version. Report, Center for Geotechnical Modeling, University of California, Davis, Davis, CA, 4 March.

Jones JM, Kalkan E, Stephens CD and Ng P (2017) *PRISM Software–Processing and Review Interface for Strong-Motion Data* (Techniques and methods, Book 12, Chapter A2). US Geological Survey, 4 pp. (December 2020). Available at: https://doi.org/10.3133/tm12A2

Joyner WB and Boore DM (1988) Measurement, characterization, and prediction of strong ground motion. *Earthquake Engineering and Soil Dynamics II*. In: *Proceedings of the American Society of Civil Engineering, Geotechnical Engineering Division Specialty Conference*, June 27–30, Park City, Utah, 43-10.

Kaklamanos J, Bradley BA, Moolacattu AN and Picard BM (2020) Physical hypotheses for adjusting coarse profiles and improving 1D site-response estimation assessed at 10 KiK-net sites. *Bulletin of the Seismological Society of America* 110(3): 1338–1358.

Kaklamanos J, Bradley BA, Thompson EM and Baise LG (2013) Critical parameters affecting bias and variability in site-response analyses using KiK-net downhole array data. *Bulletin of the Seismological Society of America* 103: 1733–1749.

Kaklamanos J, Thompson EM, Baise LG and Dorfmann LA (2011) Identifying and modeling complex site response behavior: Objectives, preliminary results, and future directions. In: *Proceedings of the 2011 NSF Engineering Research and Innovation Conference*, Atlanta, GA, 4–7 January.

Kamai R, Abrahamson NA and Silva WJ (2016) V_{S30} in the NGA GMPEs: Regional differences and suggested practice. *Earthquake Spectra* 32(4): 2083–2108.

Kottke AR (2010) *A comparison of seismic site response methods.* PhD Dissertation, The University of Texas at Austin, Austin, TX.

Ktenidou O-J, Cha´ vez-Garcı´a FJ and Pitilakis KD (2011) Variance reduction and signal-to-noise ratio: Reducing uncertainty in spectral ratios. *Bulletin of the Seismological Society of America* 101(2): 619–634.

Kuhlemeyer RL and Lysmer J (1973) Finite element method accuracy for wave propagation problems. *Journal of the Soil Mechanics and Foundations Division* 99(5): 421–427.

Li W and Assimaki D (2010) Site- and motion-dependent parametric uncertainty of site-response analyses in earthquake simulations. *Bulletin of the Seismological Society of America* 100: 954–968.

Lloret-Cabot M, Fenton GA and Hicks MA (2014) On the estimation of scale of fluctuation in geostatistics. *Georisk: Assessment and Management of Risk for Engineered Systems and Geohazards* 8(2): 129–140.

National Research Institute for Earth Science and Disaster Resilience (NIED) (2019) *NIED Kiban Kyoshin Network (K-NET) and KiK-net.* Tsukuba, Japan: NIED.

Nour A, Slimani A, Laouami N and Afra H (2003) Finite element model for the probabilistic seismic response of heterogeneous soil profile. *Soil Dynamics and Earthquake Engineering* 23(5): 331–348.

Olsen KB, Day SM and Bradley CR (2003) Estimation of Q for long-period (.2 sec) waves in the Los Angeles basin. *Bulletin of the Seismological Society of America* 93: 627–638.

Pehlivan M (2013) *Incorporating site response analysis and associated uncertainties into the seismic hazard assessment of nuclear facilities.* PhD Dissertation, The University of Texas at Austin, Austin, TX.

Phoon K-K and Kulhawy FH (1996) On quantifying inherent soil variability. In: *Proceedings of the uncertainty in the geologic environment: From theory to practice (Uncertainty'96)*, Madison, WI, 31 July–3 August, vol. 1, pp. 326–340. New York: ASCE.

Phoon K-K and Kulhawy FH (1999) Characterization of geotechnical variability. *Canadian Geotechnical Journal* 36: 612–624.

Pretell R, Ziotopoulou K and Abrahamson NA (2022) Numerical investigation of V_S spatial variability effects on the seismic response estimated using 2D and 1D site response analyses. In: *Proceedings of the Geo-Congress 2022*, Charlotte, NC, 20–23 March.

Regnier J (2013) Seismic site-response variability: From site-classification to soil non-linear behaviour. Report, Earth Sciences, Université Paris-Est Créteil, Créteil, 19 November.

Regnier J, Bonilla LF, Bard PY, Bertrand E, Hollender F, Kawase H, Sicilia D, Arduino P, Amorosi A, Asimaki D, Boldini D, Chen L, Chiaradonna A, DeMartin F, Elgamal A, Falcone G, Foerster E, Foti S, Garini E, Gazetas G, Ge´ lis C, Ghofrani A, Giannakou A, Gingery J, Glinsky N, Harmon J, Hashash Y, Iai S, Kramer S, Kontoe S, Kristek J, Lanzo G, di Lernia A, Lopez-Caballero F, Marot M, McAllister G, Mercerat ED, Moczo P, Montoya-Noguera S, Musgrove M, Nieto-Ferro A, Pagliaroli A, Passeri F, Richterova A, Sajana S, d'Avila MPS, Shi J, Silvestri F, Taiebat M, Tropeano G, Vandeputte D and Verrucci L (2018) PRENOLIN: International benchmark on 1D nonlinear site—response analysis—Validation phase exercise. *Bulletin of the Seismological Society of America* 108(2): 876–900.

Rodriguez-Marek A, Bommer JJ, Youngs RR, Crespo MJ, Stafford PJ and Bahrampouri M (2020) Capturing epistemic uncertainty in site response. *Earthquake Spectra* 37(2): 921–936.

Stewart JP, Kwok AO-L, Hashash YMA, Matasovic N, Pyke R, Wang Z and Yang Z (2008) *Benchmarking of nonlinear geotechnical ground response analysis procedures.* Report no. PEER 2008/04, August. Berkeley, CA: Pacific Earthquake Engineering Research Center (PEER), University of California, Berkeley.

Tao Y (2018) *Evaluating the site-specific applicability of one-dimensional seismic ground response analysis.* PhD Dissertation, The University of Texas at Austin, Austin, TX.

Tao Y and Rathje EM (2019) Insights into modeling small-strain site response derived from downhole array data. *Journal of Geotechnical and Geoenvironmental Engineering* 145(7): 04019023.

Tao Y and Rathje EM (2020) Taxonomy for evaluating the site-specific applicability of one-dimensional ground response analysis. *Soil Dynamics and Earthquake Engineering* 128(3): 105865.

Teague DP and Cox BR (2016) Site response implications associated with using non-unique V_S profiles from surface wave inversion in comparison with other commonly used methods of accounting for V_S uncertainty. *Soil Dynamic and Earthquake Engineering* 91(2016): 87–103.

Thompson EM, Baise LG, Tanaka Y and Kayen RE (2012) A taxonomy of site response complexity. *Soil Dynamics and Earthquake Engineering* 41: 32–43.

Thomson WT (1950) Transmission of elastic waves through a stratified solid. *Journal of Applied Physics* 21: 89–93.

Toro GR (1995) *Probabilistic models of site velocity profiles for generic and site-specific ground-motion amplification studies.* Report no. 779574, 17 November. Upton, NY: Brookhaven National Laboratory.

Vanmarcke EH (1983) *Random Fields: Analysis and Synthesis.* Cambridge, MA: The MIT Press.

Wills CJ and Clahan KB (2006) Developing a map of geologically defined site-condition categories for California. *Bulletin of the Seismological Society of America* 96(4A): 1483–1501.

Zalachoris G and Rathje EM (2015) Evaluation of one-dimensional site response techniques using borehole arrays. *Journal of Geotechnical and Geoenvironmental Engineering* 141(12): 04015053.

FIGURES

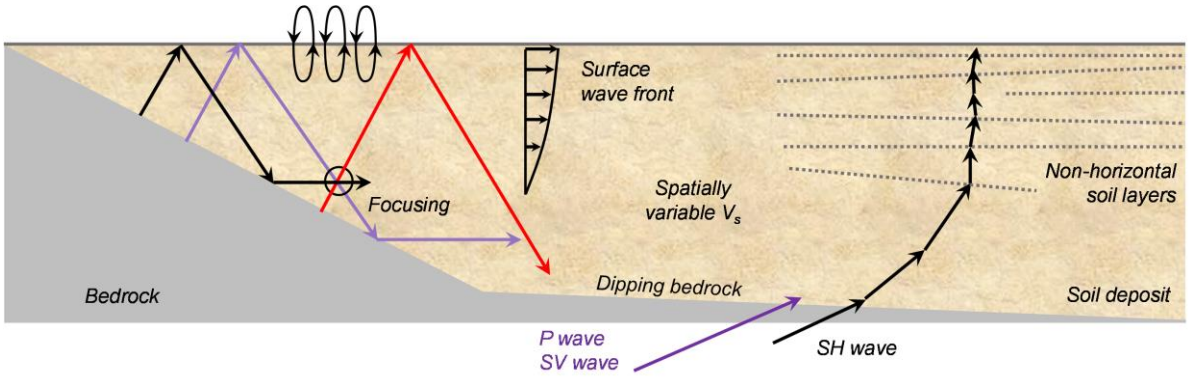

Figure 2.1. Schematic of various wave propagation phenomena in a natural environment.

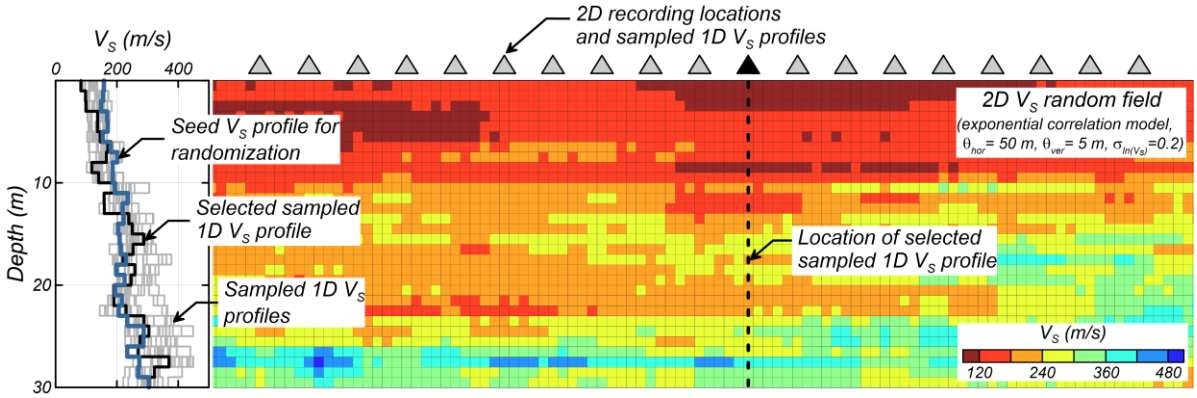

Figure 2.2. Sample window of a 2D correlation V_S random field and sampled 1D V_S profiles.

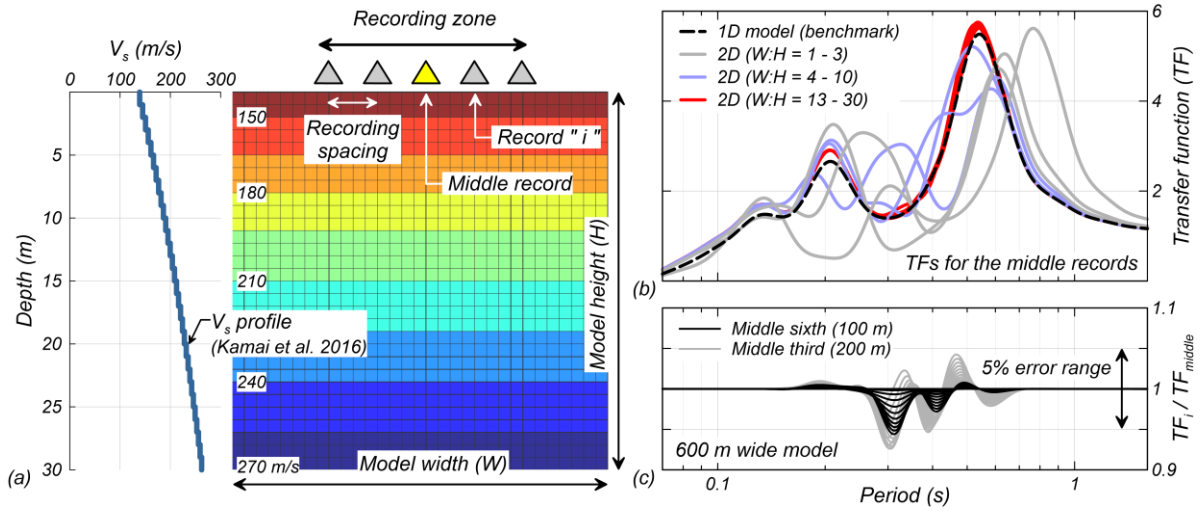

Figure 2.3. Selection of a minimum model width. (a) Model setup for evaluation. (b) Evaluation in terms of TFs against the 1D benchmark. (c) Evaluation of allowable error in the 2D response.

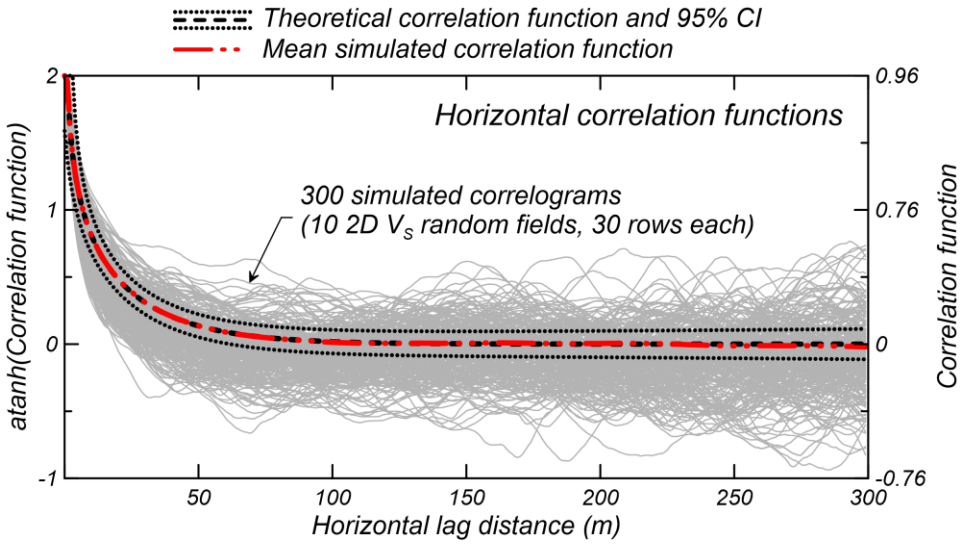

Figure 2.4. Theoretical and simulated horizontal correlation functions of $\ln(V_S)$ for the 2D random fields.

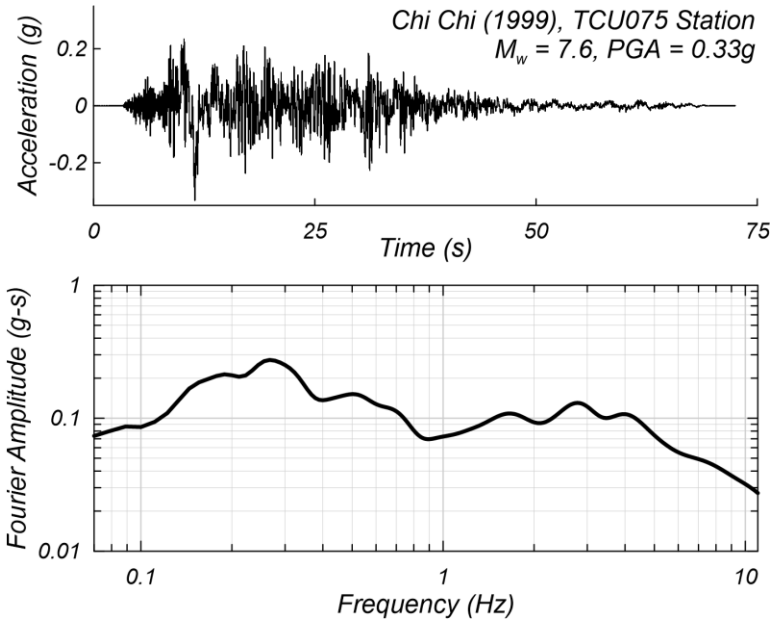

Figure 2.5. Input ground motion considered for the numerical evaluation of 2D versus 1D SRAs.

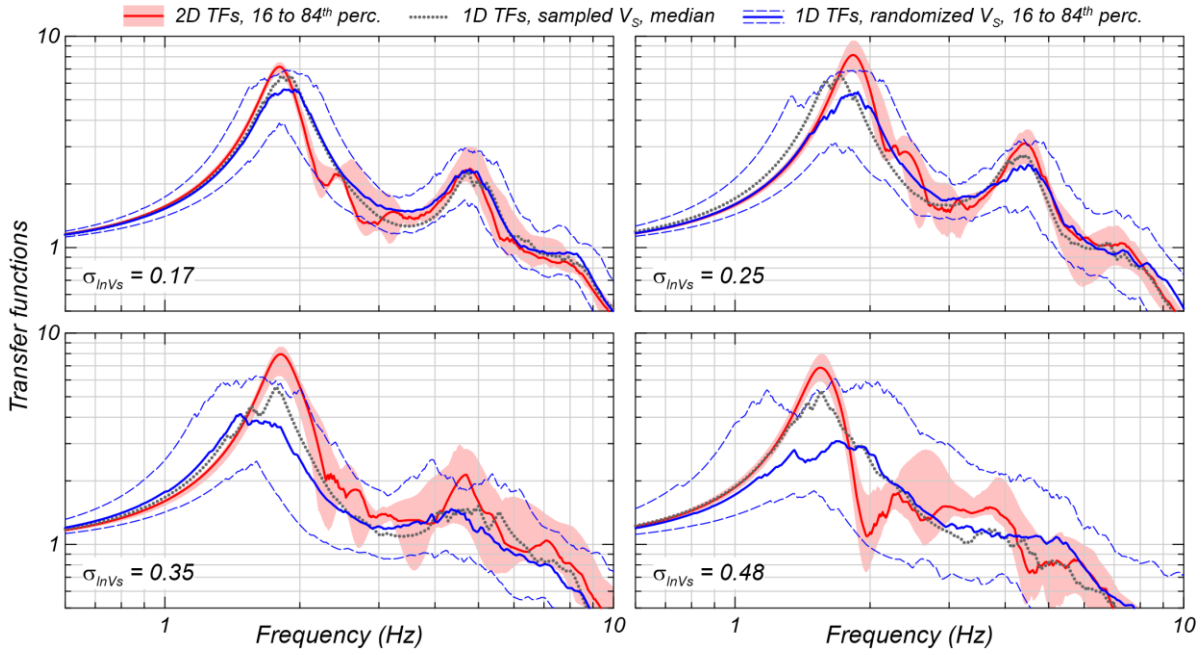

Figure 2.6. Transfer functions from 2D and 1D SRAs. Results from (a) to (d) correspond to four representative 2D V_S random field models, each with a different model-specific $\sigma_{\ln V_S}$, indicated in the bottom left corners, and the corresponding sampled 1D and randomized 1D V_S profiles. One-dimensional SRAs conducted with V_S randomization using the model-specific $\sigma_{\ln V_S}$.

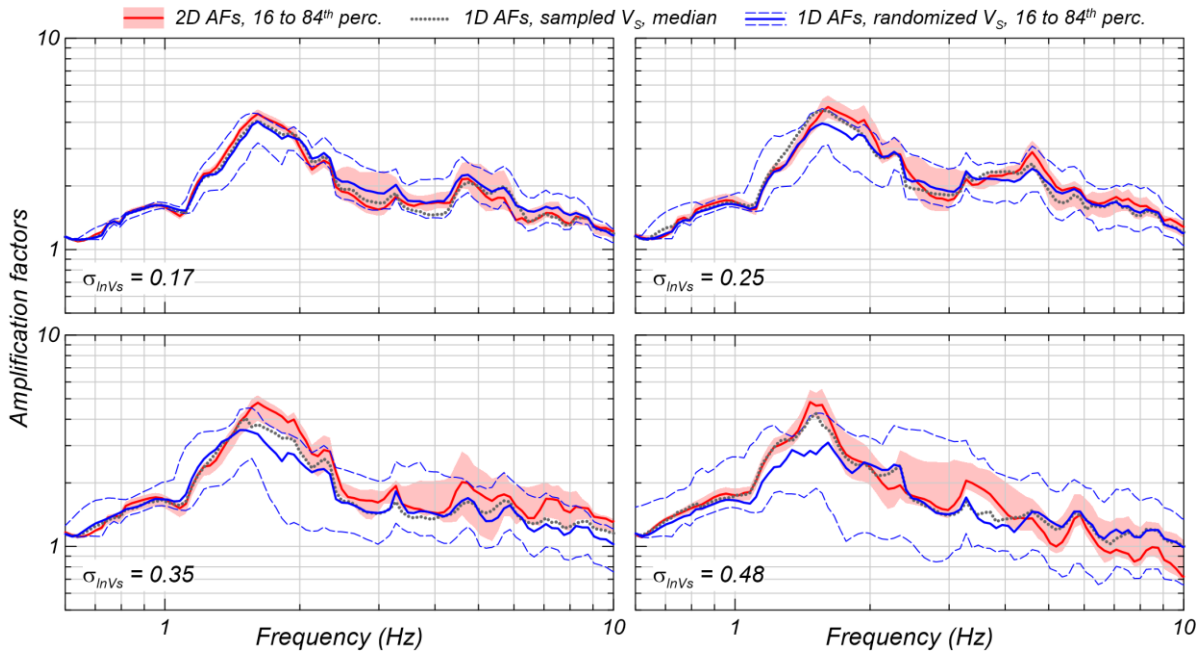

Figure 2.7. Amplification factors from 2D and 1D SRAs. Results from (a) to (d) correspond to four representative 2D V_S random field models, each with a different model-specific $\sigma_{\ln V_S}$, indicated in the bottom left corners, and the corresponding sampled 1D and randomized 1D V_S profiles. One-dimensional SRAs conducted with V_S randomization using the model-specific $\sigma_{\ln V_S}$.

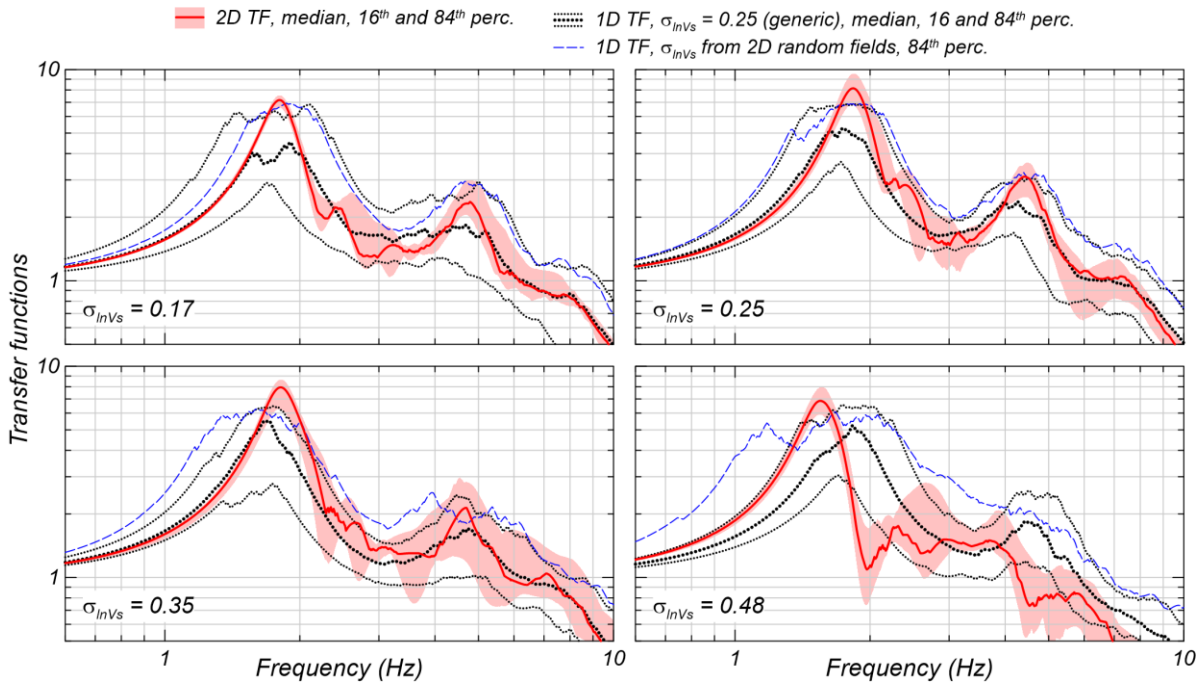

Figure 2.8. Transfer functions from 2D and 1D SRAs. Results from (a) to (d) correspond to four representative 2D V_S random fields, each with different $\sigma_{\ln V_S}$, indicated in the bottom left corners, the corresponding randomized 1D V_S profiles using model-specific $\sigma_{\ln V_S}$, and 1D V_S profiles using a generic $\sigma_{\ln V_S} = 0.25$.

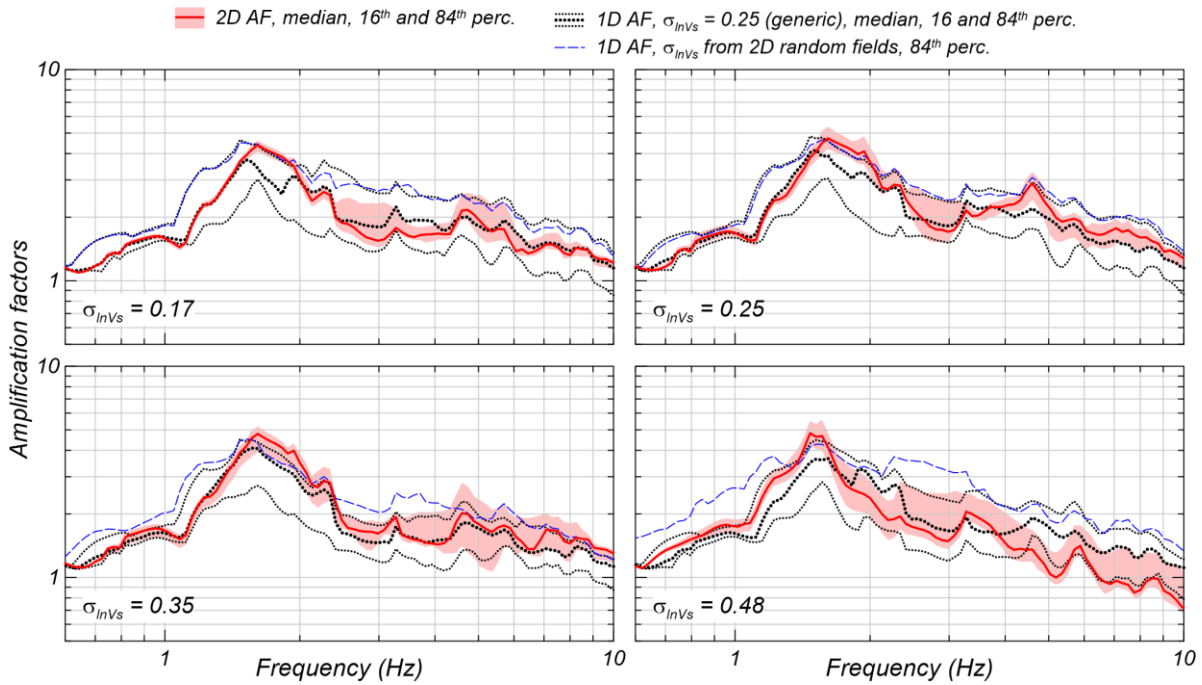

Figure 2.9. Amplification factors from 2D and 1D SRAs. Results from (a) to (d) correspond to four representative 2D V_S random fields, each with different $\sigma_{\ln V_S}$, indicated in the bottom left corners, the corresponding randomized 1D V_S profiles using model-specific $\sigma_{\ln V_S}$, and 1D V_S profiles using a generic $\sigma_{\ln V_S} = 0.25$.

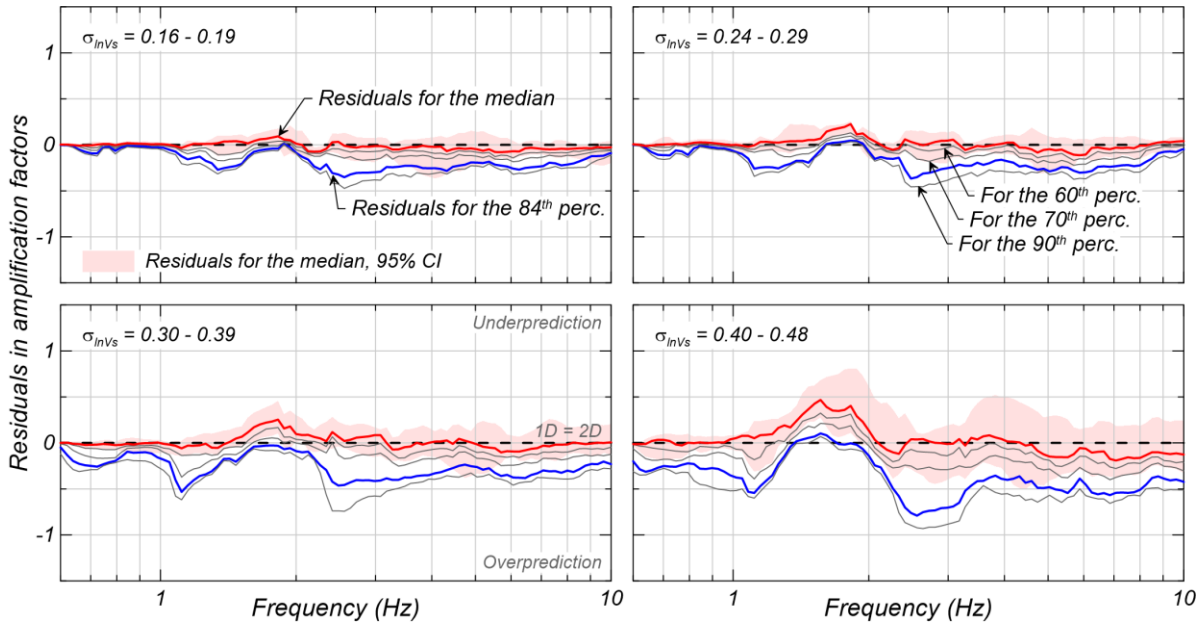

Figure 2.10. Median residuals for various percentiles of 1D SRA-based amplification factors compared to 2D SRA-based median amplification factors. V_S randomization conducted using model-specific $\sigma_{\ln V_S}$, indicated in top left corners.

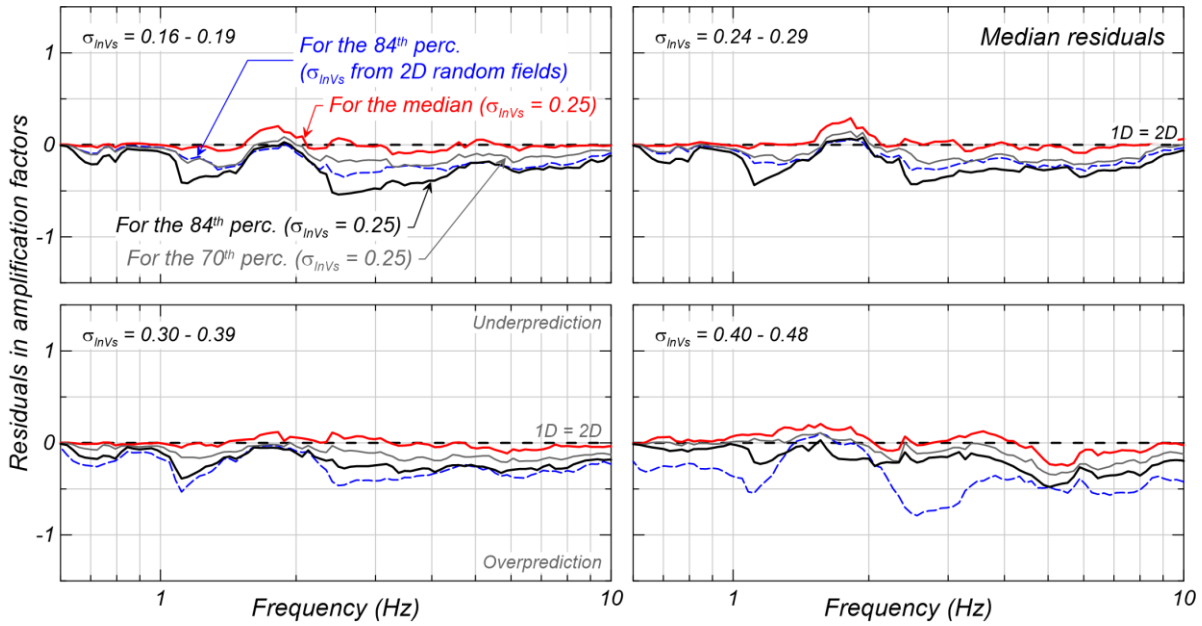

Figure 2.11. Median residuals for the 50th, 70th, and 84th percentiles of 1D SRA-based amplification factors compared to 2D SRA-based median amplification factors. V_S randomization conducted using model-specific $\sigma_{\ln V_S}$, indicated in the top left corners, and a generic $\sigma_{\ln V_S} = 0.25$. Residuals for the 84th percentile 1D SRA-based amplification factors from V_S randomization with model-specific $\sigma_{\ln V_S}$ (Figure 2.10) included for reference.

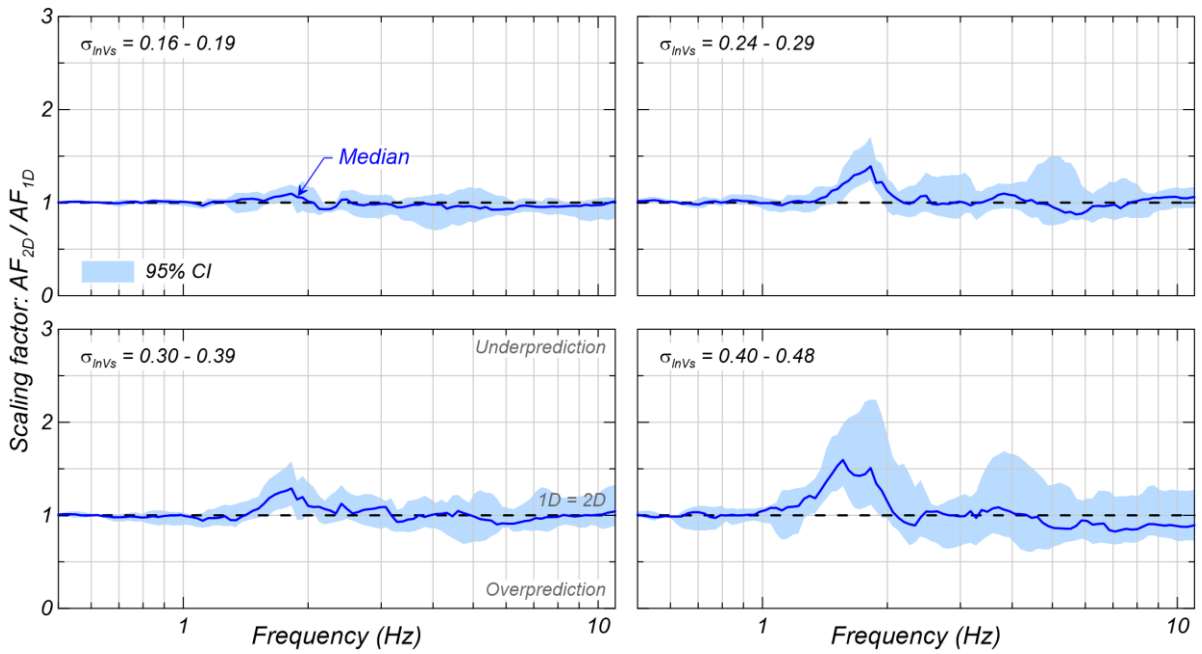

Figure 2.12. Scaling factors to estimate median 2D amplification factors accounting for V_S spatial variability based on 1D SRAs with V_S randomization using model-specific $\sigma_{\ln V_S}$, indicated in top left corners.

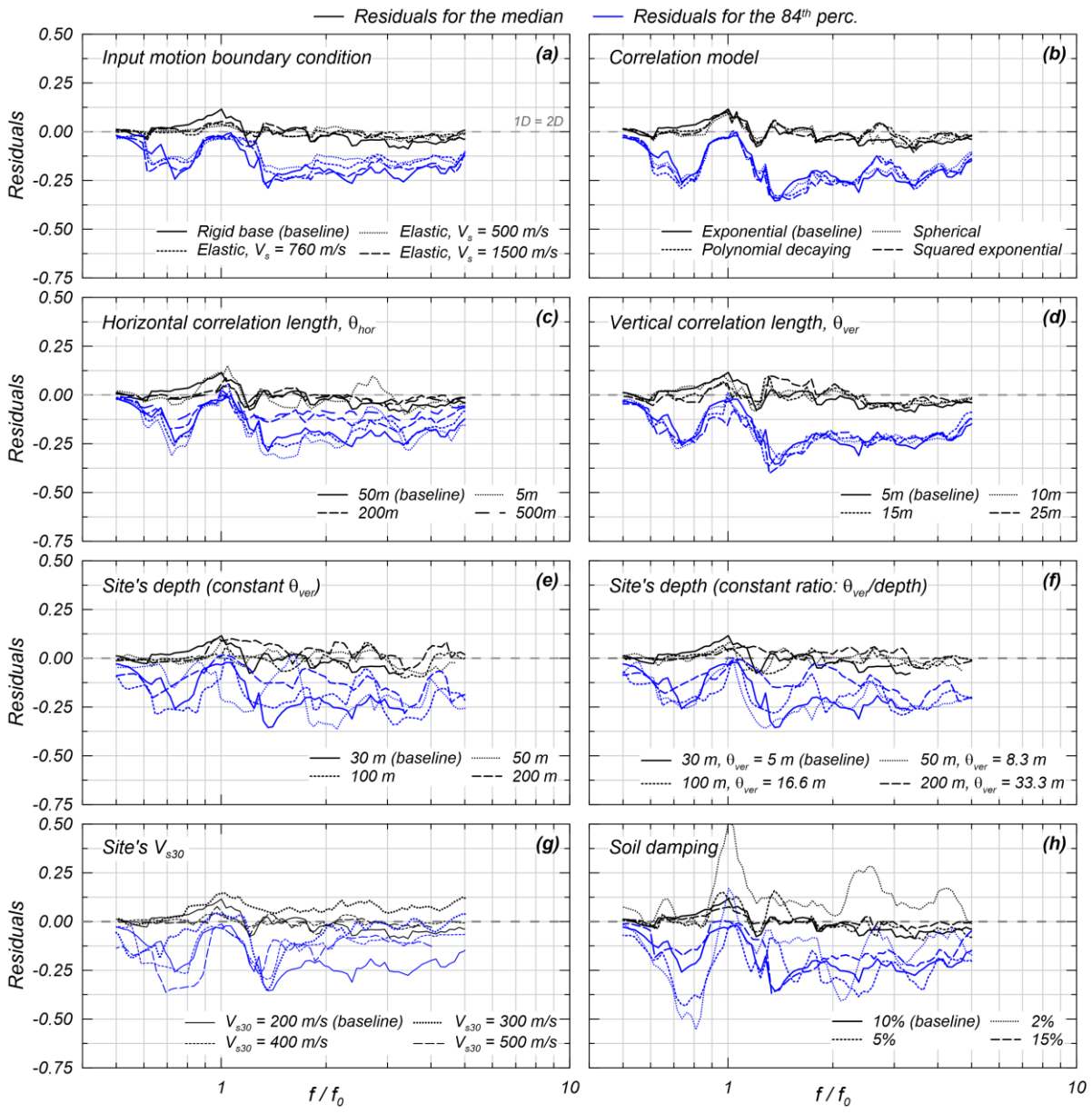

Figure 2.13. Residuals for the median and 84th percentile 1D SRA-based amplification factors relative to the median 2D SRA-based amplification factors for various site parameters related to (a): the underlying bedrock condition, (b) to (d): the V_S heterogeneity, (e) to (g): the site's stiffness and fundamental frequency, and (h): damping. One-dimensional SRAs conducted with V_S randomization using the model-specific $\sigma_{\ln V_S}$.

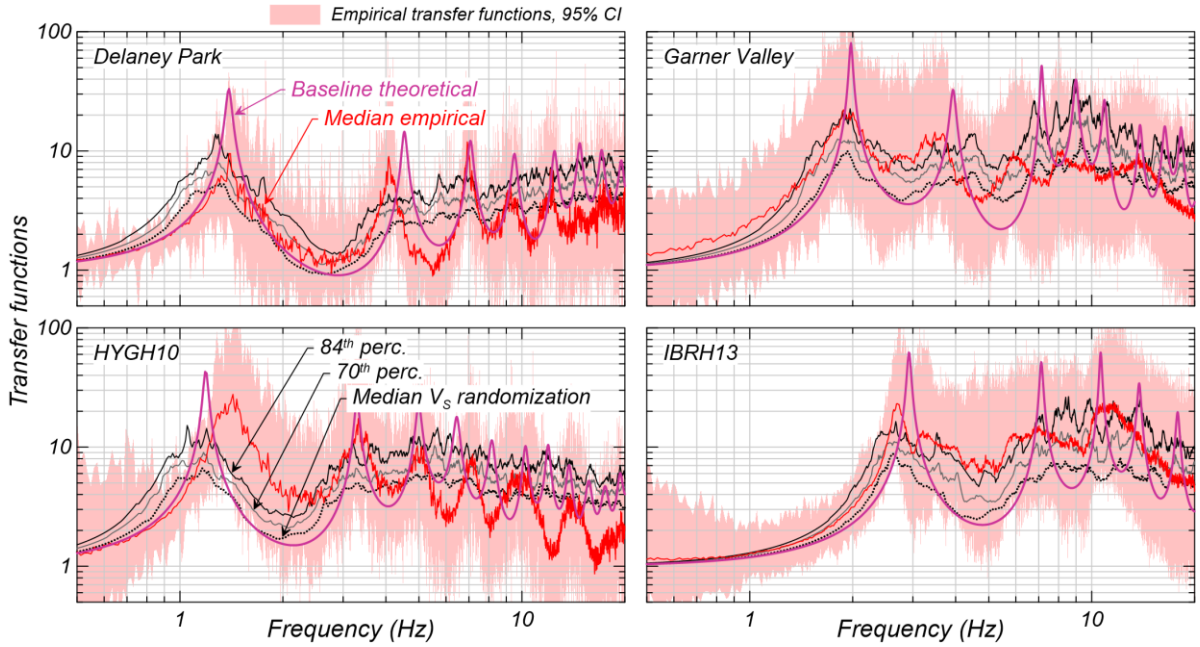

Figure 2.14. Theoretical and empirical transfer functions for four sites classified as A based on the site taxonomy by Tao and Rathje (2020). Theoretical transfer functions based on 1D SRAs with V_S randomization using a generic $\sigma_{\ln V_S} = 0.25$ to capture 2D V_S spatial variability effects.

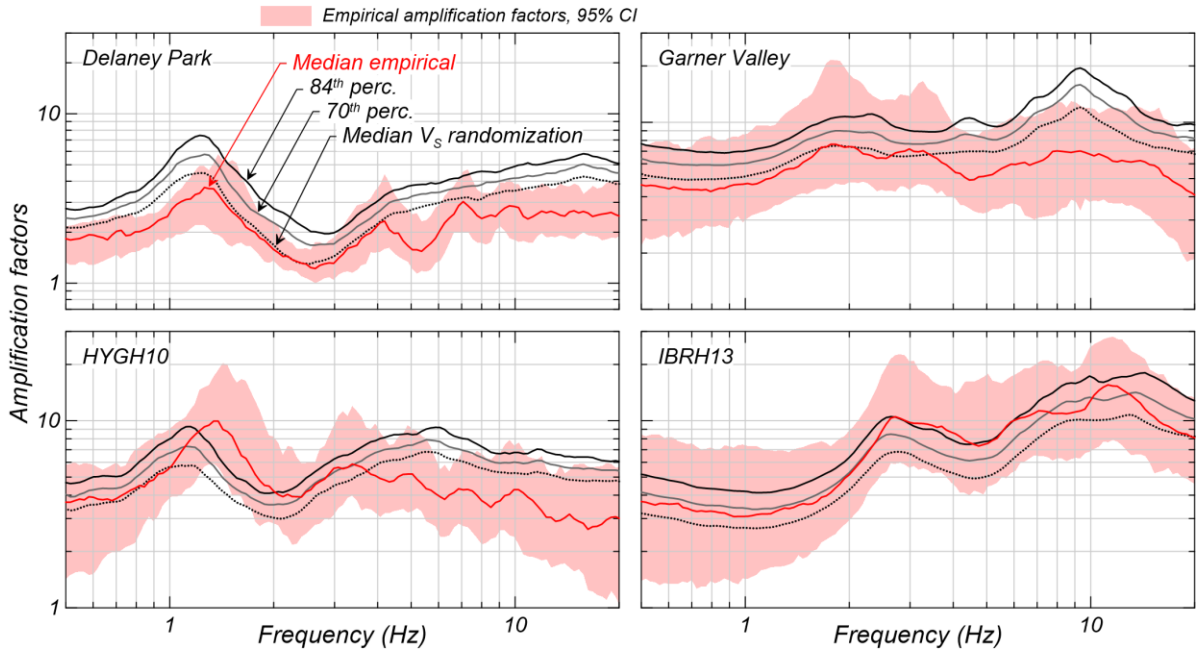

Figure 2.15. Theoretical and empirical amplification factors for four sites classified as A based on the site taxonomy by Tao and Rathje (2020). Theoretical amplification factors based on 1D SRAs with V_S randomization using a generic $\sigma_{\ln V_S} = 0.25$ to capture 2D V_S spatial variability effects.

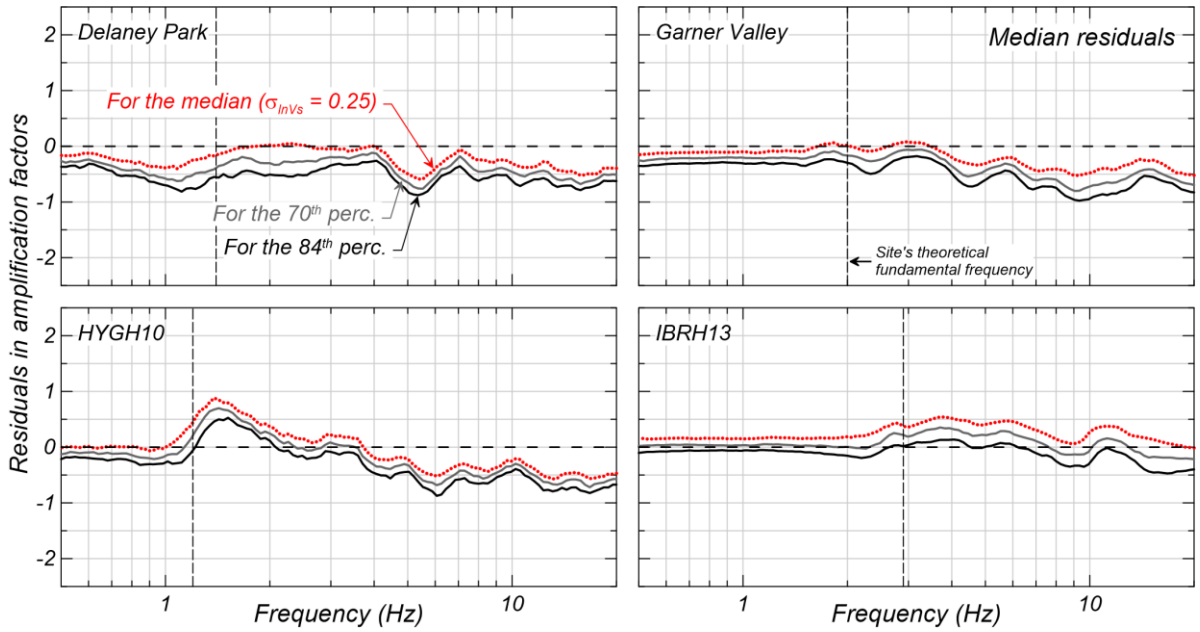

Figure 2.16. Residuals for various 1D SRA-based amplification factor percentiles. 1D SRAs conducted with V_S randomization using a generic $\sigma_{\ln V_S}$ = 0.25. *Note: Site's theoretical fundamental frequency corresponding to the first mode observed in the theoretical transfer function.*

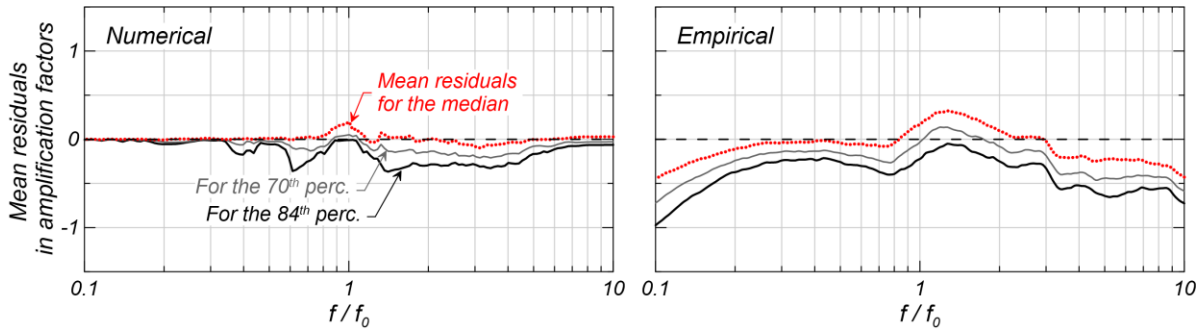

Figure 2.17. Mean of median residuals in amplification factors for the investigated numerical baseline sites (Figure 2.11) and the four downhole sites (Figure 2.16).

TABLES

Table 2.1. Summary of parameters for all the evaluated site conditions.

Parameter	Baseline case	Parametric evaluation
Input ground motion boundary condition	Rigid	Elastic (V_S = 500, 760, 1500 m/s)
Correlation model	Exponential	Spherical, polynomial decaying, squared exponential
Horizontal correlation length, θ_{hor} (m)	50	5, 25, 500
Vertical correlation length, θ_{ver} (m)	5	10, 15, 25
Site's V_{S30} (m/s)	200	300, 400, 500
Site depth (m)	30	50, 100, 200
Soil's damping ratio (%)	10	2, 5, 15

Note: In all cases, input $\sigma_{\ln V_S}$ = 0.20 ln units.

Table 2.2. Key features of the downhole sites selected for the evaluation of empirical consistency.

Downhole site	Depth (m)	V_{S30} (m/s)	Site type		Number of events [3]	Database
			TR20 [1]	Tea12 [2]		
Delaney Park	61	270	A	LG	15	NEES
Garner Valley	150	285	A	LG	89	NEES
HYGH10	100	225	A	LP	23	KiK-net
IBRH13	100	335	A	LG	120	KiK-net

[1] Tao and Rathje (2020): A: 1D sites dominated by true resonances.

[2] Thompson et al. (2012): L: Low variability; G: Good fit.

[3] Both components of each event are used.

CHAPTER 3

A BOREHOLE DATA-BASED APPROACH FOR CONDUCTING 1D SITE RESPONSE ANALYSES I: DAMPING AND V_S RANDOMIZATION

AUTHOR'S NOTE

The contents of this chapter will be submitted for journal publication by Pretell R, Abrahamson NA and Ziotopoulou K. Authorship roles are provided in Chapter 1.

3.1. ABSTRACT

One-dimensional site response analysis (1D SRA) remains the state of practice to estimate site-specific seismic response, despite the ample evidence of discrepancies between observations and 1D SRA-based predictions. These discrepancies are due to errors in the input parameters, intrinsic limitations in the predicting capabilities of 1D SRAs even for sites relatively compliant to the 1D SRA assumptions, and the inability of 1D SRAs to model 3D wave propagation phenomena. This paper aims at reducing 1D SRA mispredictions by using minimum damping profiles calibrated by a damping multiplier (D_{mul}) and randomized shear-wave velocity (V_S) profiles. An approach for conducting 1D SRAs is developed with the goal of reducing the 1D SRAs errors in magnitude and variability. First, sites from a database of 534 downhole sites are classified as 1D- and 3D-like sites depending on the substructure conditions inferred from observed transfer functions. Second, data from the 1D-like sites are compared against predictions from 1D SRAs conducted using various trials of D_{mul} and V_S standard deviations $(\sigma_{\ln V_S})$ for V_S randomization. Third, D_{mul} and

$\sigma_{\ln V_S}$ are evaluated in their combined ability to reduce the root mean square error (RMSE) in SRA predictions. Results indicate that 1D SRAs conducted with $D_{mul} = 3$, and $\sigma_{\ln V_S} = 0.25$ lead to an overall minimum RMSE and thus provide more accurate site response estimations. The use of these parameters in forward SRAs is discussed in Chapter 4.

3.2. INTRODUCTION

One-dimensional site response analysis (1D SRA) remains the state of practice to estimate site-specific seismic response, despite of the ample evidence of discrepancies between observations from borehole sites and 1D SRA predictions. These discrepancies are generally attributed to the lack of knowledge about the shear-wave velocity (V_S) profile, and the breakdown of the 1D wave propagation assumptions, and 3D effects (Kaklamanos et al., 2020; Stewart and Afshari, 2020; Hu et al., 2021). The parameterization of linear elastic 1D SRAs consists of damping and V_S profiles only. This simple parameterization, and the broad implementation of 1D SRAs in practice prevents the addition of new parameters or the adoption of more advanced numerical approaches for estimating site response (e.g., Semblat, 2011). This situation leads to three alternatives for enhancing 1D SRA-based site response predictions: (1) altering the site response input parameters (V_S and damping), (2) post-processing 1D SRA estimations such that a more accurate site response is obtained, e.g., using scaling factors, and (3) a combination of (1) and (2). In this work, a methodology for conducting 1D SRAs with altered input parameters is proposed, specifically damping profiles increased by a damping multiplier (D_{mul}) and randomized V_S profiles. The proposed approach focuses on linear elastic SRAs, henceforth referred to as "1D SRAs," and thus only the minimum or small-strain damping is discussed and referred to as "damping" for brevity.

Current practices use geophysical testing and engineering correlations to define site response input parameters. In principle, both V_S and damping profiles could be measured using geophysical testing (e.g., Foti et al., 2014). However, damping is commonly estimated based in correlations with other geotechnical or seismological parameters (Boaga et al., 2015), and V_S profiles are often measured, although to an extent that is generally insufficient to understand and account for the V_S spatial variability and potential presence of any complex geological structure underneath a given site of interest. The approach for defining damping profiles for forward site response predictions remains a choice based on the analyst's preference and available data. These approaches include correlations with the site-specific attenuation parameter κ_0 (Xu et al., 2020), quality factors, Q (e.g., Olsen et al., 2003; Campbell, 2009; Cabas et al., 2017), and laboratory-based damping formulations (e.g., Darendeli, 2001; Menq, 2003). The latter are often scaled to better represent the field conditions (e.g., Rodriguez-Marek et al., 2017; Tao and Rathje, 2019; Ruigrok et al., 2022). The V_S spatial variability is the only site-specific feature intended to be addressed when conducting 1D SRAs in engineering practice. To this end, randomized V_S profiles generated using the Toro (1995) model are used (e.g., Griffiths et al., 2016a), and the median response is considered as representative. However, studies show that this approach underpredicts the seismic response (Teague and Cox, 2016; Tao and Rathje, 2019; Kaklamanos et al., 2020; Hallal et al., 2022, Pretell et al., 2022a). To prevent these underpredictions, Pretell et al. (2022a) recommend using randomized V_S profiles generated using the model by Toro with V_S standard deviation $\left(\sigma_{\ln V_S}\right)$ = 0.25 and selecting the 84th percentile seismic response as representative at the site's fundamental frequency.

The development of the proposed approach has two main parts. The first part consists of the selection of a D_{mul} and a $\sigma_{\ln V_S}$ for V_S randomization that together lead to the lowest minimum

root square error (RMSE). The second part consists of the quantification of the 1D SRA remaining errors such that they can be considered in forward predictions of site response. This chapter focuses on the first part, and Chapter 4 describes the second part.

3.3. PROPOSED APPROACH FOR CONDUCTING 1D SITE RESPONSE ANALYSES

The state of practice for predicting site response uses 1D SRA as an approach that condenses the complexities of 3D wave propagation to an SH wave traveling vertically through a soil column. Such simplification leads to modeling errors, evident when comparing 1D SRA predictions and observations (e.g., Bonilla et al., 2002; Kaklamanos et al., 2013; Kaklamanos and Bradley, 2018; Stewart and Afshari, 2020; Zhu et al., 2022). For example, Figure 3.1 shows the theoretical and observed transfer functions (TFs), defined as the ratio of the Fourier amplitude spectra at surface and depth, for four borehole sites. Key observations in Figure 3.1 are (1) the overprediction of the theoretical fundamental mode (Figures 3.1a to 3.1d), (2) the underprediction of the high-frequency modes (Figures 3.1b, 3.1c, and 3.1d), (3) the misalignment of the fundamental and higher modes between the median observed and theoretical TFs (Figures 3.1b to 3.1d), and (4) the overall smoother observed TFs compared to the more sharply peaked theoretical TFs (Figures 3.1b to 3.1d). The commonly observed overprediction of the fundamental mode suggests that 1D SRAs have a consistent tendency at the fundamental frequency, and less clearly so at other frequencies (e.g., Kaklamanos et al., 2013). In this section, an approach for conducting 1D SRAs with D_{mul} and V_S randomization is described.

3.3.1. DAMPING MULTIPLIERS AND V_S RANDOMIZATION IN 1D SRAs

Various mechanisms lead to dissipation of energy during wave propagation, such as friction between particles and wave scattering, which are not modeled but can be captured by damping in

1D SRAs. Laboratory-based damping models (e.g., Darendeli, 2001; Menq, 2003) provide estimates of the intrinsic material damping and do not account for energy dissipation mechanisms existing in the field. As such, damping is underestimated and the site response amplitudes overestimated. Various authors propose that laboratory-based damping could be scaled to improve site response predictions (Elgamal et al., 2001; Tsai and Hashash, 2009; Stewart et al., 2014; Zalachoris and Rathje, 2015; Kokusho, 2017; Tao and Rathje, 2019). For instance, Tao and Rathje (2019) find that D_{mul} = 3 to 5 applied to damping profiles after Darendeli (2001) reduces the discrepancies between observations and 1D SRA predictions at four borehole sites, and Ruigrok et al. (2022) suggest that a D_{mul} = 0.65 to 1.6 can be used to scale laboratory damping-based κ_0 to match Q estimates at the Groningen gas field in the Netherlands.

Randomized V_S profiles generated using the Toro (1995) model for 1D SRA applications are commonly used in the nuclear industry (e.g., Abrahamson et al., 2002; Abrahamson et al., 2004; EPRI, 2013; Bommer et al., 2015; Rodriguez-Marek et al., 2021). Toro recommends different values of $\sigma_{\ln V_S}$ for V_S randomization ranging from 0.27 to 0.37, depending on site classes determined based on $V_{S30,}$ estimated as the inverse of the average slowness in a site's top 30 m. Generally, V_S profiles are randomized with the goals of (1) reducing the overpredictions at the site's fundamental mode (e.g., Figure 3.2c), and (2) capturing the V_S spatial variability across the footprint of a project site. However, it is unclear how the amount of randomization mapped through $\sigma_{\ln V_S}$ should vary for sites with different site-specific conditions regardless of V_{S30}. Overall, various studies indicate that the $\sigma_{\ln V_S}$ values recommended by Toro are excessively high and thus V_S randomization leads to unrealistically low site response estimates (e.g., Stewart et al., 2014; Griffiths et al., 2016b; Teague et al., 2018; Tao and Rathje, 2019; Passeri et al., 2020). Pretell et al. (2022a) show that not only $\sigma_{\ln V_S}$ is generally too high, but site response underpredictions also

originate from considering the median site response as representative. Based on a numerical investigation, Pretell et al. (2022a) suggest that the 84th percentile site response from 1D SRAs conducted with randomized V_S profiles ($\sigma_{\ln V_S}$ = 0.25) is an appropriate response that accounts for V_S spatial variability at the site's fundamental frequency.

Increasing damping and randomizing V_S profiles are both tools observed to improve 1D SRA predictions, but they affect the estimated responses differently. For instance, Figure 3.2 shows TFs calculated for various D_{mul} and $\sigma_{\ln V_S}$ values applied to a baseline V_S profile generated after Kamai et al. (2016) for site conditions consistent with California. Both D_{mul} and $\sigma_{\ln V_S}$ reduce the site response amplitudes at the fundamental mode, but the D_{mul} causes a stronger reduction in the high-frequency range (Figure 3.2b), whereas $\sigma_{\ln V_S}$ leads to relatively stable minimum amplitudes (Figure 3.2c).

3.3.2. APPROACH FOR IMPROVING SITE RESPONSE PREDICTIONS

In theory, 1D SRAs should provide the best possible site response predictions for sites that are more compatible with 1D SRA assumptions (1D-like sites), while larger errors are expected for sites that are more strongly affected by non-1D effects (3D-like sites). However, the assumptions of the 1D SRA approach are unrealistic and thus 1D SRAs cannot predict site response accurately even for 1D-like sites, and cases with V_S profiles exempt from measurement errors, as demonstrated in numerical investigations (e.g., De la Torre et al., 2021; Pretell et al., 2022b). Such errors are herein referred to as "intrinsic errors." Two major sources of such errors are (1) the unrealistic wave reverberations and spurious resonances that lead to overpredictions of the amplitudes at the sites' fundamental frequency (Boore, 2013), and (2) the inability to simulate energy dissipation mechanisms, thus leading to an overall overprediction of site response

amplitudes. It is hypothesized that the portion of 1D SRA mispredictions due to intrinsic 1D-SRA errors can be removed by using randomized V_S profiles and an increased amount of damping. The remaining residuals can then be attributed to 3D effects affecting the seismic response, the intrinsic complexity of the wave propagation phenomena, and randomness of ground motion waveforms.

An approach for conducting 1D SRAs using increased damping and randomized V_S profiles is proposed with two objectives: (1) to remove the bias intrinsically carried by 1D SRAs following the previously described hypothesis, and (2) to obtain the minimum variability in site response residuals. To achieve this goal, this work builds off the work by Tao and Rathje (2019) and Pretell et al. (2022a) to find the most appropriate D_{mul} and $\sigma_{\ln V_S}$ by comparing 1D SRA predictions to ground motion data from 1D-like borehole sites, whose residuals are assumed to be dominated by the intrinsic errors in 1D SRAs. Pretell et al. (2022a) hypothesized that V_S randomization can be treated as a multi-purpose tool used to capture site-specific features affecting the seismic response such as (1) V_S spatial variability (e.g., Assimaki et al., 2003; Nour et al., 2004; El Haber et al., 2019; De la Torre et al., 2021; Pretell et al., 2022a); (2) dipping bedrocks and topography (e.g., Katebi et al., 2018), wave inclination (e.g., Semblat et al., 2000; Zhu et al., 2016); and (3) other features that cannot be explicitly modeled in 1D SRAs. This approach is extended to find the right amount of $\sigma_{\ln V_S}$ for V_S randomization that along with D_{mul} removes the intrinsic errors associated to 1D SRAs. This approach does not prevent the potential for including further or lower randomization to capture site-specific features, but further work is needed in this direction. The use of D_{mul} in 1D SRAs follows a similar philosophy, motivated by the inability to explicitly model energy dissipation mechanisms in 1D SRAs.

3.3.3. FRAMEWORK OF ALEATORY VARIABILITY AND EPISTEMIC UNCERTAINTY

One-dimensional SRAs, or more generally numerical simulations and analysis tools, inevitably deal with sources of aleatory variability (AV) and epistemic uncertainty (EU) as described by Abrahamson et al. (1990) and Roblee et al. (1996). AV and EU refer to variability due to apparent randomness of the natural phenomena caused by the features uncaptured in a selected modeling approach, and the lack of knowledge about the optimal input parameters, respectively (Abrahamson et al., 2004; Baecher and Christian, 2003). Abrahamson et al. (1990) further partitioned the AV and EU into parametric and modeling components (Table 3.1). The parametric AV (PAV) results from the spatial and temporal randomness of the input parameters, whereas the parametric EU (PEU) results from the lack of knowledge about the ranges of input parameters and the values sampled for analyses. The modeling AV (MAV) is due to the site-specific features which effects are not captured by the analysis tool, and the modeling EU (MEU) is due to the limited predictive capabilities of the analysis tool.

Generally, there is a trade-off between the complexity of the analysis tool and the MAV. For instance, within the context of ground motion modeling, it is expected that ground motion models (GMMs) that only account for magnitude and distance (i.e., simple parameterization) have a larger MAV than GMMs that also account for site conditions mapped through V_{S30} and the depth to V_S = 1 km/s, Z_1 (i.e., a more complex parameterization). The reduction in MAV for the second GMM comes with an additional PEU associated with the V_{S30} and Z_1 scaling in the model that can be reduced as larger datasets are collected, or if further investigations are conducted to better estimate such parameters. Overall, there is a benefit in trading MAV for PEU as the latter can be reduced whereas the former can only be accounted for.

The framework proposed by Abrahamson et al. (1990) can be adapted to 1D SRA applications. The PAV consists of random factors affecting site response that can be explicitly modeled. The PAV includes the ground motion waveforms, an example of randomness in time, and V_S spatial variability, an example of randomness in space. The PEU consists of the plausible alternative input parameters, selected based on some criteria, such as a given mean and standard deviation of ground motion spectral accelerations, and a best estimate, lower, and upper bound V_S profiles. A part of MAV can be reduced as site-specific terms are quantified (more complex model). Finally, the remaining part of MAV consists in the variability of site response given its natural randomness that is not captured by the selected modeling approach, e.g., ground motion inclination within the context of 1D SRAs.

3.3.4. SITE RESPONSE RESIDUAL COMPONENTS

The errors carried by 1D SRA predictions can be quantified using borehole data, which consist of ground motion recordings at depth and ground surface. Within the context of 1D SRAs, the ground motions recorded at depth should explain the ground motions at surface assuming that the site's 1D V_S profile is accurate. Thus, the recordings at depth can be used as input motions and the resulting responses and recordings at surface be compared to evaluate the accuracy of 1D SRAs. For an intensity measure "IM" estimated using 1D SRAs, and the corresponding observed earthquake component "e" at a site "s," the following relation can be established:

$$IM_{es}^{obs} = IM_{es}^{SRA} + \delta_{es}^{SRA} \quad (3.1)$$

where IM_{es}^{obs} and IM_{es}^{SRA} are respectively the observed and 1D SRA-predicted IM in natural logarithm units, and δ_{es}^{SRA} is the site response residual. IM can represent transfer functions (TFs), amplification factors (AFs), or any other metric of interest. Following the separation of residuals

proposed by Al Atik et al. (2010), adapted to the approach for conducting 1D SRAs herein proposed, the residual in Equation 3.1 can be expressed as:

$$\delta_{es}^{\mathrm{SRA}} = c^{SRA} + \delta 1D_s^{SRA} + \delta 3D_{es}^{SRA} \quad (3.2)$$

where c^{SRA} is the global 1D-SRA bias, estimated as the mean of all the residuals in the available dataset, $\delta 1D_s^{\mathrm{SRA}}$ is the site-specific residual due intrinsic 1D-SRA errors (e.g., the 1D SRA overprediction at the site's fundamental mode), and $\delta 3D_{es}^{\mathrm{SRA}}$ is the residual due to non-1D features affecting the site response and the effect of different ground motion waveforms that are not accounted for by c^{SRA}. The residual $\delta 3D_{es}^{\mathrm{SRA}}$ can be further partitioned as:

$$\delta 3D_{es}^{SRA} = \delta S2S_s^{SRA} + \delta AMP_{es}^{SRA} \quad (3.3)$$

where $\delta S2S_s^{\mathrm{SRA}}$ is the mean bias-corrected residual at a site "s", and $\delta AMP_{es}^{\mathrm{SRA}}$ is the unexplained remaining bias- and site-corrected residual. The components $\delta S2S_s^{\mathrm{SRA}}$ and $\delta AMP_{es}^{\mathrm{SRA}}$ are considered random variables with zero mean and standard deviations $\phi_{S2S}^{\mathrm{SRA}}$ and $\phi_{AMP}^{\mathrm{SRA}}$, respectively. Replacing Equation 3.3 into Equation 3.2:

$$\delta_{es}^{SRA} = c^{SRA} + \delta 1D_s^{SRA} + \delta S2S_s^{SRA} + \delta AMP_{es}^{SRA} \quad (3.4)$$

Equations 3.1, 3.2, and 3.4 correspond to 1D SRAs conducted with a single best estimate V_S profile and an uncalibrated amount of damping (e.g., based on laboratory measurements or correlations with Q). Following the hypothesis herein proposed, $\delta 1D_s^{\mathrm{SRA}}$ can be removed by using the right amount (i.e., calibrated) of damping and V_S randomization through D_{mul} and $\sigma_{\ln V_S}$, respectively. Therefore, using calibrated D_{mul} and $\sigma_{\ln V_S}$, Equation 3.4 reduces to:

$$\delta_{es}^{SRA} = c^{SRA} + \delta S2S_s^{SRA} + \delta AMP_{es}^{SRA} \quad (3.5)$$

Note that δ_{es}^{SRA} in Equations 3.2 to 3.4 is calculated from Equation 3.1 with IM_{es}^{SRA} obtained from a V_S profile and an input ground motion, whereas δ_{es}^{SRA} in Equation 3.5 is calculated from Equation 3.1 with IM_{es}^{SRA} representing the median IM from a suite of randomized V_S profiles and an input ground motion. Thus, c^{SRA} in Equations 3.4 and 3.5 are conceptually different. This paper aims at finding the D_{mul} and $\sigma_{\ln V_S}$ based on comparisons with borehole data. Sites considered in the evaluation are those identified as 1D-like, thus c^{SRA} is expressed as c_{1D}^{SRA}. The more common c_{3D}^{SRA} (i.e., the bias associated with 3D-like sites), and the residual components $\delta S2S_s^{SRA}$ and δAMP_{es}^{SRA} are discussed in Chapter 4. All the terms in Equations 3.1 to 3.5 are frequency dependent.

Various sets of SRAs are conducted for D_{mul} from 1 to 10 in increments of 1, and $\sigma_{\ln V_S}$ from 0.05 to 0.40 in increments of 0.05, leading to a total of 80 D_{mul}-$\sigma_{\ln V_S}$ trials. Ten additional sets of SRAs with D_{mul} from 1 to 10 and no V_S randomization are also conducted. When randomization is used, a suite of 50 randomized V_S profiles is generated per site, and the median of the corresponding 50 theoretical TFs compared against each of the observed TFs. In the case of AFs, each ground motion recording is propagated through the 50 V_S profiles resulting in 50 AFs per recording available. The median of these 50 theoretical AFs per recording is compared against each of the observed AFs.

Several modeling decisions and assumptions are considered for the damping and the V_S profiles. Damping profiles are calculated as a function of vertical effective stress following the formulation by Darendeli (2001) considering the same layering as in the V_S profiles. The Darendeli model is used assuming a plasticity index (PI) = 0, an overconsolidation ratio (OCR) = 1, a load frequency (f_{load}) = 1 Hz, and a coefficient of lateral pressure at rest (K_0) = 0.5. The vertical effective stress is estimated considering the measured groundwater table level, when available, or

inferred water table elevations located based on the deepest location with a compressional-wave velocity (V_P) higher than 1500 m/s (Table 3.2) or site conditions (e.g., closeness to a body of water). The sites' mean effective stresses at the borehole sensor locations range approximately from 4.5 to 53 atm (assuming a $K_0 = 0.5$), with a 90^{th} percentile of 27.6 atm, which is approximately falls within the range of isotropic confining pressures considered by Darendeli in the development of the model from 0.3 to 27 atm. Sites with higher mean effective stresses are AICH09, CHBH17, IBRH17, and SZOH25. Randomized V_S profiles are generated based on measured V_S profiles using the V_S model by Toro (1995) with a constant $\sigma_{\ln V_S}$ with depth, and the coefficients recommended for sites with V_{S30} = 180 to 360 m/s, which are approximately the same as the coefficients for sites with V_{S30} = 360 to 760 m/s. The correlation between damping and V_S is not considered in the estimation of damping or randomized V_S profiles, and the same damping is used for all the randomized V_S profiles.

The theoretical TFs are computed using the computer code NRATTLE, while observed are based on borehole data. NRATTLE is included in the SMSIM programs (Boore, 2005), considering a within-motion boundary condition (e.g., Kwok et al., 2007), and smoothed after Konno and Ohmachi (1998). NRATTLE uses the Thomson–Haskell solution to compute the 1D SH-wave TF (Thomson, 1950; Haskell, 1953) based on profiles of V_S, density, and the inverse of the Q, estimated as half the inverse of damping (Joyner and Boore, 1988). AFs are estimated based on response spectra of accelerations computed using pyRotD (Kottke, 2018). Only the data from borehole sites with measured V_S profiles are used, and it is assumed that such profiles are accurate. Ground motion recordings are screened and those with a shear strain index (Idriss, 2011) lower than 0.005%, expected to yield shear strains lower than 0.01% on average (Kim et al., 2016), considered appropriate for linear elastic SRAs (Kaklamanos et al., 2013) and kept for this

investigation. The ground motions are also screened to meet an acceptable signal-to-noise ratio SNR within frequencies higher than half the site's fundamental frequency (f_0) to 12 to 20 Hz, depending on the ground motion database. The number of ground motions per usable (i.e., appropriate) SNR is presented across f/f_0 in Figure 3.3, and summarized in Table 3.2. Note that the f_0 corresponds to the first mode of the theoretical TFs computed assuming a within-motion boundary condition.

3.4. IDENTIFICATION OF 1D-LIKE SITES

Several approaches for identifying sites compatible with the 1D SRA assumptions are available in the literature (Thompson et al., 2012; Laurendeau et al., 2018; Afshari and Stewart, 2019; Pilz and Cotton, 2019; Tao and Rathje, 2020; Pilz et al., 2022) as summarized by Hallal et al. (2022). For instance, Thompson et al. (2012) assessed a given site's compliance to 1D SRA assumptions by means of the inter-event variability (σ), and the Pearson's correlation coefficient (r) between observed and theoretical TFs. The authors suggested that sites with $\sigma < 0.35$ and $r > 0.6$ are less exposed to 3D effects, and thus better modeled using 1D SRAs.

In this work, sites with theoretical TFs estimated using $D_{mul} = 1$ and no randomization whose peaks align well with those in observed TFs are considered 1D-like. To evaluate this, an approach similar to the proposed by Thompson et al. (2012) is followed, with the difference that only the Pearson's correlation coefficient is used. The goal of the evaluation is to find 1D-like sites that can be used for the calibration of D_{mul} and $\sigma_{\ln V_S}$ and thus remove the $\delta 1D_S^{SRA}$. Therefore, the inter-event variability, indicative of the azimuthal variations in the velocity structure (Ramos-Sepúlveda and Cabas, 2021; Pilz et al., 2022), is not used in the evaluation. The correlation coefficient is computed at five frequency ranges indicated in Appendix B, e.g., from the first to

either the third theoretical TF peaks or the maximum usable frequency determined based on the SNR. Considering various relatively narrow frequency intervals prevents that a single highly or negligibly correlated mode dominates the correlation coefficient across a wide frequency range, and thus allows for the identification of 1D-like sites with a proper alignment of TF peaks across frequencies. A database of 534 borehole sites from the US and Japan is used to identify the 1D-like sites. The 100 sites with the highest Pearson's correlation coefficients in at least three frequency intervals are selected as candidates and visually inspected. A total of 39 sites are identified as 1D-like, which represents about 7% of the database. Examples of 1D- and 3D-like sites' TFs are presented in Figure 3.4. A summary of the main characteristics of the 1D-like sites is presented in Table 3.2, the corresponding correlation coefficients in Appendix B, and TFs and AFs estimated using $D_{mul} = 1$ and no randomization for all the 1D-like sites are presented in Appendices C and D.

3.5. SELECTION OF D_{mul} and $\sigma_{\ln V_S}$

Various D_{mul} and $\sigma_{\ln V_S}$ are evaluated in their individual and combined ability to improve 1D-SRA predictions for 1D-like sites in terms of TFs and AFs (e.g., Figures 3.5 to 3.7). The most appropriate D_{mul} and $\sigma_{\ln V_S}$ are the pair yielding to the lowest ($\delta S2S_s^{SRA} + \delta AMP_{es}^{SRA}$) thus removing $\delta 1D_s^{SRA}$. Such a D_{mul}-$\sigma_{\ln V_S}$ combination can be found by minimizing the root mean square error (RMSE), defined as:

$$RMSE = \frac{1}{N_{site}} \sum_{s=1}^{N_{site}} \left(\frac{1}{2 \times N_{event}} \sum_{gm=1}^{2 \times N_{event}} \sqrt{\frac{1}{N_{freq}} \sum_{i=1}^{N_{freq}} \Delta_{es}^{SRA^2}} \right) \quad (3.6)$$

where the variables N_{freq}, N_{event}, and N_{site} are the number of frequencies, the number of earthquake events (Table 3.2), and the number of sites available in the database (N_{site} = 39), respectively. The number of earthquake events is factored by 2 as both horizontal components of the ground motion records are used. The frequency is normalized by each site's fundamental frequency (f_0) from the theoretical TFs, such that all the fundamental modes align at a common value of $f/f_0 = 1$. Only the normalized frequencies from 0.5 (i.e., half f_0) to 20 times f_0, or the maximum usable f in the borehole or surface recording, is used. This range is thus re-sampled with 200 points (i.e., N_{freq} = 200) with natural logarithmic spacing for a fair comparison across frequencies and sites.

In addition to the RMSE of Equation 3.6, the errors in site response predictions are also quantified as the square root of the summation of absolute values. To this end, the exponent in the innermost term in Equation 3.6 is removed. To make this distinction, this error is referred to as "L1 error", whereas the RMSE as presented in Equation 3.6 is referred to as "L2 error." The L1 and L2 errors are computed from residuals δ_{es}^{SRA} as opposed to bias-corrected residuals $\left(\delta_{es}^{SRA} - c_{1D}^{SRA}\right)$ to prevent the selection of a D_{mul}-$\sigma_{\ln V_S}$ associated to a large c_{1D}^{SRA}. If bias-corrected residuals are used, then higher values of D_{mul} are found to minimize the variability in residuals, but they also lead to significantly higher c_{1D}^{SRA} across frequencies (Figure 3.11). The results in Figures 3.8, 3.9, 3.12, and 3.13 are presented in terms of standardized L1 errors, i.e., L1 errors shifted and scaled to vary from 0 to 1, for clarity.

3.6. RESULTS

3.6.1. INDEPENDENT EFFECTS OF D_{mul} and $\sigma_{\ln V_S}$ ON THE SEISMIC RESPONSE

The standardized L1 errors in TFs and AFs are presented in Figures 3.8 and 3.9 for various D_{mul} and $\sigma_{\ln V_S}$ applied separately across f/f_0. The sharp contrasts observed starting at $f/f_0 = 5$ are partly due to the lower number of records available at high frequencies (Figure 3.3). These results indicate that increased damping and randomized V_S profiles can both improve 1D SRA predictions for 1D-like sites, but this improvement is not equally favorable across frequencies and neither for TFs nor AFs simultaneously. For example, the predictions at the fundamental mode, $f/f_0 = 1$, can be improved with $D_{mul} > 6$ for TFs and $D_{mul} \approx 5$ for AFs, but lower D_{mul} are more appropriate at higher frequencies in both cases. Similarly, Figure 3.9 suggests that using $\sigma_{\ln V_S} \approx 0.2$ and $\sigma_{\ln V_S} \approx 0.35$ can improve the predictions in TFs and AFs at $f/f_0 = 1$, respectively, but lower $\sigma_{\ln V_S}$ are more appropriate at other f/f_0. Based on these results, 1D SRAs with frequency-dependent damping are expected to be better suited to accurately estimate site response, as suggested in previous studies within the context of nonlinear 1D SRAs (Assimaki and Kausel, 2002; Kausel and Assimaki, 2002; Yoshida et al., 2002; Huang et al., 2020; Meite et al., 2020; Kuo et al., 2021). Finally, the L1 error patterns for TFs are narrower, whereas they are broader for AFs. This is due to the wider range of frequencies that affects the response of a single degree of freedom oscillator at a given frequency in AFs (Bora et al., 2016), whereas TFs vary more independently, although with some inter-frequency correlation (Bayless and Abrahamson, 2019).

The L2 errors in TFs and AFs resulting from the independent use of D_{mul} and $\sigma_{\ln V_S}$ are presented in Figure 3.10 (darker lines labeled as "All data"), and a summary for key D_{mul}-$\sigma_{\ln V_S}$ combinations in Appendix C. There is a stronger effect of D_{mul} on TFs and AFs compared to $\sigma_{\ln V_S}$.

Overall, an initial reduction of the L2 with higher D_{mul} and $\sigma_{\ln V_S}$ values is observed, followed by an increase in L2 error starting at $D_{mul} \approx 3$, and $\sigma_{\ln V_S} \approx 0.25$. The minor contribution of $\sigma_{\ln V_S}$ on the reduction of residual variability in AFs presented as L2 errors is likely due to the averaging effect of using data from multiple sites, ground motion recordings, and frequencies. The influence of $\sigma_{\ln V_S}$, even though less pronounced compared to TFs, is not negligible (e.g., Figures 3.6c and 3.6d). Based on Figure 3.10, 1D SRA predictions could be improved by $D_{mul} \approx 3$ and no V_S randomization, or V_S randomization with $\sigma_{\ln V_S} = 0.25$ and $D_{mul} = 1$. A $D_{mul} = 3$ is consistent with results by Tao and Rathje (2019), who estimated D_{mul} based on the variation of measured values of κ at borehole sites. A $\sigma_{\ln V_S} = 0.2$ to 0.3 is consistent with findings by Pretell et al. (2022a), who compared results from 2D SRAs and 1D SRAs with V_S randomization to identify the most appropriate $\sigma_{\ln V_S}$ to capture the effects of V_S spatial variability of soils on the seismic response.

The independent effects of various D_{mul} and $\sigma_{\ln V_S}$ on the bias in TFs and AFs are presented in Figure 3.11. As previously observed, increases in D_{mul} lead to a reduction of the TF amplitudes that affects more strongly the high-frequency range, thus leading to a higher bias at high f/f_0 (Figures 3.11a and 3.11c). Importantly, the bias in TF at high f/f_0 values for $D_{mul} = 1$ is low, whereas a low bias in TF at $f/f_0 = 1$ is achieved only with $D_{mul} \approx 8$ (Figure 3.11a). The variability of bias with $\sigma_{\ln V_S}$ mostly affects the low-frequency range, around $f/f_0 = 1$ (Figures 3.11b and 3.11d). Again, the variation of AF amplitudes is smoother compared to TFs.

3.6.2. COMBINED EFFECT OF D_{mul} and $\sigma_{\ln V_S}$ ON THE SEISMIC RESPONSE

The previous section shows the independent impact of D_{mul} and $\sigma_{\ln V_S}$ on site response predictions in terms of TFs and AFs. Here, the combined effect of D_{mul} and $\sigma_{\ln V_S}$ is investigated by conducting

SRAs with various D_{mul}-$\sigma_{\ln V_S}$ combinations and comparing the results against observations. The L2 errors in TFs and AFs are presented in Figures 3.12a and 3.12b respectively, and their combined effect computed as the standardized averaged L2 error is presented in Figure 3.13. The 1D SRA bias associated with the most appropriate D_{mul}-$\sigma_{\ln V_S}$ trial is compared against the bias resulting from scenarios with either D_{mul} or $\sigma_{\ln V_S}$ alone in Figure 3.11.

Results from the analyses indicate that a different combination of D_{mul} and $\sigma_{\ln V_S}$ is required to improve predictions for TFs and AFs. A $\sigma_{\ln V_S}$ = 0.25 leads to the minimum L2 error in TFs and no D_{mul} is needed (Figure 3.12a). Meanwhile, a $\sigma_{\ln V_S} \approx$ 0.2 to 0.3 and a $D_{mul} \approx$ 3 to 4 lead to the lowest L2 error in AFs (Figure 3.12b). Overall, considering that TFs and AFs are equally important, the combination D_{mul} = 3 and $\sigma_{\ln V_S}$ = 0.25 leads to most appropriate site response predictions (Figure 3.13). Thus, 1D SRAs conducted with a D_{mul} = 3 and randomized V_S profiles generated using the model by Toro with $\sigma_{\ln V_S}$ = 0.25 lead to (1) removing the intrinsic 1D SRA error $1D_S^{SRA}$, and (2) the lowest variability in site response residuals. The $\delta 1D_S^{SRA}$ removed is the difference between the c_{1D}^{SRA} corresponding to D_{mul} = 3 with $\sigma_{\ln V_S}$ = 0.25, and D_{mul} = 1 with no randomization in Figure 3.11. A similar D_{mul}-$\sigma_{\ln V_S}$ pair is obtained if the L1 error is considered as the decision metric instead of the L2 error (Appendix D). For sites in the US, damping profiles based on Darendeli (2001) with D_{mul} = 3 are similar or slightly higher in the top 10 m to those obtained based on correlations with Q, Model 1 by Campbell (2009), but dominantly lower at deeper locations.

As previously mentioned, the selection of the D_{mul}-$\sigma_{\ln V_S}$ pair focuses on minimizing the variability in residuals, not the systematic bias c_{1D}^{SRA}. Figure 3.11 shows that as D_{mul} = 3 and $\sigma_{\ln V_S}$ = 0.25 leads to an overall reduction in c_{1D}^{SRA}, but an increase at high frequencies for TFs. This

increase results from a compromise between selecting a single D_{mul}-$\sigma_{\ln V_S}$ pair that works for TFs and AFs across a wide range of frequencies and using a different pair for TFs and AFs. This increase in bias should be addressed by bias-correcting site response predictions, as explained in Chapter 4.

3.7. SENSITIVITY OF THE RESULTS

The previous results are based on the comparisons of 1D SRA predictions against data from 39 1D-like sites from Japan and the US, and damping profiles developed after Darendeli (2001) assuming PI = 0, OCR = 1, f_{load} = 1 Hz, and K_0 = 0.5. In this section, the regional differences between data from sites in California, and Japan, and the effect of damping variables on the resulting D_{mul}-$\sigma_{\ln V_S}$ recommendation is investigated.

3.7.1. REGIONAL DIFFERENCES

The selection of the most appropriate D_{mul} and $\sigma_{\ln V_S}$ leading to improved site response predictions of TFs and AFs is based on comparisons against data from six sites in California, one site in Alaska, and 32 sites in Japan. In this section, regional differences in the most appropriate D_{mul} and $\sigma_{\ln V_S}$ combination, and the resulting c_{1D}^{SRA} are investigated for California and Japan.

The most appropriate D_{mul} and $\sigma_{\ln V_S}$ to reduce the L2 error in TFs are the same for California and Japan (D_{mul} = 1 and $\sigma_{\ln V_S}$ = 0.25). However, differences are found in the case of AFs. Figure 3.14 shows the standardized L2 errors for TFs, AFs, and the average between the two. Figures 3.14c and 3.14d indicate that higher D_{mul} and $\sigma_{\ln V_S}$ are required to improve predictions in AFs in Japan. In particular, there is a clear need for a higher D_{mul} (also Figure 3.10) that is attributed to the overall more uniform amplification of seismic waves across frequencies observed

in the Japanese data as flatter TFs or median TFs with lower peak-to-trough ratios (e.g., Treasure Island versus GIFH28 in Figure E1, Appendix E), indicative of a higher V_S spatial variability (e.g., De la Torre et al., 2021) and overall less compliance to 1D SRA assumptions. Such flatter response in TFs exacerbates the overamplification of AFs given the influence of the low-frequency waves across various oscillators' frequencies (Bora et al., 2016). For instance, TFs and AFs for the site SBSH06 in Figures E3 (Appendix E) and F3 (Appendix F) respectively show how over- and underpredictions observed in TFs turn into consistent overpredictions in AFs caused by the dominance of the overpredicted TF fundamental mode.

The ultimate overall appropriate D_{mul}-$\sigma_{\ln V_S}$ combination for TFs and AFs are D_{mul} = 1 and $\sigma_{\ln V_S}$ = 0.25 for California, and D_{mul} = 3 and $\sigma_{\ln V_S}$ = 0.25 for Japan (Figure 3.14). The latter is also the global recommendation based on all 39 1D-like sites (Figure 3.13). The c_{1D}^{SRA} for California are shown in Figure 3.15, whereas the corresponding ones for Japan are very similar to the global estimates in Figure 3.11 and thus not presented. Figure 3.15 shows that SRAs for California generally underpredict the seismic response, consistent with previous studies (e.g., Stewart and Afshari, 2020). The observed differences indicate potential for improvement site response predictions for regions that share similar features affecting site response (e.g., topography, subsurface conditions, soil deposition). However, the data available for California (Table 3.2) do not currently allow for region-specific estimates of D_{mul}, $\sigma_{\ln V_S}$, and the terms in Equation 3.5.

3.7.2. EFFECT OF SMALL-STRAIN DAMPING PARAMETERS

From the previously discussed evaluation, SRAs conducted with D_{mul} = 3 and randomized V_S profiles generated using $\sigma_{\ln V_S}$ = 0.25 lead improve site response predictions. In this study, D_{mul} is applied to damping profiles developed after Darendeli (2001) assuming PI = 0, OCR = 1, f_{load} = 1

Hz, and $K_0 = 0.5$, hereafter referred to as "default parameters" yielding the baseline damping ($D^{baseline}$). These parameters must be used when following the proposed approach, nevertheless, it is worth evaluating the effect of using different values to calculate the damping profiles. Henceforth, if parameters other than the default ones are used the resulting damping is called D^{new}. The effect of any given parameter on the ultimate D_{mul} is quantified through the damping Scaling Factor (D_{SF}):

$$D_{SF} = \frac{D^{new}}{D^{baseline}} \tag{3.7}$$

Different scenarios are considered to evaluate the effect of the Darendeli model parameters on the resulting D_{SF}. The effect of these parameters on the damping values are studied at a single arbitrary depth, but results valid at any depth of a profile. The results are presented in Figure 3.16 as D_{SF} and the corresponding $3 \times D_{SF}$, i.e., the impact on the damping resulting after applying $D_{mul} = 3$. These scenarios include results for various PI (Figure 3.16a), f_{load} (Figure 3.16b), and K_0 (Figure 3.16c). For the evaluation of K_0, various geotechnically consistent scenarios for OCR and PI are considered based on data reported by Brooker and Ireland (1965) and Mayne and Kulhawy (1982).

Unsurprisingly, results from the parametric evaluation indicate that PI and f_{load} have an important effect on the D_{mul}, whereas K_0 leads to milder variations in D_{mul}. These findings are consistent with previous studies on clayey soils (e.g., Vucetic and Dobry, 1993). Variations of these parameters lead to D_{SF} values from 0.3 to 1.8, and thus $3 \times D_{SF}$ from 0.9 to 5.4. This means that applying a $D_{mul} = 3$ on damping profiles developed using parameters that differ from there assumptions herein made can excessively increase damping profiles (Figure 3.16), and consequently lead to higher L2 errors (Figure 3.13 for $D_{mul} = 3$ to 5). The ultimate impact on TFs and AFs might be milder as not all layers in a given damping profile are likely to differ from the

default parameters. Nevertheless, it is recommended that the default parameters (PI = 0, OCR = 1, f_{load} = 1 Hz, and K_0 = 0.5) be used in all cases when estimating the seismic site response following the proposed approach. Engineering problems involving soils that significantly deviate from the assumed values are expected to require analyses more advanced than 1D SRAs.

3.8. CONCLUSIONS

An approach is developed for improving site response predictions using 1D SRAs that combines damping multipliers (D_{mul}), and randomized shear-wave velocity (V_S) profiles with a V_S standard deviation $\sigma_{\ln V_S}$, where D_{mul} and $\sigma_{\ln V_S}$ are calibrated based on data from borehole sites. This paper discussed (1) the approach and framework for quantifying site response residuals, and (2) the selection of the most appropriate D_{mul}-$\sigma_{\ln V_S}$ combination by comparing observed and theoretical transfer functions (TFs) and amplification factors (AFs) from sites relatively compatible with 1D SRA assumptions (1D-like sites). Chapter 4 discusses the use of D_{mul} and $\sigma_{\ln V_S}$ in forward predictions of site response for the more commonly encountered 3D-like sites, and addresses the underprediction of high-frequency amplitudes caused by increasing the minimum damping.

The results indicate that using a D_{mul} = 3 and $\sigma_{\ln V_S}$ = 0.25 leads to an overall minimum root mean square error (RMSE) in site response predictions. However, different values are obtained if the focus is placed on TFs or AFs separately, or the available data is separated by region. A lower D_{mul} = 1 is required if TFs are the only metric of interest, and D_{mul} = 2 and 4 are respectively required for AFs for California and Japan when analyzed independently. The higher D_{mul} values required for AFs compared to TFs result from the wide range of ground-motion frequencies affecting the spectral ordinates of a single degree of freedom oscillator (Bora et al., 2016), and thus the AFs. The response of the oscillators of different frequencies gets contributions

from ground motion waves around the site's fundamental mode, which are generally overpredicted. Such waves lead to the overprediction of AFs that require higher D_{mul} values to be corrected. The factor making a difference between D_{mul} for AFs in California and Japan are similar in essence. The ground motions from the Japanese sites present a more uniform and generally higher amplification of waves across frequencies, suggested by flatter TF shapes (Appendix E). These characteristics observed in TFs turn into larger contributions to the oscillators' spectral ordinates and thus AF amplitudes.

The analyses showed that the effects of D_{mul} and $\sigma_{\ln V_S}$ on the predicted TFs and AFs vary with frequency, and thus any D_{mul}-$\sigma_{\ln V_S}$ combination does not lead to a uniform reduction of the RMSE across frequencies. This suggests that frequency-dependent SRAs are better suited for site response predictions, which is consistent with other findings within the context of nonlinear SRAs (Assimaki and Kausel, 2002; Kausel and Assimaki, 2002). Frequency dependent SRAs have yet to make its way into practice.

A total of 39 1D-like sites from a database of 534 borehole sites were identified based on the alignment of peaks and troughs of the median observed and theoretical transfer functions (TFs) measured using the Pearson's correlation coefficient, followed by a visual screening. The results indicate that only 39 of the 534 sites can be considered as 1D-like sites, which represents about 7% of the database. It is unclear whether the calibrated $D_{mul} = 3$ and $\sigma_{\ln V_S} = 0.25$ would change with larger datasets of 1D-like sites, but it is expected that these recommendations will be revised as ground motion databases become larger. Similarly, the number of sites and ground motion recordings from California do not allow for providing region-specific recommendations, but there is potential for doing so as data become available.

The D_{mul} and σ_{lnV_S} were estimated considering damping profiles after Darendeli (2001), and randomized V_S profiles generated using the V_S model by Toro (1995), without prior layer discretization. Therefore, following the proposed approach involves using these models and corresponding assumed parameters. The Darendeli model is used assuming a plasticity index (PI) = 0, an overconsolidation ratio (OCR) = 1, a load frequency (f_{load}) = 1 Hz, and a coefficient of lateral pressure at rest (K_0) = 0.5. Using site-specific values that differ from these assumptions might lead to damping values higher in a factor of 2. It is expected that engineering problems involving soils that significantly deviate from the assumed values would require analyses more advanced than 1D SRAs. Randomized V_S profiles are generated using the V_S model by Toro with the coefficients recommended for sites with V_{S30} = 180 to 360 m/s, which are very similar to those for sites with V_{S30} = 360 to 760 m/s, which together cover a wide range of V_{S30}.

The proposed approach focuses on linear elastic SRAs, but the framework can be extended to nonlinear site response applications. The extension to equivalent linear 1D SRAs could involve using damping curves (e.g., Seed and Idriss, 1970) increased by an amount equivalent to the difference between the recommended and default laboratory-based damping, as opposed to the product of D_{mul} by the entire damping curve. Alternatively, the low-strain tail of the damping curves could be scaled up (e.g., Kaklamanos et al., 2020). Further research needs to be conducted towards the application of the proposed approach for equivalent linear and nonlinear site response applications.

3.9. REFERENCES

Abrahamson NA, Birkhauser P, Koller M, et al. (2002) PEGASOS – A comprehensive probabilistic seismic hazard assessment for nuclear power plants in Switzerland. In:

Twelfth European Conference on Earthquake Engineering, London, 9-13 September, paper 633.

Abrahamson NA, Coppersmith KJ, Koller M, Roth P, Sprecher C, Toro GR and Youngs R (2004) *Probabilistic seismic hazard analysis for Swiss Nuclear Power Plant Sites (PEGASOS Project).* Final Report, Wettingen, Switzerland, July.

Abrahamson NA, Somerville PG and Cornell CA (1990) Uncertainty in numerical strong motion predictions. In: *Proceedings of the 4th U.S. National Conference on Earthquake Engineering*, 1, 407-416.

Afshari K and Stewart JP (2019) Insights from California vertical arrays on the effectiveness of ground response analysis with alternative damping models. *Bulletin of the Seismological Society of America* 109: 1250–1264.

Afshari K, Stewart JP and Steidl JH (2019) California ground motion vertical array database. *Earthquake Spectra* 35(4): 2003–2015.

Al Atik L, Abrahamson N, Bommer JJ, Scherbaum F, Cotton F and Kuehn N (2010) The variability of ground-motion prediction models and its components. *Seismological Research Letters* 81: 794–801.

Assimaki D and Kausel E (2002) An equivalent linear algorithm with frequency- and pressure-dependent moduli and damping for the seismic analysis of deep sites. *Soil Dynamics and Earthquake Engineering* 22(2002): 959–965.

Assimaki D, Pecker A, Popescu R and Prevost J (2003) Effects of spatial variability of soil properties on surface ground motion. *Journal of Earthquake Engineering* 7: 1–44.

Baecher GB and Christian JT (2003) *Reliability and statistics in geotechnical engineering.* Wiley.

Bayless J and Abrahamson NA (2019) An empirical model for the interfrequency correlation of epsilon for Fourier Amplitude Spectra. *Bulletin of the Seismological Society of America* 109(3): 1058–1070.

Boaga J, Renzi S, Deiana R and Cassiani G (2015) Soil damping influence on seismic ground response: A parametric analysis for weak to moderate ground motion. *Soil Dynamics and Earthquake Engineering* 79(2015): 71–79.

Bommer JJ, Coppersmith KJ, Coppersmith RT, Hanson KL, Mangongolo A, Neveling J, Rathje EM, Rodriguez-Marek A, Scherbaum F, Shelembe R, Stafford P and Strasser FO (2015) A SSHAC level 3 probabilistic seismic hazard analysis for a new-build nuclear site in South Africa. *Earthquake Spectra* 31:661–698.

Bonilla LF, Steidl JH, Gariel JC and Archuleta RJ (2002) Borehole response studies at the Garner Valley Downhole Array, Southern California. *Bulletin of the Seismological Society of America* 92(8): 3165–3179.

Boore DM (2005) SMSIM–*Fortran programs for simulating ground motions from earthquakes: Version 2.3–A revision of OFR 96–80-A.* US Geological Survey open-file report 2000-509 revised, 55 pp. Reston, VA: US Geological Survey. 15 August 2005.

Boore DM (2013) The uses and limitations of the square-root-impedance method for computing site amplification. *Bulletin of the Seismological Society of America* 103(4): 2356–2368.

Bora SS, Scherbaum F, Kuehn N and Stafford P (2016) On the relationship between Fourier and response spectra: Implications for the adjustment of empirical ground-motion prediction equations (GMPEs). *Bulletin of the Seismological Society of America* 106(3): 1235–1253.

Brooker EW and Ireland HO (1965) Earth pressures at rest related to stress history. *Canadian Geotechnical Journal* 2(1): 1–15.

Cabas A, Rodriguez-Marek A and Bonilla LF (2017) Estimation of site-specific Kappa (κ_0)-consistent damping values at KiK-net sites to assess the discrepancy between laboratory-based damping models and observed attenuation (of seismic waves) in the field. *Bulletin of the Seismological Society of America* 107(5): 2258–2271.

Campbell KW (2009) Estimates of shear-wave Q and κ_0 for unconsolidated and semiconsolidated sediments in Eastern North America. *Bulletin of the Seismological Society of America* 99(4): 2365–2392.

Darendeli MB (2001) *Development of a new family of normalized modulus reduction and material damping curves.* PhD Dissertation, The University of Texas at Austin, Austin, TX.

De la Torre CA, Bradley BA and McGann CR (2021) 2D geotechnical site-response analysis including soil heterogeneity and wave scattering. *Earthquake Spectra* 38(2): 1124–1147.

El Haber E, Cornou C, Jongmans D, Youssef Abdelmassih D and Lopez-Caballero F (2019) Influence of 2D heterogeneous elastic soil properties on ground surface motion spatial variability. *Soil Dynamics and Earthquake Engineering* 123: 75–90.

Electric Power Research Institute (EPRI) (2013) *Seismic evaluation guidance: Screening, prioritization and implementation details (SPID) for the resolution of Fukushima near-term task force recommendation 2.1: Seismic.* Report no. 1025287, 28 February. Palo Alto, CA: EPRI.

Elgamal A, Lai T, Yang Z and He L (2001) Dynamic soil properties, seismic downhole arrays and applications in practice. In: *Proceedings of the 4th International Conference on Recent Advances in Geotechnical Earthquake Engineering and Soil Dynamics*, Diego, CA.

Foti S, Lai CG, Rix G and Strobbia C (2014) *Surface wave methods for near-surface site characterization.* CRC Press, London.

Gibbs JF, Tinsley JC, Boore DM and Joyner WB (2000) *Borehole velocity measurements and geological conditions at thirteen sites in the Los Angeles, California region.* US Geological Survey open File Report 00-470.

Griffiths SC, Cox BR, Rathje EM and Teague DP (2016a) Mapping dispersion misfit and uncertainty in V_S profiles to variability in site response estimates. *Journal of Geotechnical and Geoenvironmental Engineering* 142(11): 04016062.

Griffiths SC, Cox BR, Rathje EM and Teague DP (2016b) Surface-wave dispersion approach for evaluating statistical models that account for shear-wave velocity uncertainty. *Journal of Geotechnical and Geoenvironmental Engineering* 142(11): 04016061.

Hallal MM, Cox BR and Vantasel JP (2022) Comparison of state-of-the-art approaches used to account for spatial variability in 1D ground response analyses, *Journal of Geotechnical and Geoenvironmental Engineering* 148(5): 04022019.

Haskell NA (1953) The dispersion of surface waves on multilayered media. *Bulletin of the Seismological Society of America* 43: 17–34.

Holzer TL and Youd TL (2007) Liquefaction, ground oscillation, and soil deformation at the Wildlife Array, California. *Bulletin of the Seismological Society of America* 97(3): 961–976.

Hu Z, Roten D, Olsen KM and Day SM (2021) Modeling of empirical transfer functions with 3D velocity structure. *Bulletin of the Seismological Society of America* 111: 2042–2056.

Huang D, Wang G, Wang C and Jin F (2020) A modified frequency-dependent equivalent linear method for seismic site response analyses and model validation using KiK-Net borehole arrays. *Journal of Earthquake Engineering* 24(5): 827–844.

Idriss IM (2011) Use of V_{S30} to represent local site conditions. In: *Proceedings of the 4th LASPEI/IAEE International Symposium Effects of Surface Geology on Strong Ground Motions*, Santa Barbara CA.

Joyner WB and Boore DM (1988) Measurement, characterization, and prediction of strong ground motion. Earthquake Engineering and Soil Dynamics II. In: *Proceedings of the American Society of Civil Engineering, Geotechnical Engineering Division Specialty Conference*, June 27–30, Park City, Utah, 43-10.

Kaklamanos J and Bradley BA (2018) Challenges in Predicting Seismic Site Response with 1D Analyses: Conclusions from 114 KiK-net Vertical Seismometer Arrays. *Bulletin of the Seismological Society of America* 108(5): 2816–2838.

Kaklamanos J, Bradley BA, Moolacattu AN and Picard BM (2020) Physical hypotheses for adjusting coarse profiles and improving 1D site-response estimation assessed at 10 KiK-net sites. *Bulletin of the Seismological Society of America* 110(3): 1338–1358.

Kaklamanos J, Bradley BA, Thompson EM and Baise LG (2013) Critical parameters affecting bias and variability in site-response analyses using KiK-net downhole array data. *Bulletin of the Seismological Society of America* 103: 1733–1749.

Kamai R, Abrahamson NA and Silva WJ (2016) V_{S30} in the NGA GMPEs: Regional differences and suggested practice. *Earthquake Spectra* 32(4): 2083–2108.

Katebi M, Gatmiri B and Maghoul P (2018) A numerical study on the seismic site response of Rocky Valleys with irregular topographic conditions. *Journal of Multiscale Modelling* 9(3): 1850011.

Kausel E and Assimaki D (2002) Seismic simulation of inelastic soils via frequency-dependent moduli and damping. *Journal of Engineering Mechanics* 128(1): 34–47.

Kim B, Hashash YMA, Stewart JP, Rathje EM, Harmon JA, Musgrove MI, Campbell KW and Silva WJ (2016) Relative differences between nonlinear and equivalent-linear 1-D site response analyses. *Earthquake Spectra* 32(3): 1845–1865.

Kokusho T (2017) *Innovative earthquake soil dynamics.* pp. 181–184. London: Taylor & Francis.

Konno K and Ohmachi T (1998) Ground-motion characteristics estimated from spectral ratio between horizontal and vertical components of microtremor. *Bulletin of the Seismological Society of America* 88(1): 228–241.

Kottke AR (2018) pyrotd v0.5.4. Zenodo. https://doi.org/10.5281/zenodo.1322849.

Kuo CH, Huang JY, Lin CM, Chen CT and Wen KL (2021) Near-surface frequency-dependent nonlinear damping ratio observation of ground motions using SMART1. *Soil Dynamics and Earthquake Engineering* 147: 106798.

Kwok AOL, Stewart JP, Hashash YMA, Matasovic N, Pyke R, Wang Z and Yang Z (2007) Use of exact solutions of wave propagation problems to guide implementation of nonlinear seismic ground response analysis procedures. *Journal of Geotechnical and Geoenvironmental Engineering* 133(11): 1385–1398.

Laurendeau A, Bard P-Y, Hollender F, Perron V, Foundotos L, Ktenidou O-J and Hernandez B (2018) Derivation of consistent hard rock ($1000 < V_S < 3000$ m/s) GMPEs from surface and down-hole recordings: Analysis of KiK-net data. *Bulletin of Earthquake Engineering* 16 (6): 2253–2284.

Mayne PW and Kulhawy FH (1982) K_0-OCR relationships in soils. *Journal of the Geotechnical Engineering Division* 108(GT6): 851–872.

Meite R, Wotherspoon L, McGann C, Green RA and Hayden C (2020) An iterative linear procedure using frequency-dependent soil parameters for site response analyses. *Soil Dynamics and Earthquake Engineering* 130(2020): 105973.

Menq FY (2003) *Dynamic properties of sandy and gravelly soils.* PhD Dissertation, The University of Texas at Austin, Austin, TX.

Nour A, Slimani A, Laouami N and Afra H (2003) Finite element model for the probabilistic seismic response of heterogeneous soil profile. *Soil Dynamics and Earthquake Engineering* 23(5): 331–348.

Olsen KB, Day SM and Bradley CR (2003) Estimation of Q for long-period (.2 sec) waves in the Los Angeles basin. *Bulletin of the Seismological Society of America* 93: 627–638.

Passeri F, Foti S and Rodriguez-Marek A (2020) A new geostatistical model for shear wave velocity profiles. *Soil Dynamics and Earthquake Engineering* 136(2020): 106247.

Pilz M and Cotton F (2019) Does the one-dimensional assumption hold for site response analysis? A study of seismic site response and implication for ground motion assessment using KiK-net strong-motion data. *Earthquake Spectra* 35(2): 883–905.

Pilz M, Cotton F and Zhu C (2022) How much are sites affected by 2-D and 3-D site effects? A study based on single-station earthquake records and implications for ground motion modeling. *Geophysical Journal International* 228(3): 1992–2004.

Pretell R, Ziotopoulou K and Abrahamson NA (2022a) Conducting 1D site response analyses to capture 2D V_S spatial variability effects. *Earthquake Spectra* 38(3): 2235–2259.

Pretell R, Ziotopoulou K and Abrahamson NA (2022) Numerical investigation of V_S spatial variability effects on the seismic response estimated using 2D and 1D site response analyses. In: *Proceedings of the Geo-Congress 2022*, Charlotte, NC, 20–23 March.

Ramos-Sepúlveda ME and Cabas A (2021) Site effects on ground motion directionality: Lessons from case studies in Japan. *Soil Dynamics and Earthquake Engineering* 147(2021): 106755.

Roblee C, Silva W, Toro G and Abrahamson N (1996) Variability in site-specific seismic ground-motion design predictions. In: *Proceedings of the uncertainty in the geologic environment: From theory to practice (Uncertainty'96)*, Madison, WI, 31 July–3 August, vol. 1, pp. 1113–1133. New York: ASCE.

Rodriguez-Marek A, Kruiver PP, Meijers P, Bommer JJ, Dost B, van Elk J and Doornhof D (2017) A regional site-response model for the Groningen Gas Field. *Bulletin of the Seismological Society of America* 107(5): 2067–2077.

Rodriguez-Marek A, Rathje E, Ake J, Munson C, Stovall S, Waver T, Ulmer K and Juckett M (2021) *Documentation report for SSHAC level 2: Site response.* Research Information Letter, Office of Nuclear Regulatory Research, November 2021.

Ruigrok E, Rodriguez-Marek A, Edwards B, Kruiver PP, Dost B and Bommer J (2022) Derivation of a near-surface damping model for the Groningen gas field. *Geophysics Journal International*, 230: 776–795.

Seed HB and Idriss IM (1970) *Soil moduli and damping factors for dynamic response analyses.* Report no. PEER EERC-70-10, Pacific Earthquake Engineering Research Center.

Semblat JF (2011) Modeling seismic wave propagation and amplification in 1D/2D/3D linear and nonlinear unbounded media. *Journal of Geotechnical and Geoenvironmental Engineering* 11(6): 440–448.

Semblat JF, Duval A-M and Dangla P (2000) Numerical analysis of seismic wave amplification in Nice (France) and comparisons with experiments. *Soil Dynamics and Earthquake Engineering* 19(5): 347–362.

Stewart JP and Afshari K (2020) Epistemic uncertainty in site response as derived from one-dimensional ground response analysis. *Journal of Geotechnical and Geoenvironmental Engineering* 147(1): 04020146.

Stewart JP, Afshari K, Hashash YMA (2014) *Guidelines for performing hazard-consistent one-dimensional ground response analysis for ground motion prediction.* Report PEER 2014/16, October. Berkeley, CA: Pacific Earthquake Engineering Research Center (PEER), University of California, Berkeley.

Tao Y and Rathje EM (2019) Insights into modeling small-strain site response derived from downhole array data. *Journal of Geotechnical and Geoenvironmental Engineering* 145(7): 04019023.

Tao Y and Rathje EM (2020) Taxonomy for evaluating the site-specific applicability of one-dimensional ground response analysis. *Soil Dynamics and Earthquake Engineering* 128(3): 105865.

Teague DP and Cox BR (2016) Site response implications associated with using non-unique V_S profiles from surface wave inversion in comparison with other commonly used methods of

accounting for V_S uncertainty. *Soil Dynamic and Earthquake Engineering* 91(2016): 87–103.

Teague DP, Cox BR and Rathje EM (2018) Measured vs. predicted site response at the Garner Valley downhole array considering shear wave velocity uncertainty from borehole and surface wave methods. *Soil Dynamics and Earthquake Engineering* 113: 339–355.

Thompson EM, Baise LG, Tanaka Y and Kayen RE (2012) A taxonomy of site response complexity. *Soil Dynamics and Earthquake Engineering* 41: 32–43.

Thomson WT (1950) Transmission of elastic waves through a stratified solid. *Journal of Applied Physics* 21: 89–93.

Thornley J, Dutta U, Fahringer P and Yang Z (J) (2019) In situ shear-wave velocity measurements at the Delaney Park downhole array, Anchorage, Alaska. *Seismological Research Letters* 90(1): 395–400.

Toro GR (1995) *Probabilistic models of site velocity profiles for generic and site-specific ground-motion amplification studies.* Report no. 779574, 17 November. Upton, NY: Brookhaven National Laboratory.

Tsai CC and Hashash YMA (2009) Learning of dynamic soil behavior from downhole arrays. *Journal of Geotechnical and Geoenvironmental Engineering* 135(6): 745–757.

Vucetic M and Dobry R (1991) Effect of soil plasticity in cyclic response. *Journal of Geotechnical Engineering* 117(1): 89–107.

Xu B, Rathje EM, Hashash Y, Stewart J, Campbell K and Silva WJ (2020) κ_0 for soil sites: Observations from KiK-net sites and their use in constraining small-strain damping profiles for site response analysis. *Earthquake Spectra* 36(1): 111–137.

Yoshida N, Kobayashi S, Suetomi I and Miura K (2002) Equivalent linear method considering frequency dependent characteristics of stiffness and damping. *Soil Dynamics and Earthquake Engineering* 22(3): 205–222.

Zalachoris G and Rathje EM (2015) Evaluation of one-dimensional site response techniques using borehole arrays. *Journal of Geotechnical and Geoenvironmental Engineering* 141(12): 04015053.

Zhu C, Thambiratnam DP and Zhang J (2016) Response of sedimentary basin to obliquely incident SH waves. *Bulletin of the Seismological Society of America* 14: 647–671.

Zhu C, Cotton F, Kawase H, Haendel A, Pilz M and Nakano K (2022) How well can we predict earthquake site response so far? Site-specific approaches. *Earthquake Spectra* 38(2): 1047–1075.

FIGURES

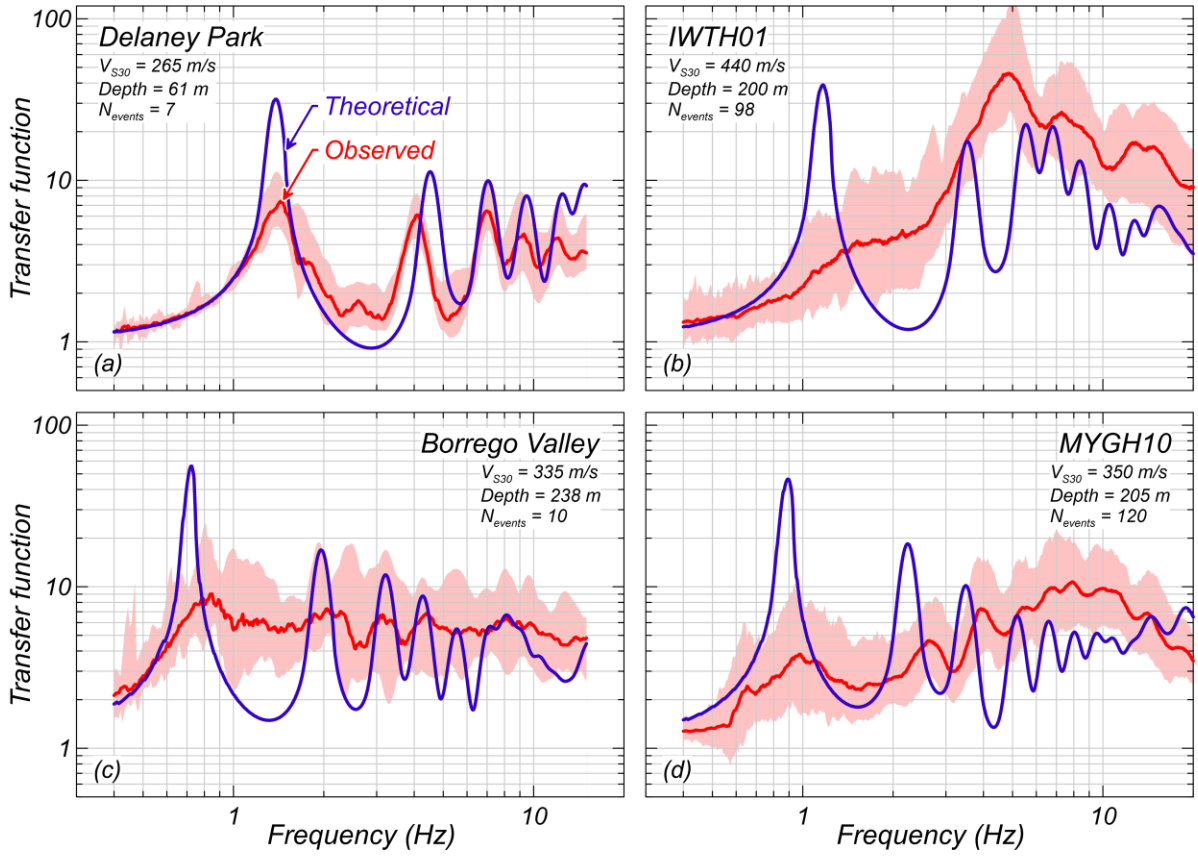

Figure 3.1. Comparison of observed and theoretical transfer functions (TFs). TFs computed using the measured V_S profiles and minimum damping after Darendeli (2001). TFs plotted within the range of usable signal based on the signal-to-noise ratio.

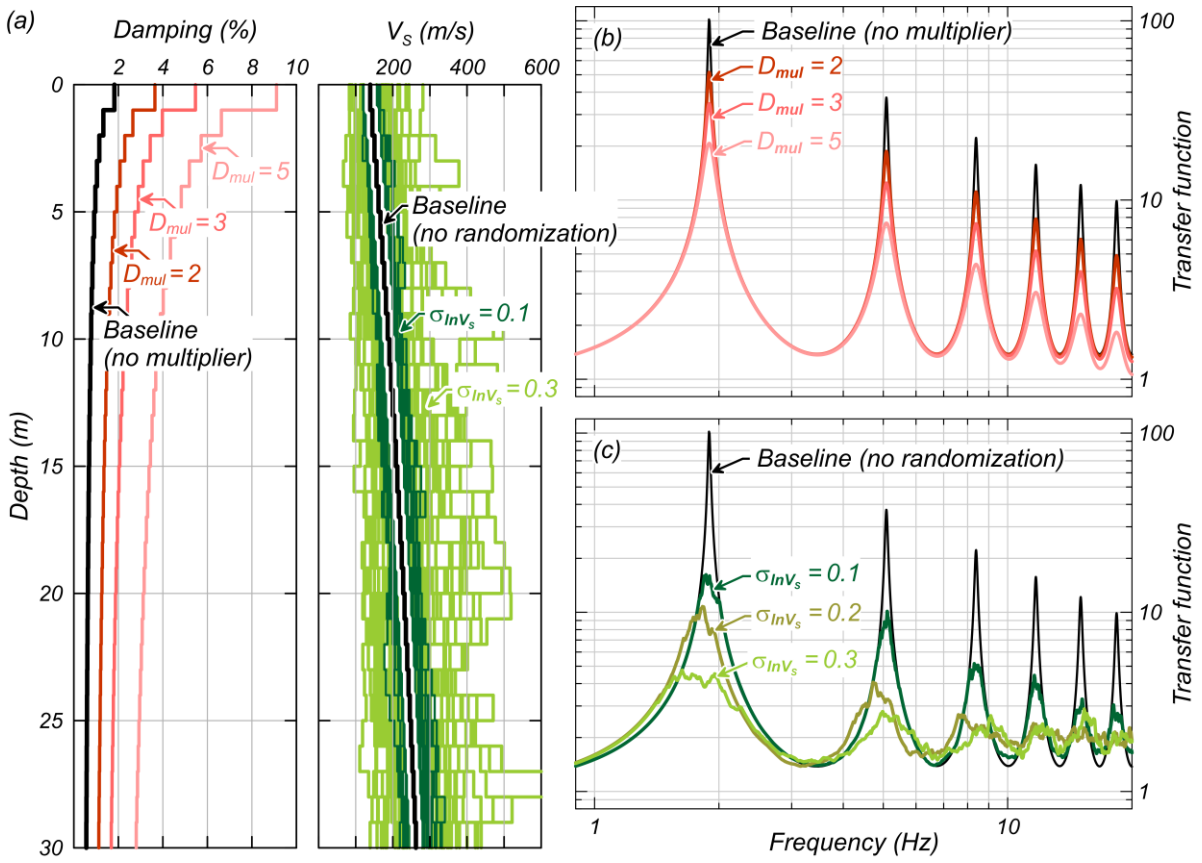

Figure 3.2. Effects of increased damping and randomized V_S profiles on transfer functions (TFs) in 1D site response analyses: (a) damping and randomized V_S profiles, (b) effect of damping on TFs for various damping multipliers (D_{mul}), and (c) effect of V_S randomization on TFs for various V_S standard deviations $(\sigma_{\ln V_S})$. Baseline TFs computed using the minimum damping after Darendeli (2001). Baselined V_S profile randomized using the Toro (1995) V_S model.

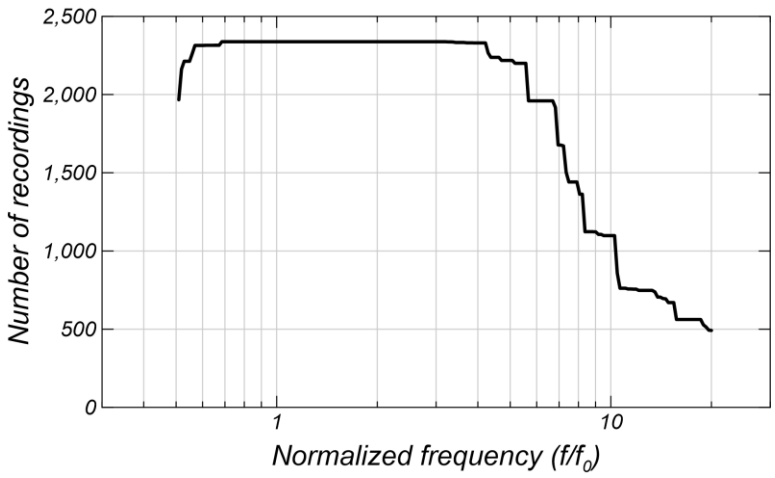

Figure 3.3. Number of ground motion recordings per normalized frequency (f/f_0).

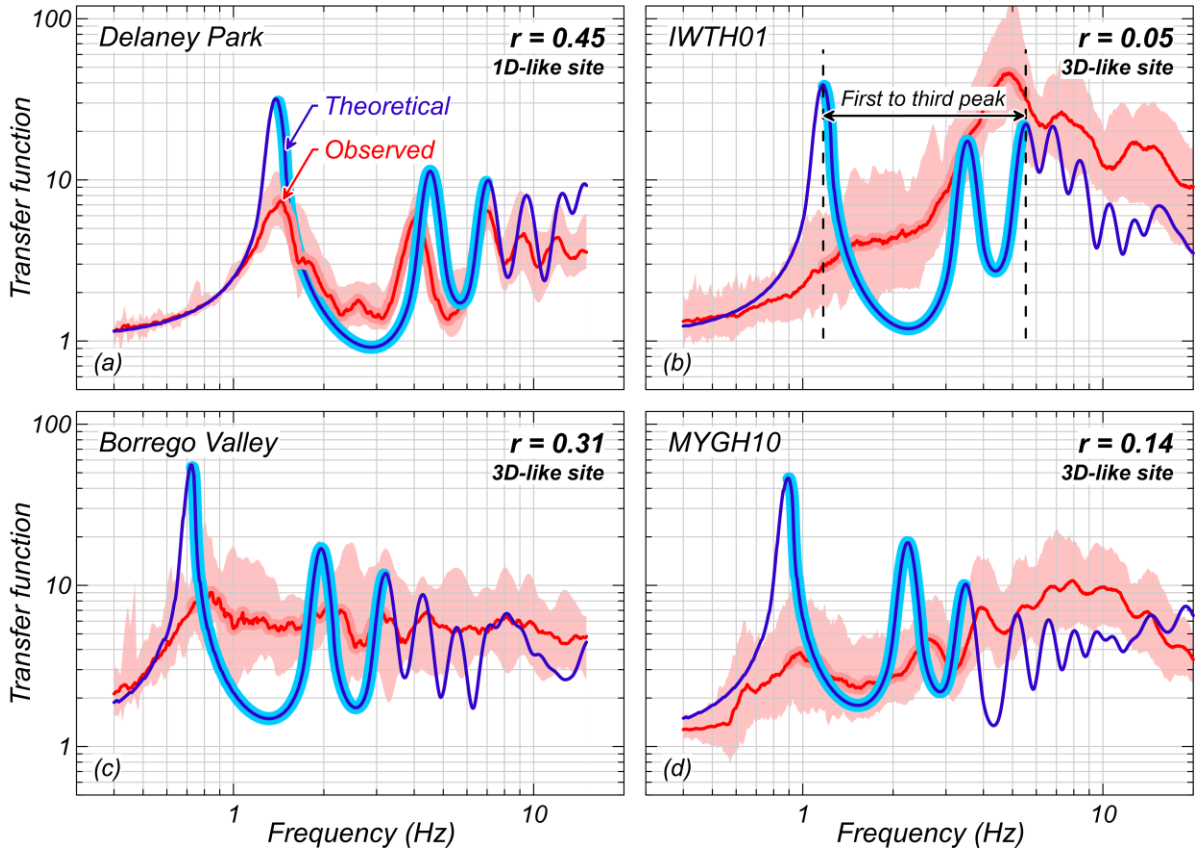

Figure 3.4. Example of 1D- and 3D-like sites. Pearson's correlation coefficient (r) between the empirical and theoretical transfer functions from the first to the third peak of the theoretical transfer functions. No specific correlation coefficient threshold is used to distinguish 1D- from 3D-like sites.

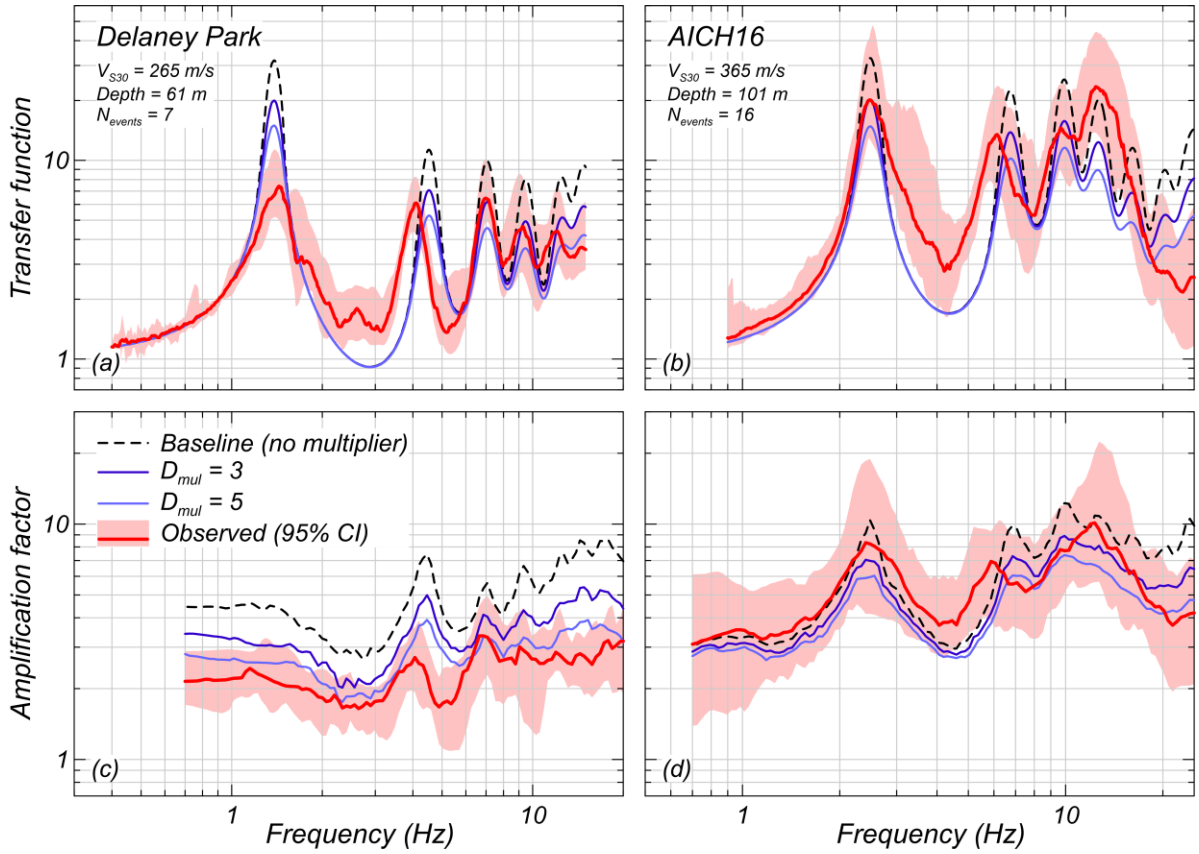

Figure 3.5. Effect of damping multipliers (D_{mul}) on 1D-like sites and comparison against observations. (a) and (b): Effect on the median theoretical transfer functions, (c) and (d): effect on the median amplification factors. Note: The median TFs result from TFs corresponding to 50 randomized V_S profiles, whereas the median AFs result from AFs from all the ground motion recordings, each one propagated through 50 randomized V_S profiles.

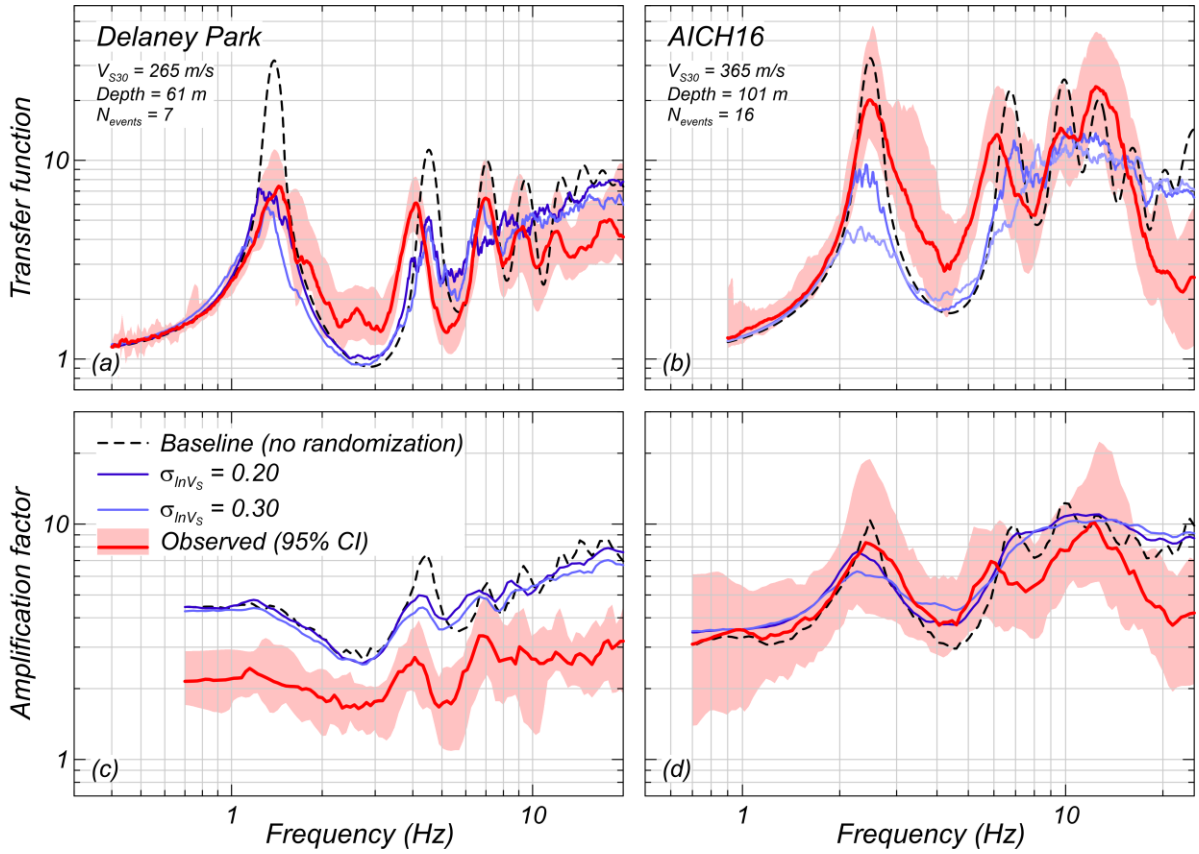

Figure 3.6. Effect of V_S standard deviation $(\sigma_{\ln V_S})$ for V_S randomization on 1D-like sites and comparison against observations. (a) and (b): effect on the median theoretical transfer functions, (c) and (d): effect on the median amplification factors. Note: The median TFs result from TFs corresponding to 50 randomized V_S profiles, whereas the median AFs result from AFs from all the ground motion recordings, each one propagated through 50 randomized V_S profiles.

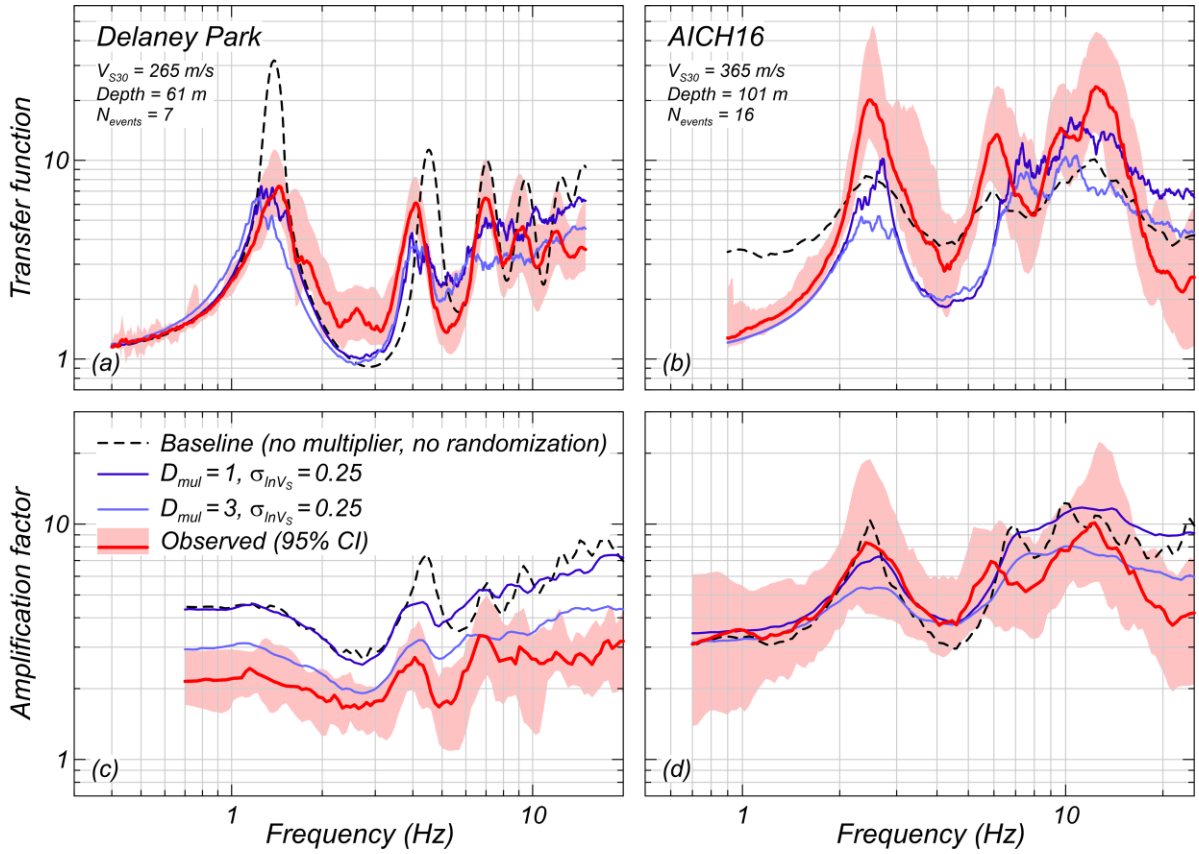

Figure 3.7. Combined effect of damping multiplier (D_{mul}) and V_S standard deviation $(\sigma_{\ln V_S})$ for V_S randomization, and comparison against ground motion recordings. (a) and (b): effect on the median theoretical transfer functions, (c) and (d): effect on the median amplification factors. Note: The median TFs result from TFs corresponding to 50 randomized V_S profiles, whereas the median AFs result from AFs from all the ground motion recordings, each one propagated through 50 randomized V_S profiles.

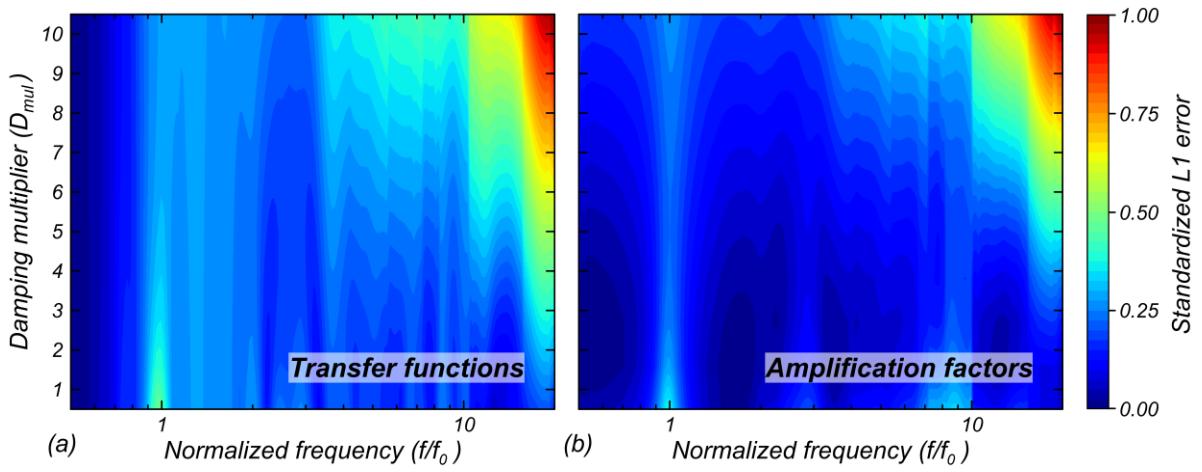

Figure 3.8. Standardized L1 error in: (a) transfer functions (TFs), and (b) amplification factors (AFs) across normalized frequency (f/f_0) for various damping multipliers (D_{mul}).

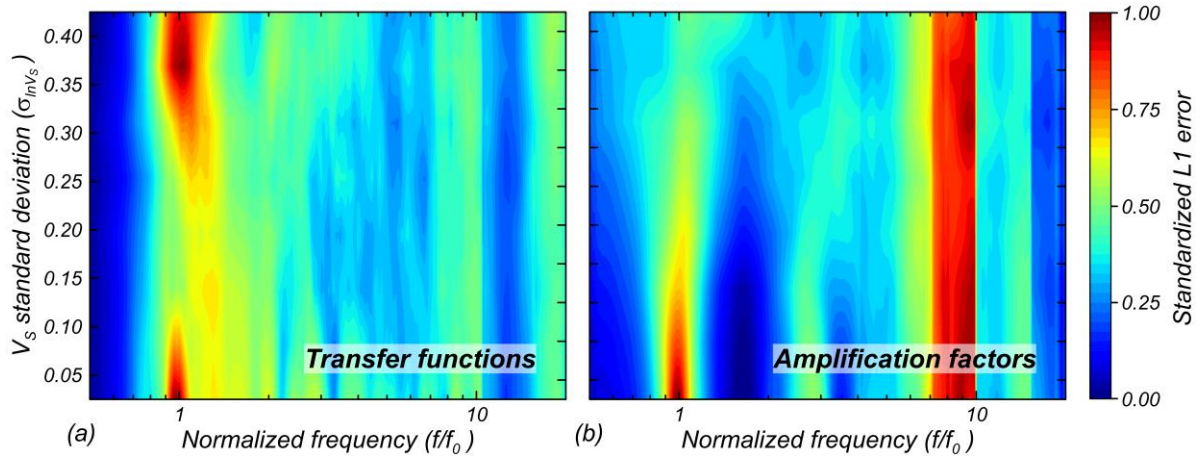

Figure 3.9. Standardized L1 error in: (a) transfer functions (TFs), and (b) amplification factors (AFs) across normalized frequency (f/f_0) for various V_S standard deviations $(\sigma_{\ln V_S})$ for V_S randomization.

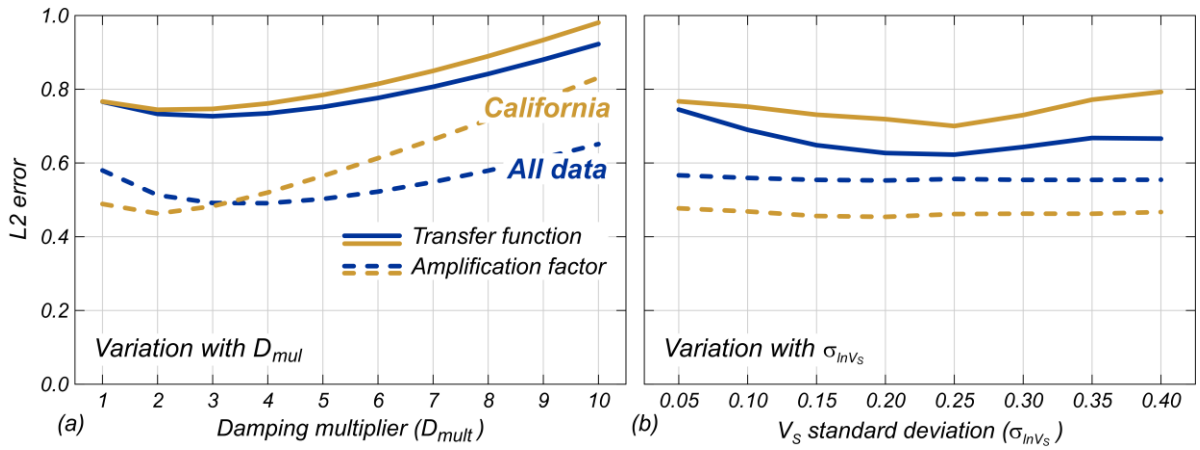

Figure 3.10. Variation of L2 error with damping multiplier (D_{mul}) and V_S standard deviation $(\sigma_{\ln V_S})$ for V_S randomization. Results labeled as "All data" based on data from all the 39 1D-like sites from the US and Japan, and results labeled as "California" based on the data from six 1D-like sites from California.

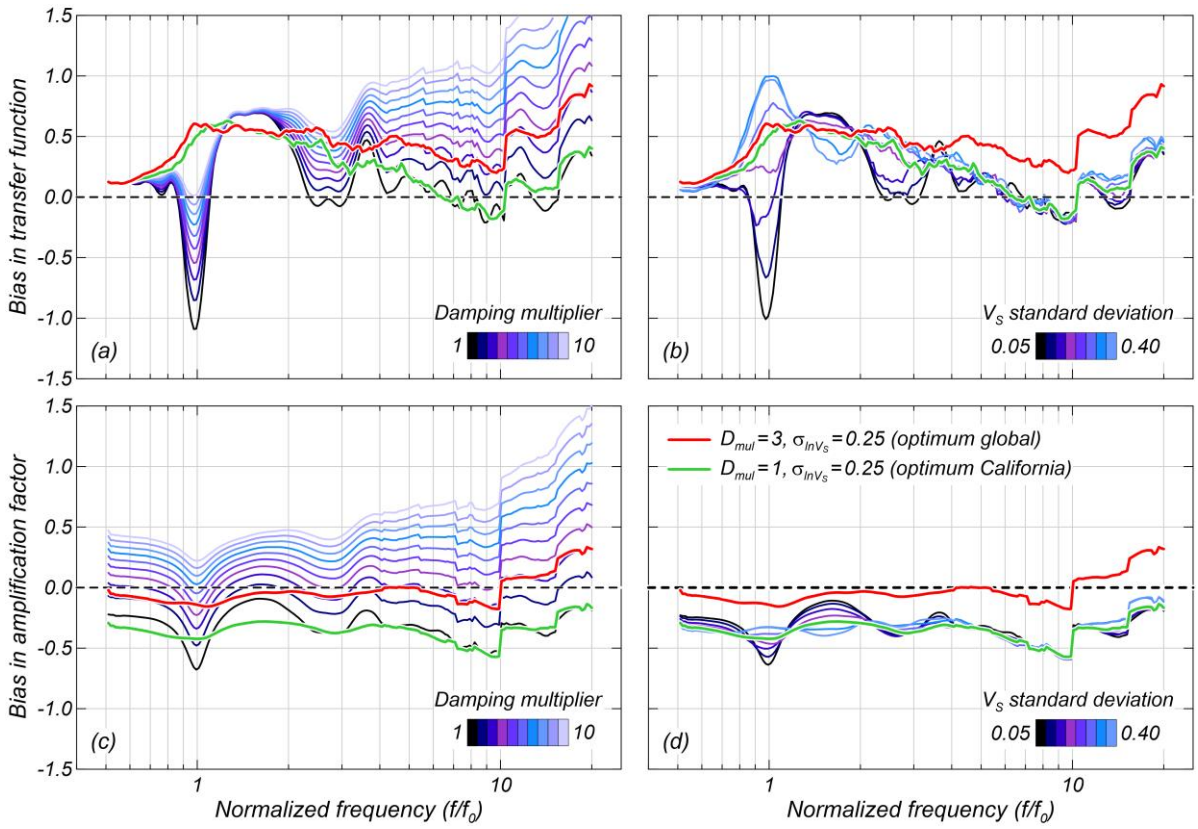

Figure 3.11. Bias in 1D site response estimates for 1D-like sites $\left(c_{1D}^{SRA}\right)$: (a) bias in transfer functions (TFs for various damping multipliers (D_{mul}), (b) bias in TFs for various V_S standard deviations $\left(\sigma_{\ln V_S}\right)$, (c) bias in amplification factors (AFs) for various D_{mul}, and (d) bias in AFs for various $\sigma_{\ln V_S}$ values.

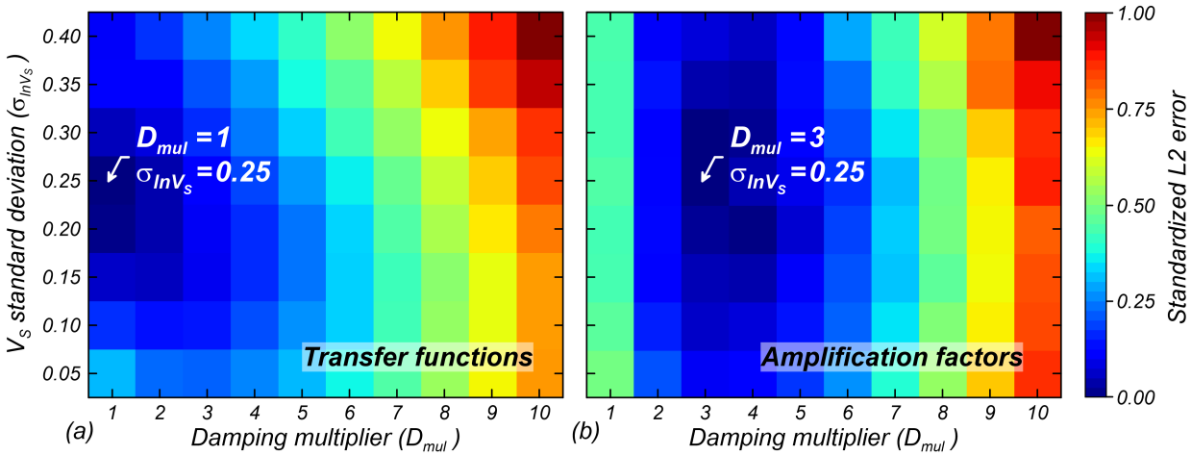

Figure 3.12. Standardized L2 error for combinations of damping multiplier (D_{mul}) and V_S standard deviation (σ_{lnV_S}) for V_S randomization: (a) Standardized L2 error in transfer functions (TFs), and (b) standardized L2 error in amplification factors (AFs). Minimum standardized L2 error in TFs for D_{mul} = 1, and σ_{lnV_S} = 0.25, and minimum standardized L2 error in AFs for D_{mul} = 3, and σ_{lnV_S} = 0.25.

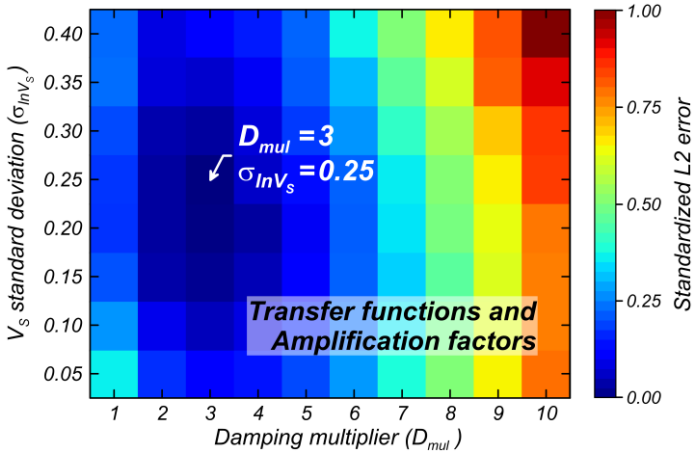

Figure 3.13. Standardized averaged L2 errors in transfer functions (Figure 11a) and amplification factors (Figure 11b) for combinations of damping multiplier (D_{mul}) and V_S standard deviation (σ_{lnV_S}) for V_S randomization. Minimum standardized L2 error for D_{mul} = 3, and σ_{lnV_S} = 0.25.

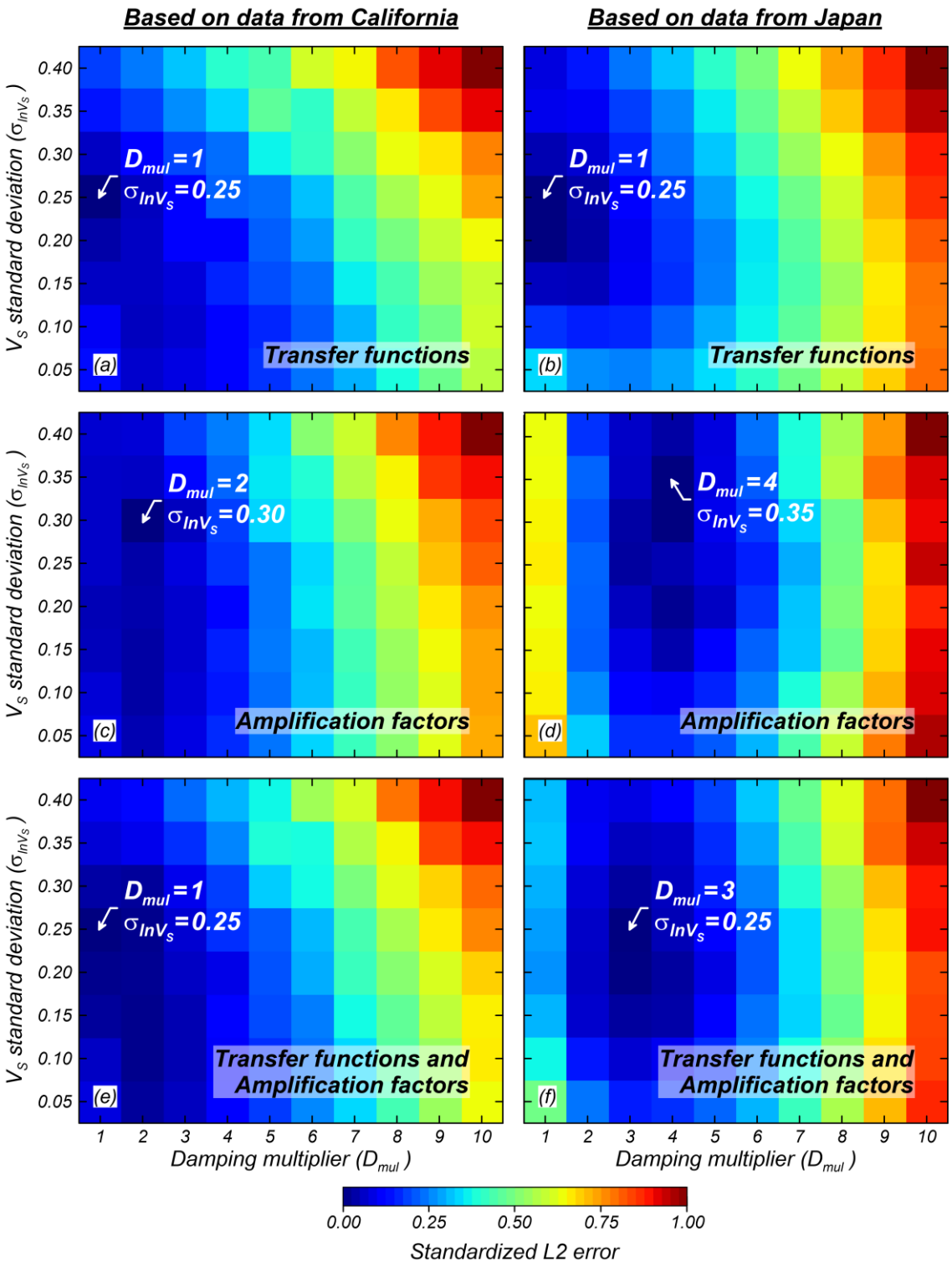

Figure 3.14. Standardized L2 errors for various combinations of damping multipliers (D_{mul}) and V_S standard deviations (σ_{lnV_S}) for V_S randomization. (a), (c), and (e): Standardized L2 errors for sites in California; (b), (d), and (f): standardized L2 errors for sites in Japan.

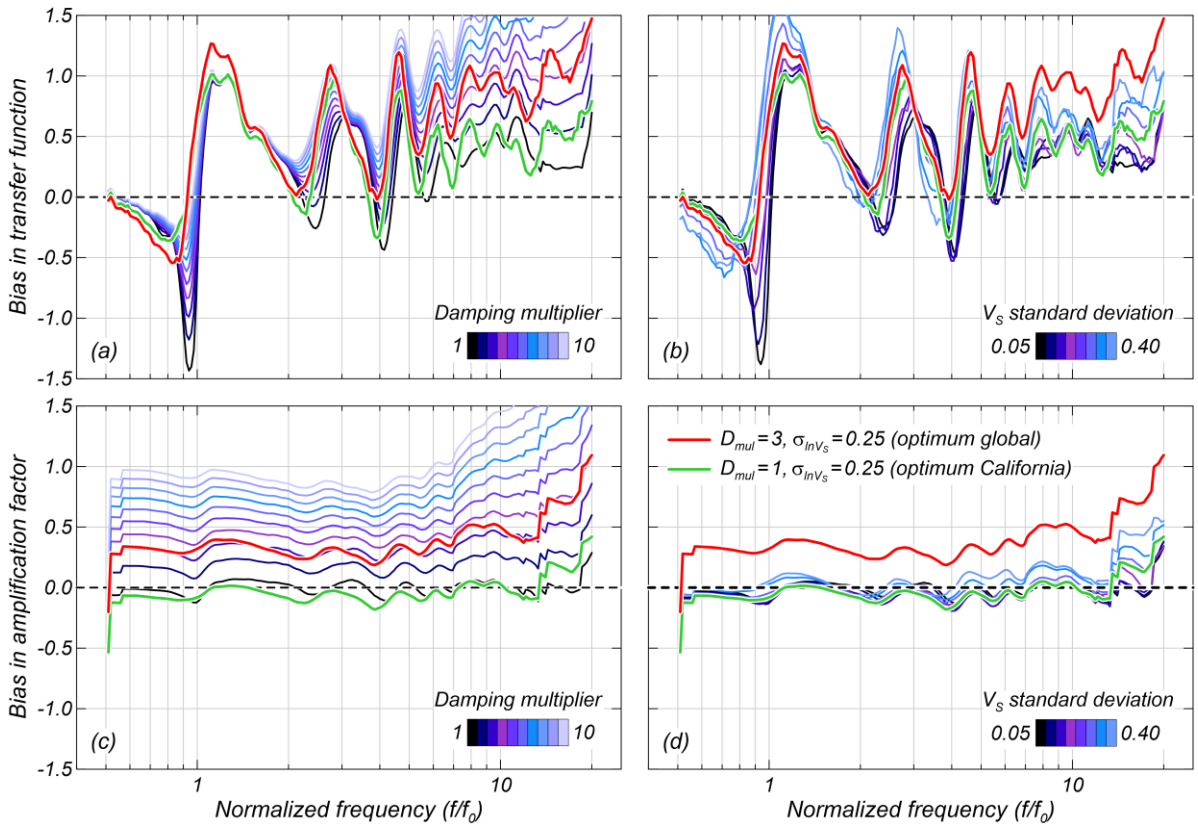

Figure 3.15. Bias in 1D site response estimates for 1D-like sites $\left(c_{1D}^{SRA}\right)$ in California. (a) Bias in transfer functions (TFs) for various damping multipliers (D_{mul}), (b) bias in TFs for various V_S standard deviations $\left(\sigma_{\ln V_S}\right)$, (c) bias in amplification factors (AFs) for various D_{mul}, and (d) bias in AFs for various $\sigma_{\ln V_S}$.

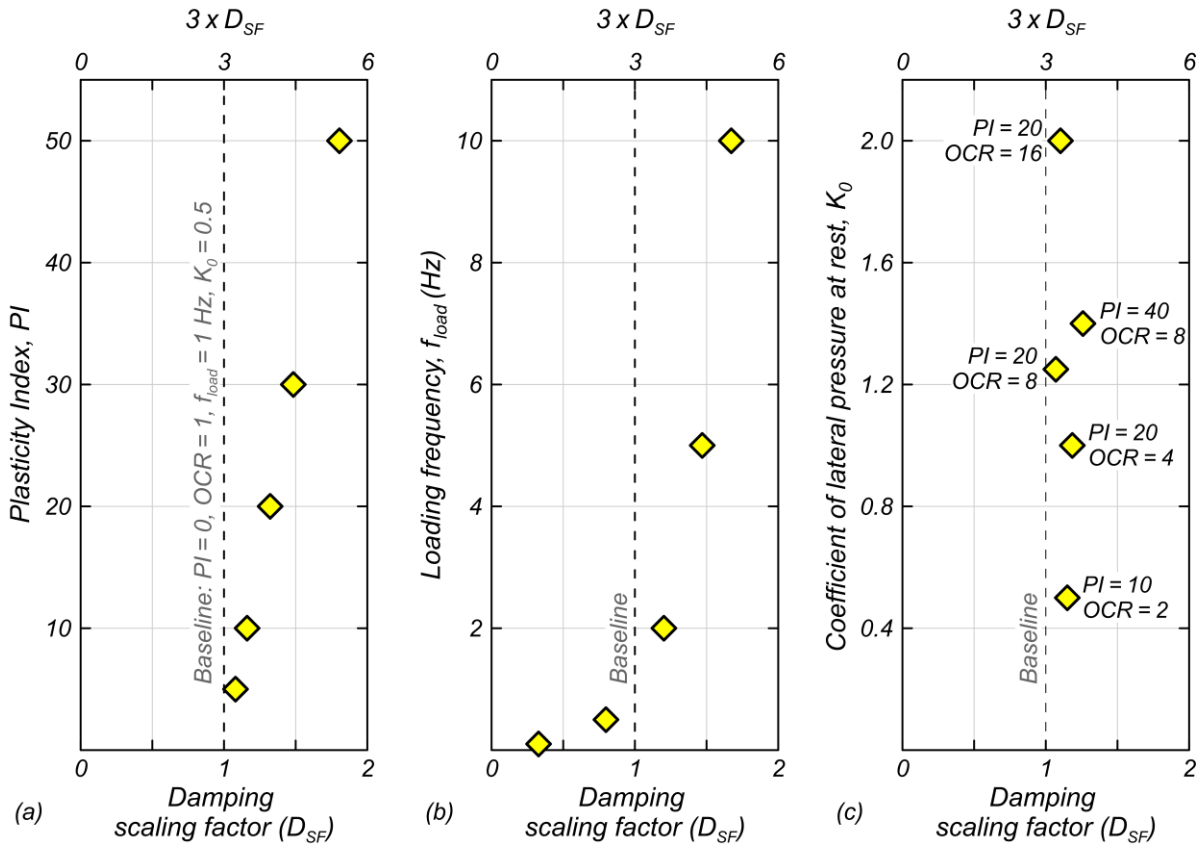

Figure 3.16. Effect of various parameters of the damping model by Darendeli (2001) on damping multiplier (D_{mul}). (a) Effect of plasticity index (PI), (b) effect of loading frequency (f_{load}), and (c) effect of coefficient of lateral pressure at rest (K_0) and overconsolidation ratio (OCR).

TABLES

Table 3.1. Matrix for the partition of sources of aleatory variability and epistemic uncertainty in numerical simulations (Abrahamson et al., 1990).

	Aleatory Variability	**Epistemic Uncertainty**
Parametric	**PAV** Effect of the randomness in time and space of input parameters on site response	**PEU** Distribution of values for input parameters and alternative selected representative input parameters
Modeling	**MAV** Randomness in predictions due to inherent complexities in natural phenomena not captured by the selected modeling approach	**MEU** Uncertainty in the predictions due to limitations of the selected modeling approach

Table 3.2. 1D-like borehole sites and main characteristics.

No	**Site** [1]	**Number of events**[2]	**Depth** [3] **(m)**	**GWT** [4] **(m)**	V_{S30} [5] **(m/s)**	$V_{S,\ average}$ [5] **(m/s)**
1	Corona I-15 Highway 91	4	42	25	334	440
2	Delaney Park	7	61	21	266	320
3	El Centro	4	195	5	199	320
4	Hayward San Mateo Bridge	4	91	11.5	184	255
5	San Bernardino	4	92	16	268	420
6	Treasure Island	22	122	2	160	295
7	Wildlife	20	100	1.2	198	240
8	AICH09	12	360	68	275	615
9	AICH16	16	101	3	365	740
10	CHBH17	12	822	5	525	907
11	FKIH05	7	122	22	190	370
12	FKSH16	35	300	0	530	840
13	GIFH18	21	107	6	555	935
14	GIFH28	11	400	5	370	785
15	IBRH11	120	103	10	245	650
16	IBRH13	120	100	16	335	795
17	IBRH17	18	510	10	277	550
18	IBUH01	48	101	12	310	520
19	IBUH05	41	177	4	380	525
20	IWTH04	120	106	15	460	935
21	IWTH08	84	100	10	305	685
22	KGSH03	32	100	0	1200	1635

No	Site [1]	Number of events[2]	Depth [3] (m)	GWT [4] (m)	V_{S30} [5] (m/s)	$V_{S,\ average}$ [5] (m/s)
23	KMMH08	23	103	10	525	790
24	KMMH13	22	177	12	405	585
25	KOCH10	10	101	2	1120	1470
26	MIEH07	8	207	8	620	1350
27	MYGH06	120	100	0	595	710
28	MYZH01	5	103	24	545	840
29	NGNH20	14	100	5	530	1115
30	NGNH21	12	180	8	510	765
31	NIGH15	26	100	0	685	890
32	NMRH03	22	228	4	190	335
33	NMRH04	23	216	8	170	290
34	NMRH05	37	220	8	210	370
35	SBSH06	5	130	0	480	640
36	SZOH25	7	450	7	330	695
37	TCGH12	54	120	4	340	505
38	TKSH04	9	100	7	475	950
39	YMTH12	10	203	4	365	675

[1] Sites number 1, and 3 to 6 from the Center for Engineering Strong Motion Data (CESMD) database. Sites number 2 and 7 from the Network for Earthquake Engineering Simulation (NEES) database. All other sites from the Kiban Kyoshin Network (KiK-net) database.

[2] Number of events after ground motion screening. Both horizontal recording components per event are used.

[3] In case of multiple sensors, the deepest one is considered.

[4] Depth to groundwater table based on the literature (Afshari et al., 2019; Holzer and Youd, 2007; Thornley et al., 2019) or the ground motion databases. When unavailable, the groundwater table was assumed as located where the measured compressional-wave velocity (V_P) > 1500 m/s. The groundwater table for the San Francisco Bridge and Benicia Martinez Bridge were assumed as 0 m, based on their closeness to bodies of water.

[5] Values estimated based on measured V_S profiles (Gibbs et al., 2000; Afshari et al., 2019; Thornley et al., 2019).

CHAPTER 4

A BOREHOLE DATA-BASED APPROACH FOR CONDUCTING 1D SITE RESPONSE ANALYSES II: ACCOUNTING FOR MODELING ERRORS

AUTHOR'S NOTE

The contents of this chapter will be submitted for journal publication by Pretell R, Abrahamson NA and Ziotopoulou K. Authorship roles are provided in Chapter 1.

4.1. ABSTRACT

Site response estimates from 1D site response analyses (SRAs) carry inaccuracies due to modeling and parametric errors. Modeling errors are due to the condensation of the 3D wave propagation phenomenon to the vertical propagation of a horizontally polarized wave through a soil column, while parametric errors are due to the incomplete knowledge of the soil parameters distribution leading to the selection of non-optimal representative input parameters for a site of interest. While parametric errors are traditionally handled by using different soil parameters (e.g., alternative shear-wave velocity profiles), modeling errors are generally neglected. In this paper, an approach is proposed for conducting linear elastic 1D SRAs in a way that improves site response predictions and accounts for modeling errors. First, ground-motion data from borehole sites are collected, processed, and screened for appropriateness (e.g., expected shear strains lower than 0.01%, signal-to-noise ratio higher than 3). Second, 1D SRA predictions in terms of transfer functions and amplification factors are compared against observations, and the discrepancies are quantified as

residuals. Finally, the residuals are partitioned into a model bias term $\left(c_{3D}^{SRA}\right)$, a site-specific mean residual with standard deviation ϕ_{S2S}^{SRA}, and a site- and event-specific residual with standard deviation ϕ_{AMP}^{SRA}, and values for these terms are recommended for forward predictions. The sensitivity of the residuals to region and site type (1D- or 3D-like), the applicability of findings to outcropping applications is discussed, and an example application for a hypothetical project site is presented.

4.2. INTRODUCTION

Predictions from one-dimensional site response analyses (1D SRAs) carry modeling and parametric errors, as well as errors intrinsic to the 1D SRA as a numerical modeling tool. The simplest approach for estimating site response consists of the propagation of the input ground motions through a soil column characterized with best estimate shear-wave velocity (V_S) and damping profiles. Modeling errors in the predicted response come from the simplification of the 3D wave propagation phenomenon to the vertical propagation of a horizontally polarized wave through a simple 1D model, which thus omits any unmodeled non-1D site-specific feature that affects the site response. Parametric errors are due to the lack of knowledge about the range of soil's properties and, in the case of linear elastic simulations, the most appropriate V_S and damping profiles. Lastly, there are errors associated with 1D SRA as an imperfect tool when conducted with a best estimate V_S profile and uncalibrated amount of damping, even for sites relatively compliant to the 1D SRA assumptions. Such errors are referred to as "intrinsic errors." While parametric errors are commonly addressed by using multiple alternative input parameters, e.g., baseline, upper, and lower V_S profiles (EPRI, 2013), intrinsic and modeling errors are generally overlooked. This and the previous chapter develop and propose an approach for conducting 1D SRAs that

removes the intrinsic errors, and accounts for modeling errors in 1D SRA-based site response predictions.

The proposed approach for conducting linear elastic 1D SRAs, hereafter referred to as 1D SRAs, consists of two main parts: (1) using calibrated input parameters (damping and randomized V_S) under the hypothesis that using the right amount of damping and V_S randomization removes the 1D SRA intrinsic errors, and (2) bias-correcting the response and computing the 5^{th} and 95^{th} site response percentiles. Damping multipliers (D_{mul}) are used to increase laboratory-based damping values and the V_S randomization model by Toro (1995) is used to generate suites of randomized V_S profiles. Based on comparisons with borehole data from 39 1D-like sites, it is observed that using $D_{mul} = 3$ and a standard deviation for V_S randomization, $\sigma_{\ln V_S} = 0.25$, leads to more accurate median site response predictions and a reduction in the site response variability. Chapter 3 discusses further the calibration of damping and V_S randomization, whereas this paper focuses on the quantification of the method bias and the estimation of the best estimate site response, and the 5^{th} and 95^{th} site response percentiles.

In this paper, a database of 490 3D-like borehole sites from Japan and the US is used to estimate the method bias $\left(c_{3D}^{SRA}\right)$ and variability in the site terms ($\delta S2S_s^{SRA}$), quantified with the standard deviation ϕ_{S2S}^{SRA}. One-dimensional SRAs are conducted with $D_{mul} = 3$ and $\sigma_{\ln V_S} = 0.25$, and residuals calculated for transfer functions (TFs) and amplification factors (AFs), following the findings from Chapter 3. Mixed-effects regression is used to separate the residuals into their components, and c_{3D}^{SRA} and ϕ_{S2S}^{SRA} values for engineering applications are recommended. The protocol for conducting 1D SRAs following the proposed approach is outlined, and an example application for a hypothetical project site is presented.

4.3. CAPTURING MODELING ERRORS IN 1D SRAs

4.3.1. FRAMEWORK

Errors carried by 1D SRA predictions can be quantified using ground-motion data from borehole sites. For an intensity measure (IM) of interest estimated using 1D SRAs and the corresponding observed earthquake component "e" at a site "s," the following relation can be established:

$$IM_{es}^{obs} = IM_{es}^{SRA} + \delta_{es}^{SRA} \quad (4.1)$$

where IM_{es}^{obs} and IM_{es}^{SRA} are respectively the observed and 1D SRA-predicted IM in natural logarithm units, and δ_{es}^{SRA} is the site response residual associated with 1D SRAs conducted using a best estimate V_S profile and an uncalibrated amount of damping (e.g., based on laboratory testing). In this work, IM represents either TFs or AFs, estimated as the ratio of the observed or the predicted ground motion at surface and the observed ground motion at depth. The residual δ_{es}^{SRA} in Equation 4.1 can be partitioned as:

$$\delta_{es}^{SRA} = c^{SRA} + \delta 1D_{s}^{SRA} + \delta 3D_{es}^{SRA} \quad (4.2)$$

where c^{SRA} is the global 1D-SRA bias estimated from a mixed-effects regression. The site-specific term $\delta 1D_{s}^{SRA}$ is due to 1D-SRA intrinsic errors (e.g., overpredictions at the site's fundamental mode) that depend on the effect of the site's damping and V_S profiles. The term $\delta 3D_{es}^{SRA}$ is the remaining modeling aleatory residual due to non-1D features affecting the site response and the effect of variability in the ground-motion waveforms that are not accounted for by c^{SRA}. $\delta 3D_{es}^{SRA}$ can be partitioned as (Al Atik et al., 2010):

$$\delta 3D_{es}^{SRA} = \delta S2S_{s}^{SRA} + \delta AMP_{es}^{SRA} \quad (4.3)$$

where $\delta S2S_s^{SRA}$ is the mean bias-corrected residual at a site "s," referred to as "site term," and δAMP_{es}^{SRA} is the remaining unexplained bias-corrected and site-corrected residual. The components $\delta S2S_s^{SRA}$ and δAMP_{es}^{SRA} are assumed random variables with zero mean and standard deviations ϕ_{S2S}^{SRA} and ϕ_{AMP}^{SRA}, respectively. Replacing Equation 4.3 into Equation 4.2:

$$\delta_{es}^{SRA} = c^{SRA} + \delta 1D_s^{SRA} + \delta S2S_s^{SRA} + \delta AMP_{es}^{SRA} \quad (4.4)$$

In Equation 4.4, the term $\delta 1D_s^{SRA}$ can be removed by conducting 1D SRAs with a calibrated amount of damping (D_{mul} = 3) and V_S randomization ($\sigma_{\ln V_S}$ = 0.25), as discussed in Chapter 3. This randomization should not be confused with the V_S randomization commonly used in engineering practice to capture spatial variability effects (e.g., Pretell et al., 2022). Given that the quantification of residuals is conducted using data from 3D-like sites, then $c^{SRA} = c_{3D}^{SRA}$. With these considerations, Equation 4.4 reduces to:

$$\delta_{es}^{SRA} = c_{3D}^{SRA} + \delta S2S_s^{SRA} + \delta AMP_{es}^{SRA} \quad (4.5)$$

Note that previously, in Equations 4.2 to 4.4, the δ_{es}^{SRA} is estimated from 1D SRAs conducted with a best estimate V_S profile and uncalibrated damping values, whereas it is estimated from 1D SRAs conducted with V_S randomization and calibrated damping in Equation 4.5. Within the context of this work, a "site" is defined as a punctual location that does not account for spatial variability of soil properties across a structure's footprint. All the terms in Equations 4.1 to 4.5 are frequency dependent.

Site response predictions can be improved by accounting for c_{3D}^{SRA} and ϕ_{S2S}^{SRA}. The c_{3D}^{SRA} represents a global bias in the estimated response, and ϕ_{S2S}^{SRA} represents the variability in the mean bias-corrected 1D SRA-based site response. The residual component $\delta S2S_s^{SRA}$ varies from site to

site, and whether it is positive (implying underprediction) or negative (overprediction) is unknown unless borehole ground motion data are available at a site of interest. To account for the 1D-SRA bias and the potential under- or overprediction, c_{3D}^{SRA} and ϕ_{S2S}^{SRA} are quantified using data from a database of borehole ground motions. Note that ϕ_{S2S}^{SRA} is different from the between-site standard deviation in ground-motion models (GMMs), herein referred to as ϕ_{S2S}^{GMM}, which represents the variability in amplification factors (e.g., Al Atik et al., 2010).

4.3.2. PROPOSED APPROACH

The proposed approach for conducting 1D SRAs (1) uses D_{mul} and V_S randomization to improve site response predictions, and (2) accounts for c_{3D}^{SRA} and ϕ_{S2S}^{SRA}. The protocol for conducting 1D SRAs consists of five steps:

Step 1: Site characterization. Selection of the best estimate V_S profile for a site of interest, and estimation of the minimum damping after Darendeli (2001). The model by Darendeli is used assuming a plasticity index (PI) of 0, an overconsolidation ratio (OCR) of 1, a loading frequency (f_{load}) of 1 Hz, a coefficient of lateral pressure at rest (K_0) of 0.5. The same layering in the V_S profiles is considered for the development of damping profiles. This site characterization is not uncommon in SRA applications.

Step 2: Input parameters. A D_{mul} = 3 is used to increase the minimum damping and a suite of 50 randomized V_S profiles is generated from the best estimate profile. The randomized V_S profiles are obtained using the Toro (1995) V_S model with $\sigma_{\ln V_S}$ = 0.25 and the parameters recommended for sites with the inverse of the slowness in the top 30 m (V_{S30}) between 180 and 360 m/s. The Toro model is implemented in widely used computer codes such as STRATA (Kottke and Rathje, 2008) and DeepSoil (Hashash et al., 2020).

Step 3: Uncorrected site response. All the randomized V_S profiles are paired with the same single damping profile (D_{mul} = 3) to compute the site response for each selected input ground motion. The median site response (μ_{IM}) from all the V_S profiles is estimated, where IM can be Fourier amplitudes or pseudo-spectral accelerations (PSAs) at ground surface. The median response of all the V_S profiles is the uncorrected best estimate for a given input motion.

Step 4: Bias correction. The estimated μ_{IM} is bias-corrected by adding c_{3D}^{SRA} (both in ln units). The resulting response is the best estimate for a given input ground motion:

Best estimate: $IM_{BE} = \mu_{IM} + c_{3D}^{SRA}$

Step 5: Accounting for modeling errors. The potential for modeling errors is accounted for by considering alternative percentiles of the bias-corrected FAS or PSA with 90% confidence interval:

5th percentile: $IM_{5^{th}} = (\mu_{IM} + c_{3D}^{SRA}) - 1.65 \times \phi_{S2S}^{SRA}$

95th percentile: $IM_{95^{th}} = (\mu_{IM} + c_{3D}^{SRA}) + 1.65 \times \phi_{S2S}^{SRA}$

The proposed approach can be repeated for alternative best estimate V_S profiles to account for parametric epistemic uncertainty, described in the next section. The estimated response at surface is valid for frequencies captured by the 1D model, approximately higher than the site's fundamental frequency (f_0). In this work, c_{3D}^{SRA} and ϕ_{S2S}^{SRA} are considered applicable to frequencies higher than half the f_0. The site response at lower frequencies can be estimated based on GMMs.

4.3.3. ALEATORY VARIABILITY AND EPISTEMIC UNCERTAINTY ASSOCIATED WITH THE PROPOSED APPROACH

A framework for the identification of sources of aleatory variability (AV) and epistemic uncertainty (EU) in ground-motion modeling (Abrahamson et al., 1990) is described in Chapter 3 within the context of site response. The separation of AV and EU helps understand the different factors affecting the response, as well as the benefits and the limitations of a selected numerical approach. This framework is developed (Table 4.1) and discussed within the context of the proposed approach and potential extensions to it.

The parametric AV (PAV) consists of random factors affecting the site response that can be explicitly modeled by the selected modeling approach. Such random factors include randomness in time given by the ground-motion waveforms, which can be captured by using multiple time histories. These time histories lead to variability in the response for PSA at surface that can be quantified as a standard deviation associated with time histories "TH": $\phi^{\mathrm{SRA}}_{\mathrm{AMP-TH}}$. Note that in the case of TFs or FAS, $\phi^{\mathrm{SRA}}_{\mathrm{AMP-TH}} = 0$. The PAV component $\phi^{\mathrm{SRA}}_{\mathrm{AMP-TH}}$ is not discussed in this paper.

The parametric EU (PEU) consists of the plausible alternative input parameters associated to the selected modeling approach. The PEU can include multiple suites of parameters depending on the available information and problem-specific needs (e.g., Rodriguez-Marek et al., 2020). Within the context of the proposed approach, the PEU consists of suites of input ground motions, selected based on some demand criteria, and best estimate V_S profiles (e.g., based on different geophysical tests). The PEU also includes D_{mul} to increase damping and $\sigma_{\ln V_S}$ to randomize V_S profiles. The best estimate and recommended values for these parameters are $D_{mul} = 3$ and

$\sigma_{\ln V_S}$ = 0.25, but alternative plausible values could be selected: D_{mul} = 1 to 4 and $\sigma_{\ln V_S}$ = 0.2 to 0.3 (see Figure 3.13 in Chapter 3).

The modeling AV (MAV) consists of the variability in the estimated site response given the factors affecting the site response but uncaptured by 1D SRAs. These factors include the wave propagation direction and wave inclination, the presence of other wave types, the presence of a dipping bedrock or complex subsurface structures, topographic and basin effects. From the perspective of the proposed approach, all these factors are regarded as random, leading to uncontrolled under- or overpredictions. The MAV, represented by c^{SRA} and $\delta 3D_{es}^{SRA}$ in Equation 4.2, is quantified using ground-motion data.

Lastly, the modeling EU (MEU) accounts for the potential misestimations of the MAV components, i.e., c_{3D}^{SRA}, ϕ_{S2S}^{SRA}, and ϕ_{AMP}^{SRA}. The MEU is quantified as standard errors (SE). Given that c_{3D}^{SRA}, ϕ_{S2S}^{SRA}, and ϕ_{AMP}^{SRA} are herein estimated based on a large database of sites and ground-motion recordings, the SE in all cases is considered negligible (Table 4.1).

4.3.4. RELATION TO SEISMIC HAZARD

The AV and EU components associated with the proposed approach should be consistent with seismic hazard calculations. In particular, the characterization of the seismic demand at the location of interest at depth (i.e., halfspace), and the subsequent convolution of the hazard at ground surface, if required, should capture different fractions of the ground-motion variability. The seismic hazard at the halfspace should be calculated using single-station sigma to remove ϕ_{S2S}^{GMM} given that site effects are explicitly modeled using site-specific 1D SRAs (Atkinson 2006; Rodriguez-Marek et al., 2011, 2013; Al Atik, 2015). To compute the seismic hazard at the ground surface, the convolution approach proposed by Bazzurro and Cornell (2004) is recommended by

EPRI (2013) and commonly used in partially non-ergodic applications in the nuclear industry (e.g., Rodriguez-Marek et al., 2014, 2021). The convolution approach requires two parameters: the median response at the ground surface (μ_{CONV}) and the standard deviation (σ_{CONV}). The μ_{CONV} corresponds to the best estimate, and the 5th and 95th percentiles resulting from the proposed approach, whereas the σ_{CONV} results from the addition of ϕ_{AMP-TH}^{SRA}. Here, we follow the approach that the component ϕ_{AMP}^{SRA} is already included in the GMM and thus is not considered in the convolution of hazard. More details are provided by Bazzurro and Cornell (2004), Pehlivan et al. (2016), and Stewart et al. (2014).

4.3.5. MAIN ASSUMPTIONS

There are four primary assumptions associated to the proposed approach:

1. *Applicability to outcropping applications*: The calibration of D_{mul} and $\sigma_{\ln V_S}$, and the quantification of c_{3D}^{SRA} and ϕ_{S2S}^{SRA} are based on borehole data. The wave cancelling effects observed in borehole recordings (e.g., Bonilla et al., 2002) raise concerns as to whether findings from borehole data are applicable to outcropping applications. An initial investigation of the validity of this assumption is presented in a later section.

2. *Perfectly measured V_S profiles*: The calibration of D_{mul} and $\sigma_{\ln V_S}$, and the quantification of c_{3D}^{SRA} and ϕ_{S2S}^{SRA} are based on comparisons of ground-motion observations and 1D SRA predictions, and discrepancies attributed to modeling errors. This implicitly assumes that the V_S profiles used in the 1D SRAs are flawless, which is hardly a realistic assumption (e.g., Zhu et al., 2022).

3. *Ergodicity*: The c_{3D}^{SRA} and ϕ_{S2S}^{SRA} are estimated based on data mainly collected from Japan but nevertheless considered to be applicable to any site. The ergodic assumption is required given

that there are not enough borehole sites that could potentially allow for differentiating aspects dominating site response in different regions. Removing the ergodic assumption requires (1) the collection of recorded ground motions at a site of interest, (2) the estimation of the components in Equation 4.5, and (3) accounting for the associated non-negligible SE of c_{3D}^{SRA} and ϕ_{S2S}^{SRA}.

4. *Applicability to any site type*: The c_{3D}^{SRA} and ϕ_{S2S}^{SRA} are recommended for any site in engineering applications. The datasets used in the estimation of c_{3D}^{SRA} and ϕ_{S2S}^{SRA} consist of 3D-like sites identified following a specific set of criteria that cannot be used in non-borehole sites or in the absence of data. Given that 93% of the sites in the database are 3D-like, it is reasonable to expect that most sites encountered in engineering practice are 3D-like. Note that the labels 1D- and 3D-like are only applicable within the context of the proposed approach and might not concur with proposed taxonomies (e.g., Thompson et al, 2012; Tao and Rathje, 2020a; Pilz et al., 2022).

4.4. PREVIOUS ESTIMATES OF SITE RESPONSE RESIDUALS

Previous studies provide estimates of c^{SRA}, ϕ_{S2S}^{SRA} and ϕ_{AMP}^{SRA} for 1D SRAs (Kaklamanos et al., 2013; Kaklamanos and Bradley, 2018; Stewart and Afshari, 2020; Zhu et al., 2022). These studies are based on different borehole datasets and damping assumptions:

- Kaklamanos et al. (2013) conducted 1D SRAs for 100 sites in the Kiban Kyoshin Network (KiK-net) database (NIED, 2019) using constant damping values optimized to fit observations at each site (Thompson et al., 2012) and computed residuals for PSA. The authors found an overall underprediction with c^{SRA} as high as 0.5, except between 0.5 and 2 Hz, ϕ_{S2S}^{SRA} from 0.4 to 0.6, and ϕ_{AMP}^{SRA} of 0.3 approximately constant with frequency. Subsequent efforts

(Kaklamanos and Bradley, 2018; Kaklamanos et al., 2020) identified the coarseness of V_S profiles in the KiK-net database as the factor leading to underpredictions in 1D-SRA estimates.

- Stewart and Afshari (2020) conducted 1D SRAs for 21 sites in California using three damping models and computed residuals for PSA. The authors found an overall trend of underprediction with c^{SRA} as high as 0.5 across frequencies up to 10 Hz for SRAs conducted with damping estimated based on correlations with quality factors (Q_S) and site-specific estimates of the high-frequency attenuation parameter (κ). The overall underprediction was not observed for 1D SRAs conducted with damping defined based on laboratory-based formulations (Darendeli, 2001; Menq, 2003). Stewart and Afshari estimated ϕ_{S2S}^{SRA} from 0.25 to 0.6, and ϕ_{AMP}^{SRA} from 0.2 to 0.4. The different damping formulations had a minor effect on ϕ_{S2S}^{SRA} and ϕ_{AMP}^{SRA}. The authors proposed a model for ϕ_{S2S}^{SRA} and provided recommendations for accounting for 1D SRA modeling errors.

- Zhu et al. (2022) conducted 1D SRAs for a large database of borehole and surface sites in Japan to investigate the efficacy of various methods for predicting FAS. Such methods include "full-resonance" 1D SRAs (i.e., the commonly used 1D SRA), the square-root-impedance (SRI) 1D SRAs (Joyner et al., 1981; Boore, 2003), and the horizontal-to-vertical spectral ratio (HVSR) correction (Nakamura, 2019). Zhu et al. used two damping formulations for SRAs and found that HVSR provides more accurate predictions, whereas the SRA and SRI have an overall poor performance, which was attributed to high parametric and modeling errors in their dataset. The authors estimated ϕ_{S2S}^{SRA} to vary from 0.25 to 0.4 from 0.1 to 2 Hz and then rapidly increase up to 0.95 for higher frequencies. The effect from using different damping models was minor.

These studies provide valuable insights into the site response bias and variability of the site terms ($\delta S2S_S^{SRA}$). In this paper, a database of borehole sites from Japan and the US is used to estimate c_{3D}^{SRA} and ϕ_{S2S}^{SRA}, and recommended values are provided along with a framework for conducting 1D SRAs to account for modeling errors. This work is different from previous studies in that SRAs are conducted using randomized V_S profiles and residual components estimated for normalized frequencies.

4.5. QUANTIFICATION OF SITE RESPONSE MODELING ERRORS

Site response residuals are quantified using publicly available borehole data from Japan and the US (California and Alaska), downloaded from the KiK-net database, and the Network for Earthquake Engineering Simulation (NEES) and the Center for Engineering Strong Motion Data (CESMD) databases, respectively.

A total of four cases are investigated for comparative purposes:

Case 1: Damping with D_{mul} = 1 and best estimate V_S profile. This is the baseline case.

Case 2: Damping with D_{mul} = 3 and best estimate V_S profile.

Case 3: Damping with D_{mul} = 1 and 50 randomized V_S profiles.

Case 4: Damping with D_{mul} = 3 and 50 randomized V_S profiles. This is the proposed approach.

4.5.1. SITE CHARACTERIZATION

The site characterization for 1D SRAs consists of profiles of minimum damping, V_S, and bulk density. Given the significant impact of V_S on the predicted site response at surface (e.g., Passeri et al., 2019; Kaklamanos et al., 2020), only sites with a measured V_S profile are used. The measured

V_S profiles from Japan are provided on the KiK-net database website, whereas various sources are used for the V_S profiles of sites in the US (Gibbs et al., 2000; Holzer and Youd, 2007; Thompson et al., 2010; Thornley et al., 2019; Afshari et al., 2019). A compromise is made to include a few sites with gaps in the V_S profile, typically at the top 1 to 2 m (e.g., KOCH05, SBSH01, YMTH02). Such V_S profiles are considered acceptable given that the shallow layer is expected to minimally impact the amplitudes at the site's fundamental mode. The V_S corresponding to the immediate underlying layer is considered for the missing portion. Figure 4.1 shows the location of the sites selected for the development of the proposed approach, including the 1D-like sites used for the calibration of D_{mul} and $\sigma_{\ln V_S}$ in Chapter 3. The measured V_S profiles are randomized to generate 50 profiles using the V_S model by Toro (1995) using $\sigma_{\ln V_S}$ = 0.25 and the other parameters recommended for sites with V_{S30} = 180 to 360 m/s. The site depths vary from 35 to 923 m, with 95% of the sites varying from 100 to 360 m, and most of them with a depth of 100 m.

The measured V_S profiles are considered flawless and discrepancies in site response predictions are attributed to modeling errors. V_S profiles could be adjusted based on the observed TF's fundamental mode as done by Tao and Rathje (2020a). However, this correcting approach implicitly assumes that deviations from a 1D-like TF are due to errors in the V_S profile, which might be accurate for some sites but could also be explained by non-vertical wave propagation and non-1D effects (Thompson et al., 2009). In lieu of a better approach, measured V_S profiles are used as published.

The damping profiles are estimated based on a laboratory-based relationship and density values are assumed based on V_S. The damping is estimated after Darendeli (2001) assuming PI = 0, OCR = 1, f_{load} = 1 Hz, and K_0 = 0.5. The resulting damping profiles are factorized by D_{mul} = 3. The

bulk density is assumed as 1,800 kg/m^3 for materials with V_S values lower than 760 m/s, and 2,200 kg/m^3 otherwise. Figure 4.2 shows examples of the input parameters for four sites.

4.5.2. GROUND-MOTION DATA

Ground-motion processing

Ground-motion data are accessed through the KiK-net, NEES, and CESMD databases. Additionally, the dataset for California is complemented with ground-motion recordings made available by Afshari et al. (2019). Ground motions from KiK-net and NEES are downloaded in raw format (count units) and processed using the software PRISM v2.1 (Processing and Review Interface for Strong Motion by Jones et al., 2017). Downloading the data in raw format allows for uniform processing across databases and the estimation of the event onset (t_0) using PRISM. t_0 is the time of the P-wave arrival estimated from the acceleration time history and is determined based on the rate of change of dissipated energy using the $P_{PHASE}P_{ICKER}$ algorithm (Kalkan, 2016). t_0 differentiates the noise from the noise and earthquake signal together in the acceleration time histories (Figure 4.3a) and thus allows for the computation of the signal-to-noise ratio (SNR) used to assess the quality of ground-motion recordings. Data from CESMD are not available in raw format, thus data in Volume 2 (V2) format are used, and data from Afshari et al. (2019) are used in their processed form.

Raw data are converted from counts to accelerations, baseline corrected, and filtered. An acausal filter is used with a lower corner frequency of 0.1 and a maximum of 25 Hz or higher, depending on the earthquake magnitude (Massa et al., 2010). The ground-motion data are only used up to 25 Hz as higher frequencies are affected by the instruments' anti-aliasing filters (Aoi et al., 2004). Most recordings have a sampling frequency of 200 Hz (time step of 0.005 s), and

recordings with lower sampling frequencies are resampled using the frequency-domain zero padding proposed by Lyons (2014) and implemented in PRISM and Matlab (Kalkan, 2021). To estimate t_0 using PRISM for the processed data from CESMD and Afshari et al. (2019), these recordings are converted to count units using arbitrary yet reasonable shifts and scaling factors. The artificially raw recordings are then processed using PRISM, the estimated t_0 is stored for the computation of SNR using the originally processed recordings, and the resulting processed recordings are disregarded.

Ground motion selection

Three criteria are considered to select ground-motion recordings appropriate for the quantification of site response residuals: (1) record component completeness, (2) SNR appropriateness, and (3) linear site response. An event is considered complete if all six components are available (three components from the sensor at depth and three from the sensor at ground surface) or at least four horizontal components, which is the case of data from CESMD and Afshari et al. (2019). The SNR of ground-motion recordings is computed as:

$$SNR = \frac{FAS_{noise+signal}}{FAS_{noise}} \tag{4.4}$$

where $\mathrm{FAS_{noise}}$ is the Fourier amplitude spectrum of the recording from the beginning (time, t = 0 s) to t_0, and $\mathrm{FAS_{noise+signal}}$ is the Fourier amplitude spectrum of the recording from t_0 to $2 \times t_0$ such that the same FAS abscissae are obtained. When available, the t_0 obtained for the vertical component is used on the two corresponding horizontal components as P waves are better observed in vertical ground motions and thus yield a more reliable t_0. Ground-motion recordings with SNR > 3 across frequencies from 0.5 Hz or at least half the site's fundamental frequency

(f/f_0 = 0.5) to 25 Hz are considered appropriate. Some of these criteria are relaxed for sites in California, given the limited number of recordings available (see Table 4.2 footnotes). Figure 4.3 shows an example of the t_0 and the SNR for a set of records.

Only ground-motion recordings not expected to yield soil nonlinearities are used. Recordings potentially leading to nonlinear behavior of soils are identified using the shear-strain index (I_γ), proposed by Idriss (2011), and defined as:

$$I_\gamma = \frac{PGV_{in}}{V_{S30}} \times 100\% \qquad (4.5)$$

where PGV_{in} is the peak ground velocity of the input motions, in the same units as V_{S30}. The ground motions yielding I_γ values lower than 0.005% are expected to yield shear strains lower than 0.01% on average (Kim et al., 2016) and are thus considered appropriate for linear elastic 1D SRAs (Kaklamanos et al., 2013). The vertical recordings are not screened based on this criterion.

Lastly, all ground motions are visually screened and recordings presenting obvious anomalies disregarded. After screening the sites based on the availability of a measured V_S profile and the ground motions, only sites with at least four two-component recorded events are kept. The maximum number of events per site is set at 120 (240 recordings) to reduce computational cost. Sites with more than 120 events are re-screened to keep the recordings with the wider frequency range of acceptable SNR values. The screened dataset consists of 534 sites, 518 from Japan and 16 from the US. From them, 39 sites are identified as 1D-like and used to calibrate D_{mul} and $\sigma_{\ln V_S}$ as discussed in Chapter 3. From the remaining 495 3D-like sites, five sites are used as examples to apply the proposed approach (Figure 4.11) and thus removed from the dataset. The remaining 490 sites are used for the quantification of c_{3D}^{SRA} and ϕ_{S2S}^{SRA}. Figure 4.4 shows the distribution of the

magnitude and epicentral distance of all the events in the dataset, and Figure 4.5 shows the number of usable recordings per normalized frequency.

4.5.3. SITE RESPONSE ANALYSIS

Site response analyses are conducted using NRATTLE, code written by C. Mueller, modified by R. Herrmann, and included in the suite of strong-motion programs Stochastic-Method SIMulations (SMSIM) by Boore (2005). NRATTLE uses the Thomson-Haskell solution to compute the 1D SH-wave TF (Thomson, 1950; Haskell, 1953) based on a V_S profile, density, and quality factors (Q_S) or small-strain damping. The ground-motion recordings at depth are input as vertically incident SH waves into the 1D models. Each of the two horizontal components is used independently in the analysis. The borehole ground-motion recordings used as input motions capture the wavefield of incident upgoing and reflected downgoing waves. Thus, a rigid base boundary condition (e.g., Kwok et al., 2007) is assumed for the analyses. All TFs are smoothed after Konno and Ohmachi (1998) with b = 40, and PSA response spectra (5% damping) computed using the package pyRotD (Kottke, 2018). Using other computer codes such as Shake2000 (Ordonez, 2012), STRATA (Kottke and Rathje, 2008), and DeepSoil (Hashash et al., 2020), leads to the same results as NRATTLE in linear elastic 1D SRAs.

Observed and theoretical TFs for four representative sites are presented in Figure 4.6. In general, the theoretical TFs present higher amplitudes than the observed TFs at the site's fundamental mode and often at some higher modes. The baseline theoretical TFs are more sharply peaked than the observed TFs and generally overpredict the fundamental and some higher modes. Results from the proposed approach (D_{mul} = 3 and $\sigma_{\ln V_S}$ = 0.25) show smoother median theoretical TFs compared to the baseline. The smoother TFs better capture the more uniform distribution of

energy across frequencies as indicated by the lower peak-to-trough ratio (e.g., Figure 4.6c) that is common in median observed TFs (De la Torre et al., 2021). These TFs more accurately estimate the observed TFs at the fundamental mode but lead to an overall underprediction of the high-frequency amplitudes. Similar trends are observed for AFs (Figure 4.7).

4.5.4. METHOD BIAS AND MODELING ALEATORY VARIABILITY

The site response residuals are calculated for TFs and AFs using Equation 4.1 and the c_{3D}^{SRA} computed using a mixed-effects regression. Figure 4.8 shows the c_{3D}^{SRA} and the residuals (95% confidence interval) for the four D_{mul}-$\sigma_{\ln V_S}$ cases. The c_{3D}^{SRA} corresponding to the baseline case (Figures 4.8a and 4.8b) shows a notorious overprediction of TFs and AFs at fundamental mode (f/f_0 = 1), which is reduced as damping is increased and by using randomized V_S profiles. Between the two, D_{mul} has a weaker effect than V_S randomization in reducing the overprediction at the fundamental mode (Figures 4.8c and 4.8d versus 4.8e and 4.8f). However, the proposed D_{mul}-$\sigma_{\ln V_S}$ combination leads to a nearly unbiased prediction of AFs, which is widely used in engineering practice (Figure 4.8f versus 4.8h). The underprediction observed at the high-frequency range is addressed in Step 3 of the proposed approach.

The site response residuals are partitioned into their components c_{3D}^{SRA}, $\delta S2S_S^{SRA}$, and δAMP_{es}^{SRA} and the results indicate that the proposed D_{mul}-$\sigma_{\ln V_S}$ pair leads to an overall reduction in c_{3D}^{SRA} and ϕ_{S2S}^{SRA} (Figure 4.9). The partition of residuals is conducted using a mixed-effects regression (Pinheiro et al., 2022) to account for the correlation among the varying number of ground-motion recordings at a given site. A significant reduction of the ϕ_{S2S}^{SRA} of TFs is obtained from Case 1 to Case 4 in the f/f_0 range from 1.6 to 8, and relatively minor differences are observed at lower and higher f/f_0 (Figure 4.9a). The ϕ_{S2S}^{SRA} of AFs presents a relatively modest reduction of

0.15 from Case 1 to Case 4 across frequencies (Figure 4.9b). The ϕ_{AMP}^{SRA} of TFs is the same for all the D_{mul}-$\sigma_{\ln V_S}$ scenarios given that TFs scale proportionally with D_{mul} and $\sigma_{\ln V_S}$ at a given frequency (Figure 4.9c). Lastly, the ϕ_{AMP}^{SRA} of AFs presents a reduction of about 0.2 at the fundamental mode from Case 1 to Case 4, and around 0.1 at higher frequencies (Figure 4.9d). A reduction in c_{3D}^{SRA} indicates that the estimated FAS or PSA at the surface are more accurate and only a small bias correction is required. A smaller ϕ_{S2S}^{SRA} indicates more confidence in the estimated response. Conducting 1D SRAs following the proposed approach leads to c_{3D}^{SRA} ranging from -0.5 to 0.5 for TFs and AFs, ϕ_{S2S}^{SRA} around 0.6 for TFs and from 0.4 to 0.5 for AFs, and ϕ_{AMP}^{SRA} nearly constant around 0.4 and 0.3 for TFs and AFs, respectively. Recommended models for c_{3D}^{SRA} and ϕ_{S2S}^{SRA} are provided as values for various f/f_0 or normalized period (T/T_0) in Table 4.3, and presented in Figures 4.8g, 4.8h, and 4.9a to 4.9d.

These results are consistent with findings from previous studies that have used a similar database. The results are not fully comparable as such studies did not use the normalized frequency in the estimation of the residual analysis, but some trends can be observed. For TFs, the estimated ϕ_{S2S}^{SRA} is higher at low frequencies and lower at high frequencies compared to Zhu et al. (2022), and a similarly minor effect of damping models is observed. For AFs, the estimated c_{3D}^{SRA} is lower (i.e., closer to zero or more negative) than Kaklamanos et al. (2013), although with similarly low values across frequencies. The ϕ_{S2S}^{SRA} of AFs is slightly lower than the estimated by Kaklamanos et al. (2013), and the ϕ_{AMP}^{SRA} of AFs similar. Various studies showed very consistent trends in the ϕ_{AMP}^{SRA} estimates.

4.6. COMPARISON AGAINST BOREHOLE DATA

To illustrate the predictive capability of the proposed approach, TFs and AFs are computed for five KiK-net sites and results compared to observations. Data from these sites were not used in the statistical analyses and were rather selected based on a preliminary evaluation indicating that their site terms in TFs at f/f_0 = 1 (i.e., $\delta S2S_s^{SRA}$) spanned across from underprediction to overprediction. These sites were also selected as they are all about 100 m deep, which are the most abundant sites in the available dataset. The cumulative distributions of site terms estimated based the recommended c_{3D}^{SRA} models (Table 4.3) for TFs and AFs including the approximate location of the five selected KiK-net sites are presented in Figures 4.10a and 4.10b, respectively. Note that the ranking of a site's site term in AFs does not uniformly translate to the ranking in site terms for TFs. This is particularly evident for the site SZOH32.

Figure 4.11 illustrates a comparison between observations and results from the proposed approach for the five KiK-net sites in terms of TFs and AFs. The best-estimate responses show an overall ability to capture well the median observed responses (Figures 4.11c to 4.11f) but also the potential for discrepancies. The discrepancies observed in AFs at the fundamental modes cover the range of possible accuracy achieved by the proposed approach. In cases where the best estimate response does not capture the observed median well, the 5th and 95th percentiles manage to envelop it. An exception to this is observed for GIFH14, a site that presents a dominant mode around 3 Hz. Such high amplitudes at the dominant frequency are explained by the additional variability in site response residuals ϕ_{AMP}^{SRA}, whose effects are assumed to be included in the input motion in seismic hazard analyses, and thus not considered to address modeling errors in the proposed approach. Overall, the proposed approach provides more accurate site response predictions compared to a more traditional approach (baseline case), as well as the ability to envelope the median responses.

4.7. EFFECT OF SITES' REGION AND TYPE

As previously described, c_{3D}^{SRA}, ϕ_{S2S}^{SRA}, and ϕ_{AMP}^{SRA} are quantified based on data from 490 3D-like borehole sites from Japan and the US (Figures 4.8 and 4.9). This approach is preferred as grouping the sites according to their compliance to the 1D assumptions (1D-like or 3D-like), or region as such an approach (1) requires a taxonomy for the identification of the site type when no ground-motion data are available, and (2) reduces the data to smaller groups of sites. In this section, c_{3D}^{SRA}, ϕ_{S2S}^{SRA}, and ϕ_{AMP}^{SRA} are calculated considering the sites' compliance to 1D assumptions and geographical location. While the geographical location is not expected to be a factor controlling site response, grouping the sites by their location either in Japan or California could capture geomorphological aspects and ground surface features (Nweke et al., 2022; Pilz et al., 2022) leading to differences in site response accuracy. There are 39 1D-like sites and 490 3D-like sites, 480 of them located in Japan, nine in California, and one in Alaska. All 1D SRAs in this section are conducted considering D_{mul} = 3, and $\sigma_{\ln V_S}$ = 0.25. A comparison of observed and theoretical TFs and AFs for the 39 1D-like sites is presented in Appendices E and F, and TFs and AFs for the nine 3D-like sites in California in Appendices G and H.

The site response residuals for 1D-like sites indicate underprediction at f/f_0 = 1 and overall lower standard deviations, compared to the 3D-like sites (Figure 4.12). The c_{1D}^{SRA} (method bias for 1D-like sites), show an overall underprediction of the TFs in 0.5 ln units across frequencies (Figure 4.12a), whereas the AFs are nearly unbiased (Figure 4.12b). Compared to c_{3D}^{SRA}, c_{1D}^{SRA} tends towards an underprediction of the fundamental mode as opposed to the overprediction exhibited by c_{3D}^{SRA} (Figures 4.12g and 4.12h). This tendency is expected as, unlike 3D-like sites, the 1D-like sites often present a good agreement between the theoretical and observed TFs' fundamental

modes. Therefore, the extent to which overpredictions occur at f/f_0 = 1 is reduced. The ϕ_{S2S}^{SRA} for 1D-like sites (Figures 4.13a and 4.13b) is slightly higher or equal than the ϕ_{S2S}^{SRA} for 3D-like sites at the fundamental mode, and mostly lower by 0.1 to 0.2 at higher frequencies. Lastly, there is no significant difference in the estimated ϕ_{AMP}^{SRA}, except at f/f_0 higher than seven, where a slight reduction is observed for the 1D-like sites in both TFs and AFs.

The site response residuals for California are similar in tendency to the global data, clearly dominated by the Japanese sites, but they show a different trend in the observed ϕ_{S2S}^{SRA} and ϕ_{AMP}^{SRA} across frequencies. The c_{3D}^{SRA} for TFs for sites in California shows stronger under- and overpredictions, although with a similar trend with frequency (Figure 4.12c), whereas minor differences are observed in c_{3D}^{SRA} for AFs (Figure 4.12d). The ϕ_{S2S}^{SRA} for TFs for sites in California is higher near the fundamental mode by about 0.3 (Figure 4.13a) and significantly lower at higher frequencies, with values nearing zero at some f/f_0 values. These near-zero values are given by the very limited data available for California that cannot capture a more realistic residual variability. The ϕ_{S2S}^{SRA} for AFs for sites in California are consistently lower in about 0.2 to 0.3 ln units (Figure 4.13b) compared to the ϕ_{S2S}^{SRA} based on the global dataset, and lower than the ϕ_{S2S}^{SRA} estimated by Stewart and Afshari (2020) overall. Lastly, there is no significant difference in the estimated ϕ_{AMP}^{SRA}, except an increase at f/f_0 lower than 1.1 and a consistent decrease at f/f_0 higher than eight. The ϕ_{AMP}^{SRA} for California is consistent with findings by Stewart and Afshari (2020). The Japanese dataset represents 98% of the global dataset and thus results are nearly the same and not described. Unsurprisingly, these results indicate that the data from the US do not contribute to the estimation of the recommended c_{3D}^{SRA}, ϕ_{S2S}^{SRA}, or ϕ_{AMP}^{SRA}.

4.8. APPLICABILITY TO OUTCROP GROUND MOTIONS

The proposed approach is developed based on borehole data, whereas forward site response predictions and ground-motion model developments are based on rock outcropping and free field data. Concerns regarding the use of borehole recordings are due to the wave cancelling effects that such recordings carry. The wave-cancelling effect refers to the destructive interference of the upgoing and downgoing waves (Bonilla et al., 2002) that leads to near-zero amplitude at some frequencies in borehole recordings and thus unrealistically high amplitudes in observed TFs (e.g., site OKYH14 at 5 Hz in Figure 14e). Given that these TF amplitudes are not associated with the subsurface structure or site-specific factors controlling the site response, they are referred to as pseudo-resonances (Tao and Rathje, 2020b).

Various researchers investigated wave-cancelling effects and proposed methods for using borehole data (e.g., Clayton and Wiggins, 1976; Mehta et al., 2007; Parolai et al., 2010; Cadet et al., 2011; Chandra et al., 2015), however, no method is established to date. Tao and Rathje (2020a, 2020b) propose a taxonomy for identifying sites affected by pseudo-resonances and recommend that these sites not be used in site response validation studies. Contrary to this, Stewart and Afshari (2020) suggest that pseudo-resonances be embraced and considered in the evaluation of the 1D SRA predicting capabilities. While the effect of pseudo-resonances leads to the overestimation of TF amplitudes, within the context of this paper, the question we try to answer is whether pseudo-resonances affect the site response bias, c_{3D}^{SRA}, and the standard deviations of the site response residual components, ϕ_{S2S}^{SRA} and ϕ_{AMP}^{SRA}.

An initial investigation to evaluate the effect of pseudo-resonances on c_{3D}^{SRA}, ϕ_{S2S}^{SRA}, and ϕ_{Amp}^{SRA} is conducted with the aim to find any distinctive difference. To this end, sites not affected

by pseudo-resonances are first selected from the database. Tao and Rathje (2020b) suggest that true resonances are those captured by outcropping theoretical TFs (i.e., TFs calculated using the outcropping boundary condition), whereas pseudo-resonances are captured by within theoretical TFs. In addition, the authors indicate that the absence of a distinct velocity contrast in the V_S profile is suggestive of the presence of pseudo-resonances. Based on these observations, sites with similar fundamental frequency from the outcropping and within TFs (D_{mul} = 1, no randomization) with 15% of similarity are considered free of pseudo-resonances. In cases where the similarity of the TFs alone does not suggest the presence of absence of pseudo-resonances, the site's V_S profile is inspected. Figure 4.14 shows examples of sites with and without pseudo-resonances, and a complete set of figures for all sites identified to be unaffected by pseudo-resonances is presented in Appendix I. Any discrepancies between the theoretical and observed TFs is not considered in this selection and rather attributed to 3D effects.

The 490 sites used for the statistical analysis are separated into 40 sites identified as free of pseudo-resonances (N-P), and the remaining 450 sites with pseudo-resonances (P). Residuals are computed for each group, and the statistical analyses conducted to recompute c_{3D}^{SRA}, ϕ_{S2S}^{SRA}, and ϕ_{AMP}^{SRA}. The results show minor differences between $\left(c_{3D}^{SRA}\right)^{P}$, $\left(\phi_{S2S}^{SRA}\right)^{P}$, and $\left(\phi_{AMP}^{SRA}\right)^{P}$ (Figures 4.15c, 4.15d, and 4.16), and the proposed global c_{3D}^{SRA}, ϕ_{S2S}^{SRA}, and ϕ_{AMP}^{SRA} (Figures 4.8g, 4.8h, and 4.9). The method bias $\left(c_{3D}^{SRA}\right)^{N-P}$ is higher than $\left(c_{3D}^{SRA}\right)^{P}$ by 0.3 to 0.7 for TFs and 0.5 for AFs at f/f_0 lower than 2; whereas it is slightly lower at higher frequencies (Figure 4.15). The standard deviation $\left(\phi_{S2S}^{SRA}\right)^{N-P}$ is higher than $\left(\phi_{S2S}^{SRA}\right)^{P}$ by about 0.2 and 0.15 for TFs and AFs around the fundamental mode, and by about 0.3 and 0.2 for TFs and AFs starting at f/f_0 = 10 (Figures 4.15c

and 4.15d). Lastly, the standard deviations $\left(\phi_{\mathrm{AMP}}^{\mathrm{SRA}}\right)^{\mathrm{N-P}}$ and $\left(\phi_{\mathrm{S2S}}^{\mathrm{SRA}}\right)^{\mathrm{P}}$ fluctuates within a 0.05 range (Figures 4.16e and 4.16f).

Overall, results for sites considered unaffected by pseudo-resonances indicate higher c_{3D}^{SRA} for f/f_0 up to around 3 and higher ϕ_{S2S}^{SRA} around f/f_0 = 1 and f/f_0 higher than 9. To remove the effect of the lower number of sites free of pseudo-resonances, mixed-effects regressions are conducted for suites of 40 sites randomly sampled without replacement from the dataset of 450 sites affected by pseudo-resonances. The results confirmed the observed trends (Figure 4.16) and variability at intermediate frequencies. Similar to the results for 1D-like sites, the higher c_{3D}^{SRA} and ϕ_{S2S}^{SRA} values near the fundamental frequency are due to the similarity in the theoretical and observed TFs' fundamental modes.

These findings show that there is potential for further underprediction of the median site response, and higher ϕ_{S2S}^{SRA} and ϕ_{AMP}^{SRA} in applications using outcropping ground-motion recordings. Given (1) the relatively low number of sites free of pseudo-resonances, (2) the assumptions made in the selection of such sites, and (3) the impact that these results would have on site response and seismic hazard applications, the values for c_{3D}^{SRA} and ϕ_{S2S}^{SRA} in Table 4.3 are still preferred for practical applications. The results presented in this section encourage the need for further investigations regarding the applicability of borehole data-based lessons to outcropping applications.

4.9. EXAMPLE APPLICATION

The proposed approach is used to estimate the site response at a hypothetical project site selected for the construction of a rigid structure with a period of approximately 0.1 s. The site is located on

30 m-thick old deposit of dense alluvial soils overlying a bedrock with V_S = 1080 m/s at the top 30 m. A single measured V_S profile available for the site (Figure 4.17b). The closest active fault is located 25 km away from the site, and the highest historical earthquake magnitude is M_w6.0. The engineers leading the design of the structure are concerned about the seismic demands during an earthquake of similar magnitude and with a predominant period close to the structure' resonant period. The analysts decide to conduct a deterministic seismic hazard analysis and 1D SRAs to estimate the seismic demand at the foundation level of the structure.

4.9.1. SEISMIC DEMAND

A deterministic scenario is defined based on the site's characteristics, and the response spectrum estimated using the Abrahamson et al. (2014) GMM (Figure 4.17c). For practical purposes, this spectrum is considered representative of the seismic demand at the base of the alluvial deposit. A more appropriate estimation requires (1) accounting for the differences in the site-specific V_S profiles and the implied by the GMM (Williams and Abrahamson, 2021), (2) the location at a depth of 30 m for the application of the input ground motions (Pretell, Ziotopoulou et al., under review), and (3) the estimation of the response spectrum at surface using a single-station sigma given that the site response is estimated using 1D SRAs (e.g., Al Atik, 2015).

Thirteen ground motions are selected from the NGA-West2 database (Ancheta et al., 2013), and scaled such that their mean approximately matches the target response spectrum (Figure 4.17c). The potential for soil nonlinearity is evaluated based on the shear strain index, I_γ, with V_{S30} = 450 m/s. All values are lower than 0.05%, thus linear elastic SRAs are appropriate, and the proposed approach is well-suited for estimating the site response.

4.9.2. PROPOSED APPROACH

Step 1: Site characterization

The site characterization consists of estimating the baseline V_S profile, and laboratory-based damping profile. The baseline V_S profile is taken from the available field measurement (Figure 4.17b), whereas the damping profile is estimated after Darendeli (2001), considering the mean effective stress at the middle of each V_S layer (Figure 4.17a).

Step 2: Increased damping profile, and randomized V_S profiles

The baseline damping and V_S profiles are adjusted to remove the errors intrinsic to 1D SRAs as a tool. The minimum damping profile estimated after Darendeli (2001) is increased by $D_{mul} = 3$. In addition, the top 30 m of the baseline V_S profile corresponding to the alluvial deposit are randomized to generate fifty V_S profiles using the V_S model after Toro (1995) with $\sigma_{\ln V_S} = 0.25$. The other parameters used for the Toro model are those recommended by Toro for sites with V_{S30} from 180 to 360 m/s. The obtained damping and randomized V_S profiles are shown in Figure 4.17.

Step 3: Uncorrected median site response

The input ground motions are propagated through each of the randomized V_S profiles to obtain the response at ground surface (Figure 4.18). An outcropping boundary condition is considered for the base of the models. Fifty FAS and acceleration response spectra per input ground motion are obtained at surface, and the median values considered the uncorrected (biased) best estimate responses for each one of the input motions (Figures 4.18e and 4.18f). Results are presented in FAS from 0.04 to 0.25 s (half the fundamental frequency ≈ 4 Hz, to 25 Hz), but PSA at shorter periods are also presented as they are often controlled by the longer period range (Douglas and

Boore, 2011). FAS and PSA estimates at periods longer the site's fundamental mode can be estimated using GMM (e.g., Bayless and Abrahamson, 2019).

Step 4: Bias correction

The median FAS and PSA response spectrum at ground surface are corrected to account for the 1D-SRA bias. The bias correction is conducted by scaling the T/T_0 in Table 4.3 by the site's fundamental period ($T_0 \approx 0.125\ s$) fundamental values and then adding the c_{3D}^{SRA} values for TFs or AFs as needed, to the median responses obtained in Step 3. The resulting bias-corrected FAS and PSA (Figures 4.18g and 4.18h) are the best estimate for a given input motion.

Step 5: Modeling epistemic uncertainty

The bias-corrected best estimate TFs and AFs assume that the proposed approach and 1D SRAs are capable of perfectly estimating the site response, which is unrealistic. To account for the potential response to be higher or lower due to unmodeled features affecting the response with a 90% confidence interval, the best estimate bias-corrected TFs and AFs are shifted by $\pm 1.65 \times \phi_{S2S}^{SRA}$. The resulting 5th and 95th percentiles, and the median of all input motions, are presented in Figures 4.18g and 4.18h. These are plausible responses that should be considered in design decisions.

4.9.3. RECOMMENDED PATH FORWARD

The site response evaluation indicates that the median PSA expected at a period of 0.1 s is approximately 0.145g. However, when accounting for modeling errors, it is possible that the PSA be as high as 0.32g. Whether the median or 95th percentile PSA value is used for design of the structure depends on the project-specific engineering and non-engineering related aspects.

However, it is recommended that at the very minimum (1) the bias-corrected median be used for design, and (2) the 95th site response percentile be checked, and the design adjusted as needed to prevent catastrophic failure caused by this seismic demand.

4.10. CONCLUSIONS

An approach for conducting linear elastic 1D site response analyses (SRAs) developed based on borehole data was presented. This approach (1) uses damping multipliers (D_{mul} = 3) and V_S randomization to improve site response predictions and (2) accounts for the 1D-SRA bias (c_{3D}^{SRA}) and the modeling errors, quantified through the standard deviation ϕ_{S2S}^{SRA}, carried by the inability of 1D SRAs to capture non-1D effects affecting site response. Current engineering practice expects 1D SRAs to provide accurate site response estimates and neglects modeling errors. This is an unrealistic expectation.

Comparisons of ground-motion data from 534 borehole sites against 1D SRA predictions in terms of transfer functions (TFs) and amplification factors (AFs) showed trends in the discrepancies. An overall site response overprediction is observed in the low-frequency range, and underpredictions in the high-frequency range. The use of randomized V_S profiles reduces the overpredictions at the frequency modes and leads to median TFs and AFs with a more uniform distribution of energy (i.e., site response amplitudes) across frequencies, similar to the observed median responses. The use of D_{mul} = 3 to increase damping leads to the estimation of nearly unbiased AFs across frequencies. Despite these improvements, site response estimates from 1D SRA conducted with D_{mul} and randomized V_S profiles are still biased and present significant variability in their site terms $\left(\delta S2S_S^{SRA}\right)$. The proposed approach addresses these concerns by bias-correcting the predicted responses and considering the 5th and 95th site response percentiles.

An investigation of the effect of pseudo-resonances on the proposed approach indicates that outcropping applications could potentially require a stronger bias-correction to prevent underpredictions and a larger shift of the bias-corrected median response to account for 1D SRA modeling errors. This finding further stresses the need for investigating the applicability of findings from site response studies using borehole data for engineering applications. Given the assumptions made in this investigation and recognizing that current practices assume $c_{3D}^{SRA} = 0$ and $\phi_{S2S}^{SRA} = 0$, using borehole-data base estimates is considered a step forward in our practice regardless of the potential issues associated with borehole data.

The recommended values for c_{3D}^{SRA} and ϕ_{S2S}^{SRA} are tied to the proposed approach for conducting 1D SRAs, and thus the provided recommendations should be closely followed. Reducing the magnitude of the recommended ϕ_{S2S}^{SRA} would likely require conducting 2D or 3D SRAs and considering the ϕ_{S2S}^{SRA} associated with those numerical approaches. The proposed c_{3D}^{SRA} and ϕ_{S2S}^{SRA} are valid for linear elastic analyses but the framework can be extended to nonlinear SRAs.

4.11. REFERENCES

Abrahamson NA, Silva WJ and Kamai R (2014) Summary of Abrahamson and Silva NGA ground-motion relation for active crustal regions. *Earthquake Spectra* 30(3): 1025–1055.

Abrahamson NA, Somerville PG and Cornell CA (1990) Uncertainty in numerical strong motion predictions. In: *Proceedings of the 4th U.S. National Conference on Earthquake Engineering*, 1, 407-416.

Afshari K, Stewart JP and Steidl JH (2019) California ground motion vertical array database. *Earthquake Spectra* 35(4): 2003–2015.

Al Atik (2015) *NGA-East: Ground-motion standard deviation models for Central and Eastern North America.* Report PEER 2015/07, June. Berkeley, CA: Pacific Earthquake Engineering Research Center (PEER), University of California, Berkeley.

Al Atik L, Abrahamson N, Bommer JJ, Scherbaum F, Cotton F and Kuehn N (2010) The variability of ground-motion prediction models and its components. *Seismological Research Letters* 81: 794–801.

Ancheta TD, Darragh RB, Stewart JP, Seyhan E, Silva WJ, Chiou BSJ, Wooddell KE, Graves RW, Kottke AR, Boore DM, Kishida T and Donahue JL (2013) *PEER NGA-West2 database.* Report PEER 2013/03, May. Berkeley, CA: Pacific Earthquake Engineering Research Center (PEER), University of California, Berkeley.

Aoi S, Kunugi T and Fujiwara H (2004) "Strong-motion seismograph network operated by NIED: K-NET and KiK-net." *Journal of Japan Association for Earthquake Engineering* 4(3): 65–74.

Atkinson GM (2006) Single-station sigma. *Bulletin of the Seismological Society of America* 96(2): 446–455.

Bayless J and Abrahamson NA (2019) Summary of the BA18 ground-motion model for Fourier amplitude spectra for crustal earthquakes in California. *Bulletin of the Seismological Society of America* 109(5): 2088–2105.

Bazzurro P and Cornell CA (2004) Nonlinear soil site effects in probabilistic seismic hazard analysis. *Bulletin of the Seismological Society of America* 94: 2110–2123.

Bonilla LF, Steidl JH, Gariel J-C and Archuleta RJ (2002) Borehole response studies at the Garner Valley Downhole Array, Southern California. *Bulletin of the Seismological Society of America* 92(8): 3165–3179.

Boore DM (2003) Prediction of ground motion using the stochastic method. *Pure and Applied Geophysics* 160: 635–676.

Boore DM (2005) *SMSIM – Fortran programs for simulating ground motions from earthquakes: Version 2.3 – A revision of OFR 96–80-A.* United States Geological Survey (USGS) Open File Report 00–509, revised.

Cadet H, Bard P-Y and Rodriguez-Marek A (2011) Site effect assessment using KiK-net data: Part 1. A simple correction procedure for surface/downhole spectral ratios. *Bulletin of Earthquake Engineering* 10(2): 421–448.

Chandra J, Gueguen P, Steidl JH and Bonilla LF (2015) In situ assessment of the G-γ curve for characterizing the nonlinear response of soil: Application to the Garner Valley Downhole Array and the Wildlife Liquefaction Array. *Bulletin of the Seismological Society of America* 105(2A): 993–1010.

Clayton RW and Wiggins RA (1976) Source shape estimation and deconvolution of teleseismic body waves. *Journal of the Royal Astronomical Society* 47: 151–177.

Darendeli MB (2001) *Development of a new family of normalized modulus reduction and material damping curves.* PhD Dissertation, The University of Texas at Austin, Austin, TX.

De la Torre CA, Bradley BA and McGann CR (2021) 2D geotechnical site-response analysis including soil heterogeneity and wave scattering. *Earthquake Spectra* 38(2): 1124–1147.

Douglas J and Boore DM (2011) High-frequency filtering of strong motion records. *Bulletin of Earthquake Engineering* 9: 395–409.

EPRI (2013) *Seismic Evaluation Guidance: Screening, Prioritization and Implementation Details (SPID) for the Resolution of Fukushima Near Term Task Force Recommendation 2.1. Seismic*, Report 1025287, February. Palo Alto, CA.

Gibbs JF, Tinsley JC, Boore DM and Joyner WB (2000) Borehole velocity measurements and geological conditions at thirteen sites in the Los Angeles, California region. United States Geological Survey (USGS) Open File Report 00–470.

Hashash YMA, Musgrove MI, Harmon JA, Ilhan O, Xing G, Numanoglu O, Groholski DR, Phillips CA and Park D (2020) *DEEPSOIL 7, User Manual.* Urbana, IL, Board of Trustees of University of Illinois at Urbana-Champaign.

Haskell NA (1953) The dispersion of surface waves on multilayered media. *Bulletin of the Seismological Society of America*, 72: 17–34.

Holzer TL and Youd TL (2007) Liquefaction, ground oscillation, and soil deformation at the Wildlife Array, California. *Bulletin of the Seismological Society of America* 97(3): 961–976.

Idriss IM (2011) Use of V_{S30} to represent local site conditions. In: *Fourth International Association of Seismology and Physics of the Earth's Interior/International Association of Earthquake Engineering International Symposium on the Effects of Surface Geology on Seismic Motion (ESG4)*, Santa Barbara, CA, 23-26 August.

Jones JM, Kalkan E, Stephens CD and Peter Ng (2017) *PRISM software – Processing and review interface for strong-motion data: U.S. Geological Survey Techniques and Methods.* Book 12, Chapter A2, 4 p.

Joyner WB, Warrick RE and Fumal TE (1981) The effect of Quaternary alluvium on strong ground motion in the Coyote Lake, California, earthquake of 1979. *Bulletin of the Seismological Society of America* 71: 1333–1349.

Kaklamanos J, Bradley BA, Moolacattu AN, et al. (2020) Physical hypotheses for adjusting coarse profiles and improving 1D site response estimation assessed at 10 KiK-net sites. *Bulletin of the Seismological Society of America* 110(3): 1338–1358.

Kaklamanos J, Bradley BA, Thompson EM and Baise LG (2013) Critical parameters affecting bias and variability in site-response analyses using KiK-net downhole array data. *Bulletin of the Seismological Society of America* 103: 1733–1749.

Kalkan E (2016) An automatic P-phase arrival time picker. *Bulletin of the Seismological Society of America* 106(3): 971–986.

Kalkan E (2021) Frequency-domain Zero-padding Resampling (Interpolation) (www.mathworks.com/matlabcentral/fileexchange/58854-frequency-domain-zero-

padding-resampling-interpolation), MATLAB Central File Exchange. Retrieved December 12, 2021.

Kim B, Hashash YMA, Stewart JP, Rathje EM, Harmon JA, Musgrove MI, Campbell KW and Silva WJ (2016) Relative differences between nonlinear and equivalent-linear 1-D site response analyses. *Earthquake Spectra* 32(3): 1845–1865.

Konno K and Ohmachi T (1998) Ground-motion characteristics estimated from spectral ratio between horizontal and vertical components of microtremor. *Bulletin of the Seismological Society of America* 88(1): 228–241.

Kottke AR (2018) pyrotd v0.5.4. Zenodo. https://doi.org/10.5281/zenodo.1322849

Kottke AR and Rathje EM (2008) *Technical manual for Strata.* Report No.: 2008/10, December. Berkeley, CA: Pacific Earthquake Engineering Research Center (PEER), University of California, Berkeley.

Kwok AOL, Stewart JP, Hashash YMA, Matasovic N, Pyke R, Wang Z and Yang Z (2007) Use of exact solutions of wave propagation problems to guide implementation of nonlinear seismic ground response analysis procedures. *Journal of Geotechnical and Geoenvironmental Engineering* 133(11): 1385–1398.

Lyons RG (2014) *Understanding digital signal processing.* Third edition: Indiana, Prentice Hall, 954 p.

Massa M, Pacor F, Luzi L, Bindi D, Milana G, Sabetta F, Gorini A and Marcucci S (2010) The ITalian ACcelerometric Archive (ITACA) – Processing of strong-motion data. *Bulletin of Earthquake Engineering* 8(5): 1175–1187.

Mehta K, Snieder R and Graizer V (2007) Downhole receiver function: A case study. *Bulletin of the Seismological Society of America* 97(5): 1396–1403.

Menq FY (2003) *Dynamic properties of sandy and gravelly soils.* PhD Dissertation, The University of Texas at Austin, Austin, TX.

Nakamura Y (2019) What is the Nakamura method? *Seismological Research Letters* 90: 1437–1443.

NIED (2019) NIED K-NET, KiK-net, National Research Institute for Earth Science and Disaster Resilience.

Nweke CC, Stewart JP, Wang P and Brandenberg SJ (2022) Site response of sedimentary basin and other geomorphic provinces in southern California. *Earthquake Spectra* 00(0): 1–30.

Ordonez G (2012) *SHAKE2000 – A computer program for the 1D analysis of geotechnical earthquake engineering problems.* Washington: GeoMotions, LLC.

Parolai S, Bindi D, Ansal A, Kurtulus A, Strollo A and Zschau J (2010) Determination of shallow S-wave attenuation by down-hole waveform deconvolution: a case study in Istanbul (Turkey). *Geophysical Journal International* 181: 1147–1158.

Passeri F, Foti S, Cox BR and Rodriguez-Marek A (2019) Influence of epistemic uncertainty in shear wave velocity on seismic ground response analyses. *Earthquake Spectra* 35(2): 929–954.

Pehlivan M, Rathje EM and Gilbert RB (2016) Factors influencing soil surface hazard curves. *Soil Dynamics and Earthquake Engineering* 83(2016): 180–190.

Pilz M, Cotton F and Zhu C (2022) How much are sites affected by 2-D and 3-D site effects? A study based on single-station earthquake records and implications for ground motion modeling. *Geophysics Journal International* 228: 1992–2004.

Pinheiro J, Bates D, DebRoy S and Sarkar D (2022) NLME: Linear and nonlinear mixed effects models. Vienna, Austria: R Foundation for Statistical Computing.

Pretell R, Ziotopoulou K, Watson-Lamprey JA, Sinha SK and Zekkos D (under review) Double convolution approach for developing input ground motions.

Pretell R, Ziotopoulou K and Abrahamson NA (2022) Conducting 1D site response analyses to capture 2D V_S spatial variability effects. *Earthquake Spectra* 38(3): 2235–2259.

Rodriguez-Marek A, Bommer JJ, Youngs RR, Crespo MJ, Stafford PJ and Bahrampouri M (2020) Capturing epistemic uncertainty in site response. *Earthquake Spectra* 37(2): 921–936.

Rodriguez-Marek A, Cotton F, Abrahamson NA, Akkar S, Al Atik L, Edwards B, Montalva GA and Dawood HM (2013) A model for single-station standard deviation using data from various tectonic regions. *Bulletin of the Seismological Society of America* 103: 3149–3163.

Rodriguez-Marek A, Montalva GA, Cotton F and Bonilla F (2011) Analysis of single-station standard deviation using the KiK-net data. *Bulletin of the Seismological Society of America* 101, 1242–1258.

Rodriguez-Marek A, Rathje E, Ake J, Munson C, Stovall S, Weaver T, Ulmer K and Juckett M (2021) *Documentation report for SSHAC level 2: Site response.* Research Information Letter, Office of Nuclear Regulatory Research. RIL2021-15. San Antonio, TX. Nov. 2021.

Rodriguez-Marek A, Rathje E, Bommer J, Scherbaum F and Stafford P (2014) Application of single-station sigma and site-response characterization in a probabilistic seismic-hazard analysis for a new nuclear site. *Bulletin of the Seismological Society of America* 104(4):1601–1619.

Stewart JP and Afshari K (2020) Epistemic uncertainty in site response as derived from one-dimensional ground response analysis. *Journal of Geotechnical and Geoenvironmental Engineering* 147(1): 04020146.

Stewart JP, Afshari KA and Hashash YMA (2014) *Guidelines for performing hazard-consistent one-dimensional ground response analysis for ground motion prediction.* Report No.: 2014/16, October. Berkeley, CA: Pacific Earthquake Engineering Research Center (PEER), University of California, Berkeley.

Tao Y and Rathje E (2019) Insights into modeling small-strain site response derived from downhole array data. *Journal of Geotechnical and Geoenvironmental Engineering* 145(7): 04019023.

Tao Y and Rathje E (2020a) Taxonomy for evaluating the site-specific applicability of one-dimensional ground response analysis. *Soil Dynamics and Earthquake Engineering* 128(2020): 105865.

Tao Y and Rathje E (2020b) The importance of distinguishing pseudoresonances and outcrop resonances in downhole array data. *Bulletin of the Seismological Society of America* 110(1): 288–294.

Thompson EM, Baise LG, Kayen RE and Guzina BB (2009) Impediments to predicting site response: Seismic property estimation and modeling simplifications. *Bulletin of the Seismological Society of America* 99(5): 2927–2949.

Thompson EM, Baise LG, Tanaka Y and Kayen RE (2012) A taxonomy of site response complexity. *Soil Dynamics and Earthquake Engineering* 41: 32–43.

Thompson EM, Kayen RE, Carkin B and Tanaka H (2010) *Surface-wave site characterization at 52 strong-motion recording stations affected by the Parkfield, California, M6.0 Earthquake of 28 September 2004.* United States Geological Survey (USGS) Open File Report 2010–1168, 117 pp.

Thomson WT (1950) Transmission of elastic waves through a stratified solid. *Journal of Applied Physics* 21: 89–93.

Thornley J, Dutta U, Fahringer P and Yang Z (J) (2019) In situ shear-wave velocity measurements at the Delaney Park downhole array, Anchorage, Alaska. *Seismological Research Letters* 90(1): 395–400.

Toro GR (1995) *Probabilistic models of the site velocity profiles for generic and site-specific ground-motion amplification studies*. Report 779574, Brookhaven National Laboratory, Upton, NY, 17 November.

Williams T and Abrahamson N (2021) Site-response analysis using the shear wave velocity profile correction approach. *Bulletin of the Seismological Society of America* 111(4): 1989–2004.

Zhu C, Cotton F, Kawase H, Haendel A, Pilz M and Nakano K (2022) How well can we predict earthquake site response so far? Site-specific approaches. *Earthquake Spectra* 38(2): 1047–1075.

FIGURES

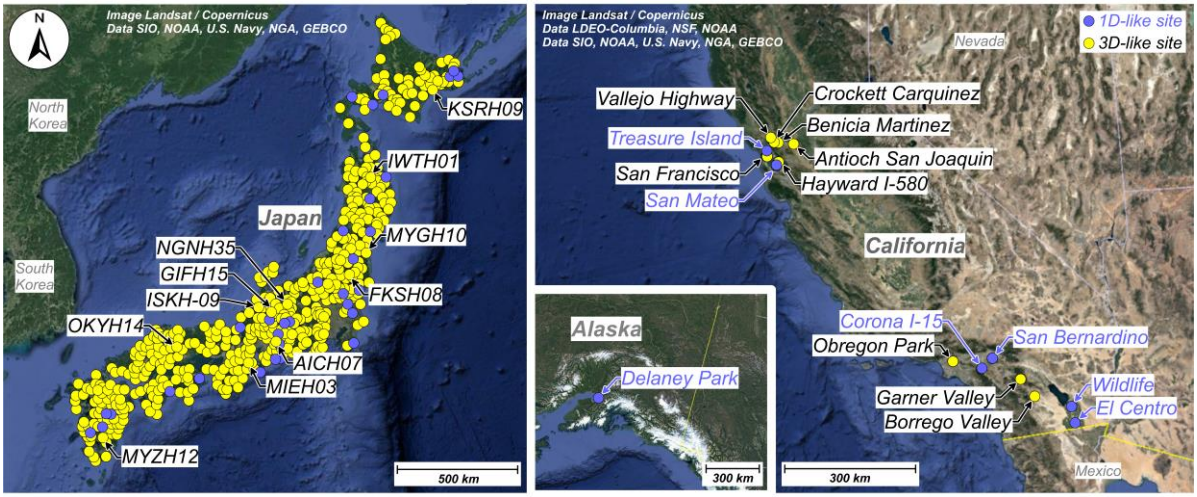

Figure 4.1. Borehole site locations differentiating types as 1D- or 3D-like: (a) sites in Japan, (b) sites in California with an insert closeup view of the Delaney Park site in Alaska. *Note: 3D-like KiK-net sites used as examples throughout this paper are labeled for reference.*

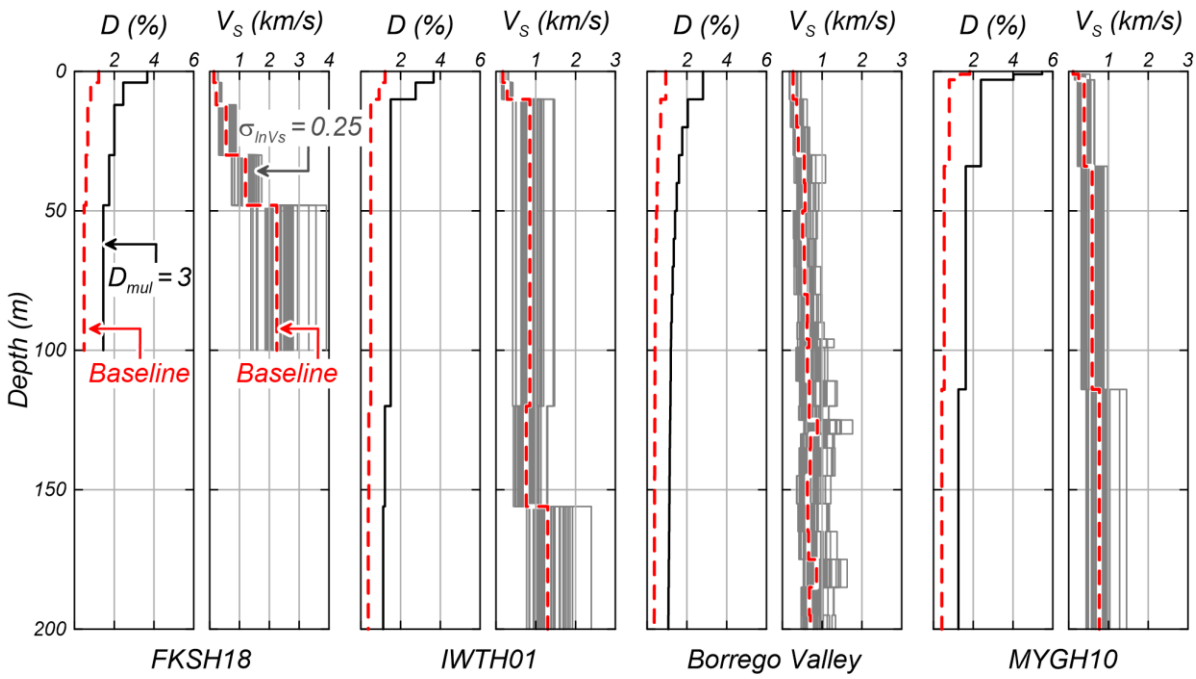

Figure 4.2. Example of input V_S and damping profiles for 1D SRAs.

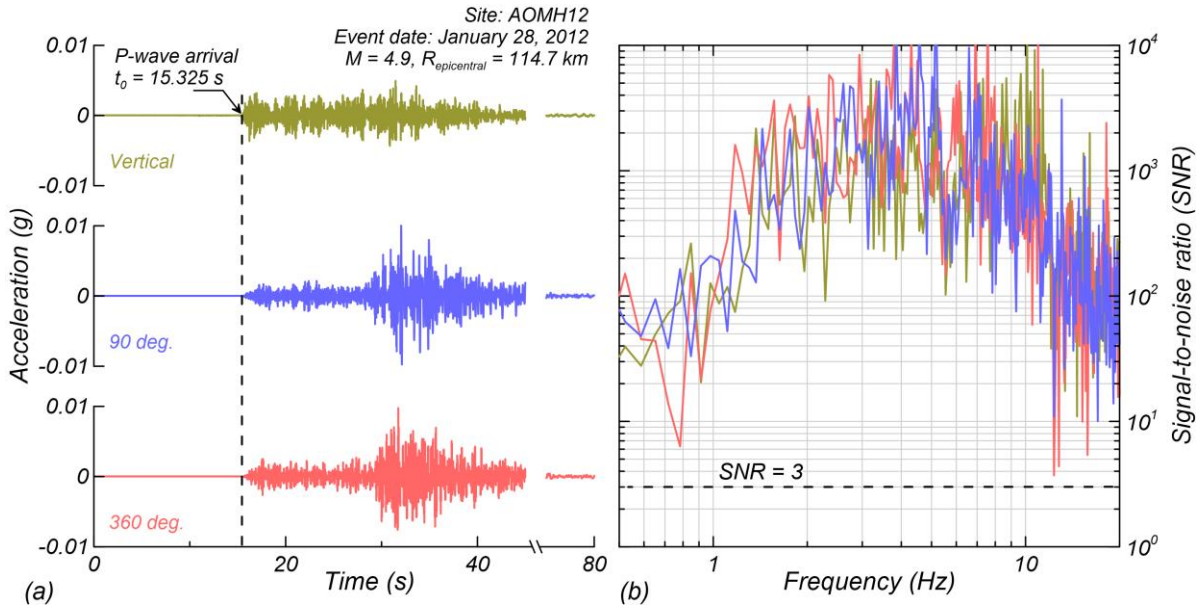

Figure 4.3. (a) P-wave arrival time in ground-motion recordings, and (b) signal-to-noise ratio (SNR).

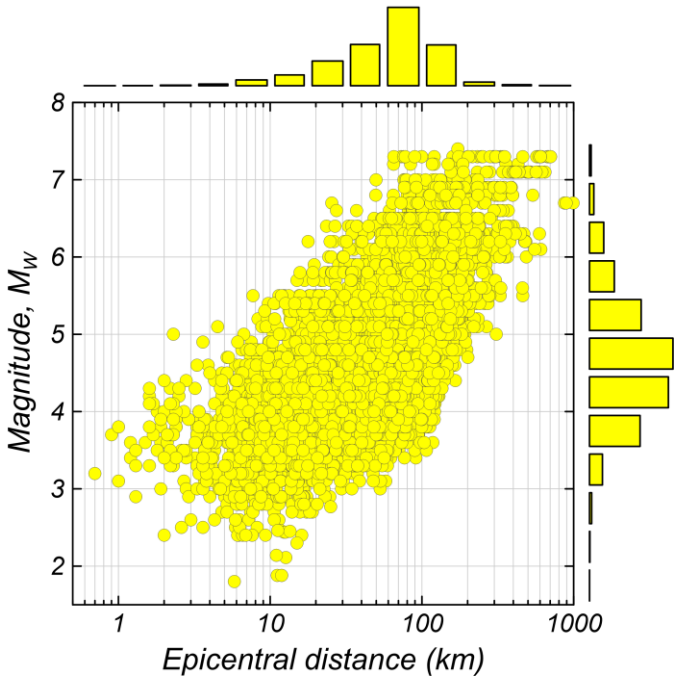

Figure 4.4. Distribution of epicentral distance and earthquake magnitude for selected events.

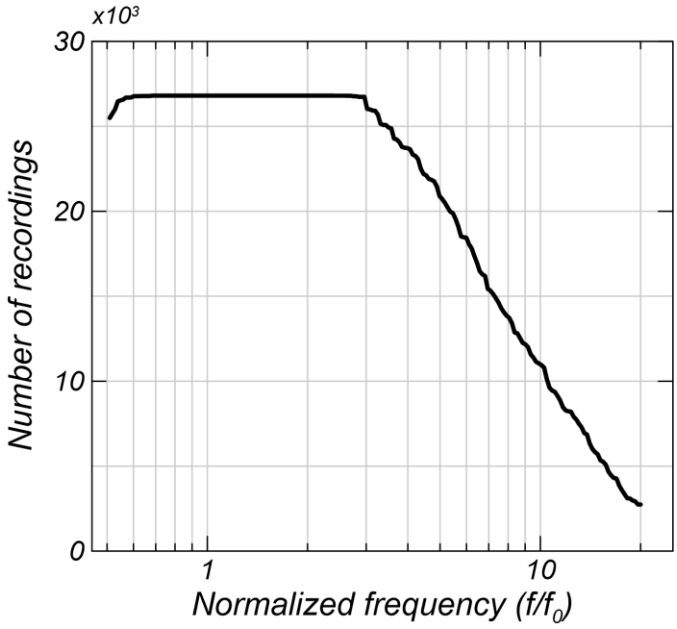

Figure 4.5. Number of usable recordings per normalized frequency.

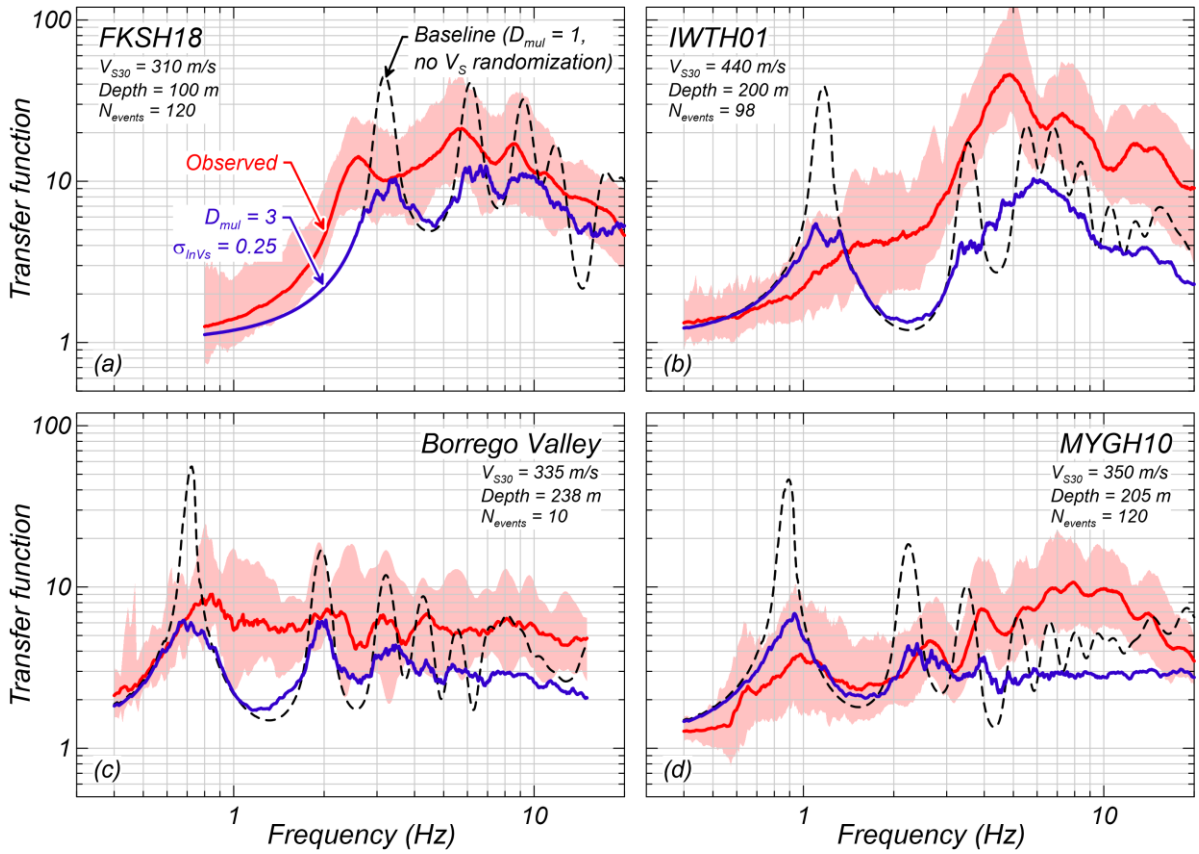

Figure 4.6. Comparison of observed transfer functions (TFs) and 1D SRA-based TFs for Case 1: Baseline (damping with D_{mul} = 1 and best estimate V_S profile), and Case 4: Proposed approach (damping with D_{mul} = 3 and randomized V_S profiles).

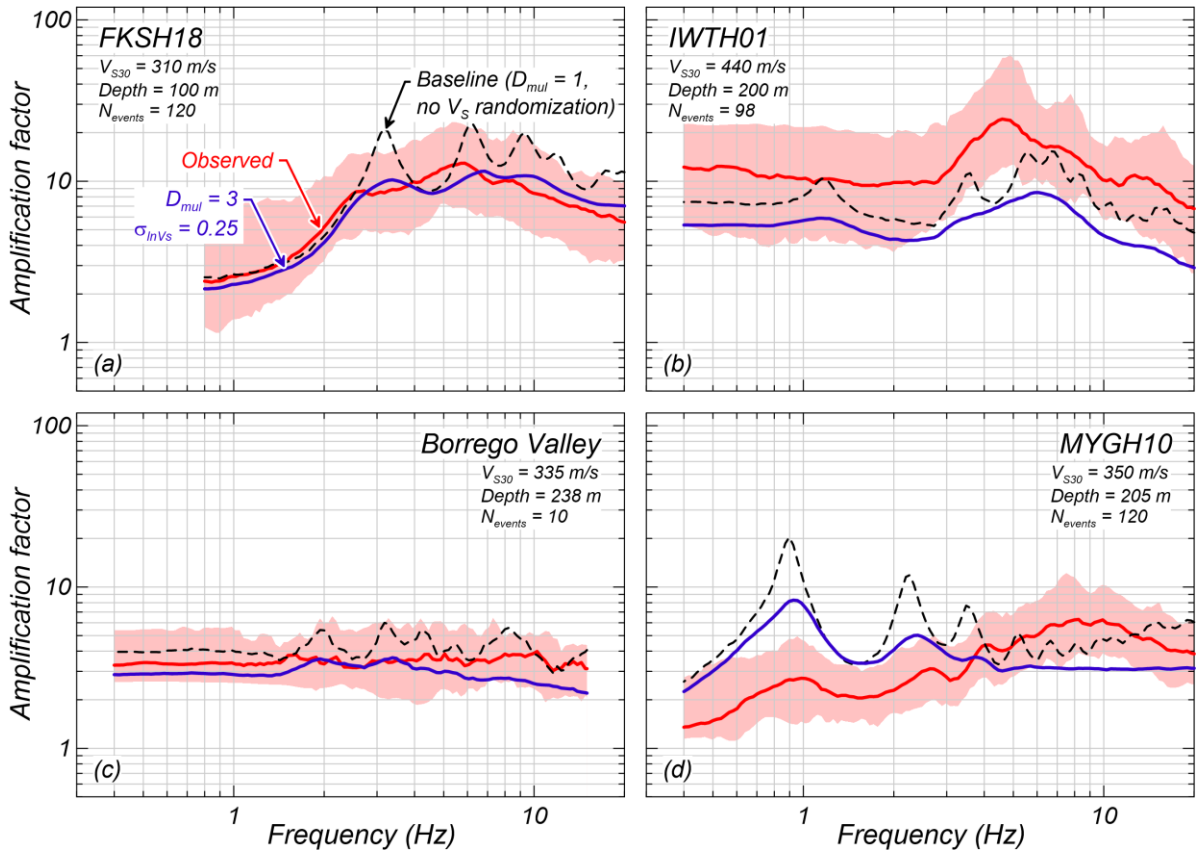

Figure 4.7. Comparison of observed amplification factors (AFs) and 1D SRA-based AFs for Case 1: Baseline (damping with D_{mul} = 1 and best estimate V_S profile), and Case 4: Proposed approach (damping with D_{mul} = 3 and randomized V_S profiles).

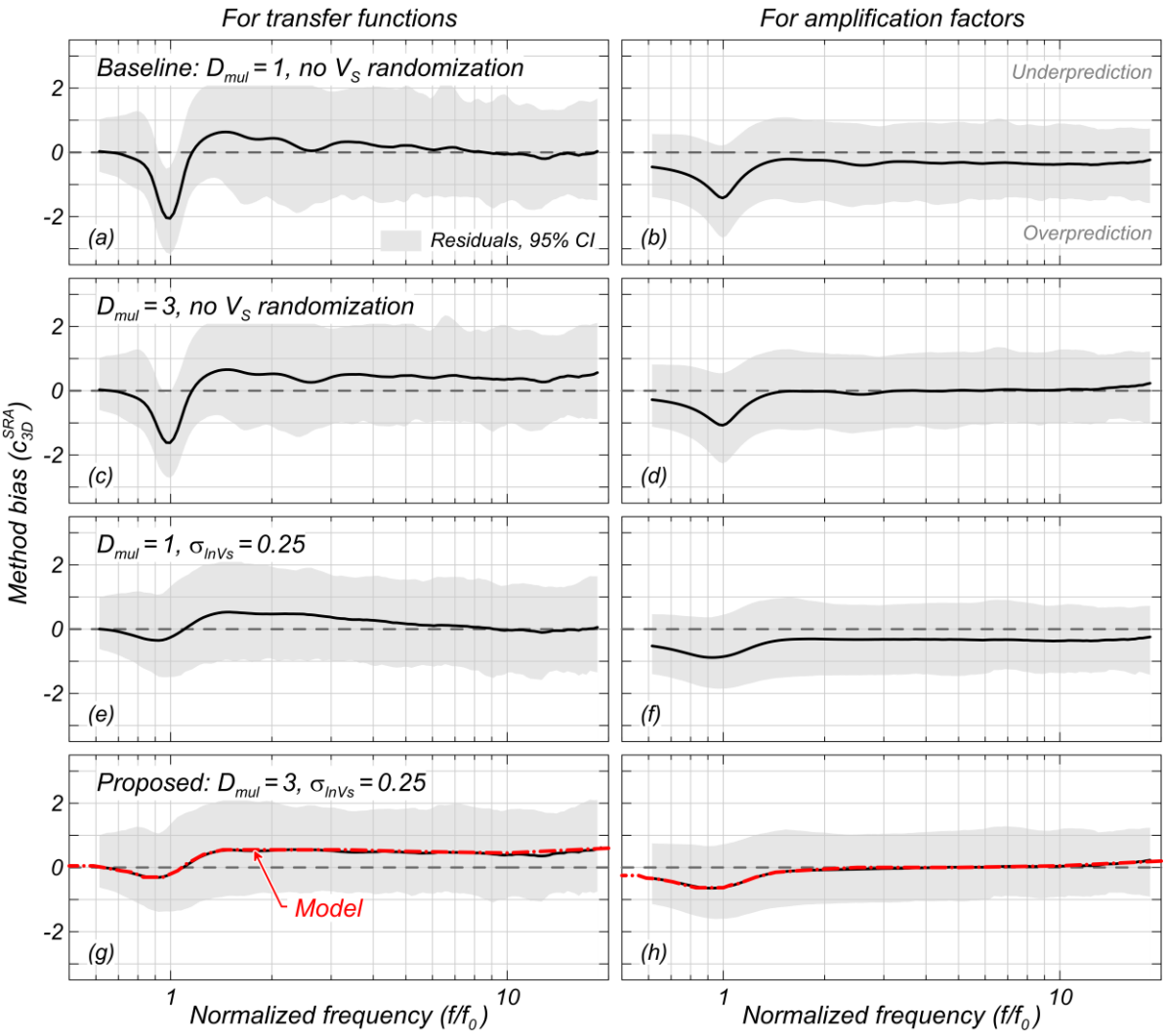

Figure 4.8. Comparison of site response method bias (c_{3D}^{SRA}) and residuals (95% confidence interval) in transfer functions and amplification Factors. (a) and (b): Case 1, baseline (damping with D_{mul} = 1 and best-estimate V_S profile); (c) and (d): Case 2 (D_{mul} = 3 and best estimate V_S profile); (e) and (f): Case 3 (D_{mul} = 1 and randomized V_S profiles with σ_{lnV_S} = 0.25); and (g) and (h): Case 4, proposed (D_{mul} = 3 and σ_{lnV_S} = 0.25).

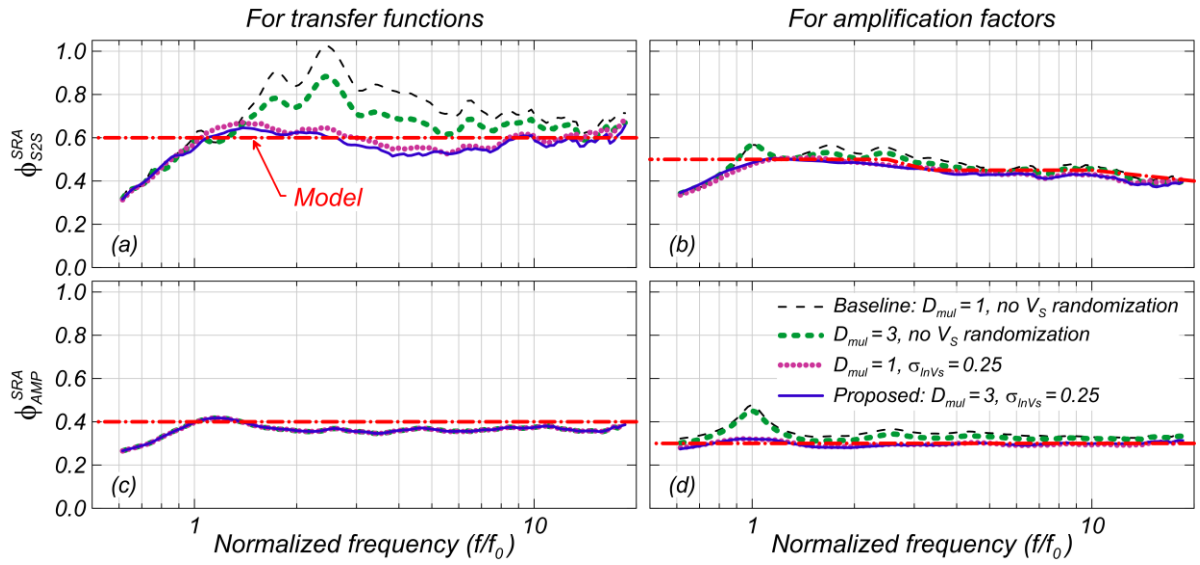

Figure 4.9. Comparison of site response residual standard deviations (ϕ_{S2S}^{SRA} and ϕ_{AMP}^{SRA}) in transfer functions and amplification factors.

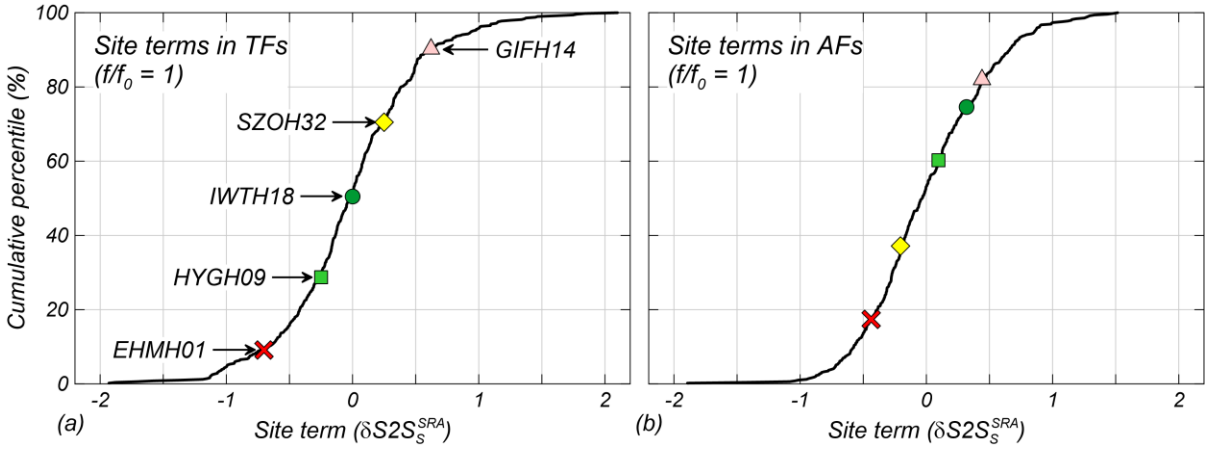

Figure 4.10. Cumulative distribution of site terms ($\delta S2S_S^{SRA}$) at $f/f_0 = 1$: (a) Site terms in transfer functions (TFs), and (b) in amplification factors (AFs). Labels indicate five selected sites with approximately uniformly spaced site terms in AFs.

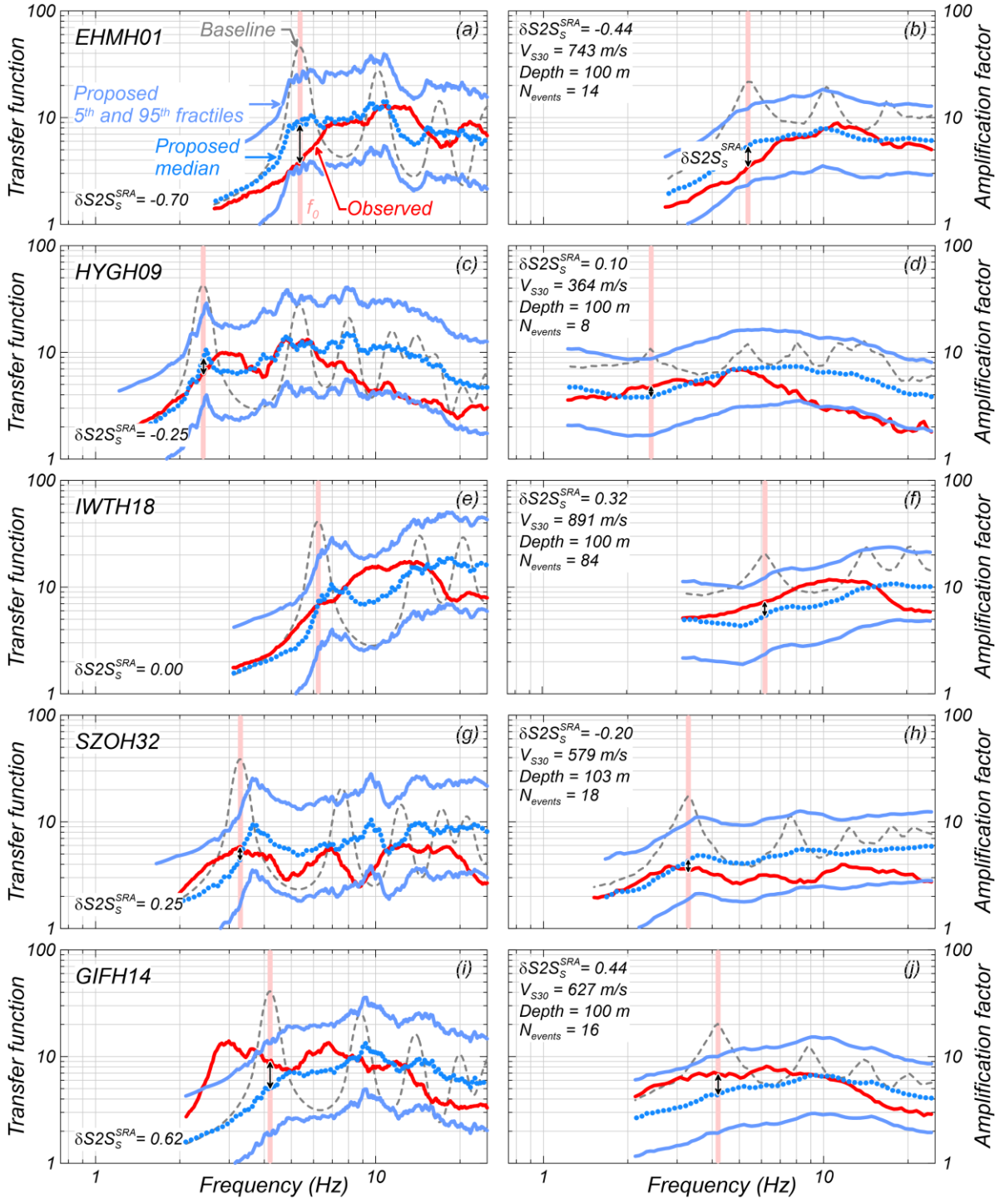

Figure 4.11. Transfer functions and amplification factors estimated using Cases 1 (baseline) and Case 4 (proposed approach) for five KiK-net sites. The sites are selected to cover the range of site term values ($\delta S2S_S^{SRA}$) in AFs.

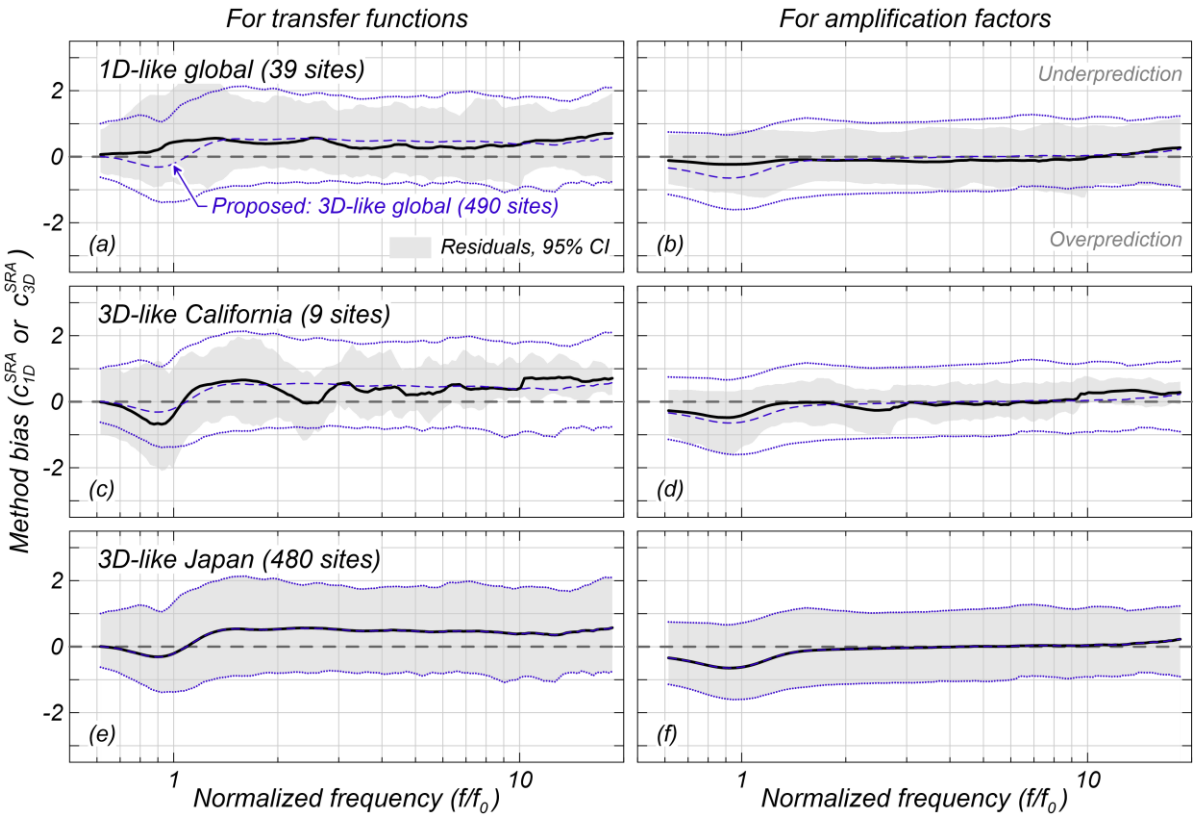

Figure 4.12. Comparison of site response method bias (c_{1D}^{SRA} or c_{3D}^{SRA}) and residuals (95% confidence interval) in transfer functions and amplification factors estimated from different datasets. (a) and (b): 1D-like sites from Japan and the US, (c) and (d): 3D-like sites from California, (e) and (f) 3D-like sites from Japan, and (g) and (h): 3D-like sites from Japan and the US (proposed).

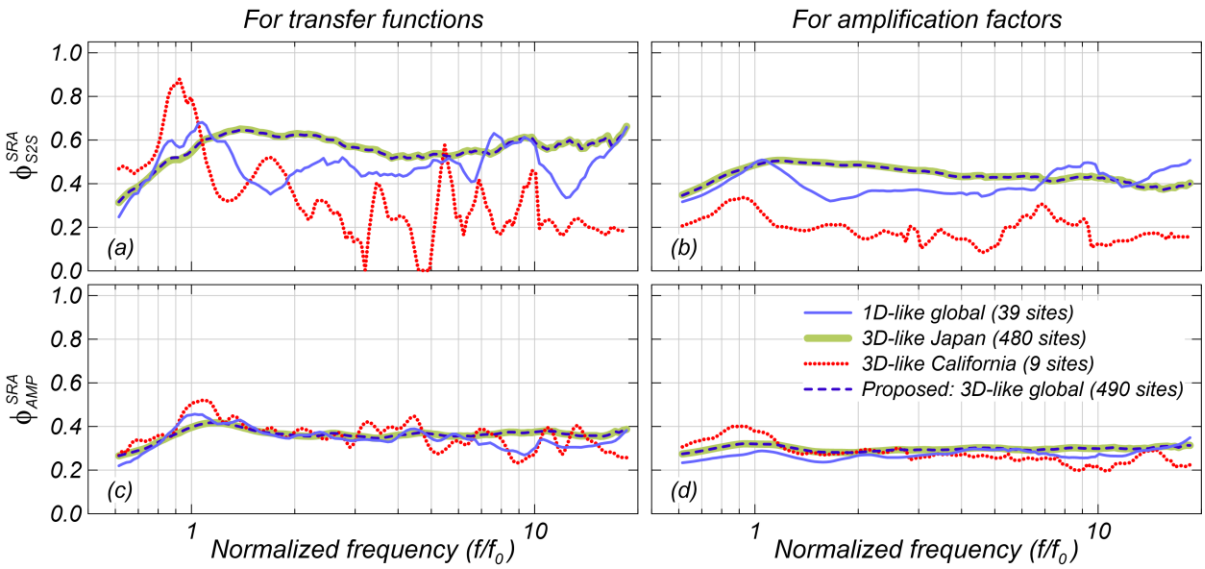

Figure 4.13. Comparison of site response residual standard deviations ($\phi^{\mathrm{SRA}}_{\mathrm{S2S}}$ and $\phi^{\mathrm{SRA}}_{\mathrm{AMP}}$) in transfer functions and amplification factors estimated from different datasets: (1) 1D-like sites from Japan and the US, (2) 3D-like sites from California, (3) 3D-like sites from Japan, and (4) 3D-like sites from Japan and the US (proposed).

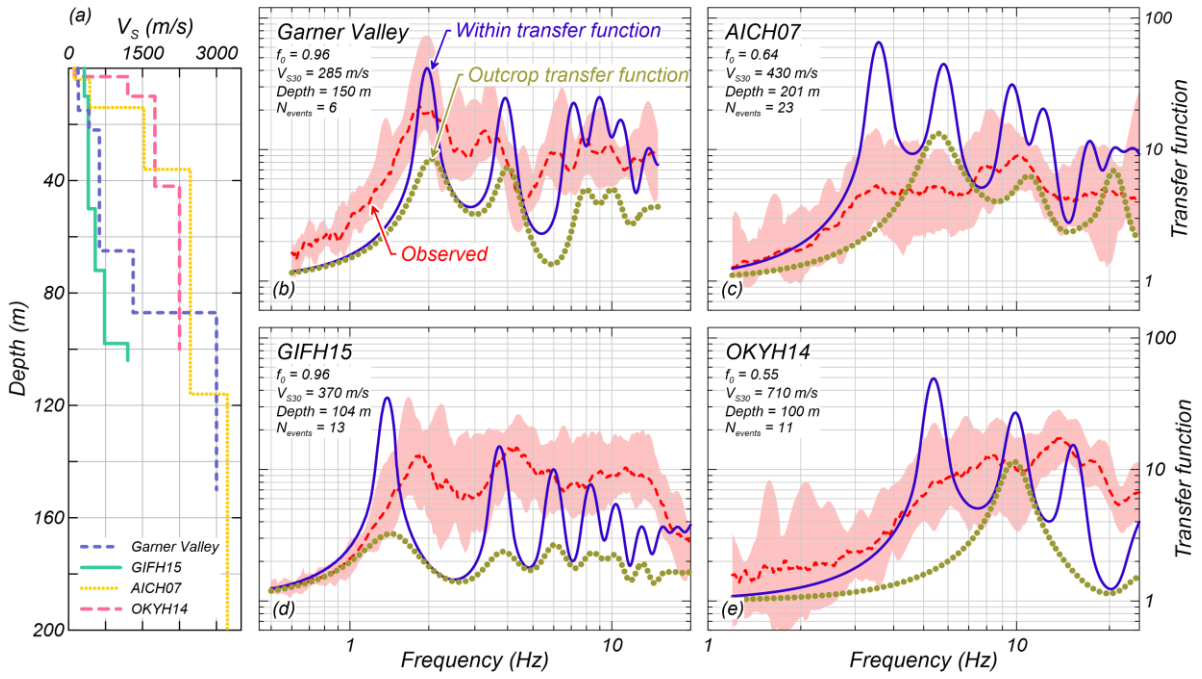

Figure 4.14. Example of sites unaffected and affected by pseudo-resonances: (a) Measured V_S profiles, (b) and (d): transfer functions (TFs) for sites free of pseudo-resonances, (c) and (e): TFs for sites with pseudo-resonances.

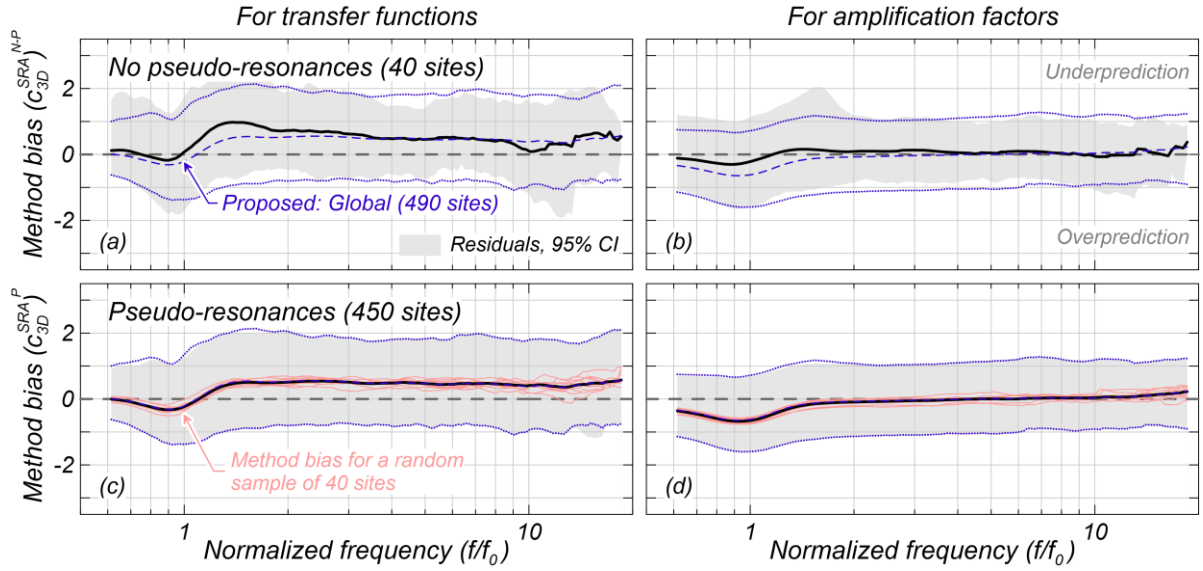

Figure 4.15. Comparison of site response method bias (c_{3D}^{SRA}) and residuals (95% confidence interval) in transfer functions and amplification factors estimated from different datasets. (a) and (b): Sites unaffected by pseudo-resonances, (c) and (d): Sites affected by pseudo-resonances.

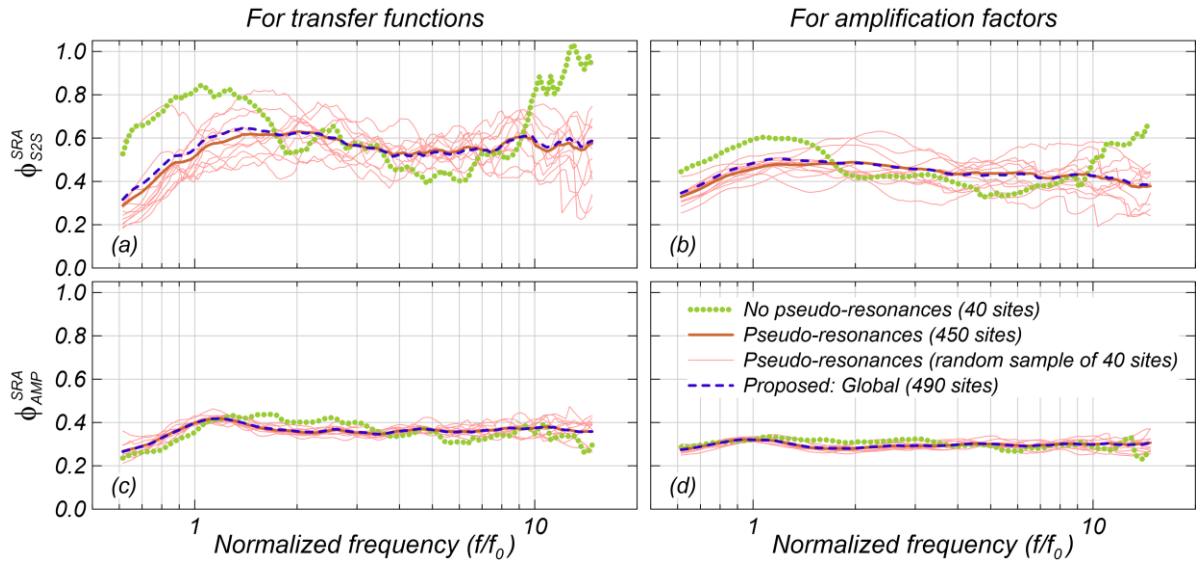

Figure 4.16. Comparison of site response residual standard deviations (ϕ_{S2S}^{SRA} and ϕ_{AMP}^{SRA}) in transfer functions and amplification factors estimated from different datasets: (1) Sites unaffected by pseudo-resonances, (2) sites affected by pseudo-resonances, (3) random sample of sites affected by pseudo-resonances, and (4) sites unaffected and affected by pseudo-resonances (proposed).

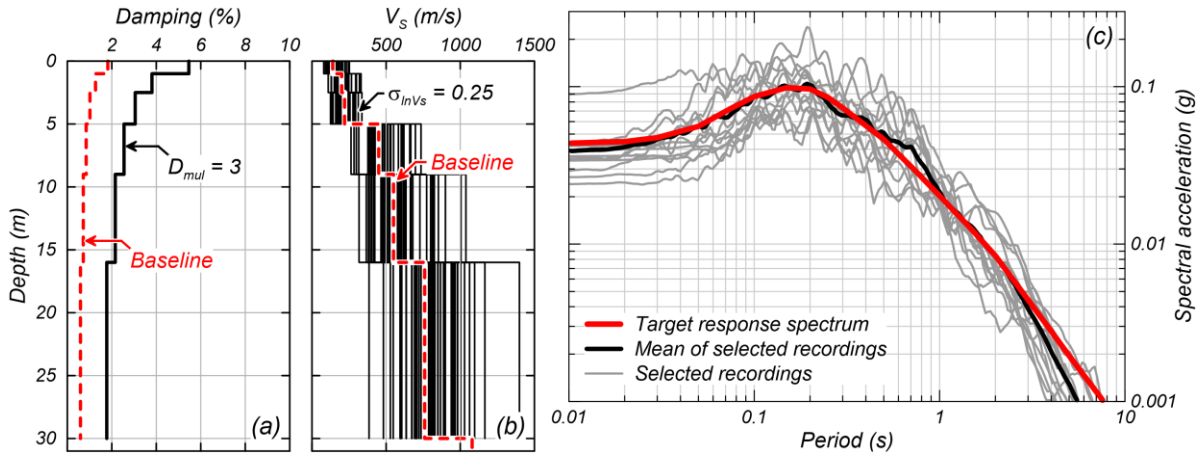

Figure 4.17. (a) Baseline and factorized damping profiles. (b) Baseline and randomized V_S profiles. (c) Target response spectrum and selected input ground motions.

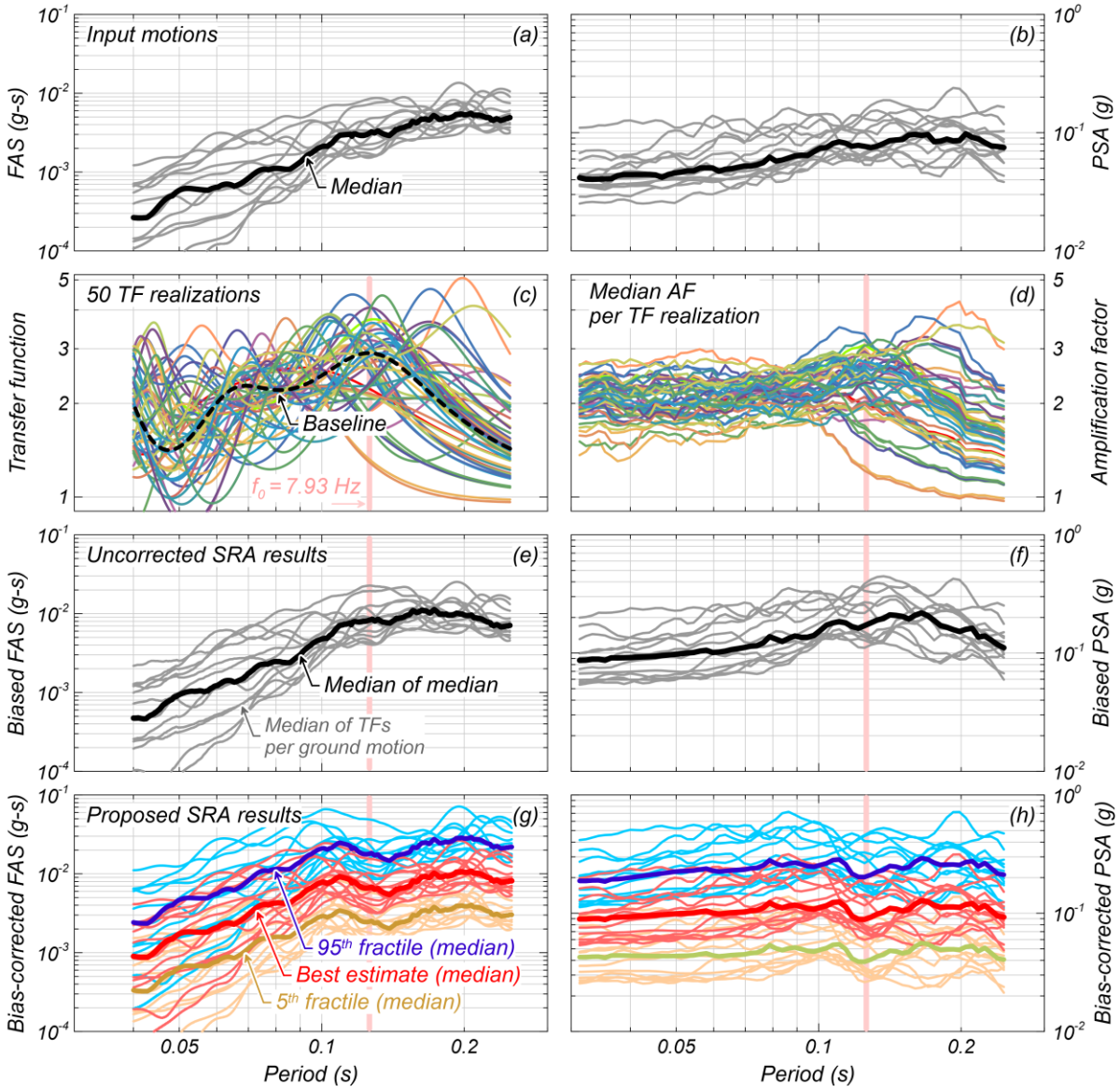

Figure 4.18. Estimated site response for a hypothetical site, step-by-step results for Fourier amplitude spectra (FAS) and pseudo-spectral acceleration (PSA) response spectra. (a) and (b): Input ground motions, (c) and (d): transfer functions and amplification factors (median of all input motions) per randomized V_S profile; (e) and (f): uncorrected FAS and uncorrected PSA response spectra (median of all input motions) at surface; (g) and (h): best estimate, and 5th and 95th percentiles of bias-corrected FAS and PSA response spectrum at surface (median of all input motions).

TABLES

Table 4.1. Matrix for the separation of sources of aleatory variability and epistemic uncertainty associated with the proposed approach for conducting 1D SRAs.

	Aleatory Variability	**Epistemic Uncertainty**
Parametric	Effect of the randomness in time on the site response, e.g., from ground-motion waveforms: ϕ_{AMP-TH}^{SRA}, only applicable to amplification factors.	Alternative suites of input ground motions consistent with design criteria. Alternative best estimate 1D V_S profile. Alternative values of σ_{lnV_S} for V_S randomization to remove $\delta 1D_s^{SRA}$: 0.2 to 0.3. Alternative values of D_{mul} for increasing damping to remove $\delta 1D_s^{SRA}$: 1 to 4.
Modeling	Standard deviation of the site-specific mean residual, $\delta S2S_s^{SRA}$: ϕ_{S2S}^{SRA} Standard deviation of remaining unexplained residuals, δAMP_{es}^{SRA}: ϕ_{AMP}^{SRA}	Standard error of c_{3D}^{SRA}, $SE(c_{3D}^{SRA}) \approx 0$ given the large database it is based on. Standard error of ϕ_{S2S}^{SRA}, $SE(\phi_{S2S}^{SRA}) \approx 0$ given the large database it is based on. Standard error of ϕ_{AMP}^{SRA}, $SE(\phi_{AMP}^{SRA}) \approx 0$ given the large database it is based on.

Table 4.2. Databases and ground motion selection criteria, including 1D- and 3D-like sites.

Database	**Maximum shear strain index, I_γ (%)** [1]	**Minimum signal-to-noise ratio, SNR**	**Accepted sites**	**Accepted events**
CESMD	0.01	3 [2]	12	105 [3]
KiK-net	0.005	3 [3, 5]	518	15,541
NEES	0.01	2.5 [4, 5]	4	43

[1] Idriss (2011)

[2] SNR estimated within frequency window from 0.5 Hz or at least half the site's frequency, up to 10 Hz. This SNR was enforced in 90% of the frequency range. Time of P-wave arrival (t_0) selected based on horizontal recordings given the absence of vertical components.

[3] Includes ground-motion recordings from the Afshari et al. (2019) database.

[4] SNR estimated within frequency window from 0.5 Hz or at least half the site's frequency, up to 20 Hz.

[5] SNR estimated within frequency window from 0.5 Hz or at least half the site's frequency, up to 12 Hz.

[6] Same SNR criteria applied for selecting vertical ground motion components. The I_γ was not evaluated.

Table 4.3. Recommended method bias (c_{3D}^{SRA}) and standard deviations ϕ_{S2S}^{SRA} and ϕ_{AMP}^{SRA} of TFs and AFs for various normalized periods and frequencies.

T/T_0	f/f_0	c_{3D}^{SRA}		ϕ_{S2S}^{SRA}	
		TF	**AF**	**TF**	**AF**
0.04	25.0	0.60	0.20	0.60	0.40
0.05	20.0	0.60	0.20	0.60	0.40
0.10	10.0	0.45	0.05	0.60	0.45
0.20	5.00	0.50	0.0	0.60	0.45
0.30	3.33	0.55	0.0	0.60	0.45
0.40	2.50	0.55	0.0	0.60	0.50
0.50	2.00	0.55	-0.05	0.60	0.50
0.60	1.67	0.55	-0.10	0.60	0.50
0.70	1.43	0.55	-0.15	0.60	0.50
0.80	1.25	0.40	-0.30	0.60	0.50
0.90	1.11	0.10	-0.50	0.60	0.50
0.95	1.05	-0.10	-0.55	0.60	0.50
1.00	1.00	-0.2	-0.63	0.60	0.50
1.05	0.95	-0.30	-0.63	0.60	0.50
1.10	0.91	-0.30	-0.63	0.60	0.50
1.20	0.83	-0.30	-0.63	0.60	0.50
1.30	0.77	-0.15	-0.55	0.60	0.50
1.40	0.71	-0.10	-0.45	0.60	0.50
1.50	0.67	-0.05	-0.40	0.60	0.50
1.60	0.63	0.0	-0.35	0.60	0.50
1.70	0.59	0.05	-0.33	0.60	0.50
1.80	0.56	0.05	-0.25	0.60	0.50
1.90	0.53	0.05	-0.25	0.60	0.50
2.00	0.50	0.05	-0.25	0.60	0.50

CHAPTER 5

SUMMARY AND FUTURE DIRECTIONS

This dissertation discussed two main topics: (1) an approach for capturing 2D shear-wave velocity (V_S) variability effects on site response using one-dimensional site response analyses (1D SRAs) conducted with randomized V_S profiles, and (2) an approach for conducting 1D SRAs to account for modeling errors by using (a) calibrated amounts of damping and V_S randomization to improve site response predictions, and (b) models for the bias $\left(c_{3D}^{SRA}\right)$ and variability in the site terms $(\delta S2S_s^{SRA})$, quantified with the standard deviation ϕ_{S2S}^{SRA}, to account for the potential under- and overprediction of site response. A summary of the main findings of interest for engineering practice and future research directions are provided in this chapter.

SUMMARY OF MAIN CONTRIBUTIONS

CHAPTER 2

The results from 2D SRAs on V_S correlated random fields and 1D SRAs on randomized V_S profiles indicated that the latter leads to underprediction of the site response around the sites' fundamental frequency when the standard deviation for V_S randomization $\left(\sigma_{\ln V_S}\right)$ was computed from the 2D random fields. Such underprediction was due to: (1) the shifting of the individual 1D responses' fundamental modes that led to coinciding peaks and troughs that canceled each other out, and (2) the intrinsic limitations of 1D SRAs in capturing non-1D amplification effects (e.g., constructive interference). The results from this chapter did not support the use of median

amplification factors (AFs) from 1D SRAs with V_S randomization for estimating the seismic demands in the design of structures.

The results indicated that the 84th percentile site response from 1D SRAs conducted with V_S randomization using the Toro model (1995) with $\sigma_{\ln V_S} = 0.25$ captures V_S spatial variability effects well at a given site's fundamental frequency. This generic $\sigma_{\ln V_S} = 0.25$ showed a similar or superior performance than the site-specific $\sigma_{\ln V_S}$ values in preventing site response underpredictions. A comparison against ground-motion data from four borehole array sites (Delaney Park, Garner Valley, HYGH10, and IBRH13) supported this finding on average.

This chapter also indicated that $\sigma_{\ln V_S}$ has a different meaning in 2D and 1D SRAs. In 2D SRAs, a higher $\sigma_{\ln V_S}$ led to mild variations of the median seismic response and a moderate increase in the response variability. In 1D SRAs with V_S randomization, a higher $\sigma_{\ln V_S}$ led to a significant decrease in the median seismic response amplitudes and a significant increase in the response variability across frequencies. This finding suggested that conducting 1D SRAs with randomized V_S profiles generated based on measured site-specific $\sigma_{\ln V_S}$ values does not necessarily lead to a more appropriate seismic response estimate.

CHAPTER 3

An approach was proposed for improving site response predictions based on 1D SRAs by using damping multipliers (D_{mul}), and randomized V_S profiles. A $D_{mul} = 3$ and $\sigma_{\ln V_S} = 0.25$ led to an overall minimum root mean square error (RMSE) in site response predictions. A lower $D_{mul} = 1$ was required for cases where transfer functions (TFs) were the only metric of interest, whereas $D_{mul} = 2$ to 4 were required for AFs. Higher D_{mul} values were needed to improve AF predictions,

given that the AF at a single degree of freedom oscillator frequency is affected by a wide range of ground-motion frequencies (Bora et al., 2016).

A framework for the sources of aleatory variability (AV) and epistemic uncertainty (EU) in ground-motion modeling initially proposed by Abrahamson et al. (1990) was adapted for 1D SRA applications. This framework differentiates between the parametric and modeling components of AV and EU. The parametric AV consists of random factors affecting the site response that the selected modeling approach can explicitly model (e.g., ground-motion waveforms). The parametric EU consists of the plausible alternative input parameters associated to the selected modeling approach (e.g., suites of input ground motions, selected based on some demand criteria). The modeling AV consists of the variability in the estimated site response given the factors affecting the site response but uncaptured by 1D SRAs (e.g., the wave propagation direction and wave inclination). Lastly, the modeling EU accounts for the potential misestimations of the MAV components such as the standard errors in the method bias associated with 1D SRAs $\left(c_{3D}^{SRA}\right)$ within the context of the proposed approach.

CHAPTER 4

This chapter follows Chapter 3 on developing an approach for conducting linear elastic 1D SRAs based on ground-motion data from borehole sites. Specifically, the c_{3D}^{SRA}, the site-specific mean residual with standard deviation ϕ_{S2S}^{SRA}, and a site- and event-specific residual with standard deviation ϕ_{AMP}^{SRA} were quantified and models for engineering applications were proposed. In summary, the proposed approach for conducting 1D SRAs consists of the following five steps:

1. *Site characterization*

   Selection of best estimate V_S profile and estimation of the minimum damping after Darendeli (2001). This site characterization is not uncommon in SRA applications.

2. *Input parameters*

   Application of $D_{mul} = 3$ to increase the minimum damping and generation of a suite of 50 randomized V_S profiles based off the best estimate profile using the V_S model by Toro (1995) with $\sigma_{\ln V_S} = 0.25$.

3. *Uncorrected site response*

   Conducting of 1D SRAs using the randomized V_S profiles and the same single damping profile ($D_{mul} = 3$). The suite of randomized V_S profiles is used for each one of the selected input ground motions. The median site response from all the V_S profiles is computed and considered the uncorrected best estimate for a given input motion.

4. *Bias correction*

   The model for c_{3D}^{SRA} is added to the uncorrected best estimate:

   Best estimate: $IM_{BE} = \mu_{IM} + c_{3D}^{SRA}$

5. *Accounting for modeling errors*

   The potential for modeling errors leading to under- or overpredictions is accounted for by considering alternative percentiles of the bias-corrected Fourier amplitude spectra (FAS) or pseudo-spectral acceleration (PSA) response spectra with 90% confidence interval:

   5th percentile: $IM_{5^{th}} = (\mu_{IM} + c_{3D}^{SRA}) - 1.65 \times \phi_{S2S}^{SRA}$

   95th percentile: $IM_{95^{th}} = (\mu_{IM} + c_{3D}^{SRA}) + 1.65 \times \phi_{S2S}^{SRA}$

Systematic trends were observed in the comparisons of ground-motion data from 495 3D-like borehole sites against 1D SRA predictions. First, there is an overall site response overprediction of the low-frequency range, and underprediction of the high-frequency range. Second, V_S randomization reduces the overpredictions at the frequency modes and leads to median TFs and AFs with a more uniform distribution of energy, i.e., smoother peaks at frequency modes. Third, using $D_{mul} = 3$ to increase damping leads to the estimation of nearly unbiased AFs across frequencies. Fourth, V_S randomization and D_{mul} can improve site response predictions; for instance, following the proposed approach. However, there is still significant bias in the results and significant variability in the site terms $\left(\delta S2S_S^{SRA}\right)$.

FUTURE DIRECTIONS

The development of the proposed approaches for conducting 1D SRAs involved the exploration of various avenues that can be further investigated in future studies. The proposed approaches are herein referred to as:

- Approach 1: To capture V_S spatial variability effects in site response (Chapter 2)
- Approach 2: To reduce and account for the modeling errors in 1D SRAs (Chapters 3 and 4)

Eight broad areas of future directions are identified and described as follows:

1. The proposed Approaches 1 and 2 were developed independently. Approach 1 offers a practical alternative for estimating a site response that captures V_S spatial variability at a given site's fundamental mode. Meanwhile, Approach 2 can be used to estimate the range of potential site amplifications accounting for modeling errors that lead to potentially lower or higher site

amplifications. Further work is needed to combine both approaches or to develop a method that meets both approaches' goals.

2. The proposed Approaches 1 and 2 were developed for linear elastic 1D SRAs which are rarely used in engineering practice. Future efforts could build on the proposed frameworks to develop approaches for conducting equivalent linear and nonlinear 1D SRAs. It is expected that such initiatives should include the randomization of the equivalent linear material properties (i.e., shear modulus reduction curves, and damping ratio curves), or any other parameters whose effect on site response is variable in the field and observed to be important. The goals of such randomization should be clearly defined.

3. The proposed Approaches 1 and 2 used V_S randomization considering the V_S model by Toro (1995). Future research efforts should also evaluate the potential for improving site response predictions by (1) randomizing V_S layer thicknesses and the depth to bedrock, (2) considering a variable $\sigma_{\ln V_S}$ with depth (e.g., Tao and Rathje, 2019), and (3) using a different randomization model.

4. The framework considered in the development of Approach 1 can be extended to evaluate the appropriate amount of V_S randomization, mapped through $\sigma_{\ln V_S}$, to capture non-1D site-specific features beyond V_S spatial variability (e.g., a dipping bedrock). Approach 1 suggests that using $\sigma_{\ln V_S} = 0.25$ and selecting the 84^{th} percentile site response leads to appropriate estimates at a given site's fundamental mode that capture V_S spatial variability effects. However, most sites are likely exposed to more than a single site-specific feature affecting site response. Future studies should therefore consider using V_S randomization to capture the independent and the combined effect of such non-1D features.

5. The evaluation of the effect of pseudo-resonances showed that higher c_{3D}^{SRA} and ϕ_{S2S}^{SRA} values could be associated with Approach 2 when used in applications involving rock outcrop ground motions. This finding stressed the need for further investigating the applicability of research findings based on ground-motion data to engineering applications.

6. The proposed Approach 2 was developed based on a large database of ground-motion recordings, which was used to quantify D_{mul}, $\sigma_{\ln V_S}$, c_{3D}^{SRA}, ϕ_{S2S}^{SRA}, and ϕ_{AMP}^{SRA}. It is unclear whether these values would increase or decrease as ground motion data are collected. It is expected that the recommended D_{mul} and $\sigma_{\ln V_S}$ values and the models for c_{3D}^{SRA}, ϕ_{S2S}^{SRA}, and ϕ_{AMP}^{SRA} will be revised as the borehole ground-motion datasets become larger.

7. The development of Approach 2 involved identifying 1D-like sites based on the similarity between observed and theoretical TFs. A total of 39 1D-like sites were identified from a database of 534 borehole sites, representing about 7%. This finding urges the development of protocols for conducting site response analyses using more advanced 2D and 3D SRAs. It is expected that such protocols would include directions from the model development stage to the implementation of the models in a numerical platform and the interpretation of results for design purposes.

8. Lastly, this dissertation adapted the framework for the parametric and modeling components of AV and EU (Abrahamson et al., 1990) to site response applications. This framework is expected to be used in future development of numerical simulations, within the context of site response applications and beyond.

REFERENCES

Abrahamson NA, Somerville PG and Cornell CA (1990) Uncertainty in numerical strong motion predictions. In: *Proceedings of the 4th U.S. National Conference on Earthquake Engineering*, 1, 407-416.

Bora SS, Scherbaum F, Kuehn N and Stafford P (2016) On the relationship between Fourier and response spectra: Implications for the adjustment of empirical ground-motion prediction equations (GMPEs). *Bulletin of the Seismological Society of America* 106(3): 1235–1253.

Darendeli MB (2001) *Development of a new family of normalized modulus reduction and material damping curves.* PhD Dissertation, The University of Texas at Austin, Austin, TX.

Tao Y and Rathje EM (2019) Insights into modeling small-strain site response derived from downhole array data. *Journal of Geotechnical and Geoenvironmental Engineering* 145(7): 04019023.

Toro GR (1995) *Probabilistic models of site velocity profiles for generic and site-specific ground-motion amplification studies.* Report no. 779574, 17 November. Upton, NY: Brookhaven National Laboratory.

APPENDIX A

NUMERICAL INVESTIGATION OF V_S SPATIAL VARIABILITY EFFECTS ON THE SEISMIC RESPONSE ESTIMATED USING 2D AND 1D SITE RESPONSE ANALYSES

AUTHOR'S NOTE

The contents of this appendix were originally published in the conference paper by Pretell R, Ziotopoulou K and Abrahamson NA, presented during GeoCongress 2022 in Charlotte, North Carolina (March 2022). Authorship roles are provided in Chapter 1.

PUBLICATION

Pretell R, Ziotopoulou K and Abrahamson NA (2022) Numerical investigation of V_S spatial variability effects on the seismic response estimated using 2D and 1D site response analyses. In: *Proceedings of the Geo-Congress 2022*, Charlotte, NC, 20–23 March. 10.1061/9780784484043.020

ABSTRACT

One-dimensional site response analyses (1D SRAs) are the most widely used tool to assess site-specific seismic response. However, compared to 2D and 3D SRAs, 1D SRAs are limited in their ability to capture some wave propagation mechanisms. Here, 2D and 1D SRAs are conducted on V_S correlated random fields to evaluate: (1) the discrepancies in the median 2D and 1D seismic responses, (2) the effects of V_S spatial variability features (e.g., correlation length, θ) on the 2D response, and (3) the effect of using 1D SRA-based ground motions to estimate intensity measures (IMs) towards getting insight into the seismic performance of geosystems. Results indicate that (1) median 2D responses are higher than median 1D responses, and the discrepancy increases with V_S variability ($\sigma_{\ln V_S}$), (2) $\sigma_{\ln V_S}$ has a stronger effect than other V_S variability features on the 2D and 1D seismic responses, and (3) IMs might be underpredicted when estimated using 1D SRA-based ground motions, and thus the expected geosystems' seismic performance overestimated.

INTRODUCTION

The state of practice for assessing site-specific seismic response consists of 1D SRAs, commonly accompanied with V_S randomization to account for V_S spatial variability (e.g., EPRI 2013). Two implicit assumptions to this are: (1) 1D SRAs can capture the seismic response of natural deposits, and (2) the combined seismic response from multiple randomized 1D V_S profiles can capture V_S spatial variability effects. Validation studies compared 1D SRAs predictions against recorded ground motions from downhole stations (e.g., Stewart et al. 2008, Kaklamanos et al. 2013, Afshari and Stewart 2019) have shown discrepancies that are often attributed to uncertainties on the input parameters such as measured V_S profiles, and non-1D effects (e.g., Kaklamanos et al. 2020).

A numerical evaluation is conducted to understand the discrepancies between the 2D SRA-based seismic responses for simple 2D sites with spatially variable V_S, but unexposed to complex geological conditions, and 1D SRA-based responses from 1D V_S profiles numerically sampled from the 2D models. Results provide insights into (1) the ability of 1D SRAs to capture the effect of V_S spatially variability, $\sigma_{\ln V_S}$, (2) the effect of V_S spatial variability features, such as correlation lengths, on the 2D seismic response; and (3) the accuracy of the expected seismic performance of geosystems when inferred from 1D SRA-based IMs.

NUMERICAL SITES

The seismic response of 2D sites with spatially variable V_S is evaluated using linear elastic 2D and 1D SRAs (Figure A.1). The sites consist of 30 m-deep V_S correlated random fields developed using the variance-covariance matrix approach (Vanmarcke 1983), based on a "seed" 1D V_S profile generated using the relationship by Kamai et al. (2016) for conditions consistent with sites in California. In reality, there are no 2D sites, but rather 3D sites that unavoidably encompass a

wide range of site conditions (e.g., variable V_S, inclined bedrock, inclined wave propagation) affecting the seismic response. However, herein the models are referred to as "2D sites with spatially variable V_S" to be explicit about the assumptions of this study, and the range of application of the conclusions drawn. 1D SRAs are conducted on columns sampled from the 2D sites, at the recording locations (Figure A.1). These columns represent V_S profiles that are exempt from measuring errors or field technique limitations, and are referred to as "sampled V_S profiles."

The model elements are 1 m by 1 m, which allows for an appropriate estimation of the seismic response for frequencies lower than approximately 12.5 Hz (Kuhlemeyer and Lysmer, 1973), and higher than the site's fundamental frequency. Multiple model widths were tested, and a reasonably small model was selected such that the seismic response measured along the middle portion was not influenced by spurious wave reflections from the model' sides (Pretell et al., 2022). This zone is hereafter referred to as "recording zone." The software QUAD4MU (Hudson et al., 2003) is used for both 2D and 1D SRAs with a damping of 10% for all soils. This damping is used to allow for a smaller model and thus a reasonable computational demand. Additional analyses indicate that using lower damping values does not significantly affect the relative difference between 2D and 1D seismic responses (Pretell et al., 2022). A fully reflective boundary condition, i.e., rigid base (Kwok et al., 2007), is used for the base of the 2D and 1D models to isolate the effects of the soil-bedrock impedance ratio. The input motion is applied as a horizontal acceleration, accompanied by a null vertical acceleration to prevent vertical displacements. Horizontal and vertical displacements are allowed along the 2D models' sides, whereas vertical displacement is prevented along the 1D models' sides. The selected 1D boundary conditions provide results that are consistent with those from conventional software.

Results from 1D and 2D SRAs are compared in terms of transfer functions (TFs) and amplification factors (AFs). The 2D seismic response is recorded at 21 locations equally spaced every 5 m along the recording zone. This zone is the only portion of the model affecting the seismic response and thus is used to quantify $\sigma_{\ln V_S}$. Ten 2D sites are used, leading to 210 2D and 1D recordings, with standard errors of the median and standard deviation TF lower than 2.5%.

BASELINE SITES

The variance-covariance matrix approach for generating random fields depends on (1) the standard deviation of V_S in natural logarithm units, $\sigma_{\ln V_S}$, (2) the correlation model, and (3) the horizontal and vertical correlation lengths selected for the model (θ_{hor} and θ_{ver}, respectively). The $\sigma_{\ln V_S}$ determines how variable V_S is within the modeled space, the correlation model determines the rate at which the V_S correlation decays with distance, and the θ_{hor} and θ_{ver} determine the span within which V_S values are similar. For the baseline sites, $\sigma_{\ln V_S}$ values commonly observed in nature are selected: 0.2, 0.3, 0.4, and 0.5 ln units (e.g., Wills and Clahan, 2006). It is worth noting that these target $\sigma_{\ln V_S}$ values are for the entire model, but only 75 to 98% is achieved within the recording zone. The correlation model and correlation lengths are arbitrarily selected. The effect of these assumptions on the seismic response is explored in a later section of this article.

INPUT GROUND MOTION

All SRAs are conducted using a ground motion record of the 1999 Mw 7.6 Chi Chi Earthquake (peak ground acceleration, PGA = 0.33g), recorded at the TCU075 station and downloaded from the PEER Database (Ancheta et al., 2013). A single ground motion is appropriate for this investigation as linear elastic SRAs are used. In addition, the amplitude of this ground motion does

not impact the observed trends given that comparisons are made in terms of either (1) TFs, (2) AFs, or (3) the relative difference between 2D SRA- and 1D SRA-based IMs.

BASELINE RESULTS

TFs and AFs estimated for the baseline site conditions are presented in Figures A.2 and A.3, respectively. The results indicate consistent trends in the relative difference between responses from the 2D and 1D SRAs. First, discrepancies in the median seismic responses mainly occur at the site's fundamental frequency and are more significant in TFs than in AFs. This trend is consistent with other investigations, e.g., Teague and Cox (2016), Tao and Rathje (2019), Hallal and Cox (2021). Second, the differences between the median TFs and AFs increase with the site's V_S variability.

Third, low V_S variability sites present modest discrepancies in the median seismic responses, but significantly different standard deviations. Unsurprisingly, these trends suggest that multiple 1D SRAs cannot compensate for the absence of 2D SRAs, even under the assumption that V_S profiles are exempt from measurement errors, which is hardly ever the case in practice. Findings from these analyses are consistent with previous similar studies (e.g., Pehlivan et al., 2012; Pehlivan, 2013).

Discrepancies in the median seismic response estimated using 2D and 1D SRAs are mainly due to (1) inherent limitations of 1D SRAs compared to 2D SRAs, given that conventional 1D SRAs can only account for wave amplification (or deamplification) due to changes in impedance contrasts, and (2) the combined effect of a greater shifting of multiple 1D models' fundamental frequency compared to that of 2D models, and the averaging effect of using the median response across frequencies. Results suggest that the seismic response estimated using 2D SRAs for sites

with low V_S variability ($\sigma_{\ln V_S}$ lower than 0.2) can be reasonably modeled using 1D SRAs (Figures A.3a and A.4a). As the site variability increases, the amplitudes of the 1D seismic response decrease significantly due to shifting of the fundamental frequency caused by the effect that soil heterogeneities have on 1D models (e.g., Roy et al.; 2020). In the case of the 2D response, a higher site variability leads to higher variability in the seismic response and a lower median second mode (Figures A.2c and A.2d). The decrease in the second mode is caused by the multiple wave reflections, scattering, and filtering effects (e.g., Nour et al., 2003; Kokusho, 2017; De la Torre et al., 2019).

PARAMETRIC INVESTIGATION

The role of V_{S30}, site depth, and V_S spatial variability features (e.g., correlation model) on the 2D seismic response is evaluated and compared to $\sigma_{\ln V_S}$. The model characteristics and number of recordings are similar to those previously described, unless otherwise indicated. The scenarios considered are summarized in Table A.1, and the estimated TFs, and the standard deviation of TFs are presented in Figures A.5 and A.6, respectively. Results in terms of AFs are similar and thus not shown.

EFFECT OF SITE'S V_{S30}

The baseline V_S correlated random fields are consistent with a V_{S30} = 200 m/s. Two-dimensional SRAs are conducted on stiffer sites consistent with the following V_{S30} values: 300, 400, and 500 m/s. Results from 2D SRAs (Figures A.5a and A.6a) show a shifting of the site's resonant frequency, but similar amplitudes of the median response and standard deviation. Amplitudes of the median second mode, however, decrease as V_{S30} increases. This is attributed to (1) a stronger

impact of $\sigma_{\ln V_S}$ on V_S spatial variability for stiffer sites and thus further shifting of the fundamental frequency, and (2) limitations of the model mesh in propagating high-frequency waves.

EFFECT OF CORRELATION MODEL

The baseline V_S random fields follow an exponential correlation model. Two-dimensional SRAs are conducted on random fields that follow alternative models: squared exponential, spherical, and polynomial decaying (e.g., Baecher and Christian, 2003), presented in Figure A.4a. These models indicate, for instance, that random fields that follow the squared exponential model are more variable within a span of 50 m than those based on the exponential model (Figure A.4a). Results from 2D SRAs suggest that there is little effect of the correlation models on the median seismic response and its standard deviation (Figures A.5b and A.6b). The seismic response for random fields generated using the squared exponential model exhibit slightly higher amplitudes in TFs at the second vibration mode, and lower standard deviations across frequencies.

EFFECT OF HORIZONTAL CORRELATION LENGTH, θ_{hor}

The baseline horizontal correlation length is 50 m. Two-dimensional SRAs are conducted on random fields consistent with different θ_{hor} values: 5, 200, and 500 m (Figure A.4b). Results from 2D SRAs indicate minor variations in the median response (Figure A.5c), partly due to the averaging of multiple responses (total of 210 recordings). There is a slight decrease of amplitudes for longer θ_{hor} values at the frequency modes, accompanied by an increase in standard deviations (Figure A.6c). Sites with shorter θ_{hor} present a mild increase in the half bandwidth due to wave scattering (De la Torre et al., 2019). Sites with longer θ_{hor} have a higher V_S lateral continuity, and thus a lower seismic response, more similar to that from 1D SRAs.

EFFECT OF VERTICAL CORRELATION LENGTH, θ_{ver}

The baseline vertical correlation length is 5 m. Two-dimensional SRAs are conducted on random fields with different θ_{ver}: 10, 25, 50 m (Figure A.4b, for reference). Results from 2D SRAs indicate that longer θ_{ver} values lead to slight decreases in the median response (Figure A.5d) and higher standard deviations (Figure A.6d). These results are due to the fact that sites with longer θ_{ver} present a more uniform V_S with depth, thus there is presence of zones that are either more consistently soft or stiff. Shifting of the fundamental frequency and averaging the seismic responses lead to a lower seismic response with a higher standard deviation.

EFFECT OF SITE DEPTH

The baseline vertical correlation length is 5 m. The baseline site is 30 m-deep with a θ_{ver} = 5 m (θ_{ver}/depth ratio = 6). Two-dimensional SRAs are conducted on deeper models generated with (1) a constant θ_{ver} = 5 m, and (2) a constant θ_{ver}/depth ratio = 6, for site depths of 50 m (θ_{ver} = 8.3 m), 100 m (θ_{ver} = 16.6 m), and 200 m (θ_{ver} = 33.3 m). To evaluate these scenarios, necessary changes were made to the model dimensions to prevent boundary effects while balancing a similar number of recording locations and computational demand. Results from 2D SRAs on deeper sites with constant θ_{ver} present a slight increase in the seismic response and a decrease in the standard deviation, while deeper sites with constant θ_{ver}/depth ratio do not exhibit changes in the median responses, but an increase in the standard deviation (Figures A.5e, A.5f, A.6e, and A.6f). In the first case (constant θ_{ver}), the observed trends are due to a more uniform response given the weaker influence of a constant θ_{ver} = 5 m on deeper sites, and thus less shifting of the fundamental frequency mode. In the second case (constant θ_{ver}/depth ratio), representative of more realistic field conditions, the effects of θ_{ver} is sustained as sites get deeper, and thus the averaging of

multiple responses still leads to stable median responses. A reduction of the seismic response's second mode is observed in both scenarios for deeper sites.

IMPLICATIONS ON INFERRED GEOSYSTEM'S PERFORMANCE

In the previous sections, discrepancies in median TFs and AFs caused by the modeling approach selected, either 2D or 1D SRAs, were investigated. In this section, the impact of using 1D SRAs as a substitute for 2D SRAs on estimated ground motion IMs that correlate to seismic performance is evaluated. The following V_S spatial variability parameters are considered: $\sigma_{\ln V_S}$, correlation model, θ_{hor}, and θ_{ver}, and four IMs: PGA, peak ground velocity, PGV, Arias intensity, AI (Arias 1970), and cumulative absolute velocity, CAV (EPRI 1998). PGA values are commonly used for the evaluation of liquefaction triggering, while PGV, AI, and CAV correlate well with seismic-induced displacements and damage (e.g., Armstrong et al. 2020).

The IMs are computed for each ground motion and the results are shown in Figure A.7. IMs estimated from 2D and 1D SRAs are plotted along the horizontal and the vertical axes, respectively. Different columns correspond to different V_S spatial variability parameters, and different rows to different IMs. Results indicate that PGAs are more strongly affected by the selected modeling approach, with 2D SRAs leading to higher values. A weaker impact on PGV, CAV, and AI, is observed. The V_S spatial variability parameter leading to the most significant difference between 2D SRA- and 1D SRA-based IMs is $\sigma_{\ln V_S}$. As $\sigma_{\ln V_S}$ goes from 0.16 – 0.19 to 0.24 – 0.29, there is a shift towards the right side, suggesting that higher values are estimated from 2D SRAs. This shift is particularly clear for PGVs. However, further increases in $\sigma_{\ln V_S}$ lead to shifting back to the left side and to a reduction of the correlation between IMs estimated from 2D and 1D SRAs. For example, the estimated correlation between IMs for sites with low $\sigma_{\ln V_S}$ is

about 0.15 for PGA, 0.5 for PGV and AI, and 0.45 for CAV, whereas the correlation for sites with high $\sigma_{\ln V_S}$ is near 0 for PGA, 0.15 for PGV, and about 0.1 for AI and CAV. These observations suggest that an initial increase in $\sigma_{\ln V_S}$ leads to reverberations and higher amplitudes of time histories of accelerations, but further increases in $\sigma_{\ln V_S}$ lead to excessive wave scattering, a decrease in the amplitudes, and thus lower IM values. The effect of other V_S variability parameters suggests some degree of underprediction of ground motion IMs when using 1D SRAs.

FINAL REMARKS

A numerical evaluation was conducted to understand the discrepancies between 2D and 1D seismic responses for simple 2D sites with spatially variable V_S, but unexposed to complex geological conditions, and 1D V_S profiles numerically sampled from these 2D models. Results indicate that (1) discrepancies between the median 2D and 1D seismic response are exacerbated by V_S spatial variability, $\sigma_{\ln V_S}$, (2) the magnitude of $\sigma_{\ln V_S}$ has a dominant effect on the 2D and 1D seismic responses compared to other V_S spatial variability features evaluated as part of this work (e.g., correlation lengths), and (3) 1D SRA-based IMs tend to be lower than those estimated based on the more realistic 2D SRAs, which could infer an unconservative expectation of the seismic performance of geosystems in common practice.

Results from 2D and 1D SRAs show consistent differences in the median transfer functions (TFs) and amplification factors (AFs) for various site conditions. The extent to which a median 2D seismic response is higher than a median 1D response depends on the site's $\sigma_{\ln V_S}$. The observed discrepancies are due to wave propagation mechanisms that are inherently uncaptured by 1D SRAs and the averaging effect of considering the median response across frequencies as representative. A parametric evaluation of V_{S30}, site depth, and V_S spatial variability features indicate that the

site's $\sigma_{\ln V_S}$ dominates the 2D median seismic response more strongly, whereas other parameters lead to modest changes in amplitude and standard deviation. Results from the estimated ground motion IMs also suggest that slnVs dominates the extent to which 2D SRA-based IMs are higher than 1D SRA-based IMs, and the strength of these two sets of IM's correlation. In the case of sites with $\sigma_{\ln V_S} > 0.3$, 1D SRA-based IMs are likely unconservative. It is recommended that 2D SRAs that explicitly model V_S spatial variability are conducted for highly variable sites.

The findings of this evaluation are limited to the conditions considered herein (e.g., 2D models with a horizontal base and the availability of numerically sampled 1D V_S profiles), as well as a relatively large number of 2D and 1D results leading to smooth median TF and AF. Further investigations such as the effects of soils' nonlinearity, more complex geological configurations, and comparisons with empirical data are deemed necessary. Discrepancies between 2D and 1D seismic responses are expected to be larger in most practical applications.

REFERENCES

Afshari K and Stewart JP (2019) Insights from California vertical arrays on the effectiveness of ground response analysis with alternative damping models. *Bulletin of the Seismological Society of America* 109: 1250-1264.

Ancheta TD, Darragh RB, Stewart JP, Seyhan E, Silva WJ, Chiou BSJ, Wooddell KE, Graves RW, Kottke AR, Boore DM, Kishida T and Donahue JL (2013) *PEER NGA-West2 database.* Report PEER 2013/03. Berkeley, CA: Pacific Earthquake Engineering Research Center (PEER), University of California, Berkeley.

Arias A (1970) *A measure of earthquake intensity.* In Seismic Design for Nuclear Power Plants (Hansen R. J., ed.), The MIT Press, Cambridge, MA.

Armstrong RJ, Kishida T and Park DS (2020) Efficiency of ground motion intensity with earthquake–induced earth dam deformations. *Earthquake Spectra* 37(1): 5-25.

Baecher G and Christian J (2003) *Reliability and statistics in geotechnical engineering.* Wiley.

De la Torre C, McGann C, Bradley B and Pletzer A (2019) 3D seismic site response with soil heterogeneity and wave scattering in OpenSees. In: *Proceedings of the 1st Eurasian conference on OpenSees: OpenSees Days Eurasia*, Hong Kong, China, 20–21 June, pp. 255–262. Hong Kong, China: Department of Building Services Engineering, Faculty of Construction and the Environment, The Hong Kong Polytechnic University.

Electric Power Research Institute (EPRI) (2008) *A criterion for determining exceedance of the operating basis earthquake.* NP-5930. February. Palo Alto, CA: EPRI.

Electric Power Research Institute (EPRI) (2013) *Seismic evaluation guidance: Screening, prioritization and implementation details (SPID) for the resolution of Fukushima near-term task force recommendation 2.1: Seismic.* Report no. 1025287, 28 February. Palo Alto, CA: EPRI.

Hallal MM and Cox BR (2021) Comparison of different methods used to account for shear wave velocity variability in 2D ground response analyses. In: *Proceedings of the International Foundation Conference,* Dallas, Texas.

Hudson MB, Idriss IM and Beikae M (2003) QUAD4MU: Addendum to user's manual for QUAD4M for updates to the QUAD4MU version. Report, Center for Geotechnical Modeling, University of California, Davis, Davis, CA, 4 March.

Kaklamanos J, Bradley BA, Moolacattu AN and Picard BM (2020) Physical hypotheses for adjusting coarse profiles and improving 1D site-response estimation assessed at 10 KiK-net sites. *Bulletin of the Seismological Society of America* 110(3): 1338–1358.

Kaklamanos J, Bradley BA, Thompson EM and Baise LG (2013) Critical parameters affecting bias and variability in site-response analyses using KiK-net downhole array data. *Bulletin of the Seismological Society of America* 103: 1733-1749.

Kamai R, Abrahamson NA and Silva WJ (2016) V_{S30} in the NGA GMPEs: Regional differences and suggested practice. *Earthquake Spectra* 32(4): 2083–2108.

Kokusho T (2017) *Innovative Earthquake Soil Dynamics.* CRC Press.

Kuhlemeyer RL and Lysmer J (1973) Finite element method accuracy for wave propagation problems. *Journal of the Soil Mechanics and Foundations Division* 99(5): 421–427.

Kwok AOL, Stewart JP, Hashash YMA, Matasovic N, Pyke R, Wang Z and Yang Z (2007) Use of exact solutions of wave propagation problems to guide implementation of nonlinear seismic ground response analysis procedures. *Journal of Geotechnical and Geoenvironmental Engineering* 133(11): 1385-98.

Nour A, Slimani A, Laouami N and Afra H (2003) Finite element model for the probabilistic seismic response of heterogeneous soil profile. *Soil Dynamics and Earthquake Engineering* 23(5): 331–348.

Pehlivan M (2013) *Incorporating site response analysis and associated uncertainties into the seismic hazard assessment of nuclear facilities.* PhD Dissertation, The University of Texas at Austin, Austin, TX.

Pehlivan M, Rathje EM and Gilbert RB (2012) Influence of 1D and 2D spatial variability on site response analysis. In: *Proceedings of the 15th World Conference on Earthquake Engineering*, Lisbon.

Pretell R, Ziotopoulou K and Abrahamson NA (2022) Conducting 1D site response analyses to capture 2D V_S spatial variability effects. *Earthquake Spectra* 00(0): 1-25.

Roy N, Mukherjee S and Sahu RB (2020) Influence of trapped soft/stiff soil layer in seismic site response analysis. *Journal of Earth System Science* 129: 171.

Stewart JP, Kwok AO-L, Hashash YMA, Matasovic N, Pyke R, Wang Z and Yang Z (2008) *Benchmarking of nonlinear geotechnical ground response analysis procedures.* Report no. PEER 2008/04, August. Berkeley, CA: Pacific Earthquake Engineering Research Center (PEER), University of California, Berkeley.

Tao Y and Rathje E (2019) Insights into modeling small-strain site response derived from downhole array data. *Bulletin of the Seismological Society of America* 110(1): 288–294.

Teague D and Cox B (2016) Site response implications associated with using non-unique V_S profiles from surface wave inversion in comparison with other commonly used methods of accounting for V_S uncertainty. *Soil Dynamics and Earthquake Engineering* 91(2016): 87–103.

Vanmarcke EH (1983) *Random fields: Analysis and synthesis.* The MIT press, Cambridge.

Wills CJ and Clahan KB (2006) Developing a map of geologically defined site-conditions categories for California. *Bulletin of the Seismological Society of America* 96(4A): 1483–1501.

FIGURES

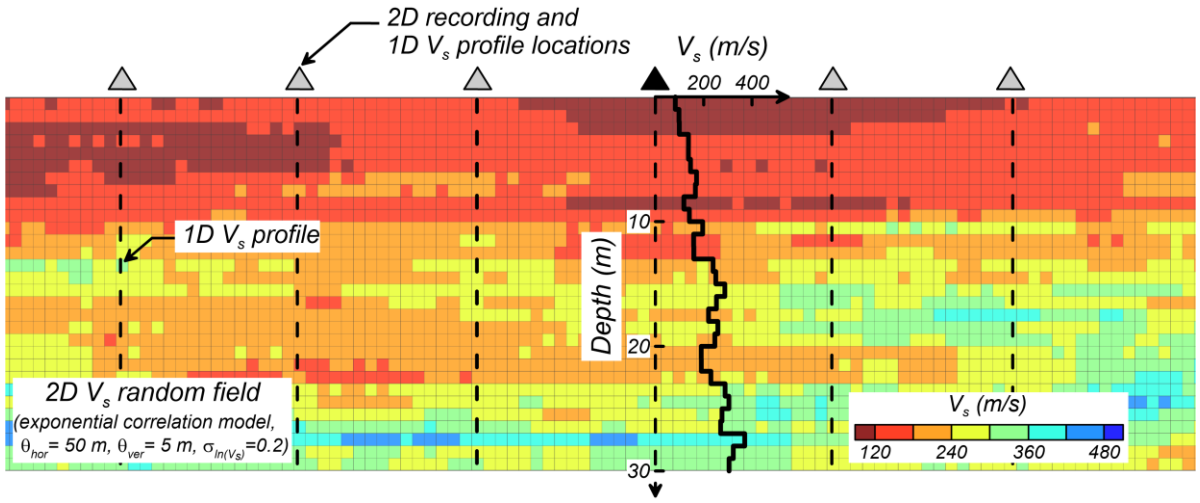

Figure A1: Example window of numerical site with spatially variable V_S.

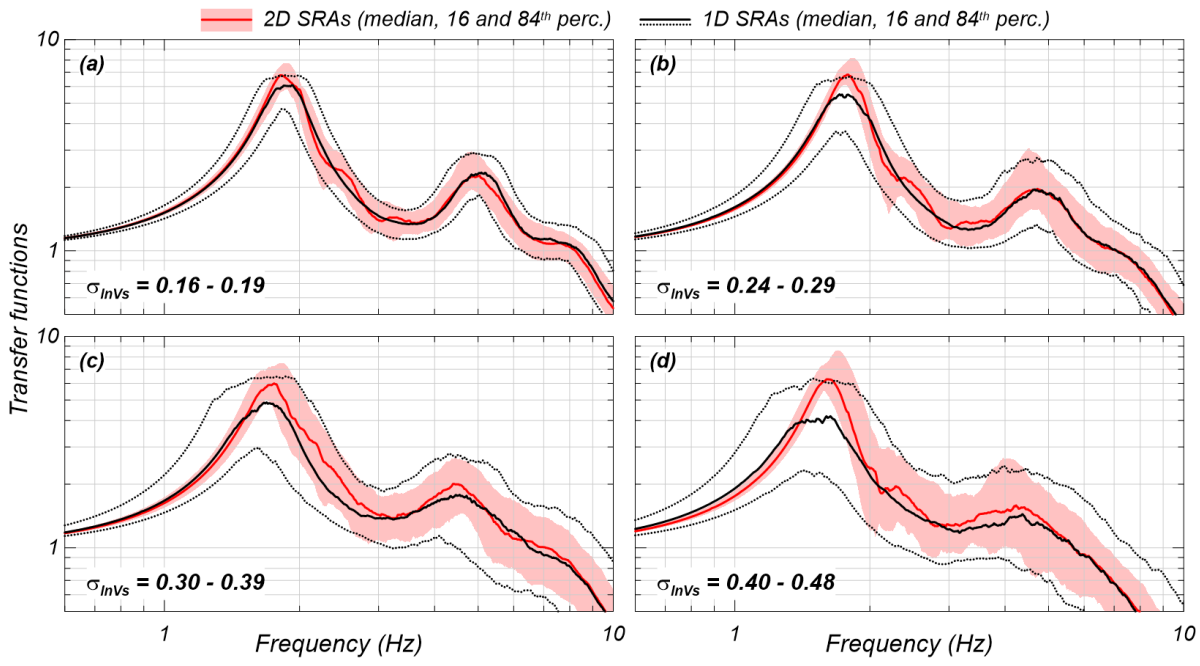

Figure A2: Transfer functions estimated using 2D SRAs on sites with increasing Vs spatial variability and 1D SRAs on columns sampled from the sites.

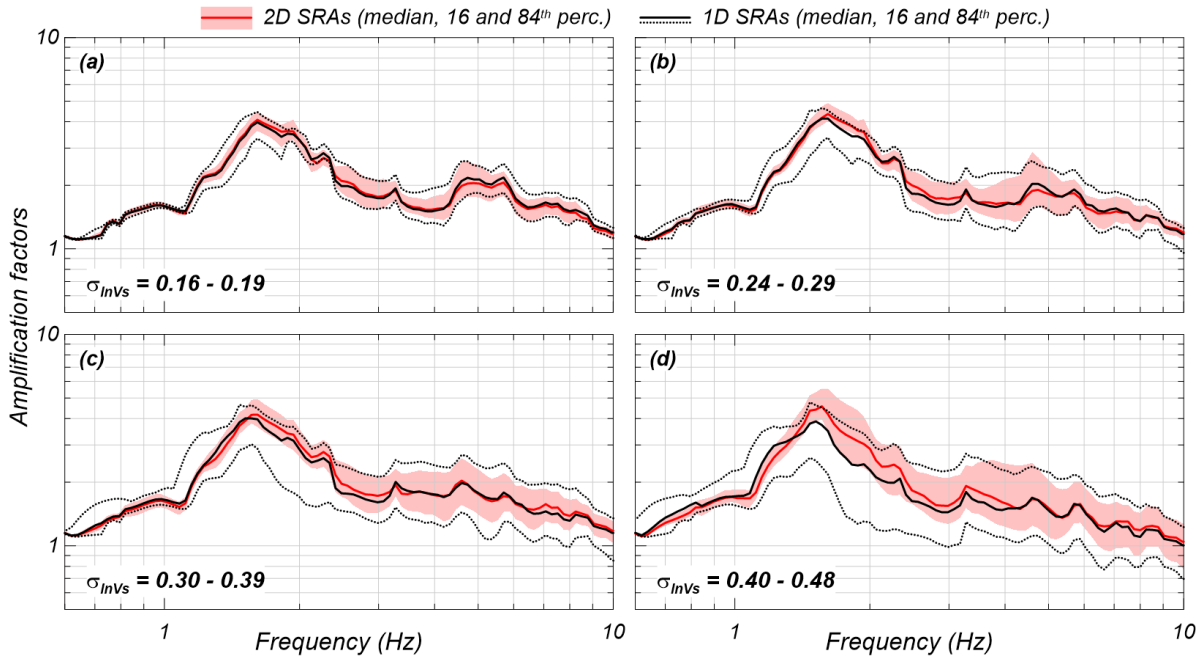

Figure A3: Amplification factors estimated using 2D SRAs on sites with increasing Vs spatial variability and 1D SRAs on columns sampled from the sites.

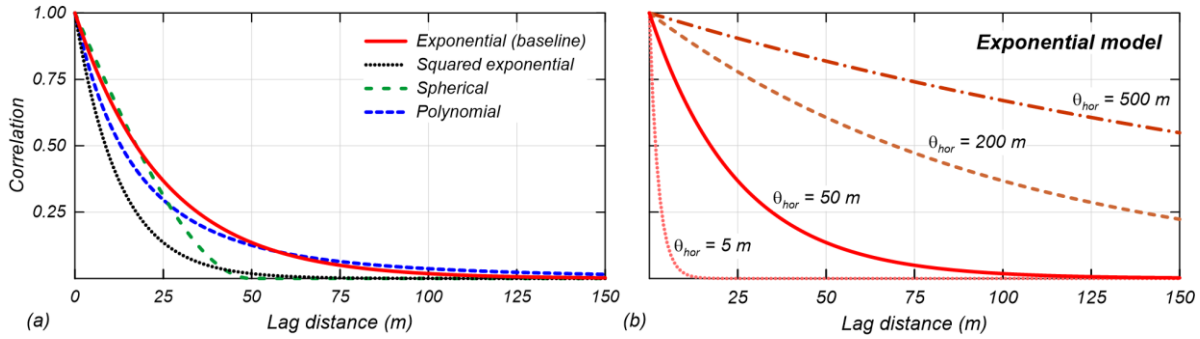

Figure A4: Correlation models: (a) various types of correlation models, and (b) the exponential model for various correlation lengths.

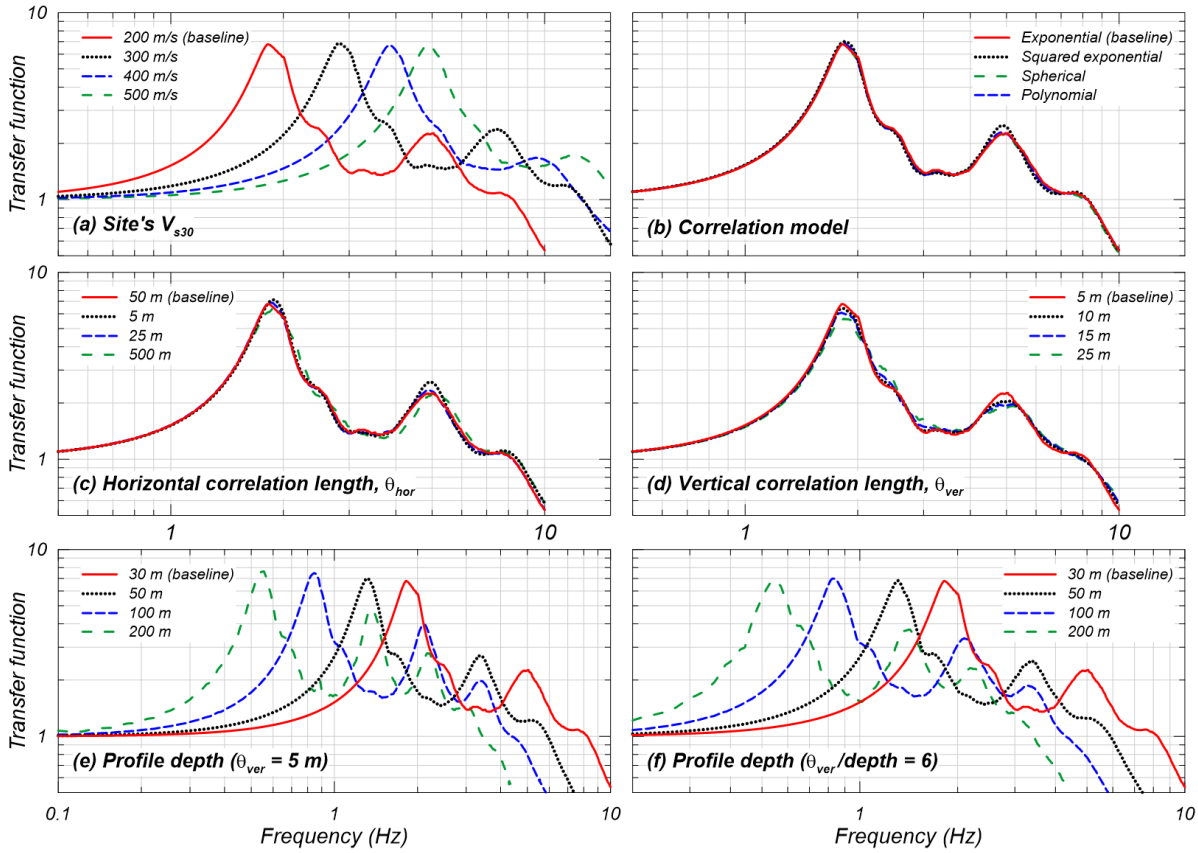

Figure A5: Effect of different site's V_S features on median 2D transfer functions.

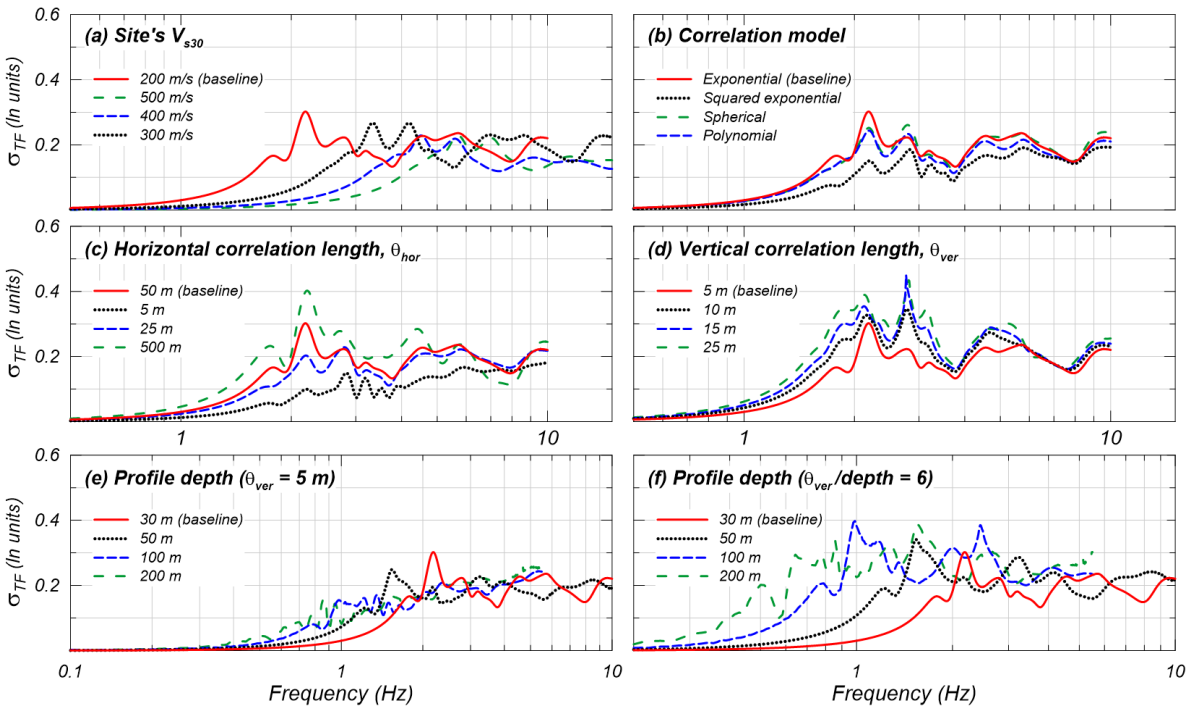

Figure A6: Effect of site's V_S features on the standard deviation of 2D transfer functions.

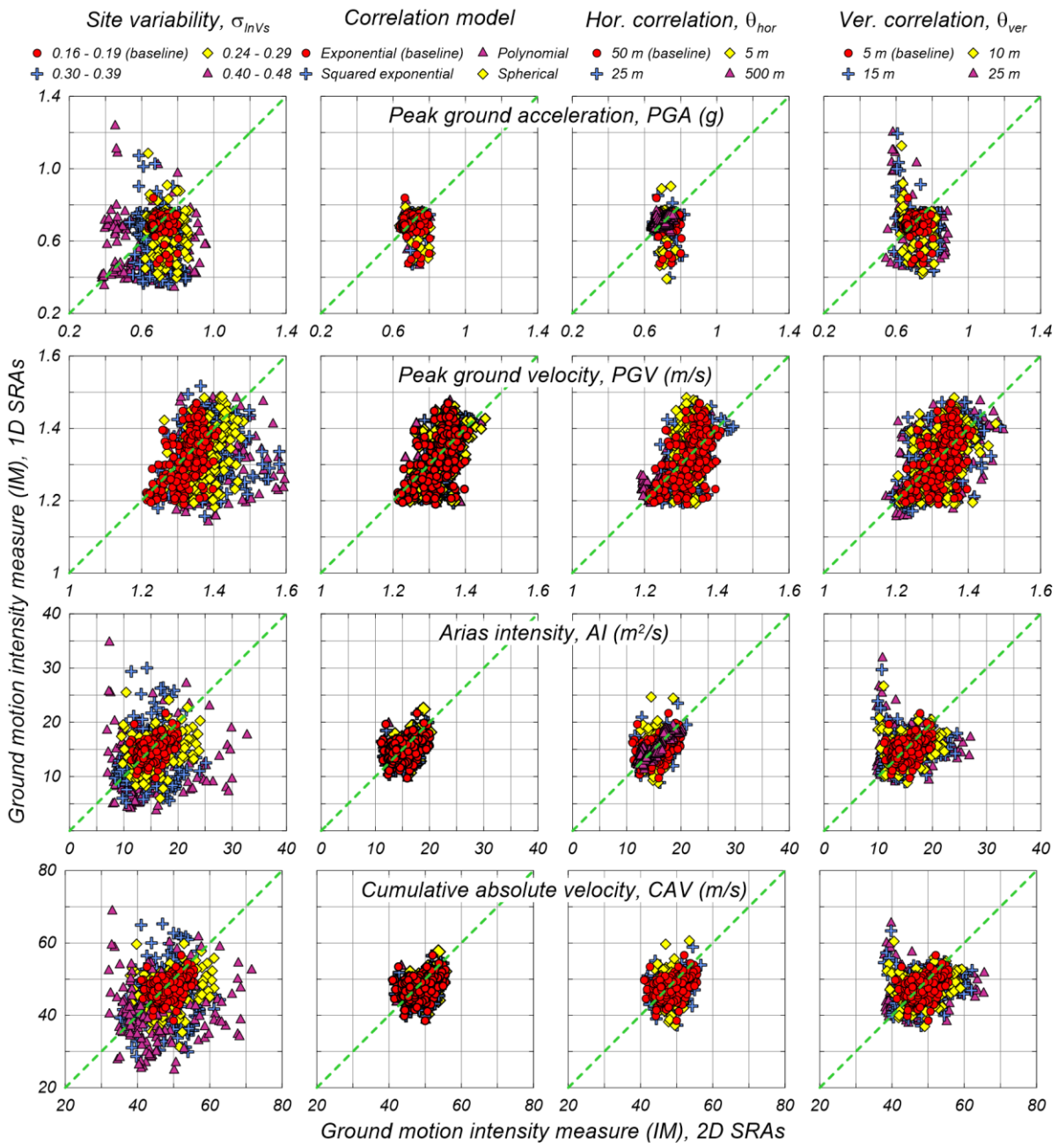

Figure A7: Effect of features of 2D V_S spatial variability on the discrepancies between 2D and 1D SRAs for common ground motion intensity measures (IMs).

TABLES

Table A1. Summary of investigated V_S spatial variability features.

Parameter	Baseline case	Parametric evaluation
Site's V_{S30} (m/s)	200	300, 400, 500
Correlation model	Exponential	Spherical, polynomial decaying, squared exponential
Horizontal correlation length, θ_{hor} (m)	50	5, 25, 500
Vertical correlation length, θ_{ver} (m)	5	10, 15, 25
Site depth with constant θ_{ver} = 5 m (m)	30	50, 100, 200
Site depth with constant θ_{ver}/depth = 6 (m)	30	50, 100, 200

Note: In all cases, input $\sigma_{\ln V_S}$ = 0.20 ln units.

APPENDIX B

PEARSON'S CORRELATION COEFFICIENTS FOR 1D-LIKE SITES

Table B1. Pearson's correlation coefficient (r) between empirical and theoretical transfer functions (TFs) for various frequency ranges.

No	Site	f_0 to f_1	f_0 to f_2	f_0 to f_3	f_1 to f_2	f_2 to f_3
1	Corona I-15 Highway 91	0.42	0.42	0.43	0.59	0.54
2	Delaney Park	0.47	0.45	0.45	0.39	0.67
3	El Centro	0.60	0.52	0.52	0.40	0.64
4	Hayward San Mateo Bridge	0.50	0.45	0.42	0.32	0.04
5	San Bernardino	0.35	0.39	0.37	0.66	-0.56
6	Treasure Island	0.52	0.52	0.52	0.56	0.34
7	Wildlife	0.58	0.56	0.53	0.61	0.49
8	AICH09	0.45	0.42	0.41	0.51	0.51
9	AICH16	0.54	0.51	0.49	0.38	0.11
10	CHBH17	0.46	0.47	0.43	0.56	0.26
11	FKIH05	0.52	0.48	0.40	0.52	0.24
12	FKSH16	0.45	0.43	0.40	0.29	-0.10
13	GIFH18	0.47	0.41	0.36	0.66	-0.07
14	GIFH28	0.61	0.60	0.57	0.53	-0.17
15	IBRH11	0.47	0.33	0.19	0.24	0.85
16	IBRH13	0.40	0.44	0.33	0.49	0.01
17	IBRH17	0.36	0.43	0.38	0.74	0.54
18	IBUH01	0.41	0.33	0.22	0.60	0.09
19	IBUH05	0.46	0.35	0.35	0.26	0.45
20	IWTH04	0.62	0.60	0.60	0.67	0.58
21	IWTH08	0.49	0.42	0.37	0.23	-0.07
22	KGSH03	0.76	0.76	0.67	0.78	0.46
23	KMMH08	0.40	0.39	0.38	0.65	-0.66
24	KMMH13	0.42	0.41	0.40	0.47	0.54
25	KOCH10	0.45	0.45	0.43	-0.14	0.09
26	MIEH07	0.44	0.45	0.43	0.63	0.23
27	MYGH06	0.76	0.70	0.54	0.73	0.46
28	MYZH01	0.49	0.35	0.32	0.45	0.76
29	NGNH20	0.55	0.38	0.32	0.17	0.21
30	NGNH21	0.68	0.60	0.55	0.22	0.44

No	Site	f_0 to f_1	f_0 to f_2	f_0 to f_3	f_1 to f_2	f_2 to f_3
31	NIGH15	0.66	0.64	0.64	0.64	0.78
32	NMRH03	0.48	0.47	0.45	0.58	0.45
33	NMRH04	0.39	0.46	0.37	0.71	0.28
34	NMRH05	0.38	0.32	0.34	0.23	0.64
35	SBSH06	0.42	0.39	0.37	0.38	0.48
36	SZOH25	0.35	0.40	0.39	0.64	0.40
37	TCGH12	0.42	0.39	0.35	0.58	0.75
38	TKSH04	0.44	0.48	0.48	0.28	-0.42
39	YMTH12	0.50	0.41	0.38	-0.04	-0.03

[1] f_0: TF's fundamental frequency, f_1 to f_3: TF's second to fourth frequency modes.

[2] The upper bound frequency could be lower if the recordings' signal-to-noise ratio (SNR) does not meet the set criterion (Pretell et al., under review).

APPENDIX C

ROOT MEAN SQUARE ERROR (RMSE) FOR 1D-LIKE SITES

Table C1. Average root mean square error (RMSE) or L2 error on transfer functions (TFs) for selected cases of damping multiplier (D_{mul}) and V_S standard deviation ($\sigma_{\ln V_S}$) for randomization.

No	Site	$D_{mul} = 1$	$D_{mul} = 3$	$\sigma_{\ln V_S} = 0.25$	$D_{mul} = 3$ $\sigma_{\ln V_S} = 0.25$
1	Corona I-15 Highway 91	0.98	0.98	1.00	1.02
2	Delaney Park	0.61	0.50	0.40	0.43
3	El Centro	0.67	0.66	0.63	0.67
4	Hayward San Mateo Bridge	0.81	0.61	0.57	0.51
5	San Bernardino	0.75	0.63	0.58	0.51
6	Treasure Island	0.73	0.82	0.79	1.00
7	Wildlife	0.66	0.78	0.63	0.86
8	AICH09	0.82	0.89	0.80	0.90
9	AICH16	0.64	0.64	0.68	0.77
10	CHBH17	0.69	0.64	0.54	0.59
11	FKIH05	1.09	1.02	1.12	1.15
12	FKSH16	0.73	0.66	0.56	0.55
13	GIFH18	0.71	0.58	0.38	0.36
14	GIFH28	0.86	0.84	0.80	0.82
15	IBRH11	0.96	0.99	0.95	1.03
16	IBRH13	0.83	0.85	0.81	0.89
17	IBRH17	0.85	0.95	0.93	1.09
18	IBUH01	0.77	0.79	0.66	0.73
19	IBUH05	0.75	0.70	0.50	0.53
20	IWTH04	0.67	0.67	0.63	0.74
21	IWTH08	0.73	0.83	0.76	0.90
22	KGSH03	0.82	0.68	0.43	0.46
23	KMMH08	0.79	0.65	0.56	0.51
24	KMMH13	0.72	0.78	0.53	0.68
25	KOCH10	0.88	0.73	0.48	0.43
26	MIEH07	0.71	0.62	0.55	0.43
27	MYGH06	0.76	0.61	0.54	0.50
28	MYZH01	0.84	0.70	0.64	0.56
29	NGNH20	0.62	0.55	0.53	0.57

No	Site	$D_{mul} = 1$	$D_{mul} = 3$	$\sigma_{lnV_S} = 0.25$	$D_{mul} = 3$ $\sigma_{lnV_S} = 0.25$
30	NGNH21	0.75	0.64	0.45	0.41
31	NIGH15	0.69	0.67	0.47	0.56
32	NMRH03	0.70	0.66	0.42	0.52
33	NMRH04	0.62	0.65	0.46	0.59
34	NMRH05	0.73	0.74	0.52	0.67
35	SBSH06	0.67	0.65	0.41	0.55
36	SZOH25	0.74	0.79	0.71	0.82
37	TCGH12	0.74	0.73	0.55	0.60
38	TKSH04	0.84	0.77	0.65	0.65
39	YMTH12	0.92	0.72	0.65	0.49

Table C2. Average root mean square error (RMSE) or L2 error on amplification factors (AFs) for selected cases of damping multiplier (D_{mul}) and V_S standard deviation ($\sigma_{\ln V_S}$) for randomization.

No	Site	$D_{mul} = 1$	$D_{mul} = 3$	$\sigma_{\ln V_S} = 0.25$	$D_{mul} = 3$ $\sigma_{\ln V_S} = 0.25$
1	Corona I-15 Highway 91	0.40	0.48	0.35	0.42
2	Delaney Park	0.70	0.42	0.67	0.31
3	El Centro	0.37	0.36	0.37	0.40
4	Hayward San Mateo Bridge	0.97	0.64	0.95	0.60
5	San Bernardino	0.61	0.41	0.55	0.34
6	Treasure Island	0.25	0.38	0.25	0.44
7	Wildlife	0.33	0.63	0.30	0.65
8	AICH09	0.40	0.42	0.36	0.35
9	AICH16	0.36	0.33	0.37	0.32
10	CHBH17	0.49	0.39	0.51	0.41
11	FKIH05	0.66	0.66	0.66	0.68
12	FKSH16	0.69	0.46	0.64	0.39
13	GIFH18	0.77	0.57	0.74	0.51
14	GIFH28	0.51	0.39	0.45	0.33
15	IBRH11	0.41	0.41	0.36	0.34
16	IBRH13	0.36	0.39	0.31	0.40
17	IBRH17	0.30	0.43	0.22	0.33
18	IBUH01	0.39	0.44	0.34	0.39
19	IBUH05	0.66	0.39	0.71	0.40
20	IWTH04	0.50	0.36	0.48	0.35
21	IWTH08	0.34	0.46	0.29	0.45
22	KGSH03	0.89	0.72	0.80	0.67
23	KMMH08	0.79	0.57	0.71	0.46
24	KMMH13	0.63	0.53	0.61	0.49
25	KOCH10	1.04	0.83	0.97	0.73
26	MIEH07	0.73	0.56	0.76	0.53
27	MYGH06	0.88	0.58	0.92	0.65
28	MYZH01	0.80	0.61	0.73	0.53
29	NGNH20	0.45	0.33	0.45	0.29

No	Site	$D_{mul} = 1$	$D_{mul} = 3$	$\sigma_{lnV_S} = 0.25$	$D_{mul} = 3$ $\sigma_{lnV_S} = 0.25$
30	NGNH21	0.75	0.58	0.77	0.56
31	NIGH15	0.46	0.38	0.43	0.32
32	NMRH03	0.61	0.44	0.65	0.42
33	NMRH04	0.24	0.43	0.26	0.39
34	NMRH05	0.53	0.45	0.53	0.43
35	SBSH06	0.78	0.54	0.77	0.52
36	SZOH25	0.42	0.38	0.39	0.38
37	TCGH12	0.39	0.40	0.51	0.36
38	TKSH04	0.52	0.41	0.40	0.33
39	YMTH12	1.23	0.97	1.18	0.90

APPENDIX D

STANDARDIZED L1 ERRORS IN TRANSFER FUNCTIONS AND AMPLIFICATION FACTORS FOR VARIOUS D_{mul}-σ_{lnV_S} COMBINATIONS

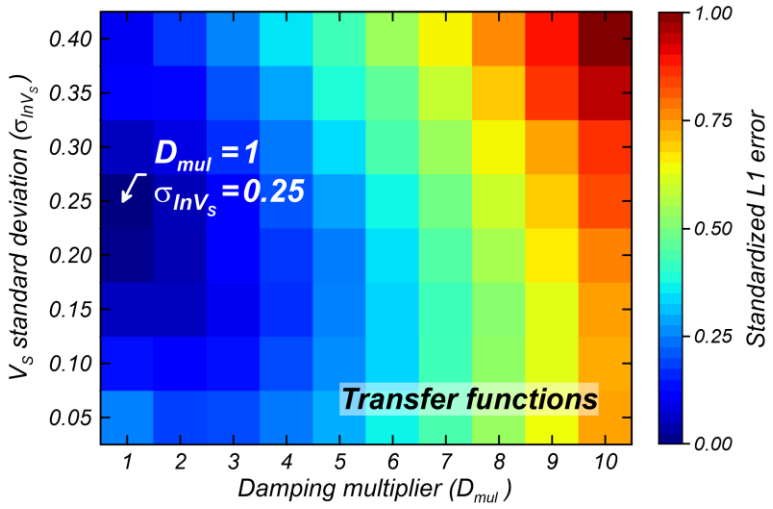

Figure D1. Standardized L1 error in transfer functions (TFs) for various combinations of damping multiplier (D_{mul}) and V_S standard deviation (σ_{lnV_S}) for V_S randomization. Minimum standardized L1 error for D_{mul} = 1, and σ_{lnV_S} = 0.25.

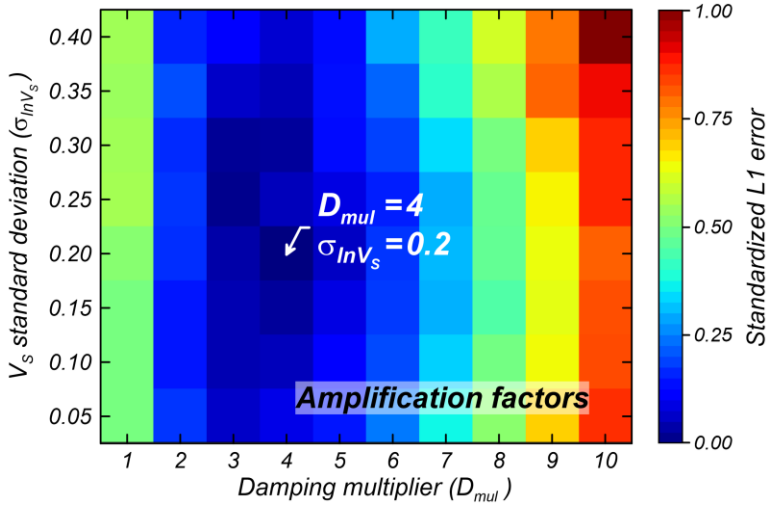

Figure D2. Standardized L1 error in amplification factors (AFs) for various combinations of damping multiplier (D_{mul}) and V_S standard deviation (σ_{lnV_S}) for V_S randomization. Minimum standardized L1 error for D_{mul} = 4, and σ_{lnV_S} = 0.2.

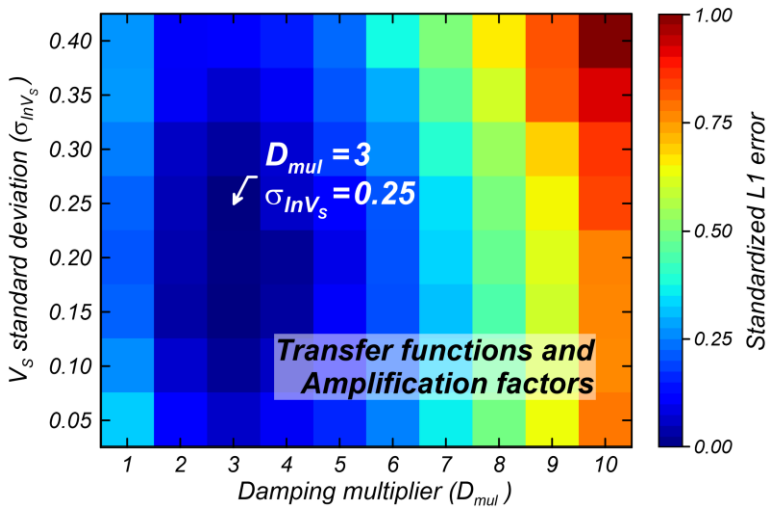

Figure D3. Standardized L1 errors for various combinations of damping multiplier (D_{mul}) and V_S standard deviation (σ_{lnV_S}) for V_S randomization. Averaged L1 error in transfer functions (Figure D1) and amplification factors (Figure D2). Minimum standardized L1 error for D_{mul} = 3, and σ_{lnV_S} = 0.25.

APPENDIX E

COMPARISON OF PREDICTED AND OBSERVED TRANSFER FUNCTIONS FOR 1D-LIKE SITES

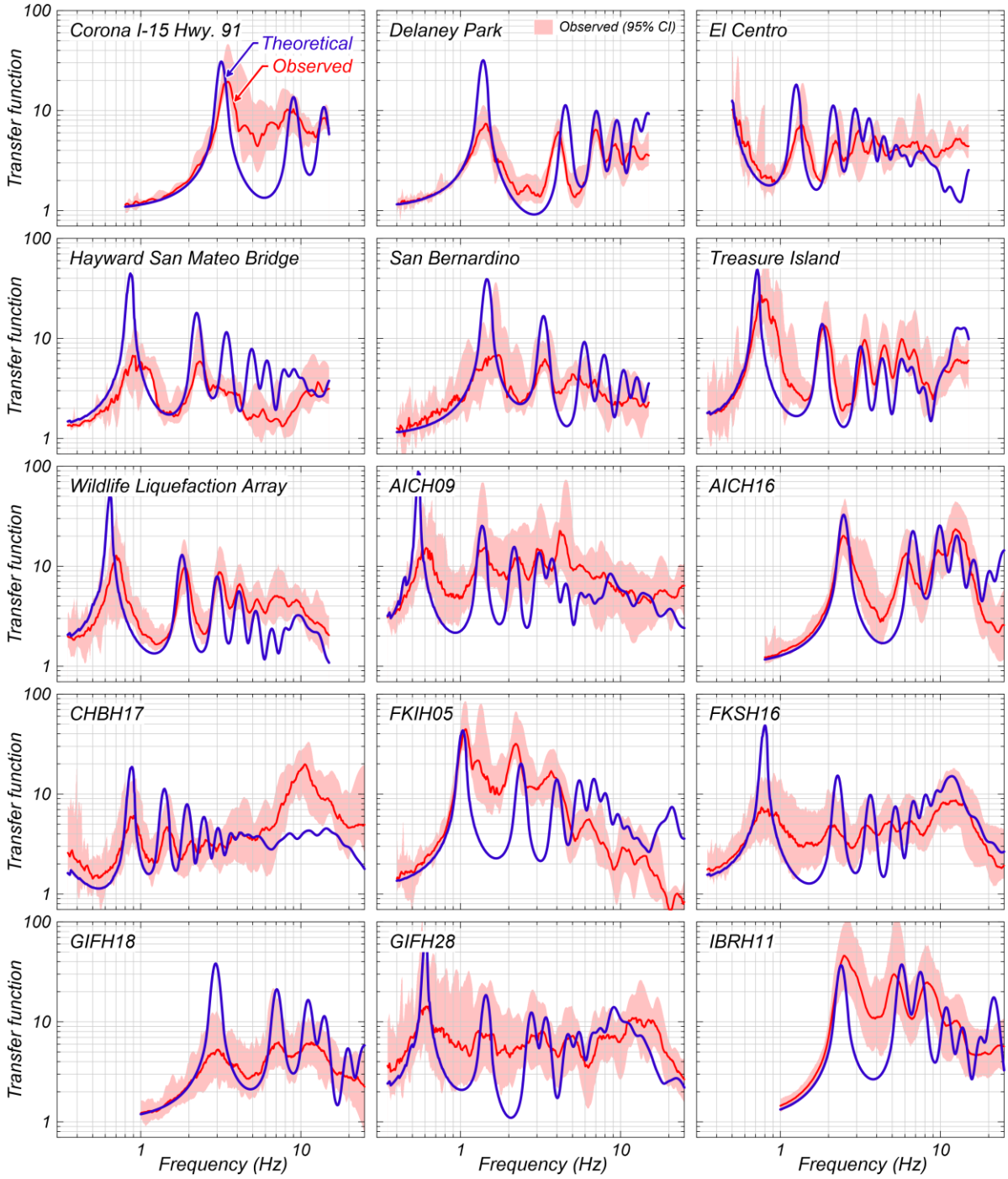

Figure E1. Transfer functions (TFs) for 1D-like sites (Part 1). Theoretical TFs based on measured V_S profiles, damping profiles after Darendeli (2001) with default parameters (PI = 0, OCR = 1, f_{load} = 1 Hz, and K_0 = 0.5). No damping multiplier (D_{mul}) or D_{mul} = 1 and no V_S randomization.

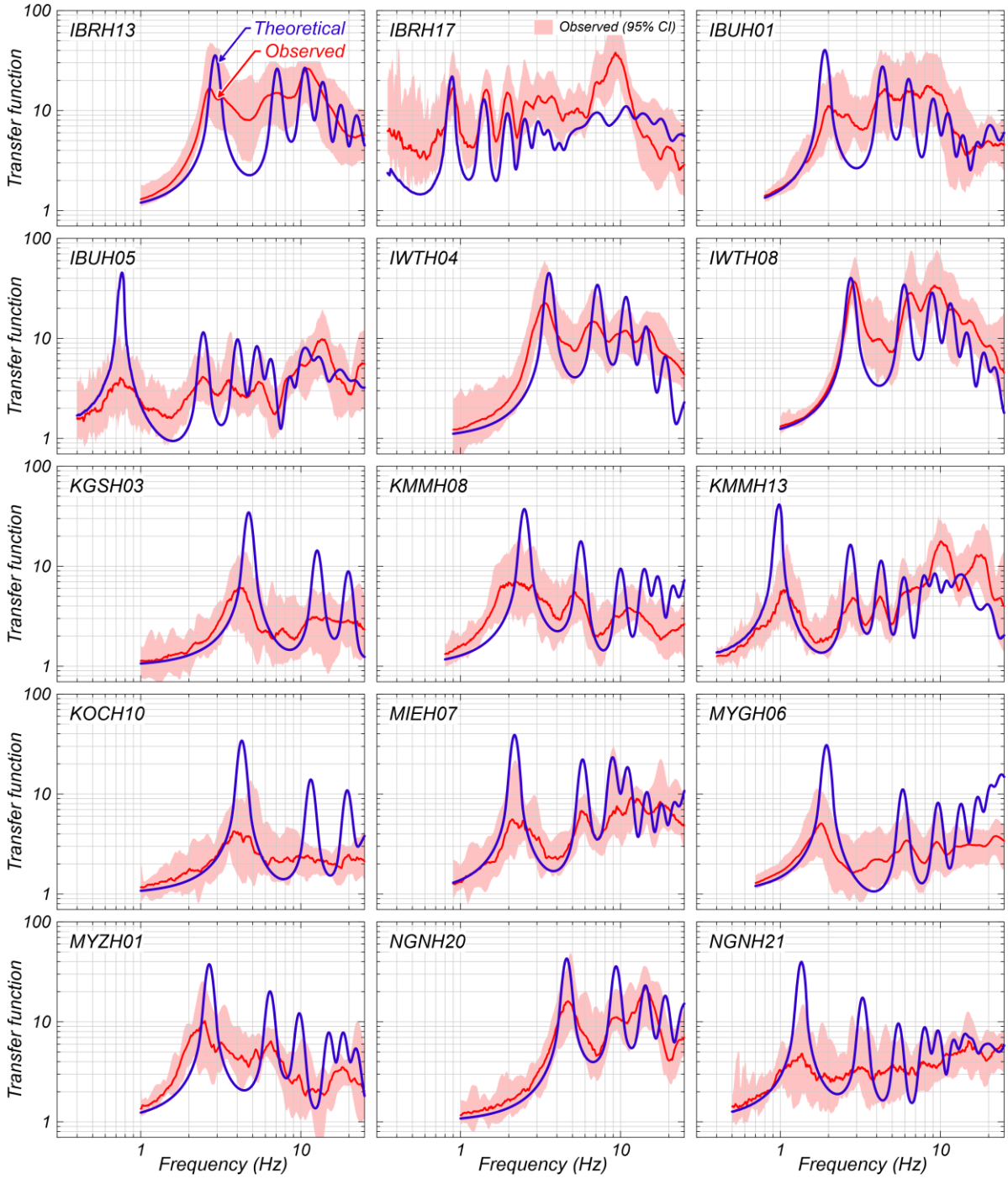

Figure E2. Transfer functions (TFs) for 1D-like sites (Part 2). Theoretical TFs based on measured V_S profiles, damping profiles after Darendeli (2001) with default parameters (PI = 0, OCR = 1, f_{load} = 1 Hz, and K_0 = 0.5). No damping multiplier (D_{mul}) or D_{mul} = 1 and no V_S randomization.

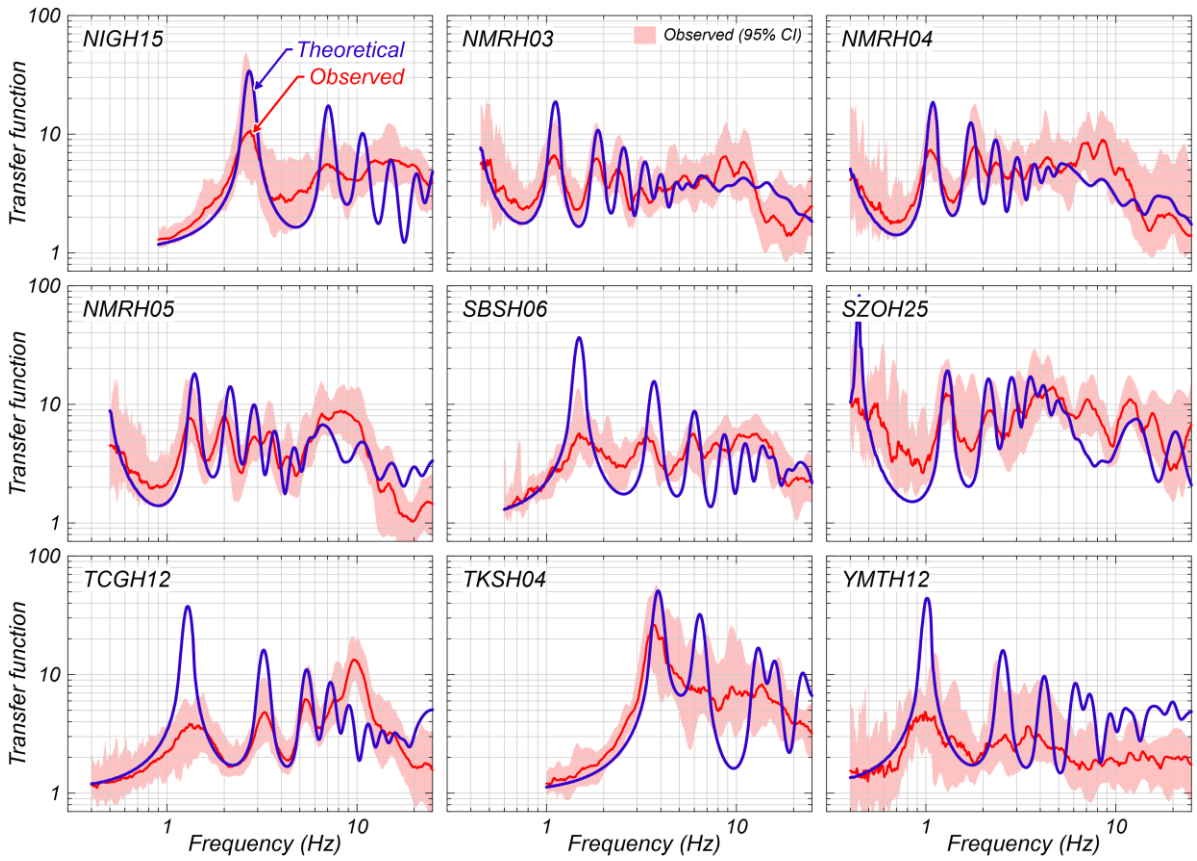

Figure E3. Transfer functions (TFs) for 1D-like sites (Part 3). Theoretical TFs based on measured V_S profiles, damping profiles after Darendeli (2001) with default parameters (PI = 0, OCR = 1, f_{load} = 1 Hz, and K_0 = 0.5). No damping multiplier (D_{mul}) or D_{mul} = 1 and no V_S randomization.

APPENDIX F

COMPARISON OF PREDICTED AND OBSERVED AMPLIFICATION FACTORS FOR 1D-LIKE SITES

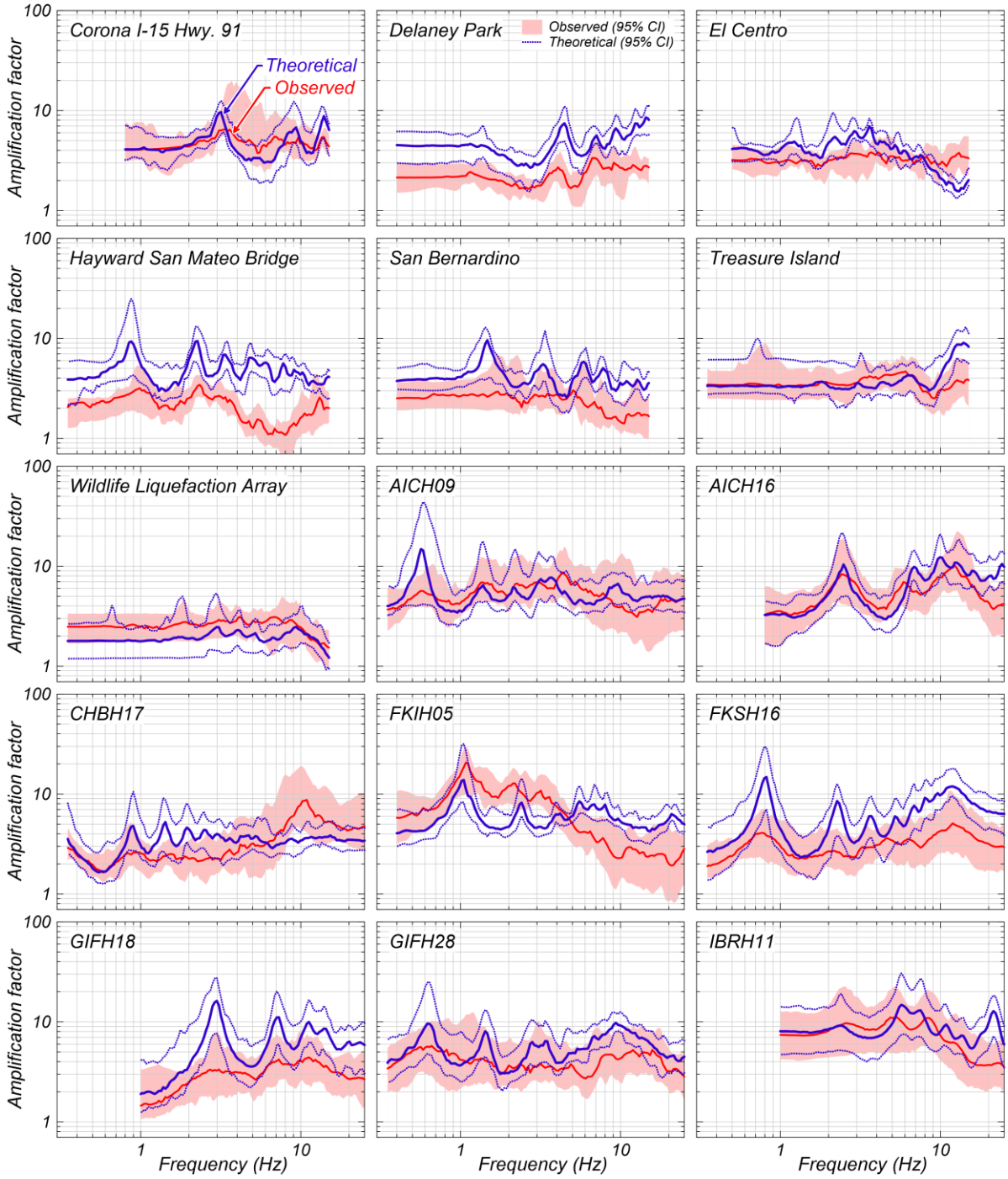

Figure F1. Amplification factors (AFs) for 1D-like sites (Part 1). Theoretical AFs based on measured V_S profiles, damping profiles after Darendeli (2001) with default parameters (PI = 0, OCR = 1, f_{load} = 1 Hz, and K_0 = 0.5). No damping multiplier (D_{mul}) or D_{mul} = 1 and no V_S randomization.

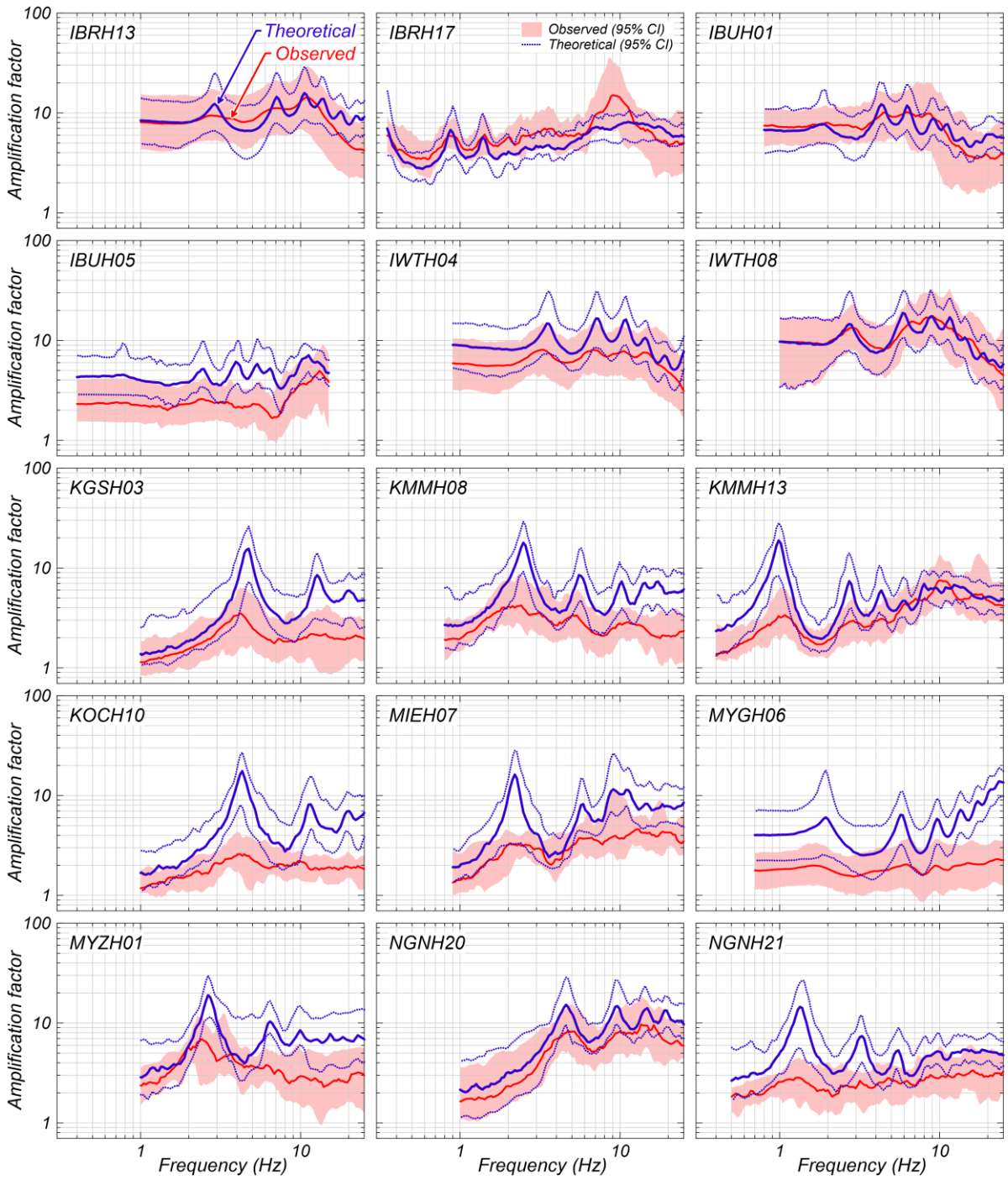

Figure F2. Amplification factors (AFs) for 1D-like sites (Part 2). Theoretical AFs based on measured V_S profiles, damping profiles after Darendeli (2001) with default parameters (PI = 0, OCR = 1, f_{load} = 1 Hz, and K_0 = 0.5). No damping multiplier (D_{mul}) or D_{mul} = 1 and no V_S randomization.

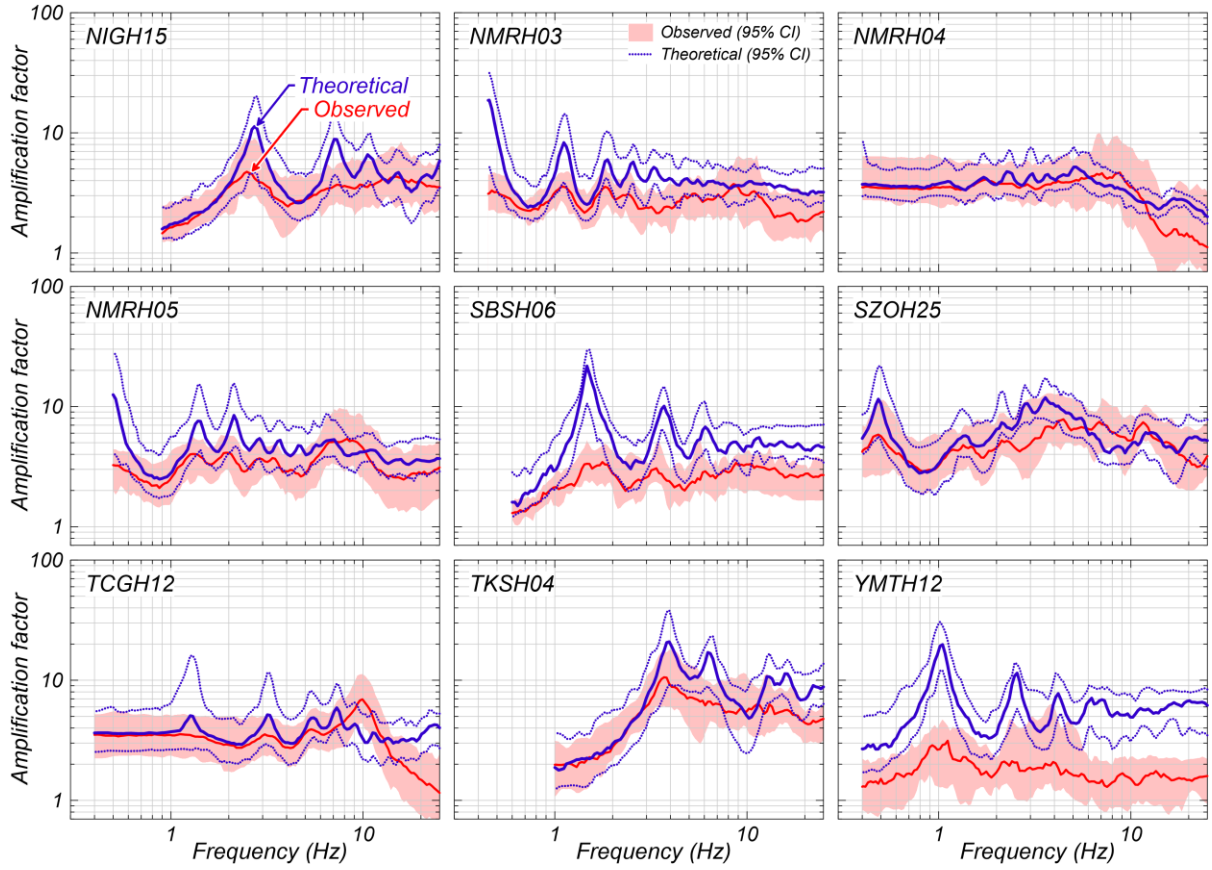

Figure F3. Amplification factors (AFs) for 1D-like sites (Part 3). Theoretical AFs based on measured V_S profiles, damping profiles after Darendeli (2001) with default parameters (PI = 0, OCR = 1, f_{load} = 1 Hz, and K_0 = 0.5). No damping multiplier (D_{mul}) or D_{mul} = 1 and no V_S randomization.

APPENDIX G

TRANSFER FUNCTIONS FOR 3D-LIKE SITES IN CALIFORNIA

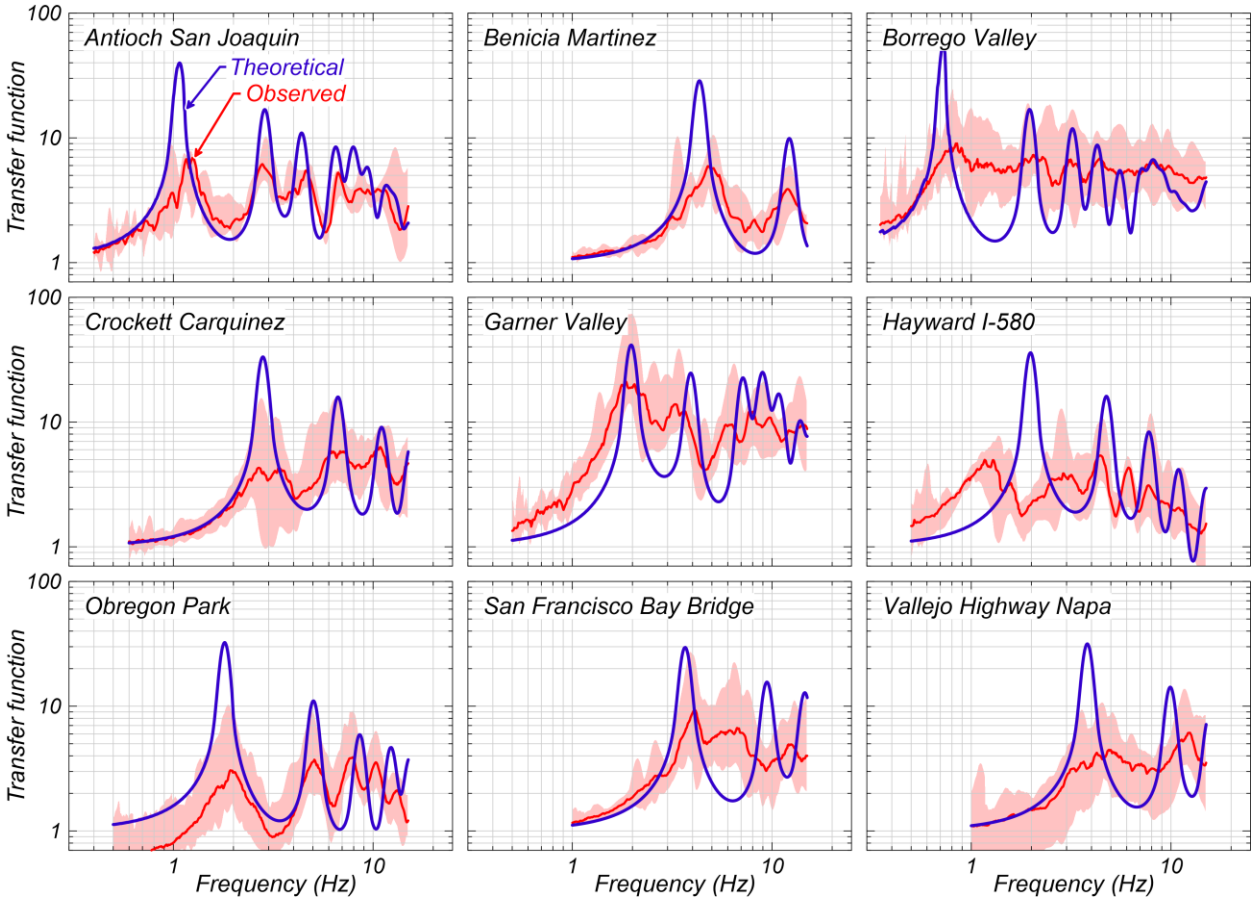

Figure G1. Transfer functions (TFs) for 3D-like sites in California. Theoretical TFs based on measured V_S profiles, damping profiles after Darendeli (2001) with default parameters (PI = 0, OCR = 1, f_{load} = 1 Hz, and K_0 = 0.5). No damping multiplier (D_{mul}) or D_{mul} = 1 and no V_S randomization.

APPENDIX H

AMPLIFICATION FACTORS FOR 3D-LIKE SITES IN CALIFORNIA

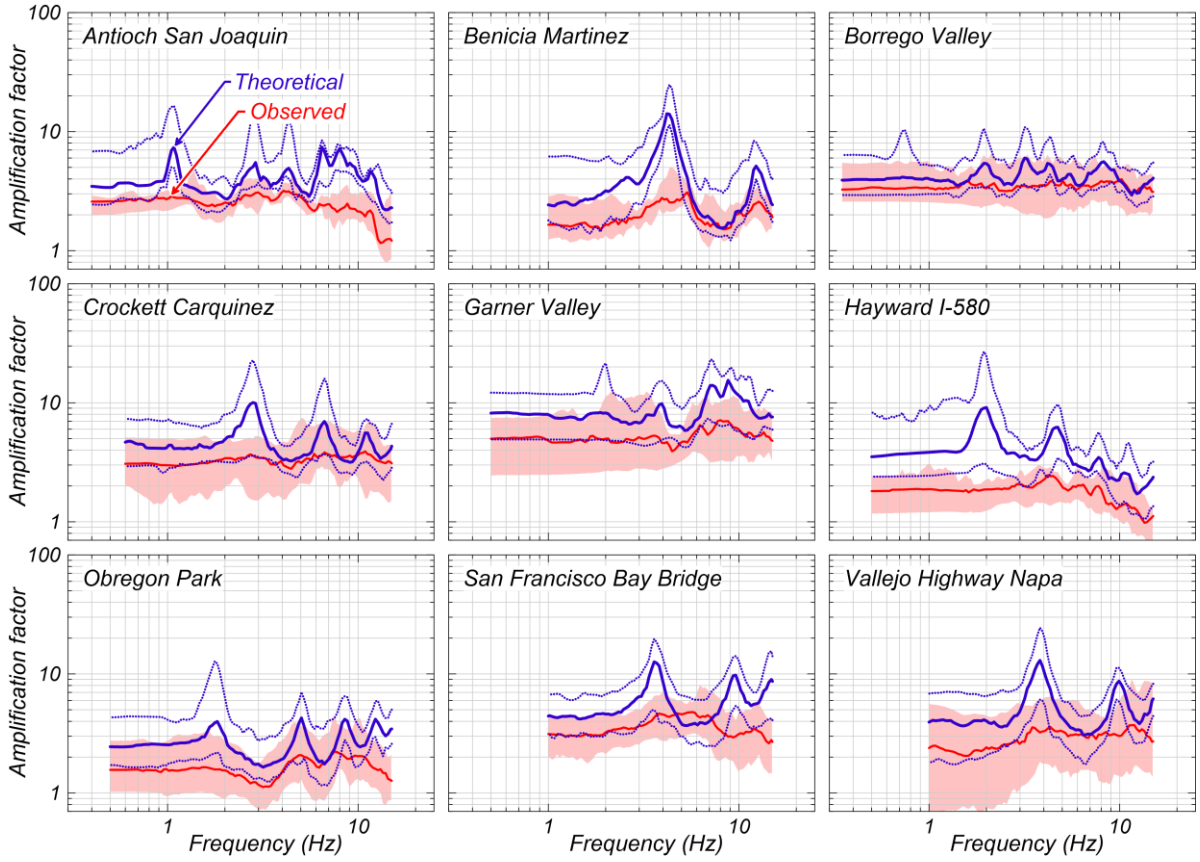

Figure H1. Amplification factors (AFs) for 3D-like sites in California. Theoretical AFs based on measured V_S profiles, damping profiles after Darendeli (2001) with default parameters (PI = 0, OCR = 1, f_{load} = 1 Hz, and K_0 = 0.5). No damping multiplier (D_{mul}) or D_{mul} = 1 and no V_S randomization.

APPENDIX I

IDENTIFICATION OF SITES
UNAFFECTED BY PSEUDO-RESONANCES

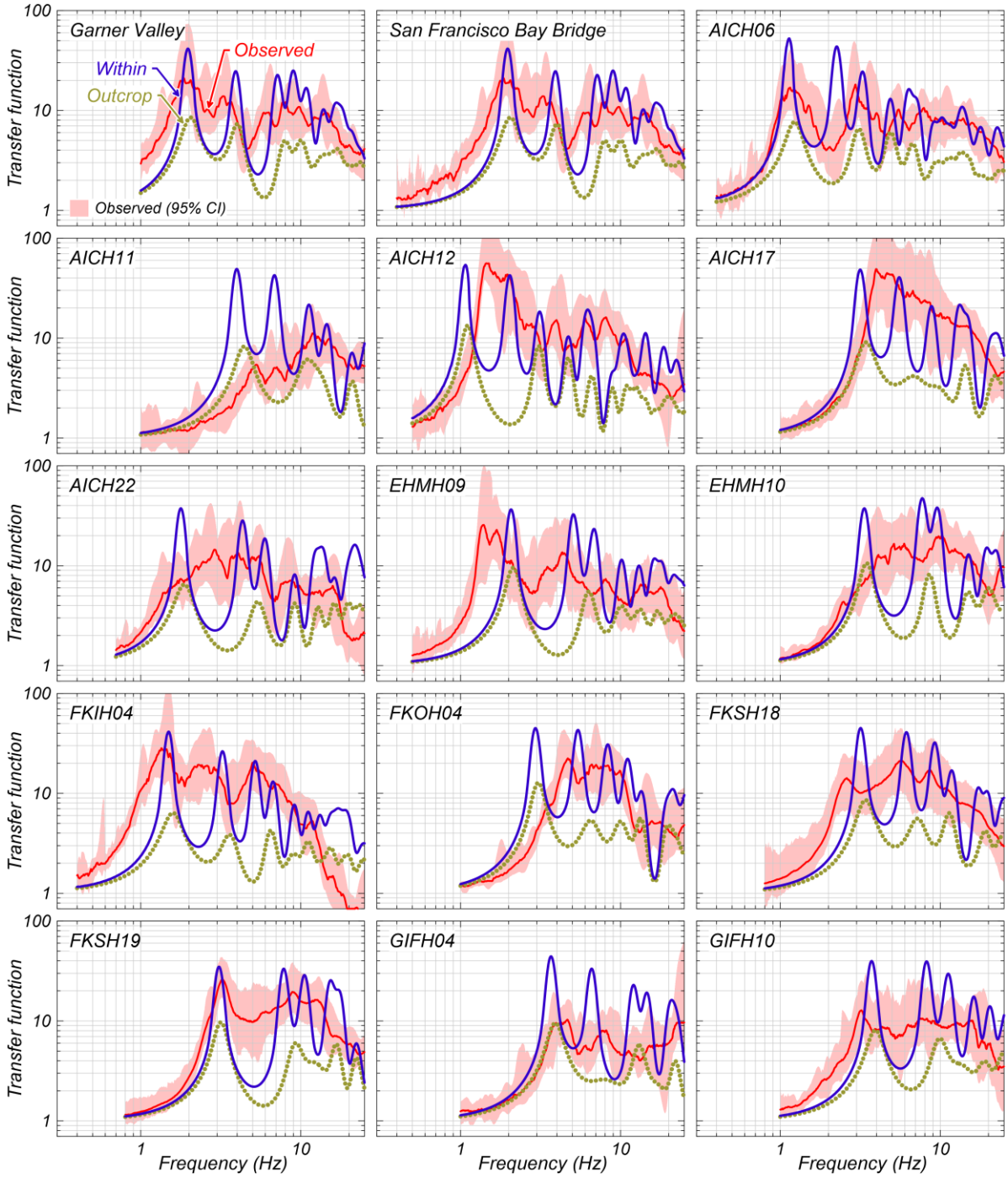

Figure I1. Transfer functions (TFs) for sites unaffected by pseudo-resonances (Part 1). Theoretical TFs based on measured V_S profiles, damping profiles after Darendeli (2001) with default parameters (PI = 0, OCR = 1, f_{load} = 1 Hz, and K_0 = 0.5). No damping multiplier (D_{mul}) or D_{mul} = 1 and no V_S randomization.

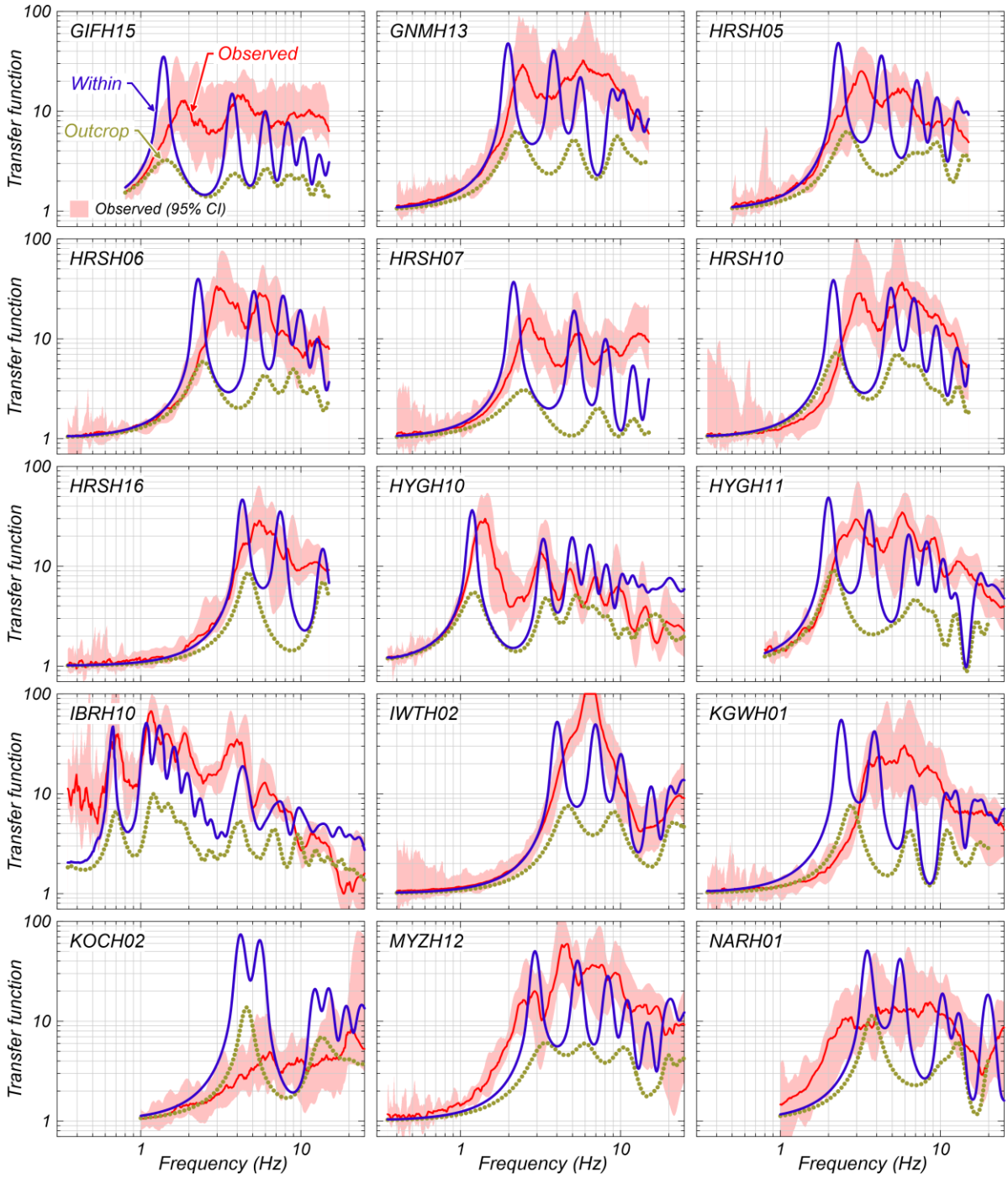

Figure I2. Transfer functions (TFs) for sites unaffected by pseudo-resonances (Part 2). Theoretical TFs based on measured V_S profiles, damping profiles after Darendeli (2001) with default parameters (PI = 0, OCR = 1, f_{load} = 1 Hz, and K_0 = 0.5). No damping multiplier (D_{mul}) or D_{mul} = 1 and no V_S randomization.

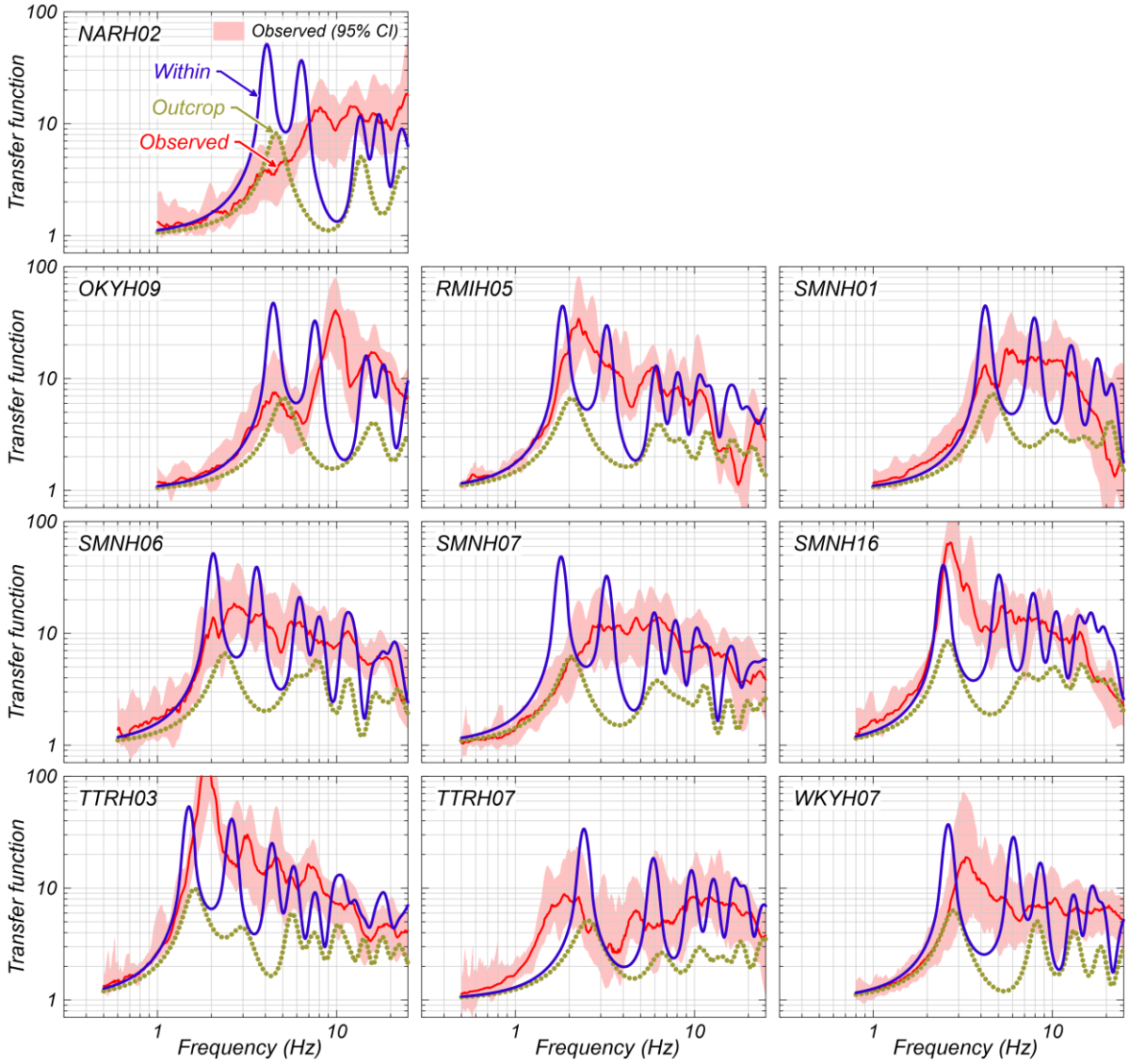

Figure I3. Transfer functions (TFs) for sites unaffected by pseudo-resonances (Part 3). Theoretical TFs based on measured V_S profiles, damping profiles after Darendeli (2001) with default parameters (PI = 0, OCR = 1, f_{load} = 1 Hz, and K_0 = 0.5). No damping multiplier (D_{mul}) or D_{mul} = 1 and no V_S randomization.